SEQUENCE-STRATIGRAPHIC CONTROLS ON RESERVOIR-SCALE ARCHITECTURE OF THE MIDDLE MESAVERDE GROUP, DOUGLAS CREEK ARCH, COLORADO

by

KIMBERLY SUE HLAVA

B.S., Purdue University, 2008

A thesis submitted to the

Faculty of the Graduate School of the

University of Colorado in partial fulfillment

of the requirement for the degree of

Master of Science

Department of Geological Sciences

2011

This thesis entitled:

Sequence-stratigraphic controls on reservoir-scale architecture of the middle Mesaverde Group, Douglas Creek Arch, Colorado

written by Kimberly Sue Hlava

has been approved for the Department of Geological Sciences

____

Matthew J. Pranter

____

Rex D. Cole

____

Edmund R. Gustason III

Date________________________

The final copy of this thesis has been examined by the signatories, and we find that both the content and the form meet acceptable standards of scholarly work in the above mentioned discipline.

ABSTRACT

Hlava, Kimberly Sue (M.S., Geology [Department of Geological Sciences])

Sequence-stratigraphic controls on reservoir-scale architecture of the middle Mesaverde Group, Douglas Creek Arch, Colorado

Thesis directed by Associate Professor Matthew J. Pranter

The middle Mesaverde Group of the Douglas Creek Arch, northwestern Colorado, is represented by a complex succession of fluvial to marine strata that serve as outcrop analogs to laterally equivalent natural gas reservoirs in the Piceance and Uinta basins. The relatively low net-to-gross (N:G) (<50% sandstone) interval includes ~380 ft (~115.9 m) of mudrock, coal, and sandstone within the lower (Kmvl) to main coal-bearing (Kmvc) intervals of the Mesaverde Group (equivalent to the upper Iles and lower Williams Fork formations).

Based on 2,488 ft (758.5 m) of measured section, facies associations include: (1) coastal plain; (2) estuarine; (3) lagoon; and (4) shallow marine. Nine architectural elements are identified and include: (1) channel bodies; (2) crevasse splays; (3) discrete flood bodies; (4) a bayhead delta; (5) an estuarine assemblage; (6) foreshores; (7) tidal barforms; (8) middle shorefaces; and (9) washover fans. Based on 480 paleocurrent values from sedimentary structures, the vector-mean azimuth is approximately 130°. The stratigraphic study interval reveals two depositional sequences, which record a retrogradation followed by a progradation. Based on 38 sandstone-body measurements, channel bodies have an apparent width (W) of 287.7 ft (87.7 m), and thickness (T) of 4.1 ft (1.3 m) and are larger than crevasse splays (W=90.5 ft [28.0 m]; T= 1.8 ft [0.5 m]) and discrete flood bodies (W=61.5 ft [18.8 m]; T=2.0 ft [0.6 m]). Facies, facies associations, and architectural elements are more diverse in the study interval (Kmvl-lower Kmvc) as compared to previous studies completed in Coal Canyon, Colorado. Sandstone bodies are larger in Coal Canyon by almost 50%. Based on thin section analysis, the relative reservoir qualities of foreshore and middle shoreface architectural elements are good to excellent. Net-to-gross ratios (N:G) in the stratigraphic study interval show direct ties to the sequence-stratigraphic framework and provide a predictive tool for subsurface reservoir characterization. High N:G ratios lie above sequence boundaries within the early lowstand systems tract and fine upward. Low N:G ratios are present within the late lowstand systems tract. Moderate N:G ratios are present within the transgressive and early highstand systems tracts.

DEDICATION

I would like to dedicate this thesis to my family. To my husband, Dustin Hlava, for being understanding, patient, and supportive. To my parents, Douglas and Deborah Peters, for being encouraging and giving me the confidence to push through. To my sister, Laura Peters, for believing in me. And to everyone, for listening.

ACKNOWLEDGEMENTS

I would like to thank my advisor and mentor Matthew Pranter for his support, guidance, encouragement, and advice throughout this research and his aid in revising this thesis. I would also like to thank my committee members who provided support, insight, and recommendations for this work, Gus Gustason III and Rex Cole. I am grateful for Rex Cole's and Matthew Pranter's aid in the field during data collection.

I would like to thank Patrick Boulas, Ericka Harper, Vern Harper, Connor Newman, Nathan Sahlin, Chris Rybowiak, Ali Sloan, and Xiangyang Xie for their assistance in the field. Without their hard work and long hours, this thesis would have never been completed. I would like to thank them for their patience and understanding throughout the intense field days. Not only did they provide assistance, but also ideas and advice in smoothing out the data collection process.

Thank you to my fellow students, and friends, Ali Sloan, Whitney Mathias, Chris Rybowiak, and Ericka Harper, for their help and support throughout this thesis compilation.

I would like to thank Donna Anderson, Jen Aschoff, David Budd, Kirt Campion, Rex Cole, Jeff Crabaugh, Gus Gustason, Mark Kirschbaum, Jeff May, Piret Plink-Björklund, Matthew Pranter, and John Warme for their time and discussions. I am appreciative of their helpful input, which aided in interpreting the strata in this thesis. Thank you to Gigi Richard for compiling spatial data and creating shape files.

The Reservoir Characterization and Modeling Laboratory (RMCL) at CU-Boulder funded this research through the Phase V sponsors. I would like to thank the Williams Fork Consortium Phase V sponsors for their generous support: Anadarko Petroleum

Corporation, Marathon Oil Corporation, Bill Barrett Corporation, Newfield, Chevron, Oxy, ConocoPhillips, Suncor Energy, ExxonMobil, Schlumberger, iReservoir.com, and Williams.

This research was also partially funded by the AAPG Grants-in-Aid program. I would like to thank the contributions from Mr. and Mrs. Larry Funkhouser, Ms. Judy Grant, and Ms. Elizabeth B. Wilson for their contribution to the James E. Wilson Memorial Grant through the AAPG Grants-in-Aid program.

CONTENTS

TABLES

Table

FIGURES

Figure

CHAPTER ONE

INTRODUCTION

1. Background

The Upper Cretaceous fluvial, marginal-marine, and marine sandstone bodies of the Mesaverde Group in the Piceance Basin, Colorado, create one of the largest, unconventional, basin-centered, natural-gas plays in the United States (Johnson, 1989; Cole and Cumella, 2005; Cumella, 2006; Pranter et al. 2007, 2008, 2009) (Fig. 1).

Sandstone-body distribution, connectivity, and petrophysical-property heterogeneities are difficult to predict in the subsurface. Recent outcrop-based studies including Cole and Cumella (2005), Ellison (2004), Anderson (2005), Caldes (2005), Panjaitan (2006), and Pranter et al. (2007; 2009), have addressed these issues. The results of these studies have been useful in characterization, modeling, and development of stratigraphically equivalent reservoirs within the Mesaverde Group in the Piceance Basin. Studies by Crabaugh (2001), Kirschbaum and Hettinger (2004), Patterson et al. (2003), Gomez-Veroiza and Steel (2010), and Aschoff and Steel (2011) have addressed the sequence stratigraphy of the Mesaverde Group and equivalent strata. These studies have established the large-scale sequence stratigraphic framework of the Western Cretaceous Interior Seaway in the Piceance, Uinta, and Sand Wash basins.

2. Objectives

This research evaluates the reservoir characteristics of the middle Mesaverde Group (upper Iles through lower Williams Fork formations equivalent) in terms of facies, facies associations, and architectural elements. Reservoir-scale paleogeography and

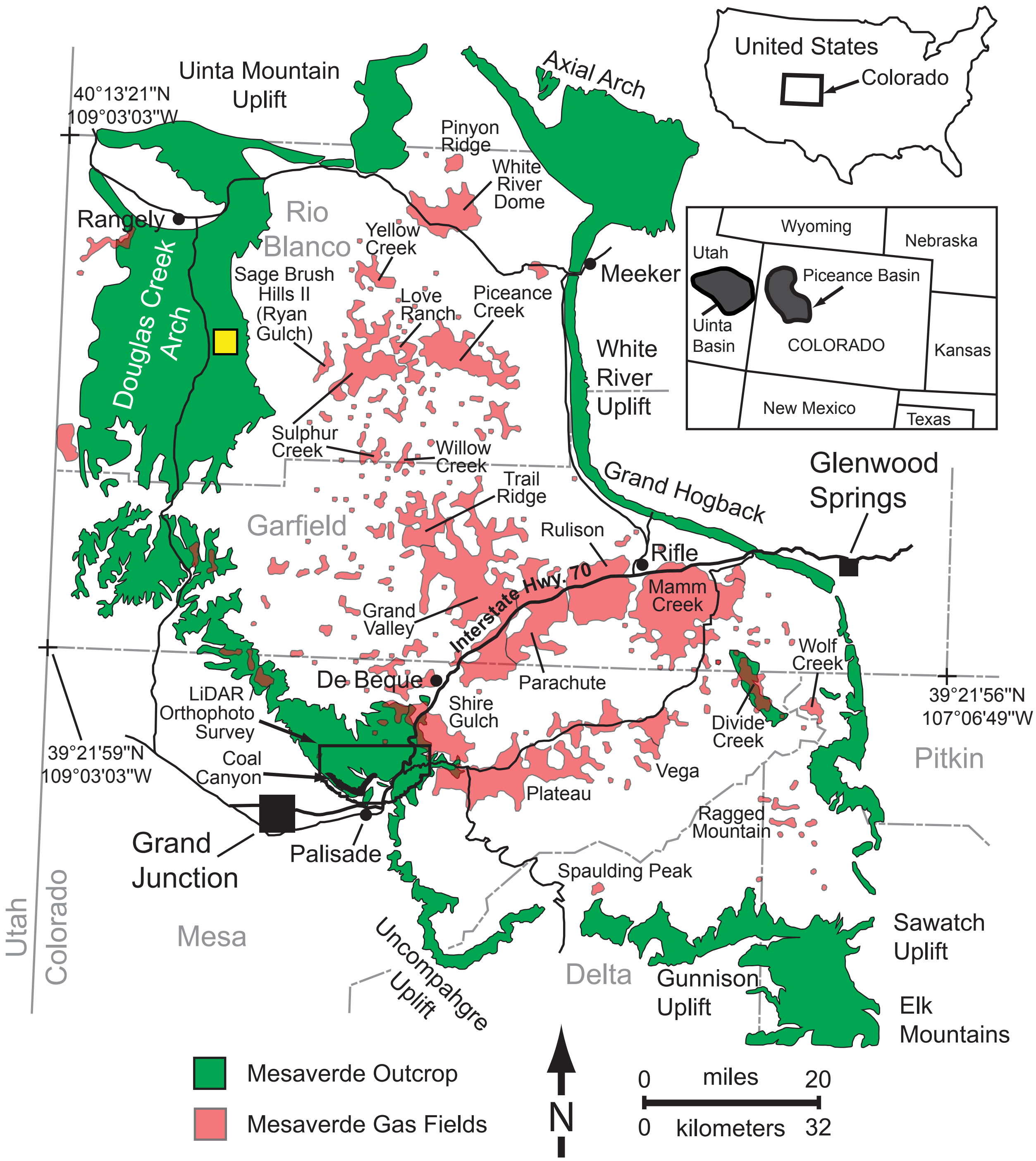

Fig. 1 Generalized Piceance Basin map showing location of outcrops and major gas fields. The Piceance Basin is located in northwestern Colorado. Major producing units are located in the Mesaverde Group. Yellow box shows approximate study area (Figs. 2 and 7). Gas fields from the Colorado Oil and Gas Commission. Modified from Hoak and Klawitter (1997) and Pranter et al. (2009).

sequence stratigraphy are also addressed. The research area lies approximately 20 mi (32.2 km) west of nearby producing fields in the Piceance Basin (Fig. 2).

This study addresses the following research questions related to the middle Mesaverde Group on the Douglas Creek Arch: (1) What lithologies, facies, and facies associations are present?; (2) What are the architectural elements and their specific characteristics and spatial distributions?; (3) What is the paleogeographic and sequence-stratigraphic framework?; and (4) How does this study apply to reservoir characterization?

3. Geologic Setting

3.1 Stratigraphy

During Cretaceous time, Sevier orogenic thrusting occurred in the present-day western United States. Erosion of the Sevier orogenic belt shed sediment eastward into the Rocky Mountain Foreland Basin, resulting in deposition of thousands of feet of Cretaceous strata. A eustaic rise in sea level flooded the present-day interior of the United States, creating the Cretaceous Western Interior Seaway, a shallow sea extending from the present-day Gulf of Mexico to the Arctic Ocean (Weimer, 1960; Johnson, 1989; Patterson et al., 2003). Numerous transgressions and regressions of the Cretaceous Western Interior Seaway into the Rocky Mountain Foreland Basin deposited a complex intertonguing of alluvial-plain, coastal-plain, and marine environments (Weimer, 1960; Johnson, 1989; Cole and Cumella, 2003; Johnson and Flores, 2003; Patterson et al., 2003). The seaway reached its maximum transgression during early Late Cretaceous time (Cenomanian-Turonian, ~91.5 Ma) (Haq et al., 1987).

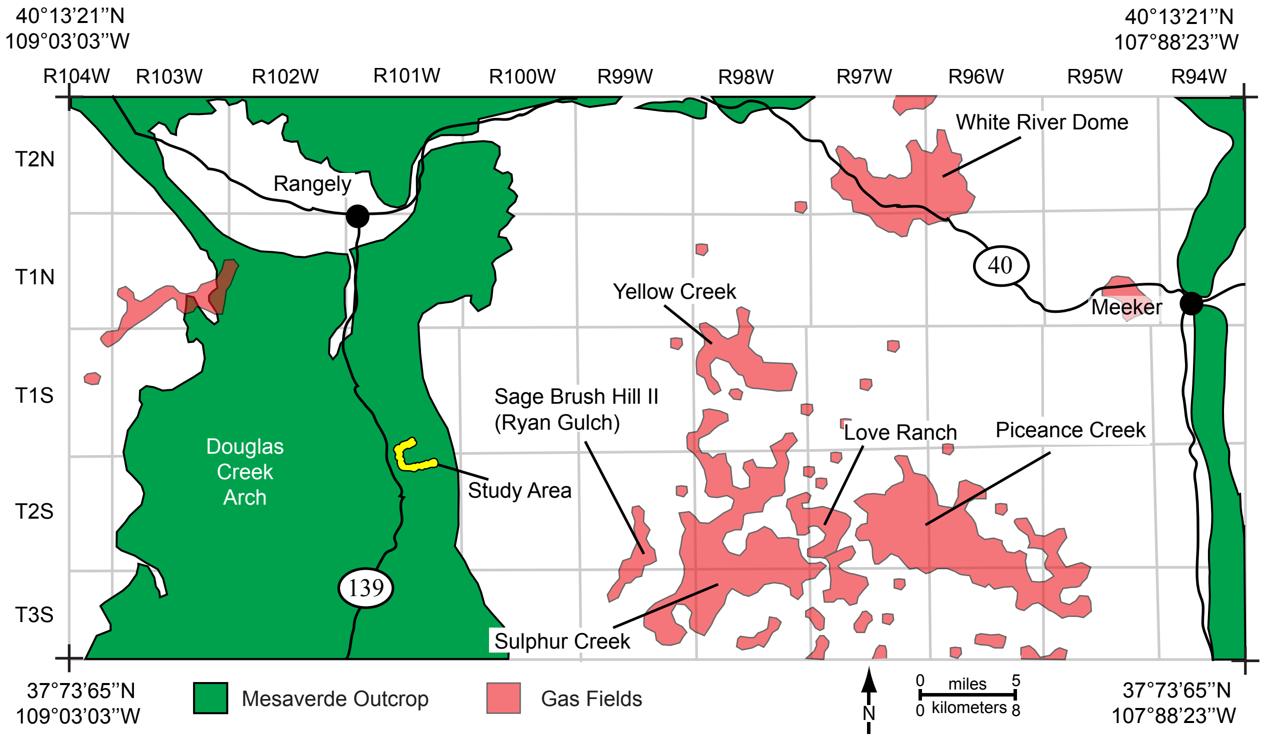

Fig. 2 Philadelphia Creek to State Bridge Draw study area in relation to major gas fields to the east, including Ryan Gulch, Yellow Creek, Love Ranch, Sulphur Creek, and Piceance Creek fields. The outcrop study area lies in a horseshoe-shaped area to the east and adjacent to Colorado Highway 139, approximately 13 mi (20.9 km) south of Rangely, Colorado within the Douglas Creek Arch. Yellow horseshoe shows the outcrop study area (Fig. 7). Gas fields from the Colorado Oil and Gas Conservation Commission.

Stratigraphic nomenclature in the area is complicated because the Mesaverde Group is subdivided differently depending upon location (Fig. 3). The standard USGS terminology, based on the Texas Mountain Quadrangle geologic map (Barnum et al., 1997), is used in this study. The top of the Mancos Shale marks the base of the Mesaverde Group. Four main units exist on the Douglas Creek Arch: 1) the lower Mesaverde Group (Castlegate-Sego interval); 2) the lower coal-bearing Mesaverde (Kmvl); 3) the main coal-bearing Mesaverde (Kmvc); and 4) the upper Mesaverde (no coal) (Kmvu) (Barnum et al., 1997). The Kmvc and Kmvu intervals are separated based on net-to-gross ratio (N:G) and the presence or absence of coal. The N:G is defined as the percentage of gross rock volume formed by the reservoir rock (i.e. sandstone percentage).

There are three main sandstone units within the lower Mesaverde Group in the study area: the Castlegate Sandstone, the lower Sego Sandstone, and the upper Sego Sandstone, which all intertongue with members of the Mancos Shale (Hettinger and Kirschbaum, 2002; 2003) (Fig. 3). Each is approximately 50-200 ft (15.2-61.0 m) thick and represents upward-coarsening, progradational shoreface sandstone bodies with minor deltaic influences (Noe, 1984; Hettinger and Kirschbaum, 2002; 2003).

The Kmvl is approximately 300-600 ft (91.4-183.0 m) thick and consists of coastal-plain, marginal-marine, and marine environments (Johnson and Smith, 1993; Barnum et al., 1997; Hettinger and Kirschbaum, 2002; 2003; Kirschbaum and Hettinger, 2004; Anderson, 2005; Caldes, 2005). In the Piceance Basin, the Kmvl is divided into three progradational shoreface members: the Corcoran, Cozzette, and Rollins sandstone members (Fig. 3), which were deposited in inner-shelf, deltaic, strandline

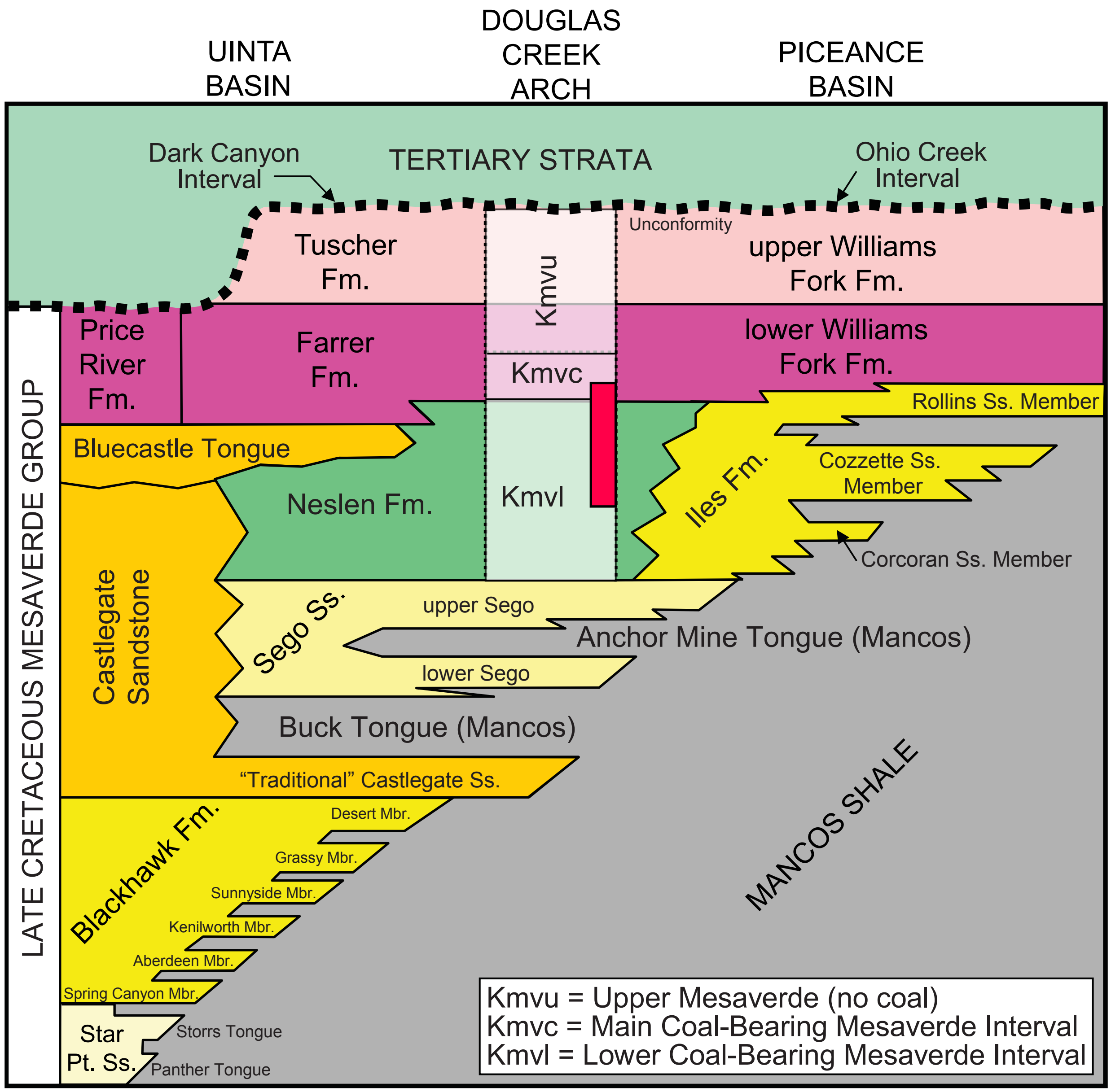

Fig. 3 Nomenclature of the study interval and the lateral equivalents to the east (Piceance Basin) and west (Uinta Basin) (Fig. 1). The red bar indicates the study interval, approximately 95 ft (29.0 m) above the top of the upper Sego Sandstone (Fig. 8). The study interval includes the uppermost Kmvl (Neslen/Iles formations) and the lowermost Kmvc (lowermost Farrer/lower Williams Fork formations). The nomenclature used is referenced from the United States Geological Survey. Modified from Hettinger and Kirschbaum (2002).

(shoreface), estuarine, and lower-coastal-plain environments (Hettinger and Kirschbaum, 2002; 2003; Kirschbaum and Hettinger, 2004; Shaak, 2010). These three members are separated by tongues of marine Mancos Shale and represent several transgressive-regressive cycles of the Cretaceous Western Interior Seaway (Hettinger and Kirschbaum, 2002; 2003; Patterson et al., 2003; Cole and Cumella, 2005; Cumella and Scheeval, 2008; Shaak, 2010). In the Uinta Basin, the Kmvl is undivided, and is referred to as the Neslen Formation. The Neslen is interpreted as coal-bearing, tidally influenced, marginal-marine deposits (Hettinger and Kirschbaum, 2002, 2003; Kirschbaum and Hettinger, 2004; Aschoff and Steel, 2011). The boundary between the Kmvl and the Kmvc is marked by an ash (tonstein) zone in the study area.

The Kmvc is a low N:G (<50% sandstone) interval that is approximately 200-500 ft (61.0-152.4 m) thick and is characterized by thin, discontinuous, isolated fluvial sandstone bodies interbedded with mudrock and coal. The Kmvc was deposited by meandering fluvial channels and extensive floodplains (Barnum et al., 1997; Johnson, 1989; Hettinger and Kirschbaum, 2002; 2003; Cole and Cumella, 2005; Pranter et. al., 2007; 2008; 2009). This unit is thought to be equivalent to the lower Williams Fork Formation, particularly, the Cameo coal zone. In the Uinta Basin, the Kmvc is undivided and referred to as the Farrer Formation (Aschoff and Steel, 2011) (Fig. 3). In the study area, no distinct boundary exists between the Kmvc and the Kmvu.

The Kmvu is a relatively high N:G (>50% sandstone) interval that is approximately 600-800 ft (182.9-243.9 m) thick and is characterized by isolated to amalgamated fluvial deposits. Deposits of the Kmvu are commonly thicker and more laterally continuous than those of the Kmvc. Sandstone bodies were deposited on the coastal and alluvial plains by meandering- to braided-fluvial channels in both the Piceance and Uinta basins (Barnum et al., 1997; Hettinger and Kirschbaum, 2002; Cole and Pranter, 2008; Pranter et al., 2008). The Kmvu is equivalent to the upper Williams Fork Formation in the Piceance Basin and the Tusher Formation in the Uinta Basin. This interval has mostly been beveled off the Douglas Creek Arch due to uplift and erosion (Johnson and Flores, 2003). The Cretaceous-Tertiary (K-T) boundary, which is exposed on the edges of the Douglas Creek Arch, marks the top of the Mesaverde Group strata (Ohio Creek and Dark Canyon intervals).

Figure 4 shows a generalized paleogeographic representation of the study area during Mesaverde Group deposition (~75 Ma). Alluvial-plain, coastal-plain, estuarine, shallow-marine, and deeper-marine depositional environments are represented between the Sevier Orogenic belt and the Western Interior Seaway.

3.2 Structural Setting

Once a part of the extensive Rocky Mountain Foreland Basin during the Sevier orogeny (~160-72 Ma) (Carroll, 2003), the Piceance Basin is one of many basins created by Laramide uplifts about 70-40 Ma (Johnson, 1989; DeCelles and Currie, 1996; Johnson and Flores, 2003; DeCelles, 2004). Late Cretaceous-Eocene age outcrops rim the Piceance Basin. The structural Piceance Basin is bounded by the Grand Hogback and the White River Uplift on the east, the Axial Arch on the northeast, the Uinta Mountain Uplift on the north and northwest, the Douglas Creek Arch on the west, the Uncompahgre and Gunnison uplifts on the south, and the Elk Mountains and the Sawatch Uplift on the southeast (Johnson, 1989; Patterson et. al., 2003, Cole and Cumella, 2005; Pranter et al., 2009) (Fig. 5). The Piceance Basin is kidney shaped, with

Fig. 4 A) Paleogeographic reconstruction of North America during the Late Cretaceous (~75 Ma). Approximate location of study area is within the red box. The study location lies to the east of the Sevier orogenic belt and within the coastal-plain to marginal-marine transition zone of the Cretaceous Western Interior Seaway. B) Close-up view of the paleogeography of the four corners area. Approximate study area outlined in red. Modified from Blakey (2004; 2009).

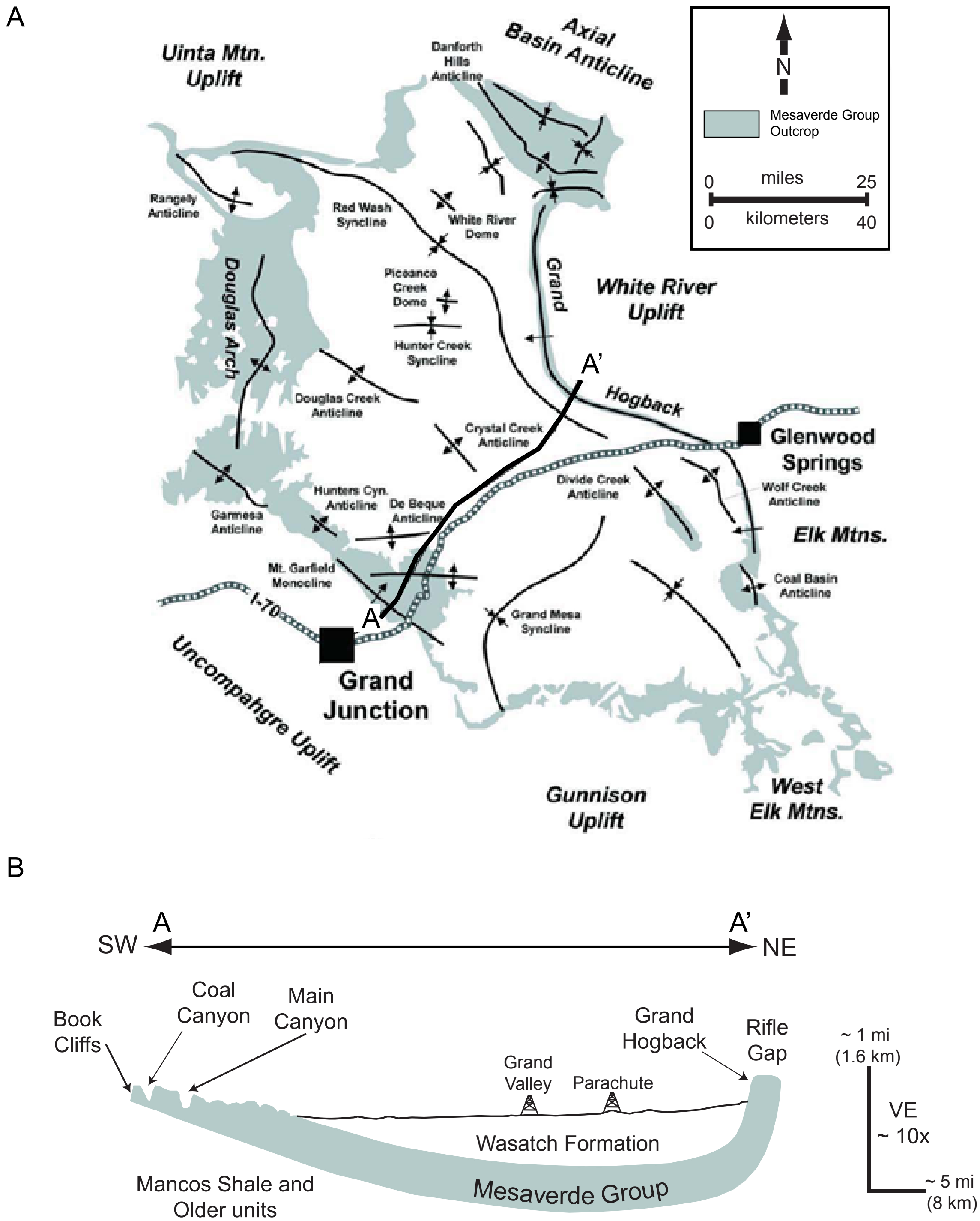

Fig. 5 A) Basic structural map of the Piceance Basin showing major structural features. B) Basic structural cross section through the Piceance Basin showing approximate locations of major gas fields and key locations. Modified from Murray and Haun (1974), Choate et al. (1981), Tyler et al. (1996), Johnson and Roberts (2003), and Cole and Cumella (2003).

an elongate northwest to southeast trend and an asymmetric structural profile where strata on the eastern side of the basin are vertical and overturned along the Grand Hogback, with a gently dipping western flank (2-5°) (Fig. 5) (Johnson, 1989; Patterson et al., 2003; Cumella, 2006; Cole and Pranter et al., 2008; 2009).

The Douglas Creek Arch is a north-south-trending, Laramide-age anticline that separates the Piceance Basin to the east from the Uinta Basin to the west, and is approximately 47 mi (75.7 km) long and 22 mi (35.4 km) wide (Bader, 2009). The Douglas Creek fault is an east-west trending strike-slip fault and is considered the master fault of the Douglas Creek Arch. The Douglas Creek fault is believed to be Precambrian in age, and was reactivated during Laramide deformation (Bader, 2009). Small normal faults throughout the Douglas Creek Arch are exposed at the surface, are northeast trending (N45°E), and high-angle (60°-90° dip), where the hanging-wall blocks are to the northwest (Fig. 6). These faults were created by left-lateral motion along the Douglas Creek fault zone. Additionally, the Rangely Dome is an east-west-trending anticline present to the north of the study area. As a result, east-west-trending normal faults with hanging-wall blocks to the south are also present in the study area. A normal fault between Vandamore Draw North and Vandamore Draw South is recognized; however, the stratigraphic interval is not significantly impacted by structural deformation. Outcrops of the area dip approximately 1-2º to the northeast. Tops of outcrops to the north (toward State Bridge Draw West) are eroded while those to the south (Philadelphia Creek West) are preserved. Because outcrops gently dip into the Piceance Basin, stratigraphically higher intervals (Kmvu) are progressively exposed to the east.

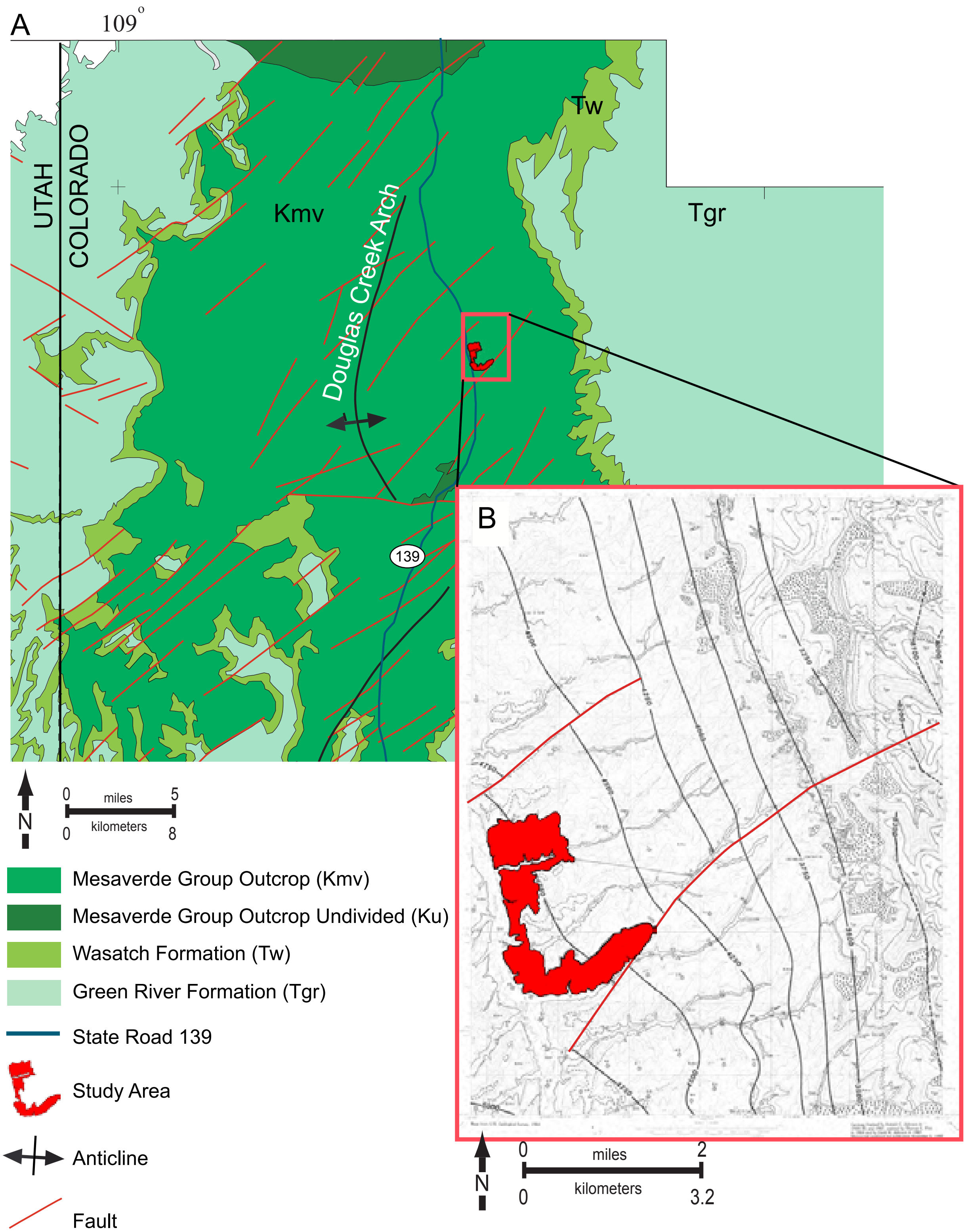

Fig. 6 A) Generalized geologic map of the Douglas Creek Arch with major faults marked. Modified from Bader (2009). Red box shows study area. B) Close-up view of the study area within the Philadelphia Creek Quadrangle geologic map. Modified from Johnson and Smith (1993).

The Uinta Basin is located in eastern Utah and lies directly west of the Douglas Creek Arch (Fig. 1). The Uinta Basin was once a part of the Cretaceous-age Rocky Mountain Foreland Basin but was isolated from the Piceance Basin by the Douglas Creek Arch during Laramide deformation.

4. Study Area and Stratigraphic Interval

The study-area outcrops are located in the central Douglas Creek Arch (T1S, R101W, Sections 33 and 34 and T2S, R101W, Sections 3 and 4) (Fig. 7). The area is located approximately 13 mi (20.9 km) south of Rangely, Colorado, and approximately 50 mi (80.5 km) north of Fruita, Colorado, along Colorado Highway (CH) 139, which runs north and south along the Douglas Creek Arch. The total outcrop area is approximately 1,280 ac (2 mi^2 [3.2 km^2]); (2.3 mi [3.7 km] north-to-south by 1.7 mi [2.7 km] east-to-west) (Fig. 7). For comparison to the area of a subsurface reservoir, approximately 128 wells with 10-ac (660 ft [201.2 m]) spacing, or 32 wells with 40-ac (2,640 ft [804.9 m]) spacing could fit within the study area. The study interval is approximately 385 ft (117.4 m) thick and lies within the upper Kmvl and the lower Kmvc intervals. The interval begins 95 ft (29.0 m) above the top of the upper Sego Sandstone (Fig. 8).

5. Previous Work

5.1 Reservoir Characterization Studies

In the southwestern Piceance Basin (Coal Canyon), studies by Cole and Cumella (2005), Ellison (2004), Panjaitan (2006), and Pranter et al. (2007; 2009) address the sedimentology, stratigraphy, and reservoir-scale characteristics of the coastal-plain deposits of the lower Williams Fork Formation. Field descriptions, global positioning

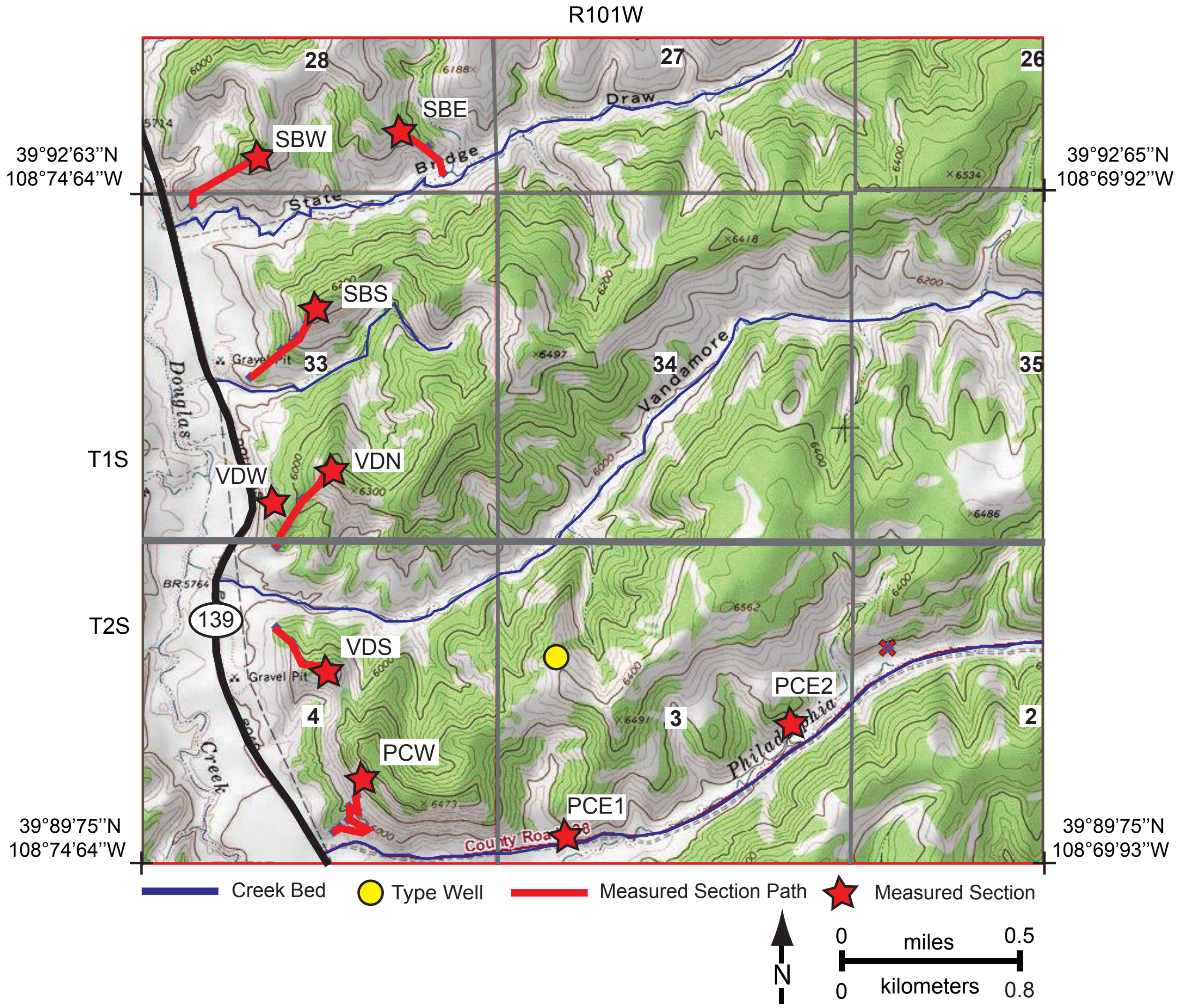

Fig. 7 Philadelphia Creek to State Bridge Draw study-area base map.The outcrop study area lies in a horseshoe-shaped area to the east and adjacent to Colorado Highway 139, approximately 13 mi (21 km) south of Rangely, Colorado within the Douglas Creek Arch (T1S R101W, Sections 28 and 33, and T2S R101W, Sections 4 and 3). Yellow dot indicates a type well used for study interval location (Fig. 8). Red stars indicate the top of the measured section and red lines indicate the measured section path.

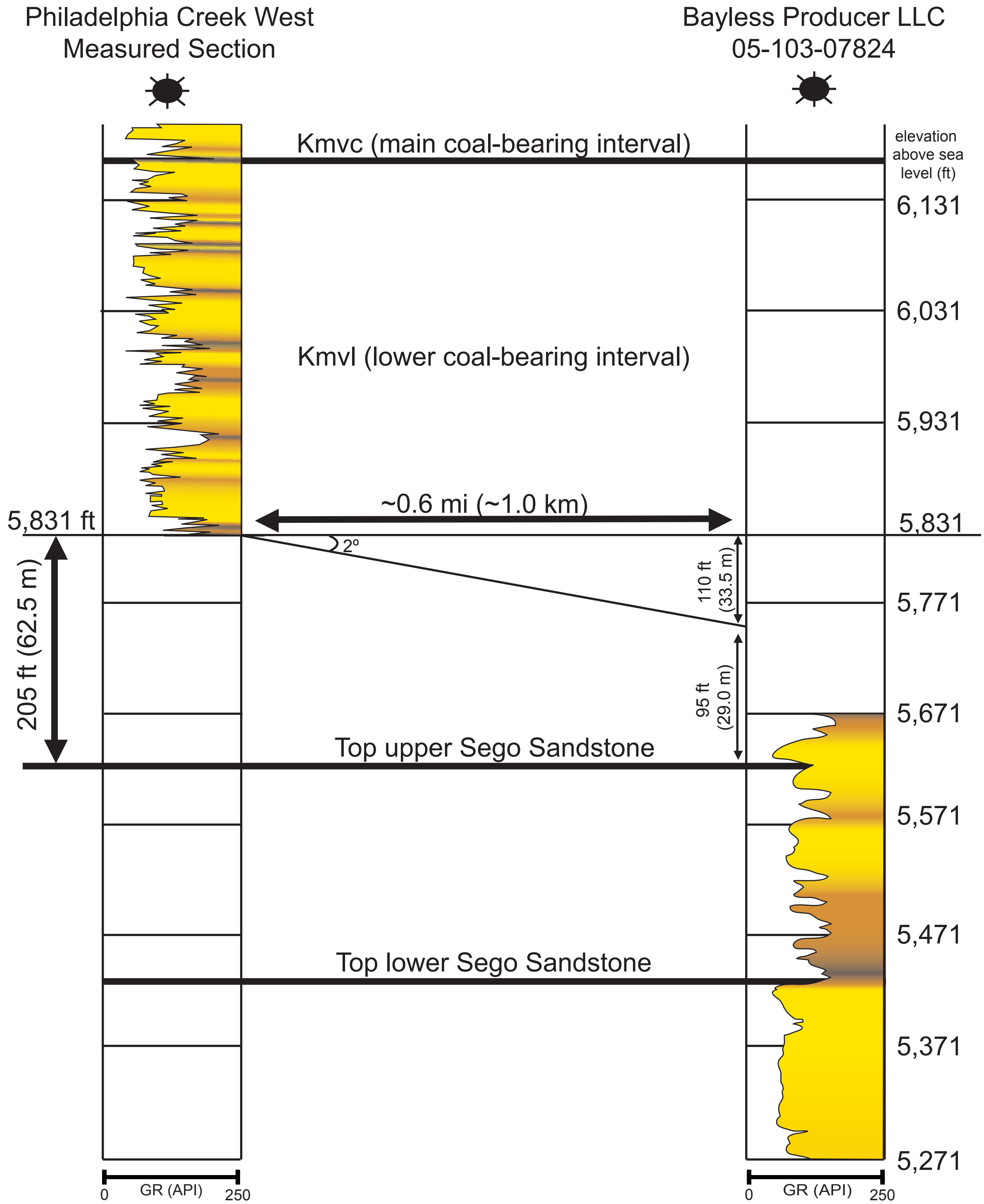

Fig. 8 Study interval with comparison to a nearby well log (Fig. 7), approximately 0.6 mi (1.0 km) (straight-line distance) to the northwest of the Philadelphia Creek West outcrop. The base of the measured section is at an elevation of 5,831 ft (1,777.7 m) above sea level. Structural dip is approximately 2º. Gamma-ray (GR) log used for comparison. The study interval begins approximately 95 ft (29.0 m) above the top of the Upper Sego Sandstone.

system (GPS) traverses, and a combination of high-resolution aerial light detection and ranging (LiDAR) data, digital orthophotography, and ground-based photomosaics were used to map and document the abundance, stratigraphic position, and dimensions of single-story and multistory channel bodies and crevasse splays. The mean thickness and apparent width of the 688 measured sandstone bodies are 12.1 ft (3.7 m), and 364.9 (111.2 m), respectively. Average apparent sandstone-body widths are equivalent to approximately 10-ac (660 ft [201.2 m]) spacing. In Cole and Cumella (2005), five types of fluvial sandstone bodies were defined, which had an average paleocurrent orientation of 74.8°. Sandstone-body types include: 1) narrow; 2) simple sinuous; 3) compound sinuous; 4) crevasse-channel; and 5) crevasse splay.

Anderson (2005) completed an outcrop study (160 ac [0.5 mi^2 (0.8 km^2)]) within the Iles Formation to characterize sandstone-body architecture in order to predict lateral continuity and directional permeability. Anderson (2005) concluded that, generally, crevasse splays have high lateral continuities, whereas point bars have low lateral continuities. Accretion surfaces, which define the macroform geometries of crevasse splays and point bars, relate to directional permeability, where permeability is higher in the average paleocurrent orientation. Individual point-bar permeability tends to be higher perpendicular to accretion sets. Crevasse-splay permeability tends to be higher parallel to accretion sets.

Caldes (2005) completed an outcrop study (1,500 ft [457.3 m] of stratigraphic section) of the coastal-plain and marginal-marine deposits of the Iles Formation in the northern Piceance Basin, east of Rangely, Colorado (near Kenney Reservoir). Four facies associations were identified and include: 1) channel; 2) crevasse splay; 3) floodplain; and 4) lake.

5.2 Sequence-Stratigraphic Studies

Studies by Patterson et al. (2003), Kirschbaum and Hettinger (2004), and Aschoff and Steel (2011) have addressed the sequence-stratigraphic framework of the Mesaverde Group in the Piceance and Uinta basins. Patterson et al. (2003) summarized the systems tracts that make up the Iles and Williams Fork formations between Rangely, Colorado and Rifle Gap, Colorado. Kirschbaum and Hettinger (2004) indentified six stratigraphic sequences between Book Cliffs, Utah, and Grand Junction, Colorado. Aschoff and Steel (2011) correlated six depositional sequences within the Mesaverde Group (between the Sego Sandstone and the lower Williams Fork Formation) between Price, Utah, and Rifle, Colorado.

Studies by Crabaugh (2001) and Gomez-Veroiza and Steel (2010) have addressed the sequence-stratigraphic framework of the Mesaverde Group in the Sand Wash basin. Crabaugh (2001) studied and characterized a transgressive-regressive cycle in the outcrop exposures of the Mesaverde Group between Highway 13 and Fish Creek, along the Williams Fork River, Colorado. Building on Crabaugh (2001), Gomez-Veroiza and Steel (2010) interpreted three systems tracts using a cross section between Rock Springs, Wyoming, and Kremmling, Colorado.

6. Methodology

The outcrops along the Douglas Creek Arch were selected because they are well exposed, accessible, and in close proximity to subsurface reservoirs that produce from the same stratigraphic interval (i.e., they are appropriate outcrop analogs) (Fig. 2). Eight stratigraphic sections (2,488 ft [758.5 m]) were measured to describe lithology, grain size, sedimentary structures, bounding surfaces, ichnofacies, paleocurrent orientations, and large-scale depositional geometries (Appendix A). Facies and architectural elements were interpreted from these observations. Stratigraphic sections are spaced approximately 2,000 ft (609.8 m) laterally (Fig. 7). Total-count gamma-ray (GR) data from a Super-Spec RS-125 scintillometer (Radiation Solutions, Inc.) were acquired for each stratigraphic section in every one foot (0.3-m) (Appendix B). Data were recorded manually and the average of the first and last reading over a 10-sec time period was computed. Dimensional data for 38 sandstone bodies were collected using a Trimble GEO-XT GPS receiver (accuracy = 3 ft [0.9 m]) to attain coordinates of lateral pinchouts of sandstone bodies (Appendix C). GPS data were imported into Arc GIS® software, where apparent-width values were recorded using the straight-line measurement tool. Along a given sandstone body, thicknesses were measured every 10-20 ft (3.0-6.1 m) using a measuring tape. Paleocurrent indicators (N=484) were determined from cross-stratification, scour surfaces, and inclined heterolithic strata using a Brunton compass (Appendix D). Additional stratigraphic sections (N = 12), between 5-20 ft [1.5-6.1 m] thick, were measured on various sandstone bodies, which were located off the main stratigraphic section paths (Appendix A). Photomosaics were acquired and assembled using a 12.3 megapixel Nikon D-90 digital SLR camera and the Adobe Photoshop software package, respectively (Appendix A). Photomosaics aided in definition of large-scale depositional geometries, surfaces, dimensions, and connectivity of the sandstone bodies. Gamma-ray data and stratigraphic sections (turned into “pseudo” grain-size logs), were imported into Petrel software and correlated laterally (Appendix E).

Additional photos were taken to show small-scale facies, ichnofaices, and geometries (Appendix F). Thin sections (N=16) stained for feldspars were created to more accurately determine grain size, composition, sorting, and maturity (Appendix G).

CHAPTER TWO

FACIES, FACIES ASSOCIATIONS, SANDSTONE BODIES, AND ARCHITECTURAL ELEMENTS

1. Introduction

Sedimentological descriptions, geometries, dimensions, gamma-ray and paleocurrent data were used to define facies, facies associations, sandstone bodies, and architectural elements. *Facies* is defined as a body of rock characterized by a particular combination of lithology, physical structures, and biological structures that bestow an aspect different from the bodies of rock above, below, and laterally adjacent (Walker, 1992). *Facies associations* are defined as groups of facies genetically related to one another and which have some environmental significance (Collinson, 1969; Walker, 1992). For the purposes of this study, a *sandstone body* is defined as a volume of sandstone and associated mudrock that forms a three-dimensional outcrop with a discrete thickness and lateral extent (Cole and Cumella, 2005), where no genetic interpretation is attached. An *architectural element* is a sandstone body, which is defined by the nature of the lower and upper bounding surfaces, external geometry, thickness and lateral extent (scale), and internal geometry (Miall, 1985).

Kirschbaum and Hettinger (2004) described 18 lithofacies and nine facies associations in outcrop and core for the Neslen Formation and equivalent strata. Five general depositional environments were identified: alluvial plain, coastal plain, estuarine complex, shoreface/delta front, and offshore marine. Cole and Cumella (2005) identified 14 lithofacies and five architectural elements within the lower coastal-plain deposits in outcrop for the Cameo coal zone near Coal Canyon, Colorado. Architectural elements included: 1) narrow, 2) simple sinuous, 3) compound sinuous, 4) crevasse-channel, and 5) crevasse splay. Caldes (2005) identified five sandstone lithofacies and two main architectural elements in the fluvial deposits in the Iles Formation near Rangely, Colorado. Crevasse splay bodies and point bars of a meanderbelt were identified and mapped across the study area. Aschoff and Steel (2011) identified 24 lithofacies within the Neslen strata. Four lithofacies assemblages were identified and included: (1) conglomeratic; (2) sandstone-dominated; (3) heterolithic; and (4) mudstone-dominated.

2. Facies

Facies were described based on eight, foot-by-foot measured sections, totaling 2,488 ft (758.5 m). Lithology, sedimentary structures, grain size, grain-size trends, texture, composition, biogenic features, thickness, bed contacts, and lateral continuity were described and used to define facies. Percentages of facies are based on the footage of measured section represented by each facies divided by all of the measured section footage combined. For example, if 250 ft (76.2 m) of the measured sections contained facies “A” then 250 ft (76.2 m) divided by 2,488 ft (758.5 m) is approximately 10% of the total study area. Therefore, facies “A” represents 10% of the total study-area footage. Seventeen facies (Table 1) are recognized and divided into four categories based on lithology (lithofacies): (1) mudstone; (2) muddy sandstone; (3) sandstone; and (4) other.

1. Mudstone and Mudrock

Mudstone is defined as a sedimentary rock with approximately equal proportions of silt-, clay-, and sand-sized grains; the sand grains are usually very fine-to-fine grained. Mudrock is defined as a sedimentary rock dominated by silt and clay. Mudstone and

Color	Name (Code)	Description	Depositional Processes	Image
	Fissile/Laminated Mudrock (Mf)	**Textures:** >80% mudrock **Structures**: fissile/planar laminated **Bioturbation:** rare to moderate, traces unknown **Thickness:** 5-10 ft (1.5-3 m) **Lateral continuity:** 5,000 ft (1,524.4 m) up to 2 mi (3.2 km) **Comments:** grayish green to dark grey, can be coal-bearing, may contain carbonaceous debris	Slow deposition rate Low energy	
	Mottled Mudrock (Mm)	**Textures**: moderately to poorly sorted, >80% mudrock **Structures**: convoluted to structureless **Bioturbation**: rare to intense with rooting **Thickness**: 5-10 ft (1.5-3 m) **Lateral continuity:** 5,000 ft (1,524 m) up to 2 mi (3.2 km) **Comments:** black to grey mottled with orange, red, green or brown, can be coal-bearing and contain carbonaceous debris, coal seams, hematite and siderite concretions	Slow deposition rate Low energy Secondary: Rooting/Bioturbation	
	Structureless Siltstone (Fs)	**Textures**: >80% siltstone **Structures**: structureless **Bioturbation**: rare to intense, traces unknown **Thickness**: 2-3 ft (0.6-1 m) **Lateral continuity:** 5,000 ft [1,542 m) up to 2 mi (3.2 km) **Comments:** grey to dark grey, can be coal-bearing, may contain carbonaceous material and siderite, may contain iron, with loading at the basal contact	Slow deposition rate Low energy Poorly drained Anoxic/Oxygen limited Secondary: Rooting/Bioturbation	
	Bioturbated Muddy Sandstone (Mb)	**Textures:** poorly sorted, with 30-80% very fine- to fine- grained sandstone, mudrock, and siltstone **Structures:** bioturbation **Bioturbation:** intense by *Planolites* and *Palaeophycus* **Thickness:** 0.5-1 ft (0.15-0.3 m) **Lateral continuity:** variable **Comments:** can be coal-bearing, may contain carbonaceous debris and siderite concretions and layers	Waning flow Low energy Bidirectional currents Oxic/Nutrient-rich Secondary: Bioturbation	

Color	Name (Code)	Description	Depositional Processes	Image
	Wavy-Laminated, Wavy Sandy Mudstone to Flaser Muddy Sandstone (Swl)	**Textures**: moderately to well sorted, very fine- to fine-grained, (30-80%) sandstone, siltstone, and mudrock **Structures**: wavy laminations, may contain round crested bidirectional-ripple foresets **Bioturbation**: rare to moderate, by *Planolites, Palaeophycus,* and rare *Teichichnus* **Thickness**: 3-5 ft (1-1.5 m) **Lateral continuity:** 5 ft (1.5 m) to up to 2+ mi (3.2+ km) **Comments:** syneresis cracks common, coarsens upward	Bidirectional currents Waning flow Ephemeral flows Seasonal flows Low to moderate energy Shifting regimes of salinity (where syneresis cracks are present)	
	Asymmetric-Ripple Cross-Stratified Sandstone (Sra)	**Textures**: well to moderately sorted, very fine- to fine-grained, >80% sandstone **Structures**: asymmetric ripple foresets, may contain climbing ripple foresets (10-50° climb) **Bioturbation**: rare insect burrows, *Planolites and Palaeophycus* **Thickness**: 1-2 ft (0.3-0.6 m) **Lateral continuity:** 50 ft (15.2 m) to 500 ft (152.4 m)	Steady flow Unidirectional current	
	Symmetric-Ripple Cross-Stratified Sandstone (Srs)	**Textures**: moderately sorted, very-fine to fine-grained, >80% sandstone **Structures**: symmetrical ripples, round-crested **Bioturbation**: 1-3/5 by *Planolites, Thallassinoides,* and rare *Rhizocoralium* **Thickness**: 1-3 ft (0.3-1 m) **Lateral continuity:** 500 ft (152.4 m) to 5,000 ft (1,524.4 m) **Comments:** straight to sinuous in plan view, may be laminated with mudrock and siltstone	Wave oscillation (small, symmetric wave orbitals) Moderate to low energy Slow sedimentation rate	
	Bidirectional-Ripple Cross-Stratified Sandstone (Srr)	**Textures**: well to moderately sorted, very fine- to fine- grained, >80% sandstone **Structures**: bidirectional ripple foresets, round crested **Bioturbation**: moderate to intense by *Ophiomorpha, Skolithos,* and *Planolites* **Thickness**: 1-3 ft (0.3-1 m) **Lateral continuity:** 500 ft (152.4 m) to 5,000 ft (1,524.4 m) **Comments**: may contain sharp-crested symmetric ripples, or combined-flow ripples, which may be climbing	Flood- and ebb- tide currents Oscillatory flow (in presence of combined-flow or symmetric ripples) Moderate to high wave- and tide- energy Nutrient rich/oxic (where burrows are present)	

Color	Name (Code)	Description	Depositional Processes	Image
	Planar-Laminated Sandstone (Sll)	**Textures**: well to moderately well-sorted, fine- to medium-grained, >80% sandstone **Structures**: very thin to thick planar lamina, may have parting lineations **Bioturbation**: rare by *Ophiomorpha* **Thickness**: 1-2 ft (0.3-0.6 m) **Lateral continuity:** 500 ft (152.4 m) to 5,000 ft (1,524.4. m) **Comments:** may contain ridge- and runnel-cross-stratification	Unidirectional traction current (upper flow regime) Rapid deposition rate Bidirectional curents (swashing) Eolian	
	Swaley to Hummocky Cross-Stratified Sandstone (Sls)	**Textures**: well sorted, subrounded to rounded, very-fine to fine-grained, >80% sandstone **Structures**: small-scale swales and hummocks **Bioturbation**: moderate to intense by *Ophiomorpha, Skolithos,* and rare *Arenicolites* and *Diplocriterion* **Thickness**: 2-4 ft (0.6-1.2 m) **Lateral continuity:** 5,000 ft (1,524 m), possibly greater **Comments:** may contain pyrite concretions and combined-flow ripples, very clean, quartz-rich	Wave oscillation (small symmetrical wave orbitals) High level of wave or current energy/Storm Nutrient rich/Oxic	
	Trough Cross-Stratified Sandstone (Slt)	**Textures:** well- to moderately sorted, fine- to medium-grained, >80% sandstone **Structures**: trough cross-stratification **Bioturbation**: none observed **Thickness**: 2-3 ft (0.6-1 m) **Lateral continuity:** 50 ft (15.2 m) to 5,000 ft (1,524.4 m) **Comments:** may contain heterolithic debris	Unidirectional current High energy Erosive (cut and fill)	
	Planar Cross-Stratified Sandstone (Slp)	**Textures**: well to moderately sorted, fine- to medium-grained, >80% sandstone **Structures:** planar/tangential cross-stratification, foresets may be draped by coal or mudstone **Bioturbation**: none observed **Thickness:** 2-4 ft (0.6-1.2 m) **Lateral continuity:** 50 ft (15.2 m) to 5,000 ft (1,524 ft) **Comments**: may contain heterolithic debris, laminasets may be in thin and thick couplets	Unidirectional current Moderate to high energy Eolian Bidirectional Current (Swashing)	
Color	Name	Description	Depositional Process	Picture

	Structureless Sandstone (Ss)	**Textures**: moderately to poorly sorted, very-fine to medium-grained, >80% sandstone **Structures**: none observed **Bioturbation**: rare to intense by *Palaeophycus* and *Planolites,* if recognized and/or rooting **Thickness**: 0.5-3 ft (0.15-1 m) **Lateral continuity:** 50 ft (15.2 m) to 5,000 ft (1,524.4 m) **Comments:** may contain hematite nodules	Rapid Deposition Secondary: Bioturbation/rooting	
	Convoluted Sandstone (Sc)	**Textures:** moderately to poorly sorted, very-fine to medium-grained, >80% sandstone **Structures**: flames, contorted stratification **Bioturbation**: none observed **Thickness:** 1-2 ft (0.3-0.6 m) **Lateral continuity:** 50 ft (15.2 m) to 500 ft (152.4 m) **Comments:** may contain heterolthic debris	Rapid Deposition Dewatering Sediment Loading	
	Heterolithic Debris (Hsd)	**Textures:** poorly sorted, very fine- to coarse-grained sandstone, siltstone, and mudrock **Structures:** none observed **Bioturbation**: none observed **Thickness**: 0.5-1 ft (0.15-0.3 m) **Lateral continuity:** 10 ft (3.0 m) to 100 ft (30.5 m) **Comments:** may contain *Teredolites* -bored logs, carbonaceous debris, chert pebbles, mud-chip and sandstone clasts, and siderite and hematite concretions	Erosional (lag) Rapid deposition rate High energy	
	Coal (C)	**Textures**: 80-100% dull to sub-vitreous coal **Structures**: cleated to non-cleated **Bioturbation**: none observed **Thickness**: 1-2 ft (0.3-0.6 m) **Lateral continuity:** 5 ft (1.5 m) up to 2 mi (3.2 km), possibly greater	Swamp/Marsh/Mire Poorly drained	

Color	Name (Code)	Description	Depositional Processes	Image
	Ash - Bentonite (A)	**Textures**: 80-100% powdery to porcelaneous ash **Structures**: structureless and convoluted **Bioturbation**: none observed **Thickness**: 0.5-1 ft (0.15-0.3 m) **Lateral continuity:** 500 ft (152.4 m) to 2 mi (3.2 km) **Comments:** white or pink, may be reworked into the sediment by channels, contains shell fragments	Volcanic Ash (air-fall)	

Table 1 Summary of facies described in the stratigraphic study interval, including characteristic features and their interpreted depositional processes. Facies are identified based on eight measured sections (2,488 ft [758.5 m]) and subdivided into four categories based on lithology (e.g., mudrocks/mudstones, muddy sandstone, sandstone, and other).

mudrock comprises 43.9% of the stratigraphic interval (Fig. 9). Three facies are identified: 1) fissile/laminated mudrock (20.6%); 2) mottled mudstone (17.9%); and 3) structureless mudstone (5.4%) (Fig. 9). These facies have a wide range of lateral continuities, from <10 ft (3.0 m) to up to 2 mi (3.2 km). Due to poor exposure and vegetation on the outcrops, it is difficult to subdivide facies, and bioturbation is difficult to identify, therefore, many of the depositional settings are unknown but can be generalized based on type and abundance of accessories (e.g. rooting, leaves, etc).

Fissile/Laminated Mudrock (Mf).

Fissile/laminated mudrock is commonly 5-20 ft (1.5-6.1 m) thick, coal-bearing, carbonaceous, and grayish-green to dark-grey in color. Bioturbation is variable and trace fossils are not determined.

Mottled Mudstone (Mm).

Mottled mudstone is commonly 5-20 ft (1.5-6.1 m) thick, carbonaceous, grey to black in color and mottled with orange, red, green, and/or brown mudstone. Contortion and hematite and siderite concretions are common. Bioturbation is variable and trace fossils are not determined.

Structureless Mudstone (Ms).

This facies is commonly 2-7 ft (0.6-2.1 m) thick, carbonaceous, grey or dark grey in color, and commonly contains more silt- and sand-sized grains than the mottled mudstone and siderite concretions. In some cases, this facies contains siderite concretions, is well cemented, and has a nodular weathering appearance. Loading is

Color	Facies Code	%
	Mf	20.6
	Mm	17.9
	Ms	5.4
	Mb	1.3
	Swl	10.9
	Sra	6.1
	Srs	0.5
	Srr	1.1
	Sll	2.9
	Sls	2.2
	Slt	9.6
	Slp	6.1
	Ss	10.3
	Sc	1.7
	Hsd	1.6
	C	1.5
	A	0.3

Lithology Statistics

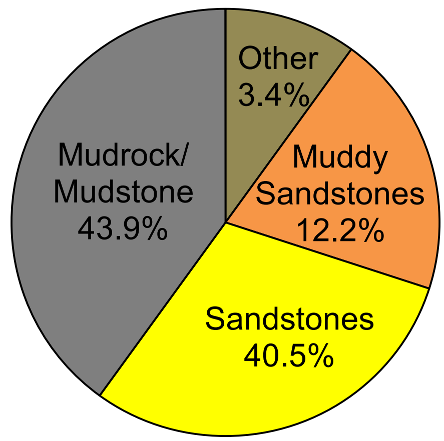

Facies Statistics

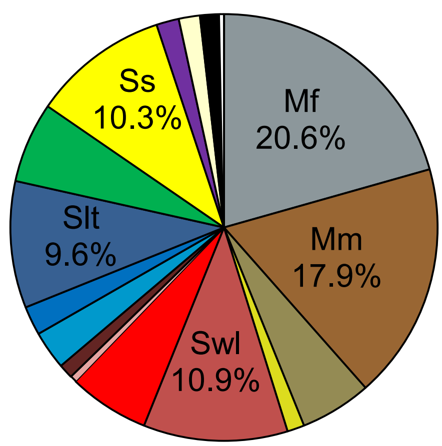

Fig. 9 Facies statistics calculated from the total footage of all the measured sections combined, based on eight measured sections (2,488 ft [758.5 m]) (N=2,488).

common at the basal contact. Bioturbation is unknown, but may be the reason for the structureless character.

Interpretation

The presence of mudstone and mudrock suggests low energies and deposition rates, such as in deep water or on the floodplain (e.g. oxbow lake, marsh, mire). All mudstone and mudrock are interpreted as floodplain derived (Table 1). Mottled mudstone indicates rooting and bioturbation. Siderite and iron precipitation occur within a restricted or anoxic environment where rapid accumulation and decomposition of organic matter takes place (Gautier, 1982; Beynon and Pemberton, 1992).

2. *Muddy Sandstone/Sandy Mudrock*

Muddy sandstone facies average 12.2% of the study-area footage (Fig. 9). Muddy sandstone is composed of 50-80% sandstone. Sandy mudrock is composed of 20-50% sandstone. Two facies are identified: 1) bioturbated muddy sandstone (1.3%); and 2) wavy-laminated, wavy sandy mudrock to flaser muddy sandstone (10.9%) (Fig. 9; Table 1). Lateral continuities vary from 10 ft (3.0 m) to up to 2 mi (3.2 km).

Bioturbated Muddy Sandstone (Mb).

This facies is commonly 0.5-5 ft (0.15-1.5 m) thick, composed of poorly sorted mudstone and very fine-to-fine grains. Bioturbation is intense, usually by *Planolites* and *Palaeophycus* plus rare *Teichichnus*. This facies is commonly carbonaceous with siderite layers and concretions.

Wavy-Laminated, Wavy Sandy Mudrock to Flaser Muddy Sandstone (Swl).

This facies can be divided into two groups: (1) flaser (50-80% sandstone); and (2) wavy (20-50% sandstone) (Table 1). The sandstone is very fine-to-fine grained (often coarsening upward), and is moderately to well sorted. This facies is typically 3-7 ft (0.9-2.1 m) thick. Sedimentary structures include 0.25-1 in (1-3 cm) wavy laminations, and commonly also contains 0.25-1 in (1-3 cm) round-crested bidirectional-ripple foresets with mudstone drapes. Bioturbation is low to moderate, by <1-2 in (3-5 cm) *Palaeophycus* and *Planolites* burrows. Syneresis cracks and siderite nodules and layers are common. Fragile particulates (such as leaves) are preserved within mudstone drapes.

Interpretation

Muddy sandstone is deposited in settings with: (1) low energies, (2) waning flows, (3) bidirectional flows (tides), and/or (4) ephemeral or seasonal flows (Table 1). The tail of a waning flow deposits the last of the suspended mud after a flood, storm, or at the base of an abandoned channel. Bidirectional currents (ebb and flood tides) produce sandstone layers while a slack-water period creates a mud drape. In a tidal environment, mud drapes in couplets are termed double-mud drapes (Reineck and Wunderlich, 1968; Collinson and Thompson, 1989; De Boer, et al., 1989; Dalrymple, 1992; Reinson, 1992). Brackish water is common in tidal settings, causing clay flocculation. This process creates grains of clay that act similar to sand grains, therefore, can be deposited similar to sand. Ephemeral and seasonal flows can act similar to tidal currents, where a slack-water period can deposit mudstone drapes between sandstone laminations. Syneresis (or synaeresis) cracks are sinuous in shape with a “V”- or “U”-shaped cross section. The presence of syneresis cracks indicates shifting salinities (brackish water) (Burst, 1965; Plummer and Gostin, 1981; Wightman et al, 1987; Pemberton and Wightman, 1992; Finzel et al., 2010). In the absence of loading or dewatering, syneresis cracks provide evidence that the depositional environment was subject to periodic extreme salinity fluctuations (Burst, 1965; Plummer and Gostin, 1981; Wightman et al, 1987; Pemberton and Wightman, 1992; Finzel et al., 2010). The feeding structures of *Planolites* and dwelling structures of *Palaeophycus* indicate shallow, subtidal, or submergent environments (Pemberton and Wightman, 1992). Small, low-diversity bioturbation is indicative of stressed environments, common in brackish water (Beynon and Pemberton, 1992; Pemberton, 1992).

3. Sandstone

Sandstone facies average 40.5% of the total study-area footage (Fig. 9). These facies are moderately continuous (5,000 [1,524.4 m]) to discontinuous (10 ft [3.0 m]), and contain >80%, very fine-to-medium-grained sandstone (Table 1). Specific facies are defined by the dominant sedimentary structure, which generally includes: 1) ripple cross-stratification; 2) dune cross-stratification; 3) planar lamination; and 4) convoluted or structureless.

Asymmetric-Ripple Cross-Stratified Sandstone (Sra).

This facies is commonly 1-7 ft (0.3-2.1 m) thick, and contains asymmetric ripple foresets. Ripples may climb at an inclination between 10-50°, herein called climbing ripple cross-stratification. Bioturbation is rare and include insect burrows, *Palaeophycus,* and *Planolites* burrows. This facies comprises 6.1% of the total study-area footage (Fig. 9).

This facies suggests deposition by a steady, non-pulsating, unidirectional traction current, such as a fluvial channel (Table 1) (Southard, 1982; Collinson and Thompson, 1989). Climbing ripples are deposited by a unidirectional current, with a high sedimentation rate, where the angle of climb reflects the balance between rate of upward bed growth and ripple migration (Collinson and Thompson, 1989). The lack of bioturbation also supports this interpretation.

Symmetric-Ripple Cross-Stratified Sandstone (Srs).

This facies is commonly quartz-rich, well sorted, and rarely contains organic debris. Sedimentary structures include round-crested, straight to sinuous, thinly bedded, symmetric ripples, which commonly are interstratified with lamina of mudstone. Bioturbation is low to moderate by the *Cruziana* ichnofacies (*Thallassinoides*, *Planolites,* and rare *Rhizocorallium*) (Appendix F). This facies is commonly 1-3 ft (0.3-0.9 m) thick and comprises 0.5% of the total study-area footage (Fig. 9).

This facies was deposited by gravity waves that generate wave oscillation, where the wave orbital’s period, size, and velocity highly affects the ripple-crest shape (Table 1). Small, symmetric wave orbitals below fair-weather wave base are more likely produce round-crested ripples (Clifton, 1976; Southard, 1982; Collinson and Thompson, 1989; Dumas and Arnott, 2006). The presence of the *Cruziana* ichnofacies indicates softground, shallow-marine environments below fair-weather wave base, but above storm-wave base, where sedimentation rate is relatively low (Frey and Pemberton, 1984; Pemberton et al., 1992).

Bidirectional-Ripple Cross-Stratified Sandstone (Srr).

Bidirectional-ripple cross-stratified sandstone is recognized by round-crested, opposed asymmetrical-ripple foresets (paleocurrents are in opposing directions). Occasionally, peak-crested symmetrical ripples, or combined-flow ripples (may be climbing) are interstratified. Bioturbation is moderate and defined by the *Skolithos* ichnofacies (*Ophiomorpha, Skolithos,* and *Planolites)* (Appendix F). This facies is typically 1-3 ft (0.3-0.9 m) thick and comprises 1.1% of the total study-area footage (Fig. 9).

This facies is deposited by bidirectional (flood- and ebb-tide) currents (Table 1). The flood-tide current produces ripple foresets in a landward direction, while the ebb-tide current rounds off the crests of the ripples and commonly produces ripple foresets in a seaward orientation. This rounding off of the crest of the ripple is called a “reactivation surface” (Collinson, 1970; Miall, 1992). A period of slack water exists between ebb and flood currents, producing a mud drape. Slack-water periods occur twice within the day and produce a double-mud drape. Depending on the energy level, and grain sizes available, the mud drape may or may not exist (Southard, 1982; Dalrymple, 1992). In this facies, the mud drape is small or nonexistent, producing >80% sandstone content. Peak-crested symmetrical ripples and combined-flow ripples are formed by shallow-water oscillatory flow (Collinson and Thompson, 1989). Combined-flow ripple cross-stratification results from storm deposition or mixed oscillatory and unidirectional flows, which result in bidirectional currents (Arnott and Southard, 1990; Myrow and Southard, 1991). The *Skolithos* ichnofacies is indicative of nutrient-rich, oxygenated environments, with high levels of wave or current energy (e.g. foreshore and shoreface of beaches) (Frey and Pemberton, 1985; Pemberton, 1992).

Planar-Laminated Sandstone (Sll).

This facies is moderately well to well sorted, very fine-to-medium grained with very thin (pinstriped) to thick planar laminations. Parting lineations are commonly seen in plan view. Bioturbation is absent to low, and where present, includes *Ophiomorpha* burrows. This facies is often 1-7 ft (0.3-2.1 m) thick and moderately (500 ft [152.4 m]) to highly (2 mi [3.2 km]) laterally continuous. Planar laminated sandstone comprises 2.9% of the total study-area footage (Fig. 9).

Planar laminations can indicate many different depositional processes: 1) unidirectional traction current; 2) rapid deposition; 3) bidirectional swashing currents; or 4) eolian (Table 1) (Schwartz, 1982; Reinson, 1992). All processes are present within the stratigraphic interval. Facies trends and subtle clues aid in determining depositional processes. Upper-flow regime unidirectional traction currents in shallow waters parting lineations, and commonly indicate washed out dunes, such as within a fluvial channel (Southard, 1982; Miall, 1992; Kirschbaum and Hettinger, 2004). These deposits are laterally discontinuous (<500 ft [152.4 m]), and stack vertically with other facies produced by fluvial-channel deposition (trough and asymmetric-ripple cross-stratification, etc). Rapid deposition and unidirectional currents in deep waters commonly result in normally graded laminations with no parting-current lineations. Rapid deposition rates do not allow sufficient time for dunes to develop. These deposits are laterally continuous (~5,000 ft (1524.4 m]) and are typically associated with other facies produced by rapid-deposition rates (climbing-ripple cross-stratification, structureless sandstone, etc), and are associated with deep water (e.g. prodelta). Bidirectional currents produce planar laminations in the swash zone (e.g. foreshore, shoreface, high-energy sand flats) (Kreisa and Moiola, 1986; MacEachern and Pemberton, 1992). Typically, swash in the foreshore to upper-shoreface environment produces seaward-dipping planar laminations (Komar, 1976; Heward, 1981; Walker and Plint, 1992). These deposits commonly contain ridge and runnel cross-stratification, parting lineations, and have gradational contacts with the facies below. *Ophiomorpha* burrows may be locally present. Planar-laminated sandstone can also be produced by eolian processes such as within back-barrier sand flats (washover deposits), which are thin deposits formed behind the barrier bar in an estuary (Schwartz, 1982; Reinson, 1992). These planar laminations are commonly pinstriped, very well sorted, and have sharp basal contacts with facies below.

Swaley Cross-Stratified Sandstone (Sls).

This facies is characterized by well-sorted, quartz-rich sandstone with subrounded-to-rounded grains (containing pyritic concretions and rare carbonaceous debris). Sedimentary structures include 0.25-1 ft (0.08-0.3 m) thick swales and hummocks and occasional 0.25 ft (0.08 m) thick combined-flow ripple cross-stratification. Bioturbation is moderate to intense by *Ophiomorpha, Skolithos,* and rare *Diplocriterion* and *Arenicolites* (*Skolithos* ichnofacies). This facies is commonly 2-4 ft (0.6-1.2 m) thick and moderately continuous 5,000 ft (1,524.4 m). Swaley cross-stratified sandstone comprises 2.2% of the total study-area footage (Fig. 9).

This facies is deposited by storm events, where the wave orbital’s period, size, and velocity highly affect the size and shape of the swale or hummock (Table 1). Sediment torn up during storms settles out of suspension, creating graded laminations within the swale. This facies is common in upward-coarsening, shallow-marine progressions (Leckie and Walker, 1982; Dumas and Arnott, 2006). Dwelling burrows of the suspension-feeding *Skolithos* ichnofacies indicates agitated, oxic, and nutrient-rich bottom waters (Pemberton, et al., 1992; Beynon and Pemberton, 1992).

Trough Cross-Stratified Sandstone (Slt).

Trough cross-stratified sandstone is recognized by 1-3 ft (0.3-0.9 m) thick, concave-upward, amalgamated, trough cross-stratified bedsets, and is more likely to contain mudstone and sandstone clasts, siderite and hematite concretions, chert pebbles, and carbonaceous debris than any other forms of cross-stratified facies. This facies is not bioturbated and has variable thicknesses, commonly 2-17 ft (0.6-5.2 m) thick. Trough cross-stratified sandstone comprises 9.6% of the total study-area footage (Fig. 9).

This facies is created by many depositional processes: 1) unidirectional currents; 2) bidirectional currents; or 3) eolian (Table 1). All processes are represented in the stratigraphic interval, and may be recognized by associated facies. Unidirectional traction currents, strong enough to produce 2-D, but not 3-D subaqueous dunes, can exist in a fluvial channel (Southard, 1982; Collinson and Thompson, 1989). Other landward-dipping and alongshore cross-stratification can exist in a backshore beach setting produced by bidirectional currents (Soliman, 1964; Heward, 1981). Small- to medium-scale foresets occur behind a barrier bar as a backshore dune or washover deposit, especially in conjunction with planar laminations, and may indicate deposition by eolian processes (Bridges, 1976; Schwartz, 1982; Reinson, 1992).

Planar Cross-Stratified Sandstone (Slp).

Planar cross-stratified sandstone is recognized by 0.5-2 ft (0.15-0.6 m) thick, planar or tangential cross-stratified bedsets. This facies is often 2-8 ft (0.6-2.4 m) thick and commonly contains siderite and hematite concretions, mudstone and sandstone clasts, and carbonaceous debris. On occasion, foresets may be coal or mudstone draped. In a rare case, the foresets thin and thicken in rhythmic bundles. This facies is not bioturbated. Planar cross-stratified sandstone comprises 6.1% of the total study-area footage (Fig. 9).

This facies is formed by many of the same depositional processes as trough cross-stratified sandstone (Table 1). The coal or mudstone drape is produced by a pause in sedimentation (e.g. tidal, seasonal, or ephemeral slack-water periods) (Southard, 1982; Collinson and Thompson, 1989). Laminations which thicken and thin in rhythmic bundles indicate neap/spring cyclicity, where neap cycles produce thinner lamina sets, and spring cycles produce thicker lamina sets, in bundles of 14/14, giving a total 28 day lunar tidal cycle, termed “tidal rhythmites” (Kreisa and Moiola, 1986; De Boer, et al.; 1989; Dalrymple, 1992), a diagnostic feature for determining deposition within the lower intertidal zone.

Structureless Sandstone (Ss).

Structureless sandstone contains no obvious internal stratification. This facies commonly contains rootlets, or hematite concretions, which may have formed around rootlets. Structureless sandstone is 0.5-6 ft (0.15-1.8 m) thick, and comprise 10.3% of the total study-area footage (Fig. 9).

Structureless sandstone can be deposited by rapid deposition and intense soft-sediment deformation. Previously stratified sandstone may be modified by intense secondary processes (i.e. rooting and/or bioturbation) (Table 1).

Convoluted Sandstone (Sc).

Convoluted sandstone is commonly 1-5 ft (0.3-1.5 m) thick, and contains flame structures and contorted cross-stratification. This facies commonly also contains siderite concretions, sandstone and mudstone clasts, and carbonaceous debris. No bioturbation is present. Convoluted sandstone comprises 1.7% of the total study-area footage (Fig. 9).

Overturned cross-stratification is produced when formerly cohesionless sand grains become cohesive after deposition and respond to an increase in shearing due to high current velocity (Sanders, 1960). Convolution is also often associated with dewatering, sediment loading, and/or rapid deposition, which can be caused by numerous processes including: channel slumping, flooding events, and earthquakes (Table 1). A water escape (flame) structure indicates escape of over-pressured fluids up through cohesionless sediment (Lowe, 1975; Pemberton et al., 1992).

4. Other

These facies comprise 3.4% of the total study-area footage (Fig. 9) and include the heterolithic debris (1.6%), coal (1.5%), and ash (0.3%) lithofacies (Table 1).

Heterolithic Debris (Hsd).

Heterolithic debris is composed of a poorly sorted, heterolithic mixture of very fine-to-coarse-grained sandstone and mudstone. It commonly contains *Teredolites*-bored logs, hematite concretions, siderite nodules, mudstone and sandstone clasts, chert pebbles, and large fragments of carbonaceous material (logs and branches). This facies is often present at the base fluvial channel deposits, is 0.5- 5 ft (0.15-1.5 m) thick, and is generally laterally discontinuous <50 ft (15.2 m).

The presence of heterolithic debris often indicates high energies, and rapid deposition rates (Table 1). *Teredolites* are sand-filled burrows into wood. These burrows are found in brackish-water environments, and indicate a marginal-marine source (Bomley and Pemberton, 1984; Cole and Cumella, 2005). The presence of logs and branches indicates a source from a coastal or alluvial plain setting. When this facies is present at the base of large sandstone bodies, it can indicate a channel-lag or channel-collapse feature (Miall, 1992).

Coal (C).

Thin (1-4 ft [0.3-1.2 m]) beds of black, cleated or non-cleated, dull to sub-vitreous coals are present. Layers are either discontinuous (<5 ft [1.5 m]) or laterally continuous (>2 mi [3.2 km]).

Coal is associated with peat accumulation in swamp environments. It is located on the coastal plain within highly vegetated, poorly drained environments (Table 1) (McCabe, 1984; Bohacs and Suter, 1997). Coal is associated with rising water tables in fresh- to brackish-water environments, or where an overall increase in accommodation space approximately equals the production rate of peat (Bohacs and Suter, 1997). Raised mires likely produce thick coals. Small lakes or low-lying mires commonly produce thin coals (McCabe, 1991).

Ash (A).

Volcanic ash and reworked volcanic ash (tonstein) is recognized by 0.5-2 ft (0.15-0.6 m) thick, powdery to porcelaneous, white to pink colored layers. Layers are discontinuous (<10 ft (3.0 m) to greater than 2 mi (3.2 km), and is present only near the top of the section (Appendix F). In some cases, the ash is commonly reworked into the surrounding sediment.

The ash was derived from nearby Late Cretaceous volcanic activity north (southwestern Montana) of the study area (Brownfield and Johnson, 2008). One such ash layer is known as the "Yampa Ash Bed" near Craig, Colorado, and was dated at 72.2 ± 0.1Ma (using the K-Ar Method), and can be used as an important correlation tool (Brownfield and Johnson, 2008). In the study area, ashes form a zone consisting of at least three layers (Appendix F). One is presumed to be the Yampa Ash, but not for certain.

3. Facies Associations and Architectural Elements

Nine architectural elements (Table 2) are identified based on their vertical and lateral facies assemblages, geometries, internal and external bounding surfaces, dimensions (apparent width and thickness), and ichnofacies. Paleocurrent orientations were used to distinguish architectural-element type with respect to architectural-element macrofeatures (bedform orientation vs. bedset orientation). Percentages of architectural elements are based on total footage represented by each architectural element on the measured sections divided by the total footage of all architectural elements combined. This calculation does not include undivided intervals (mudrock and mudstone). For example, if architectural element "A" represents 50 ft (15.2 m) of the stratigraphic

Color	Architectural Element	Vertical (base to top) and Lateral Facies Successions	Geometries and Dimensions	Internal/External Bounding Surfaces (IBS/EBS)	Comments
	Discrete Flood Body	**Vertical:** one single bed of blocky to fining upward sandstone and muddy sandstone facies **Lateral:** no obvious variation observed	**2D Geometry:** Lenticular **Avg. Thickness:** 2 ft (0.6 m) **Avg. Apparent Width:** 61.5 ft (18.8 m)	**IBS:** none **EBS:** sharp at the base, rooted to gradational at the top	Basal contact may contain heterolithic debris and convoluted and structureless sandstones. Commonly bioturbated and rooted at the top. Grey in color, coal fragments common
	Crevasse Splay	**Vertical**: Vertically stacked discrete flood bodies of muddy sandstone to sandstone (higher energy facies upward) **Lateral:** no obvious variation observed	**2D Geometry:** Lenticular and irregular sheets **Avg. Thickness:** 2.5 ft (0.8 m) **Avg. Apparent Width:** 85 ft (26 m)	**IBS:** gradational, **EBS:** sharp at the base, rooted and/or gradational at the top If trough cross-stratification or planar lamination are present near the top, the basal contact of the facies is scoured	May have an erosional surface, rooting and bioturbation at the top by *Skolithos, Planolites, Palaeophycus, Teichichnus*, Escape structures and cryptic features grey in color, coal fragments common
	Channel Body	**Vertical:** Heterolithic debris to sandstone to muddy sandstone at top (lower energy facies upward) **Lateral:** ***Into channel base***: Heterolithic debris, trough cross-stratification, and convoluted sandstone ***Into channel margin***: structureless and asymmetrical ripple cross stratified sandstone and muddy sandstone	**2D Geometry:** Lenticular or trapezoid **Avg. Thickness:** 4.3 ft (1.3 m) **Avg. Apparent Width:** 258.8 ft (78.9 m)	**IBS:** Inclined heterolithic strata which may or may not be draped with mud, may have siderite cementing the surface, and are internally scoured and erosional or sharp **EBS**: Scoured to sharp at the base and gradational and/or rooted at the top	Basal scour of heterolithic heterolithic debris and convoluted and structureless sandstones common. Bioturbation and rooting locally present at the top (0-2/5 BI). Abundant terrestrial material, siderite, and hematite concretions throughout.

Color	Architectural Element	Vertical (base to top) and Lateral Facies Successions	Lateral Continuity/Dimensions	Internal/External Bounding Surfaces	Comments
	Bayhead Delta	**Vertical:** ***lower 1/2:***interbedded structureless sandstone and mudstone ***upper 1/2:*** bidirectional ripple cross-stratified, planar-laminated, and planar cross-stratified sandstone (higher energy facies upward) **Lateral:** no obvious variation observed	**2D Geometry:** sheet **Avg. Thickness:** 5 ft (1.5 m) **Avg. Apparent Width:** 5,000 ft (1,524.4 m)	**IBS:** planar/tabular, normally graded mudrock to sandstone cycles to sandstone **EBS**: sharp and horizontal at the base, gradational at the top	Contains cycles of fining-upward units, overall sandier-upward, and an overall cleaning upward trend
	Estuarine Assemblage	**Vertical:** ***lower 1/3:***planar-laminated sandstone ***middle 1/3:***wavy-laminated muddy sandstone ***upper 1/3***:swaley cross-stratified sandstone **Lateral:** small lenticular sandstones present in the middle 1/3 to the south and lower 1/3 more common to the north	**2D Geometry:** sheet **Avg. Thickness:** 11.6 ft (3.5 m) **Avg. Apparent Width:** >2 mi (>3.2 km) (beyond limits of study area)	**IBS:** gradational to scoured if swaley and planar-laminated facies are present at the top **EBS:** sharp at the base to sharp to gradational at the top	Tripartite facies distribution. Contains very small *Planolites* burrows, syneresis cracks, coal fragments abundant with some highly preserved fragile debris (leaves), coarsens and cleans upward, *Ophiomorpha* burrows at the top
	Tidal Barform	**Vertical:** muddy sandstones to swaley and trough cross-stratified sandstone (higher energy facies upward) **Lateral:** Higher energy facies common toward up depositional dip of IHS and vice versa	**2D Geometry:** wedge **Avg. Thickness:** 9 ft (2.7 m) **Avg. Apparent Width:** 500 ft (152.4 m) - 5,000 ft (1,524.4 m)	**IBS:** Low angle (1-2°) inclined heterolithic strata which are sharp to gradational **EBS:** sharp to gradational at the base and top	Moderate to high bioturbation with abundant *Ophiomorpha*, *Skolithos, Planolites,* and *Palaeophycus.* Syneresis cracks and loading structures abundant

Color	Architectural Element	Vertical (base to top) and Lateral Facies Successions	Lateral Continuity/Dimensions	Internal/External Bounding Surfaces	Comments
	Foreshore	**Vertical:** wavy-laminated muddy sandstones to planar laminated sandstone (higher energy facies upward) **Lateral:** no obvious variation observed	**2D Geometry:** sheet **Avg. Thickness:** 4 ft (1.2 m) **Avg. Apparent Width:** unknown	**IBS:** gradational facies changes upward **EBS:** gradational at the base to sharp at the top	Gradational basal contact, *Ophiomorpha* the only burrows present if burrows are present, cleans upward, siderite common at the base
	Washover Fan	**Vertical:** planar laminated and planar cross-stratified sandstone (higher energy facies upward) **Lateral:** no obvious variation observed	**2D Geometry:** sheet **Avg. Thickness:** 4 ft (1.2 m) **Avg. Apparent Width:** ~500 ft (152.4 m)	**IBS:** gradational facies changes upward **EBS:** gradational at the base to sharp at the top	Sharp basal contact, no bioturbation, well sorted
	Middle Shoreface	**Vertical:** muddy sandstone to swaley cross stratified and structureless sandstone (higher energy facies upward) **Lateral**: less bioturbation to the south more symmetrical ripple cross-stratification to the south	**2D Geometry:** sheet **Avg. Thickness:** 6 ft (1.8 m) **Avg. Apparent Width:** ~5.000 ft (1,524.4 m) possibly up to to 2 mi (3.2 km)	**IBS:** gradational facies changes upward **EBS:** gradational at the base to sharp at the top	Moderate to highly bioturbated with abundant *Ophiomorpha, Skolithos, Thallassinoides, Planolites, Palaeophycus,* with rare *Diplocriterion* and *Rhizocorlirium* Bioturbation increases upward

Table 2 Summary of architectural elements in the stratigraphic study interval, including characteristic features, lateral continuity, and dimensions. Eight architectural elements are described based on eight measured sections (2,488 ft [758.5 m]) and subdivided into four major depositional environments (e.g. coastal plain, estuarine, shallow marine embayment, and shallow marine). Colors correspond to colors represented on Figure 10B.

interval, and the total footage of architectural elements is 500 ft (152.4 m) then "A" represents 10% of the architectural elements.

Facies associations are determined on the basis vertical facies-stacking patterns. Ichnology is used as an indicator of environments. For example, estuaries are typically composed of a mixture of *Skolithos* and *Cruziana* ichnofacies (*Skolithos, Monocriterion, Thallassinoides, Ophiomorpha, Planolites,* and *Palaeophycus*). Similar to facies, facies-association percentages are calculated based on the total footage represented by the facies association divided by the total footage of the stratigraphic interval (2,488 ft [758.3 m]). Facies associations include mudstone and mudrock facies. Architectural elements represent four facies associations: (1) coastal plain; (2) wave-dominated estuarine (estuarine); (3) lagoon; and (4) open wave-dominated shoreface (shallow marine) (Fig. 10A).

3.1 The Coastal-Plain Facies Association and Architectural Elements

The *coastal plain* is defined as strata that accumulated mainly in freshwater environments adjacent to a paleoshoreline (Hettinger and Kirschbaum, 2004) (Fig. 10A). The coastal-plain association is dominantly mudstone (40-70%), with subordinate sandstone and coal (Cole and Cumella, 2005) and commonly contains tidal- or brackish-water indicators. Coastal-plain deposits comprise 76.1% of the stratigraphic interval (Fig. 11). The coastal plain is composed of three types of deposits: (1) mudstone and coal; (2) isolated sandstone bodies; and (3) amalgamated sandstone bodies. Mudstone is typically structureless and mottled. Isolated sandstone bodies contain sandstone and muddy sandstone facies. Amalgamated sandstone bodies contain primarily sandstone facies and heterolithic debris. Three architectural elements

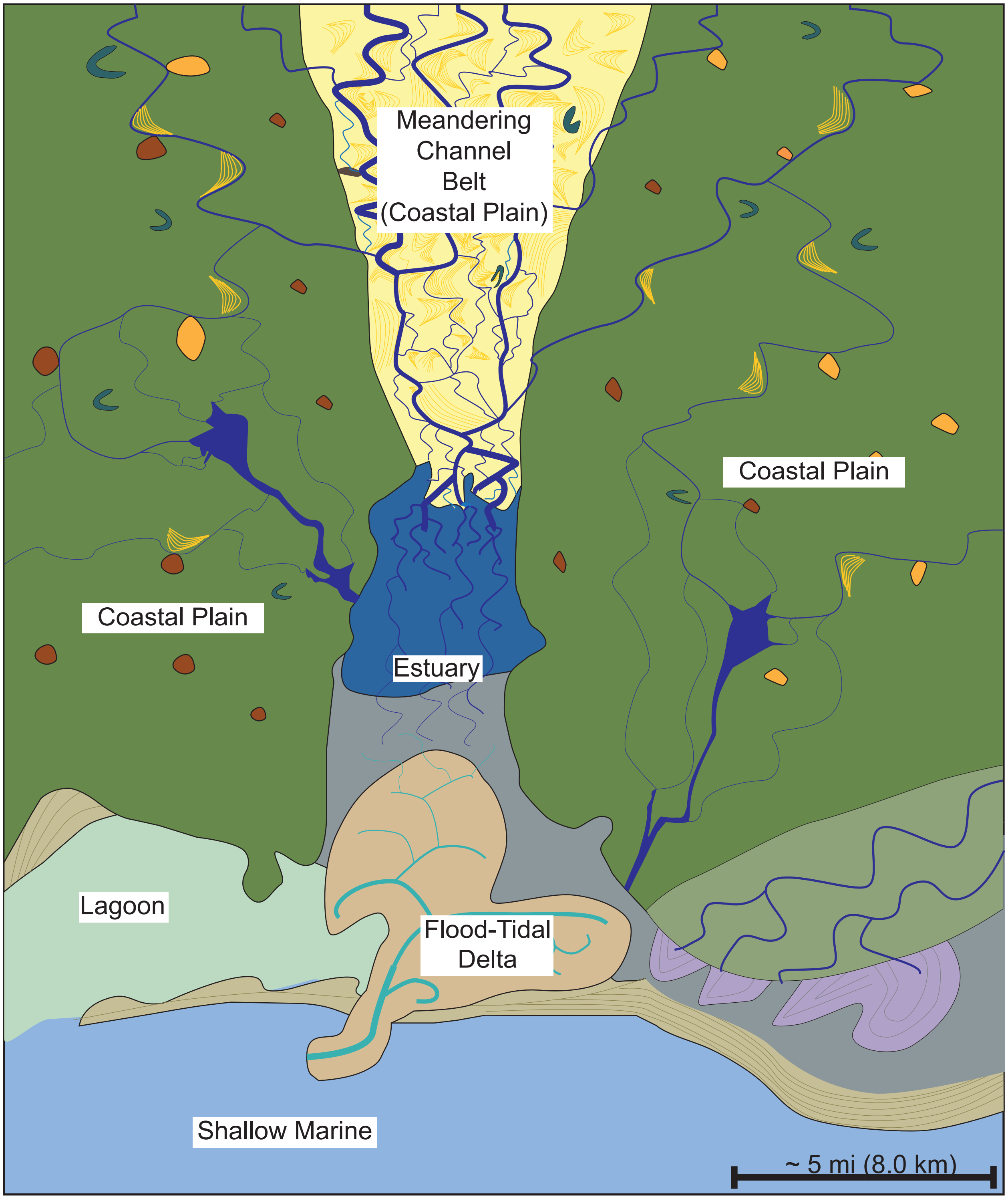

Fig.10A Schematic diagram for the facies asssociations (depositional environments) represented in the stratigraphic study interval. The different colors and shapes represent specific architectural elements within the system (see Fig. 10B). This figure is diagrammatic and does not represent the entire paleogeography of the stratigraphic study interval. Colors and shapes correspond to those represented in Table 2.

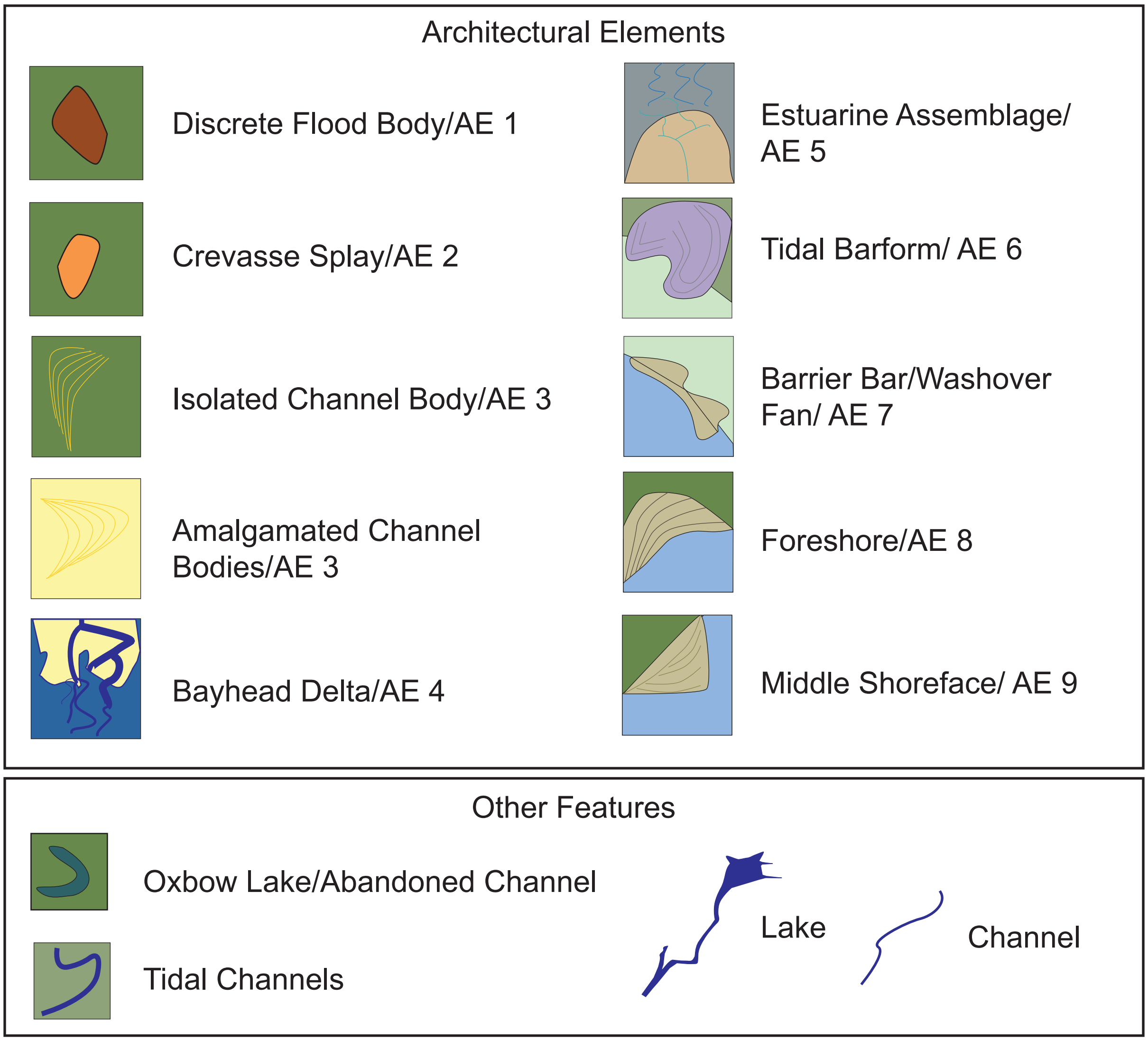

Fig. 10B Interpretation key for Figure 10A. Facies association and architectural element colors are those represented in Table 2.

Color	Facies Association	%
	Coastal Plain	76.1
	Estuarine (Est.)	12.5
	Lagoon	4.8
	Shallow Marine	6.6

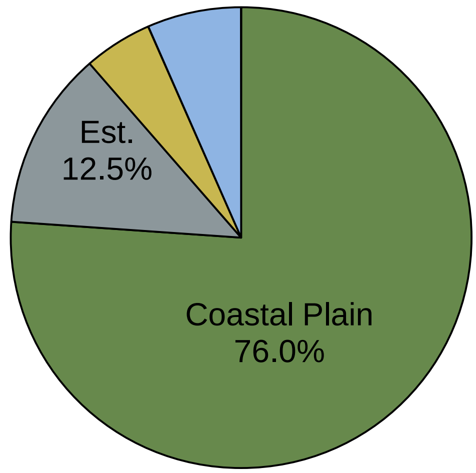

Color	Architectural Element	%
	Discrete Flood Body	2.4
	Crevasse Splay	16
	Channel Body	54
	Bayhead Delta	3.9
	Estuarine Assemblage	7.2
	Tidal Barform	7.4
	Foreshore	3.7
	Washover Fan	0.7
	Middle Shoreface	4.7

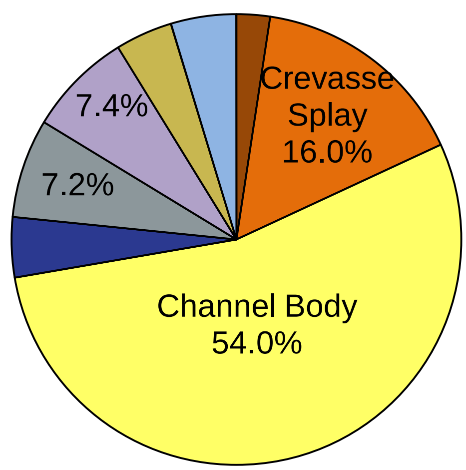

Fig. 11 Facies associations and architectural element statistics. Facies associations calculated based on total stratigraphic footage (N=2,488). Architectural element statistics calcuated based on total footage of identified architectural elements (no mudstones and mudrocks) (N=1,149 or 46.2% of the stratigraphic interval). All statistics based on eight measured sections (2,488 ft [758.5 m]).

are identified within the coastal plain: (1) discrete flood body; (2) crevasse splay; and (3) channel body (Fig. 12).

The fine-grained strata are considered to be floodplain deposits (e.g. freshwater mires, marshes, and oxbow lakes) (Fig. 10A). Floodplain deposits are composed of structureless and mottled mudstone and coal (<1%). Structureless and mottled mudstone facies typically contain localized veins of coal, root traces, carbonaceous debris, and hematite and siderite concretions. Units are slope forming and are generally 10-40 ft (3.0-12.2 m) thick, based on measured-section thicknesses and photopans.

Architectural Element 1: Discrete Flood Body.

The discrete flood body is a result of a single flooding event, where sediment overflows the levee, depositing sand, and later, silt and mud falls out of suspension into the floodplain (Bridge, 1984). The discrete flood body is composed of a single bed of sandstone and muddy sandstone facies (i.e. asymmetrical-ripple cross-stratified, and structureless sandstone) (Table 2) enveloped in mudrock (Fig. 13). Escape structures, intense bioturbation, and rooting are common. Specific trace fossils are not recognizable. Soft-sediment deformation and the presence of escape burrows indicate de-watering and rapid sediment deposition. The discrete flood body has a blocky- or fining-upward grain-size trend, with a sharp basal contact, and a gradational upper contact (Fig. 13). There are no apparent vertical or lateral facies trends (Fig. 13). Based on six (N=6) sandstone-body measurements, the average apparent width is 61.5 ft (18.8 m). The average thickness is 1.6 ft (0.5 m), based on ten measurements (N=10) (Table 3). Geometries are lenticular in two-dimension (2D) (Fig. 13). The gamma-ray data are difficult to discern due to their thickness, therefore they have no specific pattern (Fig.

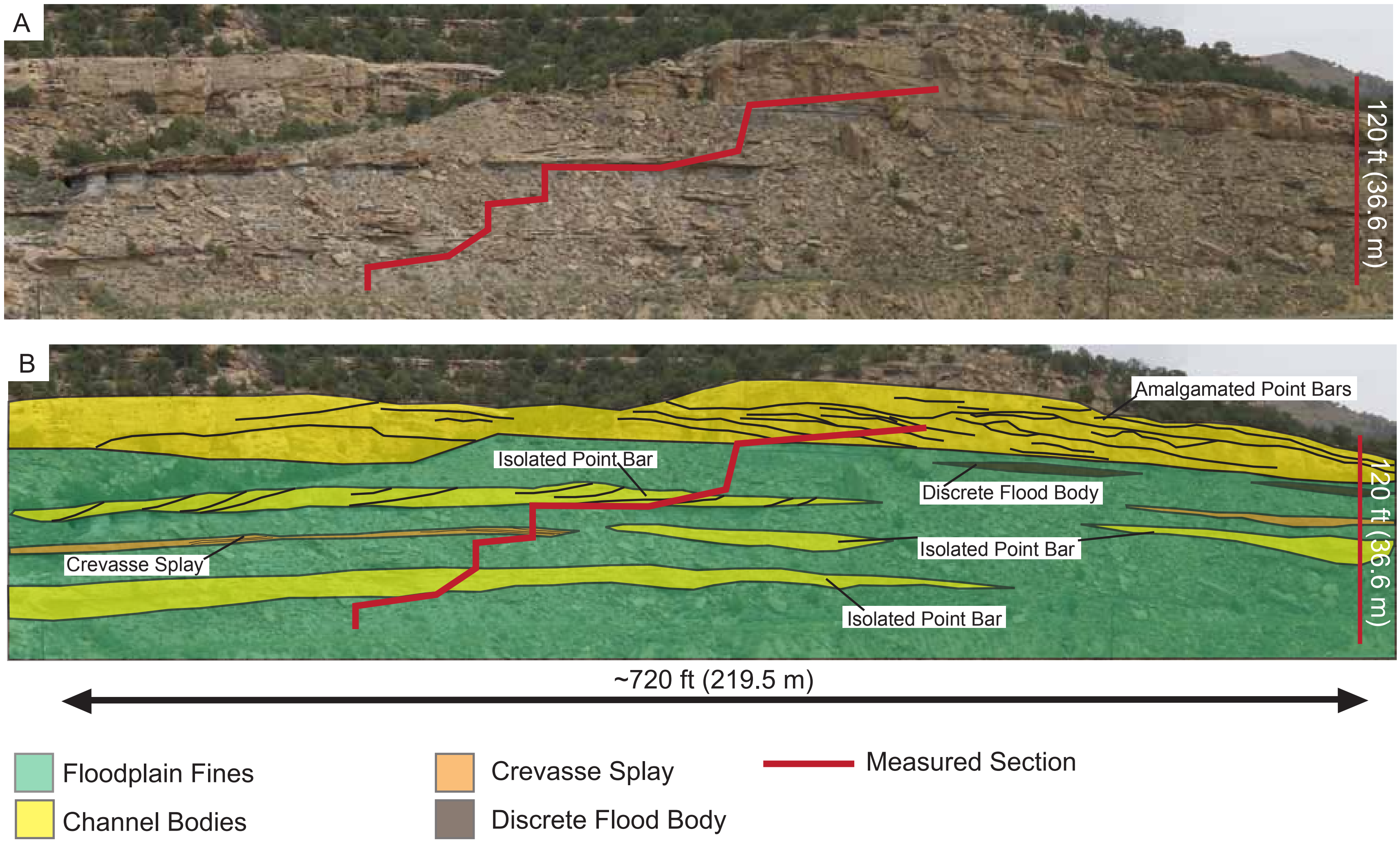

Fig. 12 Photopan of the Vandamore Draw West (VDW) measured section (0-117 ft [0-35.7m]) showing the general spatial distribution between floodplain fines and architectural elements of the coastal-plain facies association. Fine lines within architectural elements show generalized internal geometries (if applicable). A) uninterpreted. B) interpreted. (see Appendix A for measured sections and locations).

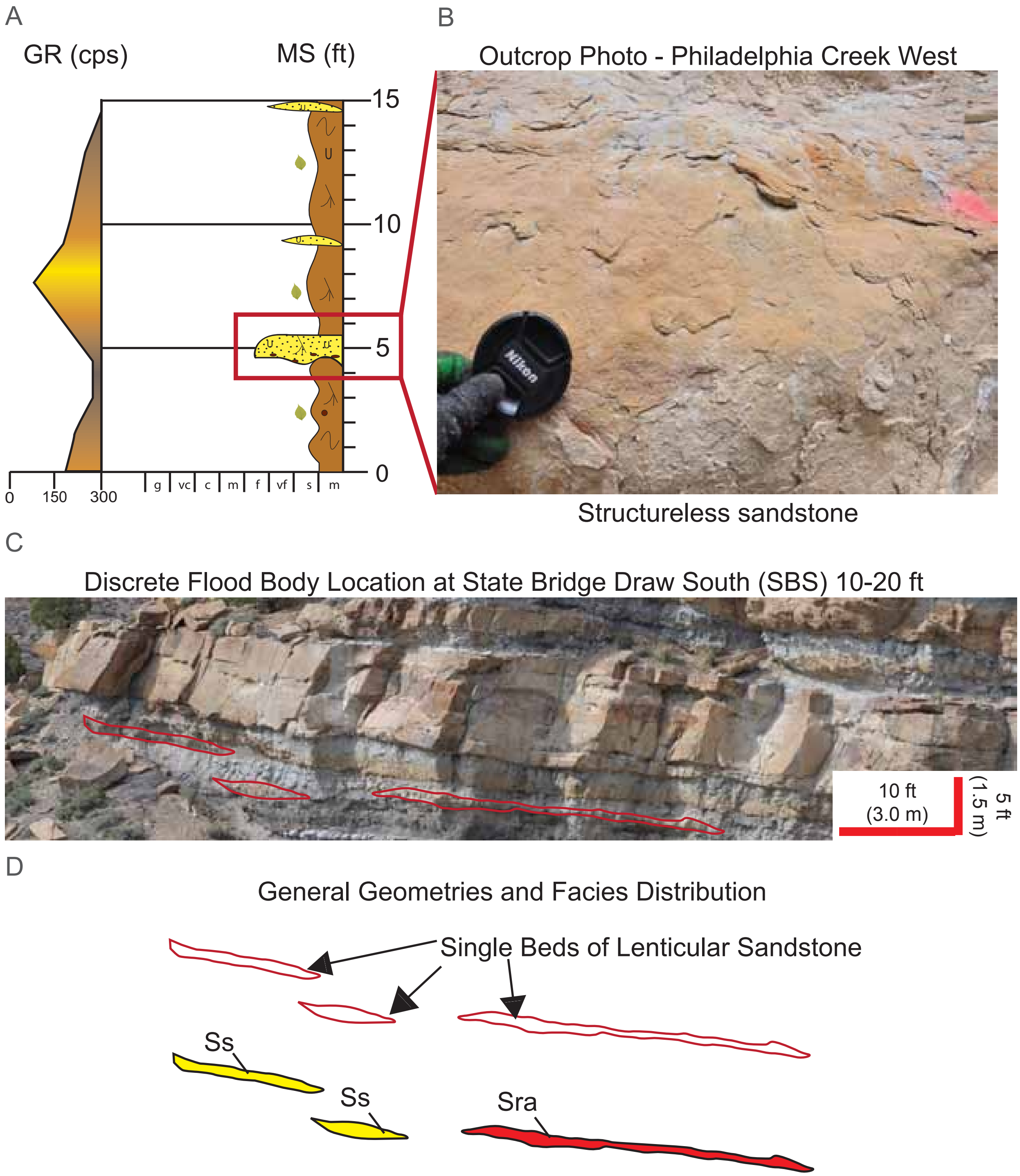

Fig. 13 Characteristics of the discrete-flood body architectural element (AE1). A) Measured section (MS) of Philadelphia Creek West with a variable gamma-ray (GR) profile. See key (Fig. 14) for symbols. Red box shows location of image in part B. B) Facies photo of AE1. C) Photopan showing locations of AE1 on the SBS measured section. D) AE1 geometries and generalized facies distribution. Red lines show external-bounding surfaces, AE1 does not have internal-bounding surfaces. Colors and abbreviations match those in Table 1. See Appendix A for measured sections.

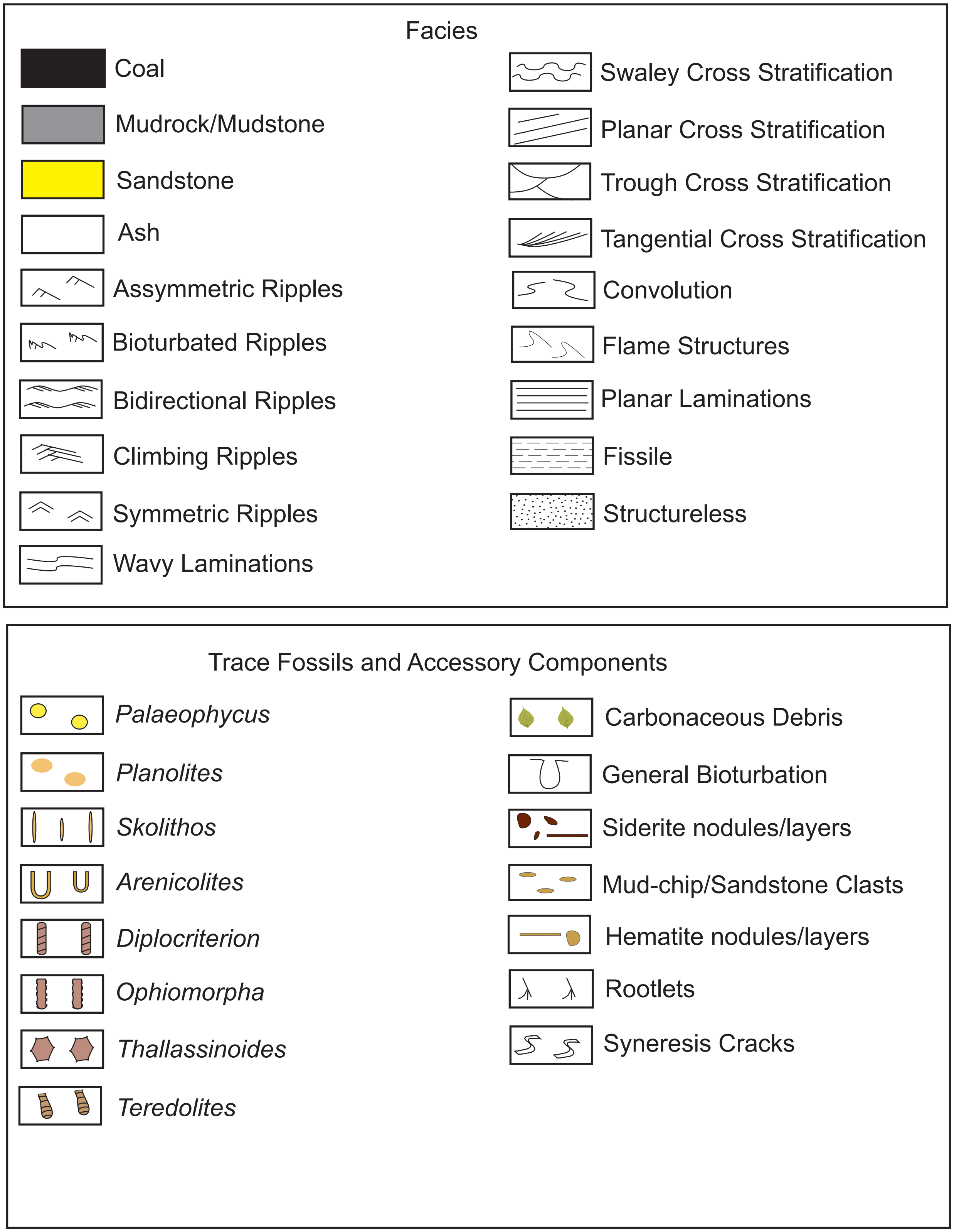

Fig. 14 Key for measured sections.

Architectural Element and Number	Location, Footage (ft)	Average Thickness (ft)	Number of thickness measurements	Apparent Width (ft)
Channel Body				
CB1	VDS, 16	2.3	3	196.8
CB2	VDS, 42	5.7	5	487.0
CB3	VDS, 67	1.0	1	266.7
CB4	VDS, 76	7.7	7	685.1
CB5	VDS, 82	2.7	3	40.4
CB6	VDS, 87	2.3	5	249.5
CB7	VDS, 87	3.0	1	60.4
CB8	SBW, 215	5.0	1	44.5
CB9	SBW, 216	5.0	3	1048.1
CB10	SBW, 105	6.0	9	450.7
CB11	SBW, 110	4.9	4	252.6
CB12	SBW, 98	4.8	3	181.8
CB13	SBW, 77	2.8	3	121.1
CB14	SBW, 77	8.6	7	228.0
CB15	SBW, 77	3.7	2	219.6
CB16	SBW, 68	2.6	3	199.6
CB17	SBW, 65	4.6	5	186.1
CB18	SBW, 135	18.5	5	377.0
CB19	SBW, 120	2.5	1	324.3
CB20	SBE, 122	2.5	1	134.0
CB21	VDW, 55	6.1	3	123.3
CB22	VDW, 75	8.1	11	812.0
CB23	SBE, 125	3.0	1	132.0
CB24	SBS, 360	4.4	5	83.0
Total	-	4.9	92	287.6
Crevasse Splay				
CS1	VDS, 32	2.5	1	48.0
CS2	VDS, 56	1.5	1	30.0
CS3	SBW, 213	2.3	6	145.5
CS4	SBW, 87	1.1	1	66.2
CS5	SBW, 80	1.0	1	55.0
CS6	SBW, 98	1.5	1	43.1
CS7	SBW, 140	1.5	1	38.8
CS8	VDW, 55	3.1	5	347.4
CS9	VDW, 85	2.0	1	40.6
Total	-	1.8	18	90.5
Discrete Flood Body				
DF1	SBW, 223	4.5	2	117.6
DF2	SBW, 215	1.0	1	61.9
DF3	SBE, 224	1.5	1	29.0
DF4	VDW, 10	1.0	1	56.0
DF5	VDW, 0	1.5	1	20.0
DF6	SBS, 352	2.6	4	84.6
Total	-	2.0	10	61.5

Table 3 Dimensional statistics of channel bodies, crevasse splays, and discrete flood bodies. For locations of measurements, see Appendix C.

13). Discrete flood bodies comprise 2.4% of the architectural elements (Fig. 11) and are common throughout the entire stratigraphic interval (Fig. 15).

Architectural Element 2: Crevasse Splay.

A crevasse splay is the result of multiple flooding events, and is composed of prograding, slightly inclined discrete-flood bodies which stack to form a delta-like feature onto the floodplain (typically in a standing body of water adjacent to a channel). The crevasse splay is commonly characterized by a coarsening-upward grain-size trend (Fig. 16). It contains a variety of sandstone and muddy sandstone facies (Table 2). Crevasse splays have gradational lower and upper contacts, and contain multiple horizontal to low-angle beds of muddy sandstone and sandstone facies, displaying higher-energy facies upward (Table 2; Fig. 16). Lateral facies changes are not obvious (Fig. 16). Crevasse splays are 1.8 ft [0.5 m] thick (N=18) and more laterally continuous (90.5 ft [28.0m]) (N=9) than the discrete flood body (Table 3). Geometries are lenticular (Fig. 14). The gamma-ray data shows a funnel-shaped profile (Fig. 16). Crevasse splays comprise 16.0% of the architectural elements (Fig. 11), and are distributed throughout the entire stratigraphic interval (Fig. 15).

Architectural Element 3: Channel Body.

Channel bodies are point bars and channel fills, which can be: (1) isolated; (2) amalgamated; and/or (3) tidally influenced. A point bar is a fluvial-dominated sandstone body composed of lateral-accretion deposits (LADs). LADs dip at angles between 5-15° into the channel base, where the direction of dip indicates direction of bar growth, and is perpendicular to the direction of channel flow (Allen, 1965; Edwards et al., 1983; Thomas, et al., 1987; Miall, 1992; Cole and Cumella, 2003).

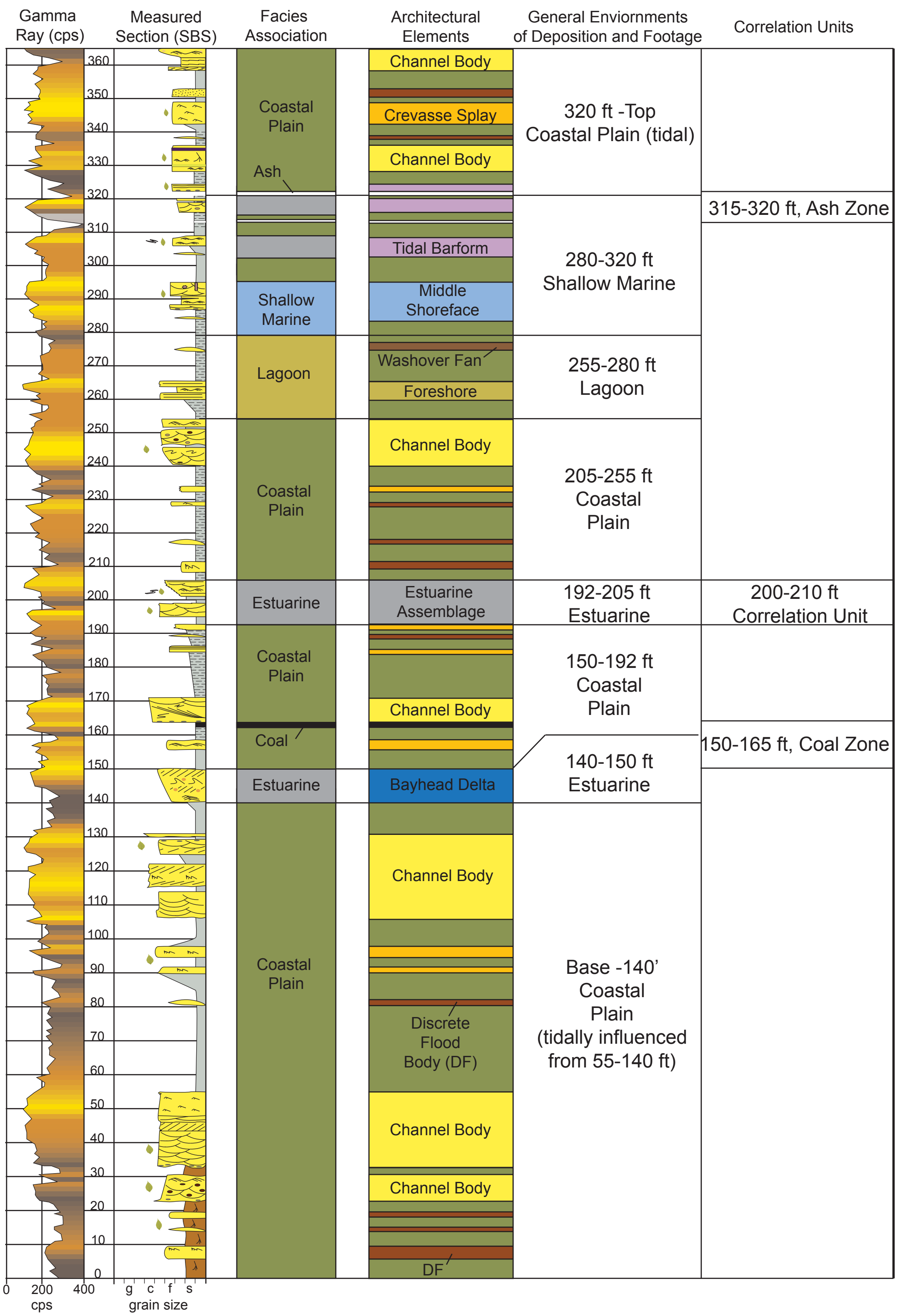

Fig. 15 Stratigraphic variability of the major depositional environments, facies associations, and architectural elements, as well as major zones used for correlations for the State Bridge Draw South (SBS) measured section (in feet) (Appendix A). Specific interval thickness can vary as much as 20 ft (6.1 m) throughout the study area due to structural dip and faults.

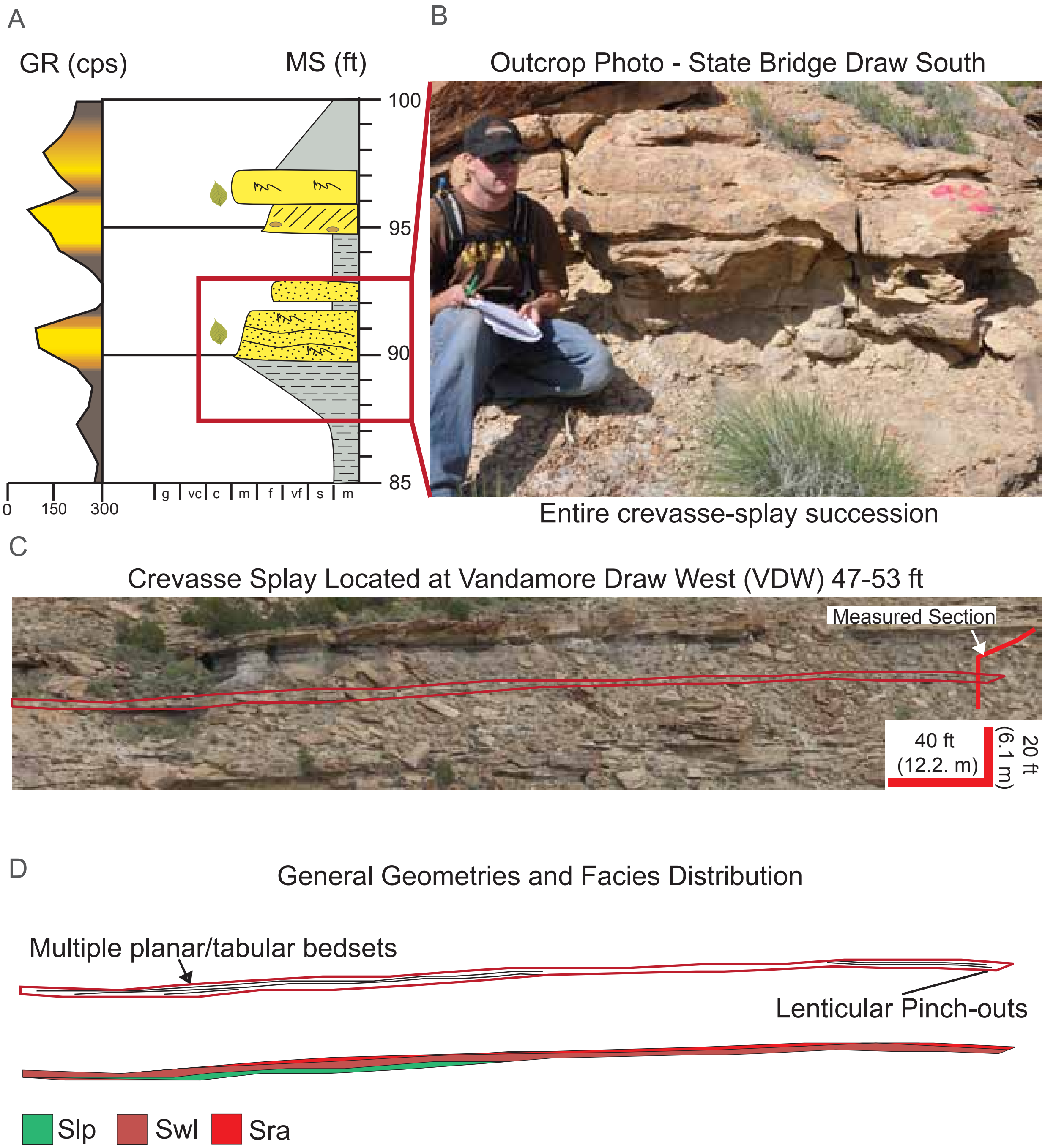

Fig. 16 Characteristics of the crevasse-splay architectural element (AE2). A) Measured section (MS) of State Bridge Draw South with a wide, funnel-shaped gamma-ray (GR) profile. See key (Fig. 14) for symbols. Red box shows location of image in part B. B) Photo of AE2. C) Outcrop photopan showing location of AE2 (outlined in red) on the VDW measured section (in red). D) AE2 geometries and generalized facies distribution of AE2. Red line shows external-bounding surfaces, and black lines show internal-bounding surfaces. Colors and abbreviations match those in Table 1. See Appendix A for measured sections.

A channel body commonly has a sharp/erosional base overlain by heterolithic debris. It is composed of multiple LADs, which are commonly draped with siderite layers, mottled mudstone, or bioturbated or wavy-laminated muddy sandstone facies (Table 2; Fig. 17). Vertical facies stacking is as follows (base to top): (1) convoluted or trough cross-stratified sandstone; (2) planar cross-stratified sandstone; (3) asymmetric-ripple cross-stratified sandstone; and (4) structureless sandstone interbedded with mottled mudstone and structureless siltstone (Fig. 17). They commonly contain local root traces and burrows at the top (Appendix F). Siderite concretions and carbonaceous debris are abundant. Facies become lower energy upward. Laterally, facies are higher-energy into the channel base and are lower energy toward the channel edge (Fig. 17). Gamma-ray data of individual (single-story) channel bodies show a bell-shaped or cylindrical profile (Fig. 17). Individual channel bodies are approximately 5.3 ft (1.6 m) thick (N=92), with an average apparent width of approximately 287.6 ft (87.7 m) (N=24) (Table 3). Geometries are lenticular (Table 2; Fig. 17). Channel bodies comprise 54.0% of the architectural elements (Fig. 11), and are distributed throughout the entire stratigraphic interval (Fig. 15).

Amalgamated channel bodies form high N:G (20:>80) intervals. Cut-and-fill (scour) geometries are common, and indicate multiple scours and erosional events, likely due to channels migrating and truncating older channel deposits. Common facies include heterolithic debris, trough cross-stratified, and convoluted sandstone. Isolated channel bodies form moderate-to-low N:G (60:<40) intervals. They commonly contain lower-energy facies than amalgamated channel bodies. Cut and fill geometries are less

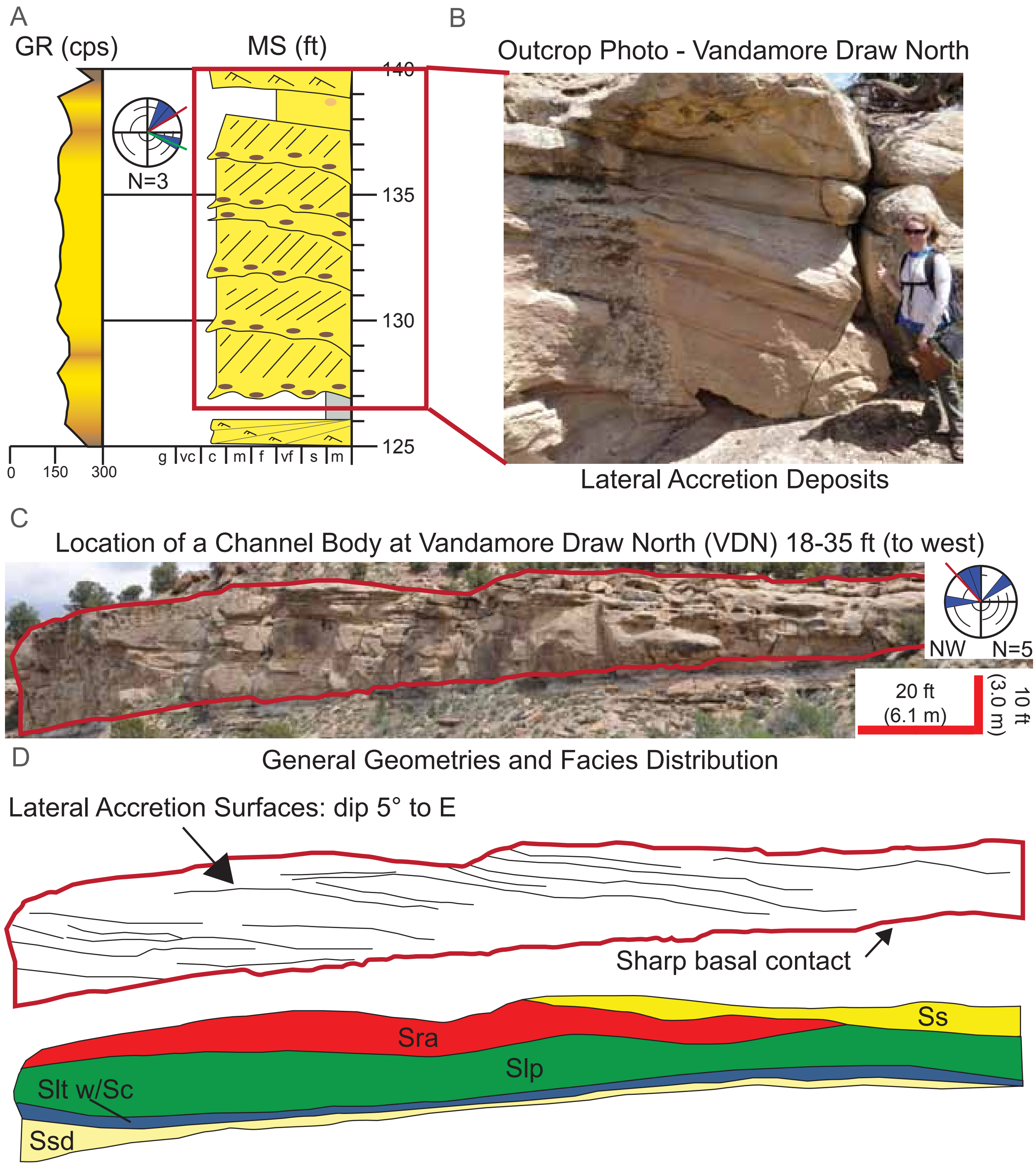

Fig.17 Characteristics of the channel-body architectural element (AE3). A) Measured section (MS) of Vandamore Draw North with a blocky gamma-ray (GR) profile. See key (Fig. 14) for symbols. Red box shows location of image in part B. B) Photo of AE3. C) Outcrop photopan showing location of AE3 at VDN measured section. Rose diagram shows average paleocurrent orientations (red line), and orientation of lateral-accretion deposits (green line). D) Geometries and generalized facies distribution of AE3. Red line shows external-bounding surfaces. Black lines show internal-bounding surfaces. Colors and abbreviations match those in Table 1. See Appendix A for measured sections.

common. A representation of amalgamated and isolated channel bodies is shown on Figure 12.

Tidally influenced channel bodies can be isolated or amalgamated. A tidally influenced channel body is distinguished from a fluvial channel body using brackish-water indicators. For example, higher bioturbation, *Teredolites*-bored logs, and mixed tidal- and fluvial-process-generated facies indicate brackish water. Occasionally, there is wavy-laminated and bioturbated muddy sandstone, and mudstone- and coal-draped planar/tangential cross-stratified, and convoluted sandstone facies. Mudstone commonly drapes LADs and thickness of mudstone increases up depositional dip (outward from the channel base). Gamma-ray data for tidally influenced channel bodies can be more serrated than the fluvial deposits due to the mudstone-draped LADs. Because the amount of mudstone between LADs depends on location of within the channel, the tidally influenced point bar is grouped with the channel body due to lack of recognizable features on a gamma-ray profile. Tidally influenced channel bodies are observed in the middle and the top of the stratigraphic interval (55-140 ft [16.8-42.7 m] to 323-365 ft [98.5-111.3 m]).

3.2 The Estuarine Facies Association and Architectural Elements

An *estuary* is defined as a semi-enclosed coastal body of water, commonly drowned river valleys produced by a rise in sea level. This is where freshwater, derived from land drainage, mixes with sea water. Estuaries are subject to wave, tidal, and fluvial processes, and usually lie within incised valleys (Fraser, 1989; Boyd, et al., 1992; Dalrymple et al., 1992; Dalrymple, 1992; Yoshida et al., 2004). A wave-dominated estuary is present within the stratigraphic interval. A wave-dominated estuary is controlled at its mouth (seaward) by wave processes and possesses a free connection with the open sea via a barrier-bar tidal-inlet complex. Estuaries include a variety of sub-environments including the: barrier bar, washover fan, tidal-inlet channel (and its associated flood- and ebb-tidal deltas), central basin, tidal barforms, and the bayhead-delta complex (Dalrymple et al., 1992) (Fig. 10A). The estuarine depositional environment comprises 12.5% of the stratigraphic interval (Fig. 11), and is more common toward the middle (190-205 ft [57.9- 62.5 m]) and top (300-323 ft [91.5-98.5 m]) of the stratigraphic interval (Fig. 15). Estuarine facies are shown in Figure 18.

The fine-grained strata within this association are considered to be estuarine mudstone deposits. They are composed of horizontal, laterally continuous (up to 2 mi [3.2 km]) units of carbonaceous fissile mudrock. Units are slope forming, and are generally 10-20 ft (3.0-6.1 m) thick, based on measured-section thicknesses and photopans.

Architectural Element 4: Bayhead Delta.

A bayhead delta is located at the head of an estuary and deposits land-derived sediment into a wave-dominated estuary (Dalrymple et al., 1992). A delta front often experiences hypopycnal flow, which occurs when the density of the materials entering from the river is less than those of the standing body of water (Bates, 1953). This creates buoyant sediment, which falls out of suspension slowly, depending on energy levels (coarser sediment will fall out proximal to the delta mouth and finer sediment in more distal settings). The process creates an upward-fining grain-size trend in beds. Overall, the delta progrades and creates an upward-coarsening grain-size trend. The

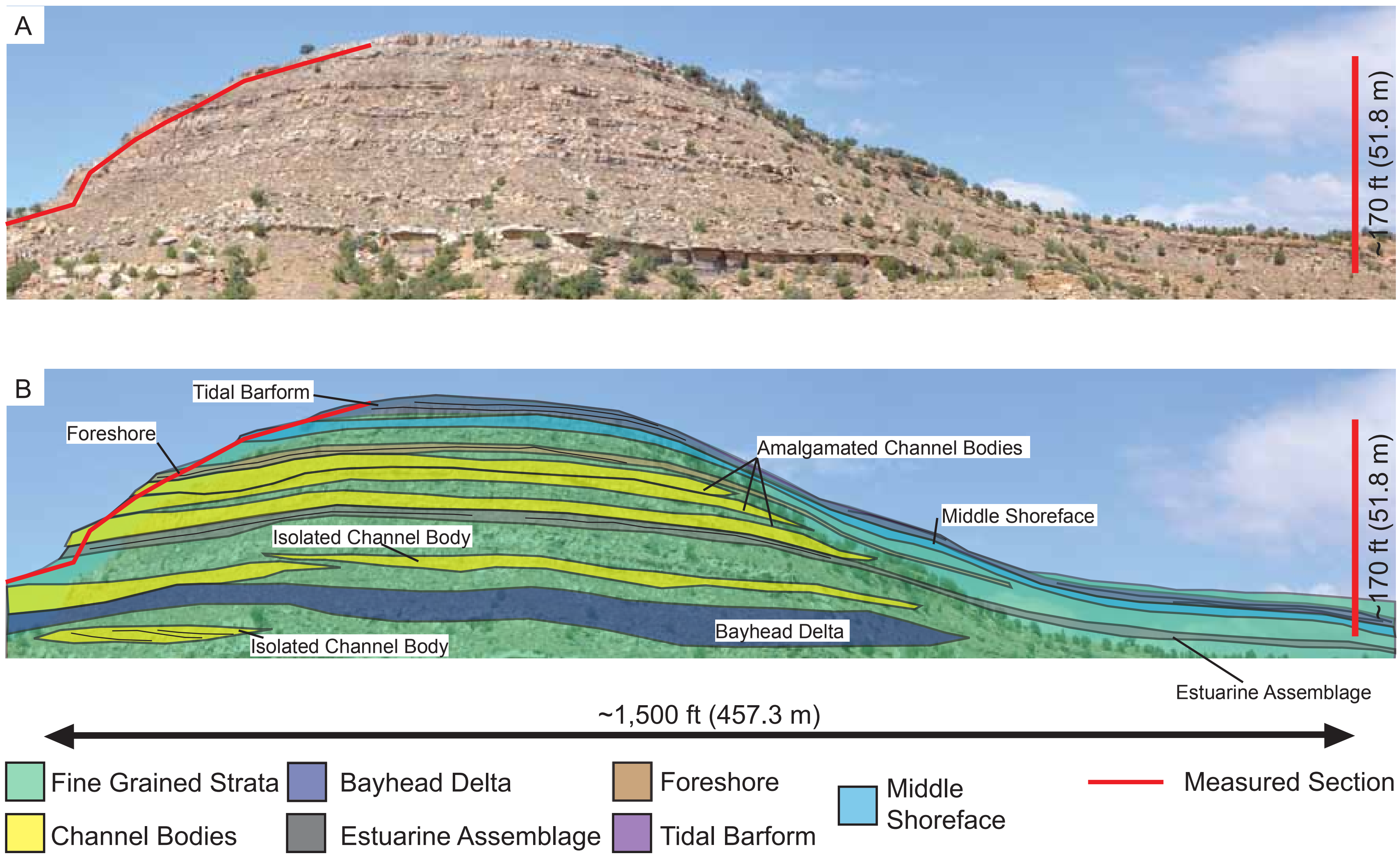

Fig. 18 Photopan of the State Bridge Draw West (SBW) measured section (~120-333 ft [36.6-101.5 m]) showing the general spatial distribution between all the architectural elements. Fine lines within architectural elements show generalized internal geometries (if applicable). A) Uninterpred. B) Interpreted. (see Appendix for measured sections and exact locations).

bayhead delta contains planar-tabular bedsets that are horizontal to gently inclined (Bates, 1953; Bhattacharya and Walker, 1992).

The bayhead delta is composed of coarsening-upward, tabular-bedded sandstone units (Table 2; Fig. 19). The exposure has basal contact, which lies sharply on carbonaceous structureless mudstone or coal (Fig. 19). At the base, 2-5 in (5-13 cm) thick bedsets of fissile mudstone are interbedded with structureless sandstone and siderite layers (which fine upward in cycles). The basal mudstone units commonly contain small (1-2 ft [0.3-0.6 m] thick, 5-10 ft [1.5-3.0 m] wide), lenticular, structureless sandstone bodies (Appendix F). In a rare case, a swaley cross-stratified sandstone bed was observed. Fining-upward sandstone cycles, combined with localized swaley cross-stratification, could represent pulsating discrete depositional events, possibly due to storm activity (Kirschbaum and Hettinger, 2004). Interbedded 2-5 ft (0.6-1.5 m) thick bedsets of bidirectional- and climbing-ripple cross-stratified, planar-laminated and coal- and mudstone-draped, planar/tangential cross-stratified sandstone facies (with local thinning and thickening of laminasets) are common at the top (Table 2; Fig. 19). Convoluted sandstone is locally present. Trace fossils are not abundant or diverse, but include rare *Palaeophycus* and *Planolites.* The upper contact grades into mudstone or is locally scoured by channel bodies, as can be seen in Figure 19. The bayhead delta contains lower-energy facies basinward (VDS and PCW measured sections) and higher-energy facies landward (SBW and SBE measured sections). The bayhead delta in the study area is ~5,000 ft (1,524.4 m) based on photopans and is 11 ft (3.4 m) thick on average based on measured section thicknesses and has a wedge-shaped geometry based on it’s thinning to the south and thickening to the north (Table 2). The

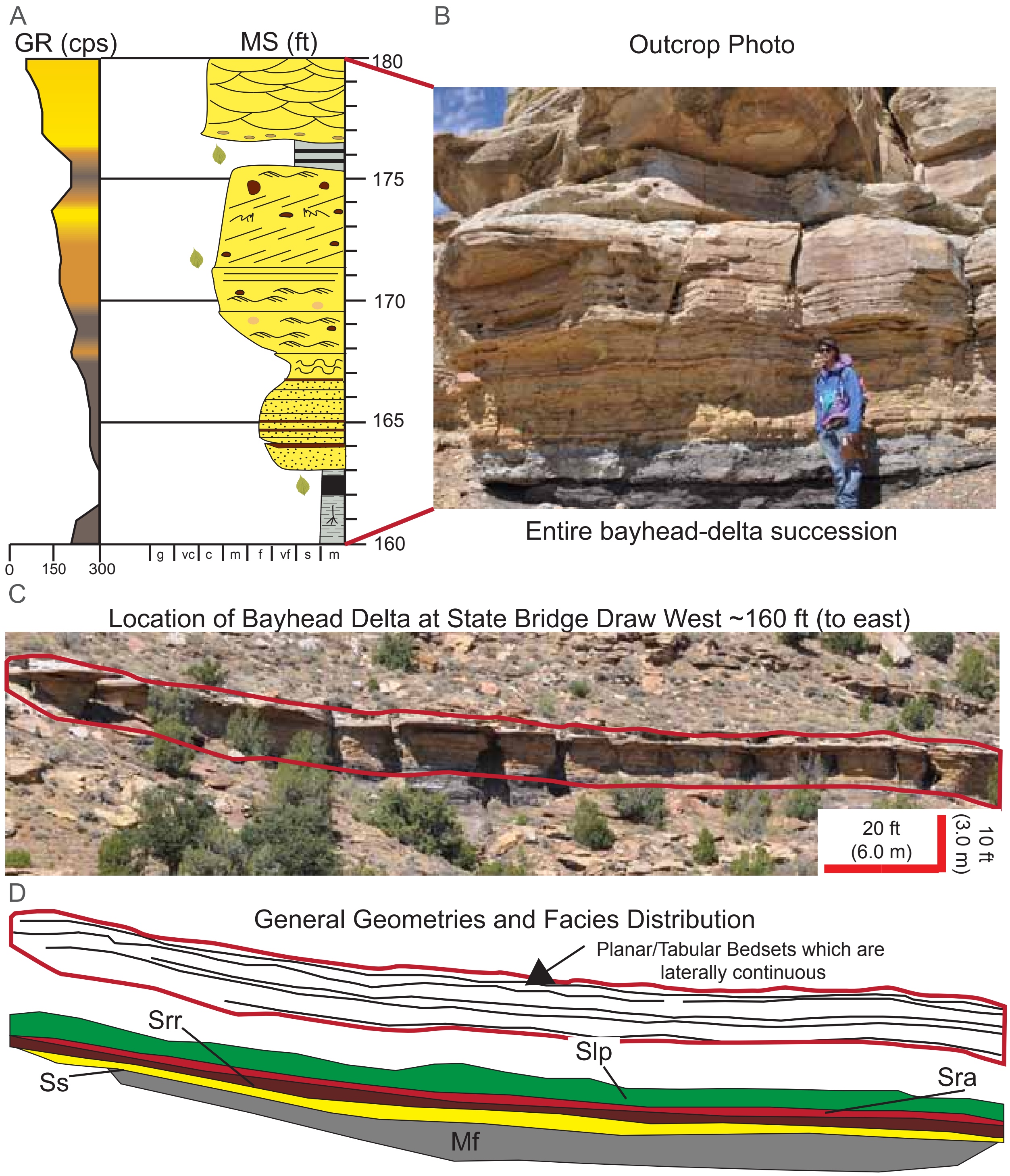

Fig. 19 Characteristics of the bayhead-delta architectural element (AE4). A) Measured section (MS) of State Bridge Draw West with a thin funnel-shaped gamma-ray (GR) profile (in feet). See key (Fig. 14) for symbols. B) Photo of AE4. C) Outcrop photopan showing location of AE4 on the SBW measured section. D) Geometries and generalized facies distribution of AE4. Red line shows external-bounding surfaces, and black lines show internal-bounding surfaces. Colors and abbreviations match those in Table 1. See Appendix A for measured sections.

gamma-ray data show a funnel-shaped profile, with a sharp basal contact (Fig. 19). The bayhead delta comprises 3.9% of the architectural elements (Fig. 11). It only appears in the middle of the stratigraphic interval (140-150 ft [43.7-46.7 m]) (Fig. 15). It thickens northward and thins southward.

Architectural Element 5: Estuarine Assemblage.

The estuarine assemblage is interpreted as deposits of the distal bayhead delta to the central basin to the flood-tidal delta (Fig. 10A). The central basin acts as the prodelta region of the bayhead delta (Dalrymple et al., 1992). Central-basin mudrock is flanked by sandstone of the bayhead delta and the tidal-inlet delta, which together represent a tripartite facies zonation (Pattison, 1992). The central basin is a complicated area, where fluvial, tidal, and marine processes interact. The flood-tidal delta is composed of sandstone bodies deposited inside the inlet. Inlets in areas with microtidal and lower mesotidal ranges and high wave energies have large flood-tidal deltas and small ebb-tidal deltas (Hayes, 1975). In vertical profile, fine-grained central-basin sediment ideally exhibits a symmetrical grain-size trend. The basal fining represents fluvial bayhead delta deposits to more distal prodelta sediments. The finest sediments represent the deepest part of the central basin. The coarsening-upward succession represents the flood-tidal delta and washover sediments (Dalrymple et al., 1992).

The estuarine assemblage in the present study is composed of fining- to coarsening-upward (hourglass profile), tabular- to slightly-inclined bedsets with three distinct units (tripartite facies stacking) (Table 2; Fig. 20). The lower bounding surface is sharp, and overlies mudrock or coal. The sandstone-rich basal unit contains 1-2 ft (0.3-0.6 m) thick bedsets of planar-laminated and/or convoluted sandstone, which suggests

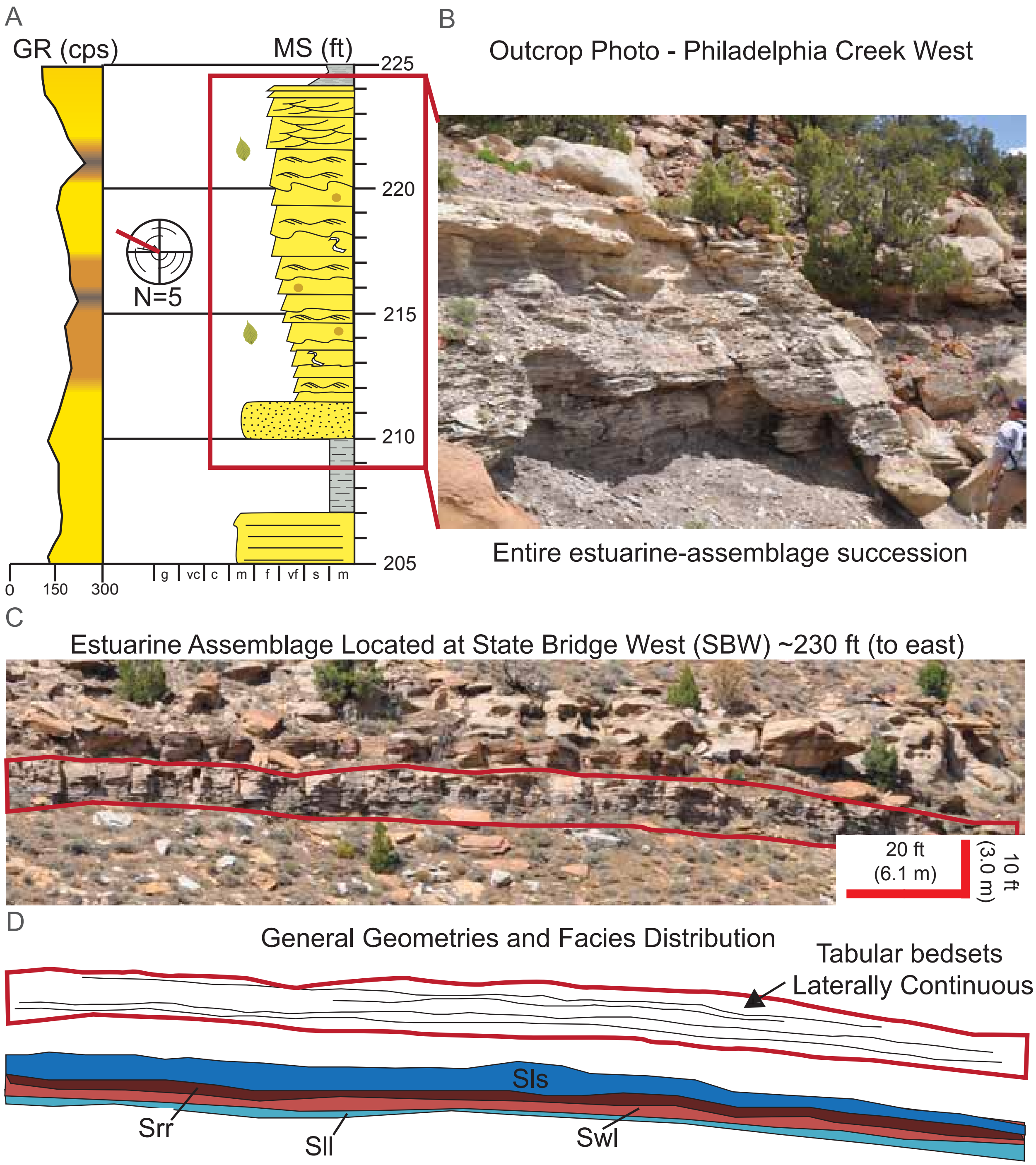

Fig. 20 Characteristics of the estuarine-assemblage architectural element (AE5). A) Measured section (MS) of Philadelphia Creek West and an hourglass-shaped gamma-ray (GR) profile. See key (Fig. 14) for symbols. Red box shows location of image in part B. B) Outcrop photo of AE5. C) Outcrop photopan showing location of AE5 (outlined in red) on the SBW measured section. D) AE5 geometries and generalized facies distribution of AE5. Red line shows external-bounding surfaces, and black lines show internal-bounding surfaces. Colors and abbreviations match those in Table 1. See Appendix A for measured sections.

distal bayhead-delta deposition. The fissile mudrock and wavy-laminated muddy sandstone facies represent deposition in the central basin. The muddy unit contains 1-3 in (3-8 cm) thick bedsets of quartz-rich sandstone mixed with mudstone containing carbonaceous debris, and indicates a combined fluvial and marine source. The muddy unit also contains abundant syneresis cracks and 0.25 in (0.64 cm) *Planolites* burrows. In the absence of loading or dewatering, syneresis cracks provide evidence that the depositional environment was subject to periodic extreme salinity fluctuations (Burst, 1965; Plummer and Gostin, 1981; Wightman et al, 1987; Pemberton and Wightman, 1992; Finzel et al., 2010). The muddy unit is commonly interbedded with 1-2 ft (0.3-0.6 m) thick, 3-5 ft (0.3-1.5 m) wide, lenticular, structureless, or swaley cross-stratified sandstone (Appendix F). These deposits suggest submarine tidal channels, likely sourced from either the bayhead delta or flood-tidal delta. The upper sandstone-rich unit contains symmetric- and bidirectional-ripple cross-stratified to swaley and trough cross-stratified sandstone. The upper sandstone bedsets are 0.5-1 ft (0.15-0.3 m) thick, with wavy-to-tabular geometries, and minor bioturbation by *Ophiomorpha.* The upper contact is sharp with overlying mudstone, but may be also locally scoured by channel bodies. The upward transition to wave-dominated facies indicates a transition to a tidal inlet-dominated source. The upward increase in *Ophiomorpha* suggests a change into more oxygenated waters and higher energies. The estuarine assemblage is laterally continuous, and can be traced across the entire study area (2 mi [3.2 km]). Average thickness is 12 ft (3.7 m) based on measured section thicknesses (Table 2). Sandstone of the lower interval is thicker to the north (SBW measured section) and thins to the south (PCW measured section) (Appendix A). Isolated channels in the central unit are more common to the south. The gamma-ray data shows a funnel-shaped profile, with a gradational basal contact (Fig. 20). The estuarine assemblage comprises 7.2% of the architectural elements (Fig. 11), and is only present in the middle of the stratigraphic interval (190-205 ft [57.9-62.5 m]) (Fig. 15).

Architectural Element 6: Tidal Barform.

A tidal barform is a basinward-migrating macroform, which is sourced from coastal-plain fluvial channels and flood-tidal inlet channels (Fig. 10A). Tidal barforms are composed of low-angle, inclined heterolithic strata (IHS) and tidal facies. Sedimentary structures have been reworked by tides, on the basis of paleocurrent measurements from ripples and cross-stratification, oriented opposite to the dip of the IHS (Fig. 21). These barforms could be equivalent to the middle estuary zones of mixed-energy estuaries, noted in Dalrymple et al. (1992).

The tidal barform is composed of low-angle (1-3°) inclined heteroltihic strata (IHS) (Fig. 21), which are draped with mudstone and/or wavy-laminated muddy sandstone facies. Tidal barforms coarsen upward, are wedge-shaped, and enveloped in mudrock (Fig. 21). Tidal barforms have a sharp basal contact and transition upward into wavy-laminated muddy sandstone and bidirectional- ripple, swaley cross-stratified and structureless sandstone facies (Table 2; Fig. 21). A mix of tidal- and wave-generated sedimentary structures indicates a low to moderate tidal influence, possibly within a microtidal setting (<6.6 ft [<2.0 m] tidal range) (Davies, 1964). Local convoluted sandstone and syneresis cracks exist. Bodies are moderately to intensely bioturbated (bioturbation increases upward) by the *Skolithos* ichnofacies. The gamma-ray data show a funnel-shaped profile (Fig. 21). Average thickness is 9 ft (2.7 m) and average

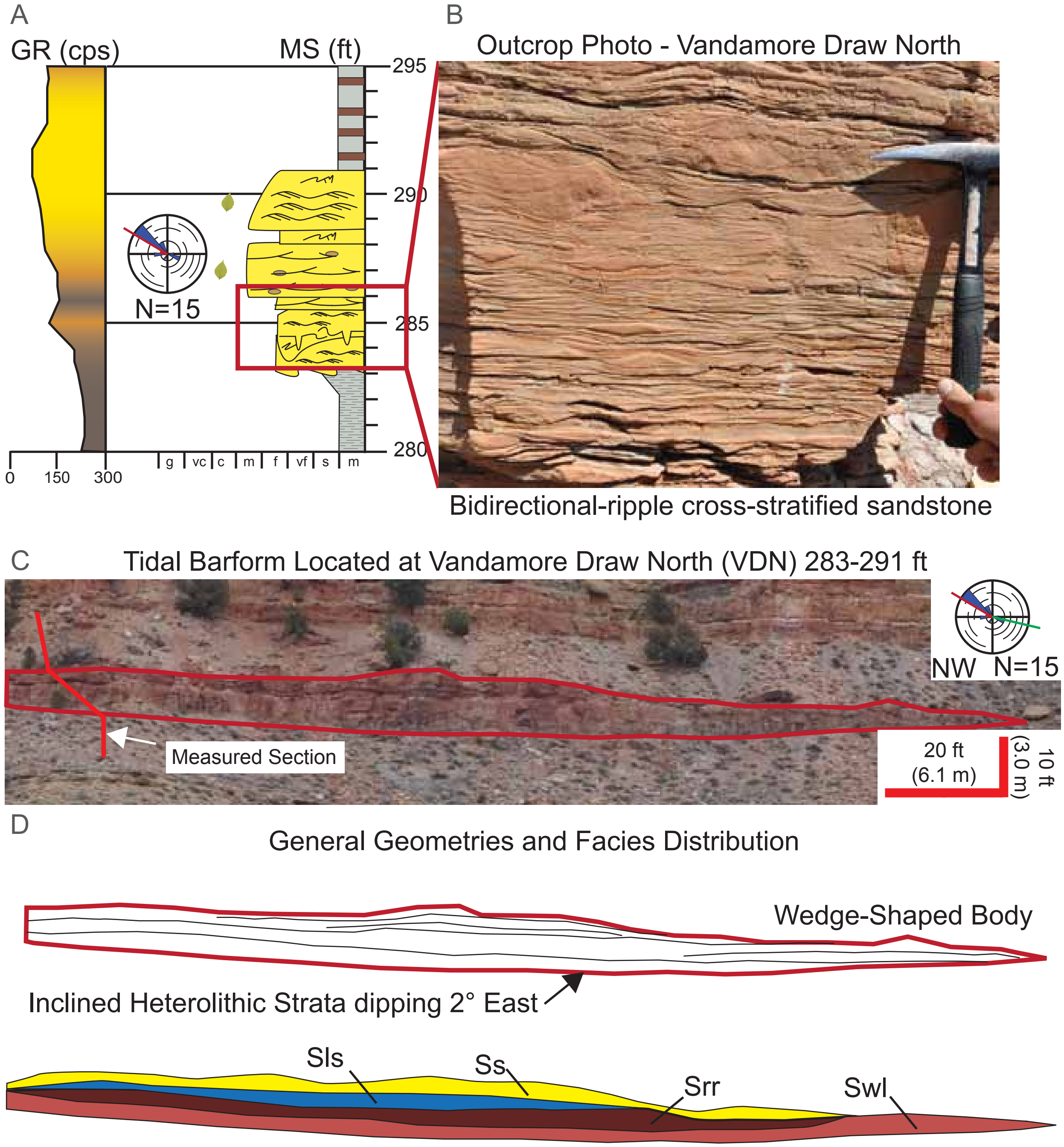

Fig. 21 Characteristics of the tidal-barform architectural element (AE6). A) Measured section (MS) of Vandamore Draw North and a funnel-shaped gamma-ray (GR) profile. See key (Fig. 14) for symbols. Red box shows location of image in part B. B) Facies photo of AE6. C) Location of AE6 (outlined in red) on the VDN measured section (red line), shown in part A. Rose diagram shows average paleocurrent orientation (red line), and inclined-heterolithic strata orientation (green line). D) AE6 geometries and generalized facies distribution of AE6. Red line shows external-bounding surfaces. Black lines show internal-bounding surfaces. Colors and abbreviations match those in Table 1. See Appendix A for measured sections.

apparent width is 500 ft (152.4 m), on the basis of measured sections and photopans (Table 2). Tidal barforms comprise 7.4% of the architectural elements (Fig. 11), and are present at the top of the stratigraphic interval (300-323 ft [91.5 – 98.5 m]) (Fig. 15).

3.3 The Lagoon Facies Association and Architectural Elements

A *lagoon* is defined as a body of water behind a barrier island that fills with fresh water after the inlet is healed. A lagoon receives nearly all its sediment from marine sources and fluvial input is negligible (Boyd et al., 1992). Subenvironments include thin foreshores, washover fans, barrier bars, and the flood-tidal delta (Boyd et al, 1992) (Fig.10). The lagoon environment comprises 4.8% of the stratigraphic interval (Fig. 11), and is only present near the top of the stratigraphic interval (255-280 ft [77.7-85.4 m]) (Fig. 15). It is thickest to the north, specifically in the State Bridge Draw West (SBW) measured section (Appendix A).

The fine-grained strata within these intervals are considered to be lagoon deposits and are composed of carbonaceous and fissile mudrock. Units are highly continuous (possibly up to 2 mi [3.2 km]), however it is unknown due to poor exposures and erosion between outcrops. Units are slope forming, and generally 10 ft (3.0 m) thick, based on measured-section thicknesses and photopans.

Architectural Element 7: Lagoon Foreshore (Foreshore).

The foreshore is confined to the intertidal zone occupying the area of wave swash, which provides the seaward-dipping planar laminations (Komar, 1976; Heward, 1981; Walker and Plint, 1992; MacEachern and Pemberton, 1992). A lagoon foreshore contains similar facies, however, is closely associated with the floodplain facies association (especially marginal-marine coals). It also contains lower-energy facies than a typical strandplain beach setting.

The lagoon foreshore has a gradational contact with carbonaceous and fissile mudstone below. The lagoon foreshore coarsens upward, from mudstone to medium-grained sandstone. It is composed of 0.25-1 ft (0.15-0.3 m) thick, tabular bedsets. Facies include wavy-laminated muddy sandstone at the base, overlain by symmetrical-ripple cross-stratified, to planar-laminated and planar cross-stratified sandstone at the top (Table 2; Fig. 22). The grain-size and facies-stacking pattern suggests a change from low to high energies upward. The upper contact is sharp with overlying mudstone. Wavy-laminated sandstone contains siderite. Trace fossils (*Ophiomorpha*) are rare, local, and low diversity due to the harsh environments (Howard and Frey, 1984; MacEachern and Pemberton, 1992). A rare runnel cross-stratification is observed within the planar laminations shown in Figure 22. The lateral continuity of the foreshore is unknown due to poor exposure and erosion between outcrops. Average thickness is 4 ft (1.2 m) (Table 2). The lagoon foreshore comprises 3.7% of the architectural elements (Fig. 11), and is present in the upper part of the stratigraphic interval (255-280 ft [77.7-85.4 m]) (Fig. 15).

Architectural Element 8: Washover Fan.

A washover fan is a thin deposit formed behind a barrier bar in an estuary or lagoon (Schwartz, 1982; Reinson, 1992; Boyd et al., 1992). Barrier bars separate lagoon and estuaries from the marine environment. Barrier bars migrate inland, and are commonly preserved as washover fans.

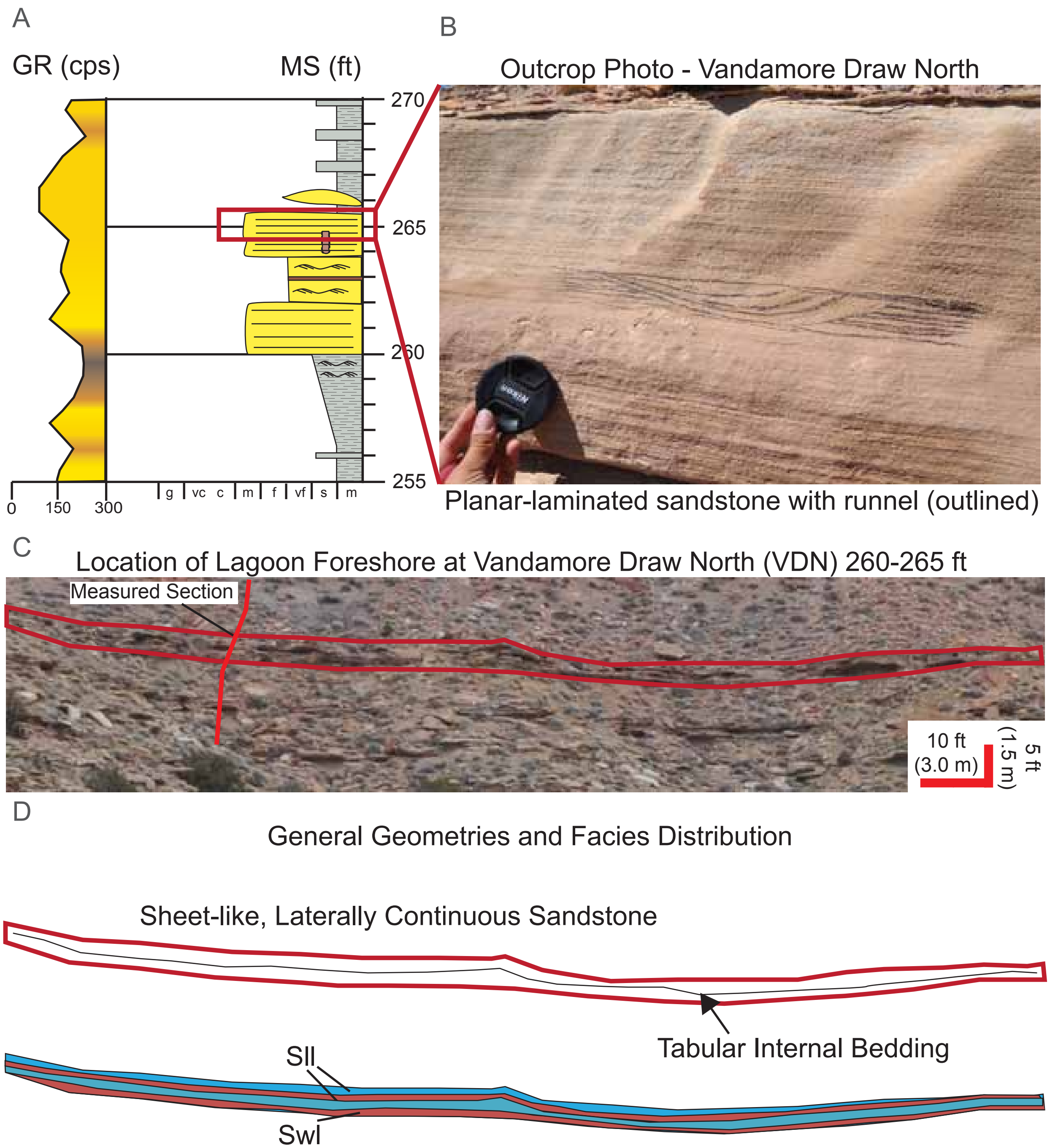

Fig. 22 Characteristics of the lagoon-foreshore architectural element (AE7). A) Measured section (MS) of Vandamore Draw North, with a funnel-shaped gamma-ray profile. See key (Fig. 14) for symbols. Red box shows location of image in part B. B) Facies photo of AE7. C) Outcrop photopan with location of AE7 (outlined in red) and measured section (red line) shown in part A. D) AE7 geometries and generalized facies distribution. Red line shows external-bounding surfaces, and black line shows internal-bounding surfaces. Colors and abbreviations match those in Table 1. See Appendix A for measured sections.

Washover fans in the study area have sharp basal contacts with mudrock below (Fig. 23). They are composed of blocky sandstone, which is very fine-to-fine grained and very well sorted. Facies include asymmetric- and bidirectional-ripple cross-stratified, planar-laminated and planar cross-stratified sandstone (Fig. 23; Table 2). Upper contacts are sharp with overlying mudstone. No bioturbation is observed. In a washover fan, a mix of eolian and swashing processes commonly produces the deposit due to its proximity to wave processes and its exposure at the surface with no vegetation. Washover fans appear in two measured sections (SBE, SBW; Appendix A), and are laterally equivalent to middle shoreface sandstone bodies on measured sections to the south. Average thickness is 4 ft (1.2 m) (Table 2). Average width is unknown due to poor exposures and erosion between outcrops. Based on a single outcrop photopan, the washover fan is lenticular and laterally discontinuous (<300 ft [91.5 m]) (Fig. 23). The gamma-ray profile shows a funnel-shape (Fig. 23). The washover fan comprises 0.7% of the architectural elements (Fig. 11), and is present in the upper part of the stratigraphic interval (275-280 ft [77.7-85.4 m]).

3.4 The Shallow-Marine Facies Association and Architectural Element

Shallow marine is general term for environments including modern shelves as well as epeiric seas and the shallow parts of foreland basins, and includes a continuum of depositional environments, from beach to shoreface, through inner and outer shelf settings (Walker and Plint, 1992). A shoreface is a seaward-sloping depositional wedge, which is composed of the offshore-, lower-, middle- and upper-shoreface, and the foreshore and backshore subenvironments (MacEachern and Pemberton, 1992). The most important distinguishing feature between the lagoon and the open shallow-marine

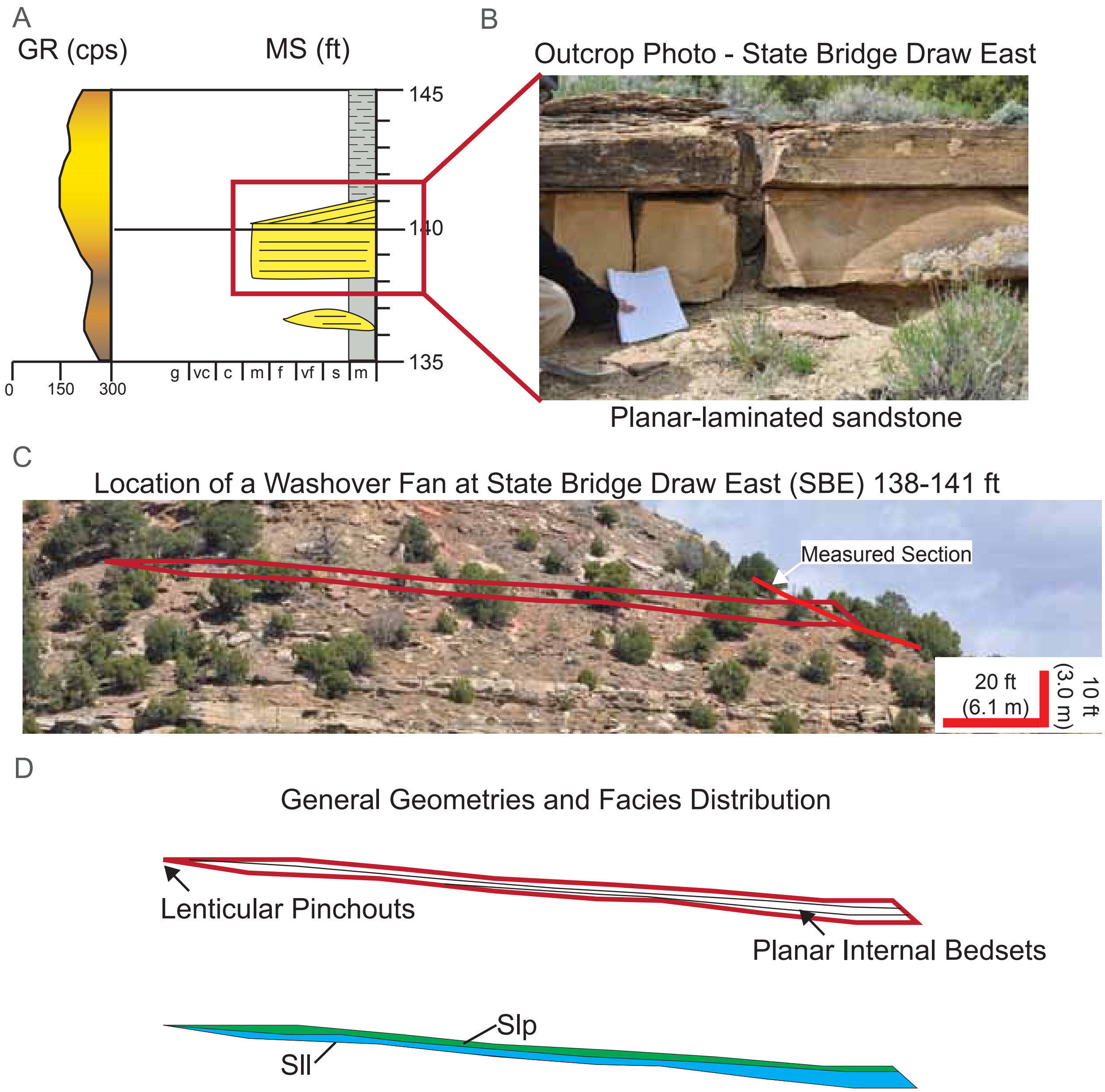

Fig. 23 Characteristics of the washover-fan architectural element (AE8). A) Measured section (MS) of State Bridge Draw East with a funnel-shaped gamma-ray (GR) profile. See key (Fig. 14) for symbols. Red box shows location of image in part B. B) Photo of AE8. C) Outcrop photopan showing location of AE8 on the SBE measured section (red line). D) Geometries and generalized facies distribution of AE8. Red line shows external-bounding surfaces, and black lines show internal-bounding surfaces. Colors and abbreviations match those in Table 1. See Appendix A for measured sections.

environment is the dominance of wave-generated sedimentary structures, and the more diverse and abundant ichnoassemblage. The shallow-marine setting comprises 6.6% of the stratigraphic interval, and is only present at the top (280-300 ft [85.4-91.5 m]) (Fig. 15). It is thickest to the north, specifically in the State Bridge Draw West (SBW) measured section.

Architectural Element 9: Middle Shoreface.

The middle shoreface refers to the body of sandstone, which was deposited between storm wave base and within fair-weather wave base within a wave-dominated shallow-marine setting (Fig. 10A). Commonly, the tops of the middle-shoreface architectural element are intensely bioturbated, thus, the upper shoreface and foreshore may be present, although unrecognizable. The upper shoreface only appears in one measured section (PCW; Appendix A), and is correlated as the up-dip equivalent to the middle shoreface. However, for the purposes of this study, all are lumped as middle-shoreface architectural elements.

The middle shoreface is gradational with underlying mudstone. It is composed of a sheet-like, coarsening-upward, mudstone to sandstone succession (Fig. 24). Facies include fissile mudstone and wavy-laminated muddy sandstone at the base, where as Symmetrical-ripple, swaley cross-stratified, and bioturbated sandstone is common at the top (Table 2; Fig. 24). Hummocky to swaley cross-stratification represent deposition at or above storm-wave base on the lower to middle shoreface (Dott and Bourgeois 1982; Male, 1992; Walker and Plint, 1992; Dumas and Arnott, 2006). The upper contact is sharp with overlying mudstone or coal. Bioturbation is rare to abundant, by the *Cruziana* (at the base) to *Skolithos* ichnofacies (at the top). Trace fossils include prevalent

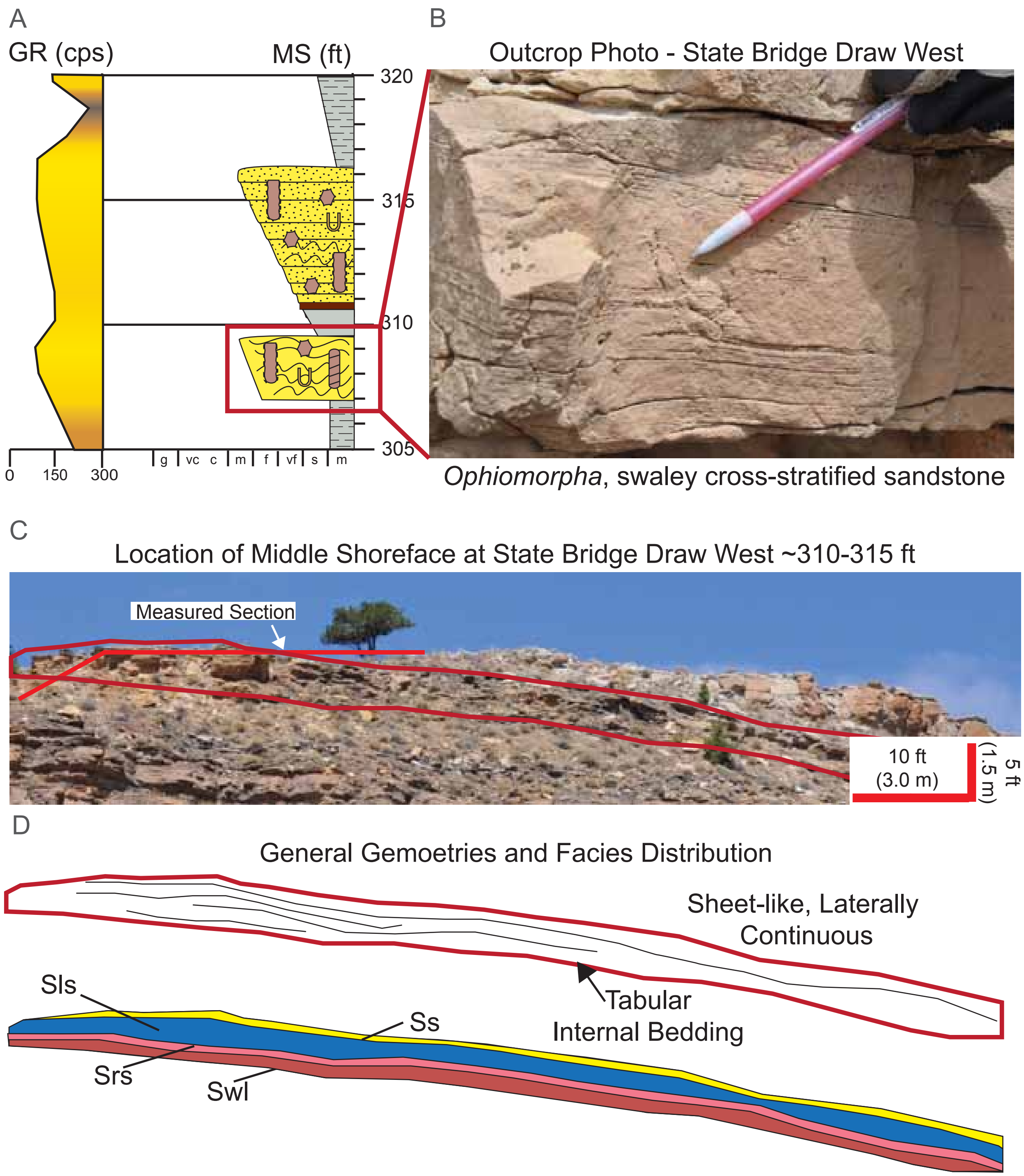

Fig. 24 Characteristics of the middle-shoreface architectural element (AE9). A) Measured section (MS) of State Bridge Draw West, with a funnel-shaped gamma-ray (GR) profile. See key (Fig. 14) for symbols. Red box shows image location in part B. B) Facies photo of AE9. C) Location of AE9 on SBW and measured section (red line) shown in part A. D) AE9 geometries and facies distribution. Red line shows external-bounding surfaces and black lines show internal-bounding surfaces of AE9. Colors and abbreviations match those in Table 1. See Appendix A for measured sections.

Thallassinoides, Ophiomorpha, Arenicolites, Skolithos and rare *Rhizocorallium* and *Diplocriterion* (Fig. 24; Appendix F). The grain-size and facies trends suggest a change from low to high energies upward, consistent with the classic shoreface model. The gamma-ray data show a funnel-shaped profile (Fig. 24). The middle shoreface comprises 4.7% of the architectural elements (Fig. 11). Average thickness is 6 ft (1.8 m), and apparent widths are at least 5,000 ft (1,524.4 m) (Table 2), however due to poor exposures and erosion between outcrops, measurements and geometries are unclear (Fig. 24). The middle shoreface is only present at the top of the stratigraphic interval (280-295 ft [85.4-89.9 m]) (Fig. 15), thickens to the north (SBW, SBE measured sections), and thins to the south (VDS, PCW measured sections).

4. Summary

Based on detailed sedimentological description, photopan correlations, and gamma-ray data, the stratigraphic interval presents four facies associations (coastal plain, estuarine, lagoon, and shallow marine). The coastal-plain facies associations are the most abundant in the stratigraphic interval (76.1%). These depositional environments were defined by 17 facies. The most common facies included fissile mudrock (20.6%), mottled mudstone (17.9%), and wavy-laminated wavy to flaser muddy sandstone (10.9%).

Nine architectural elements are identified based their vertical and lateral facies assemblages, geometries, internal and external bounding surfaces, dimensions (apparent width and thickness), and ichnofacies. Architectural elements are placed within a specific facies association. Coastal-plain architectural elements include the discrete flood body, crevasse splay, and channel body. Estuarine architectural elements include the bayhead delta, estuarine assemblage, and tidal barform. Lagoon architectural elements include the foreshore and washover fan. The shallow marine environment includes the middle shoreface architectural element. The channel body is the most common (54.0%) architectural element in the composite stratigraphic interval and the washover fan is the least common (0.7%).

CHAPTER THREE

PALEOGEOGRAPHIC AND SEQUENCE-STRATIGRAPHIC FRAMEWORK: DEPOSITIONAL EVOLUTION

1. Introduction

Stacking patterns of architectural elements, previous regional stratigraphic studies, and sequence-stratigraphic concepts were used to develop a paleogeographic and sequence-stratigraphic framework. Because the Kmvl and Kmvc (Iles and lower Williams Fork formations) intervals are primarily composed of coastal-plain strata, utilizing traditional sequence-stratigraphic concepts is challenging. This is because coastal-plain strata may not show the same coarsening- and fining-upward trends as documented in shallow-marine strata. coastal-plain and estuarine deposits described in this study are evaluated based on stratigraphic concepts of Shanley and McCabe (1991; 1993; 1994; 1995), Shanley et al., (1992), Hettinger (1993), Bohacs and Suter (1997), Plint et al., (2001), and Fanti and Catuneanu (2010). Each of these studies is briefly described in the following section. Lagoonal and shallow-marine deposits are evaluated using the terms and concepts of Van Wagoner et al. (1988; 1990).

Shanley and McCabe (1991; 1993; 1994; 1995) evaluated depositional sequences in terms of depositional architecture, sandstone connectivity, sandstone-to-mudstone ratios, coal-bed geometry, and degree of shoreface and foreshore preservation. A balance between the rate of change in base level, sediment supply, and accommodation results in changes of these elements, and allows for correlation and placement of major sequence-stratigraphic boundaries. High N:G sheet sandstone bodies overlie sequence boundaries, and represent low accommodation space during an early lowstand systems tract. Low N:G isolated sandstone bodies create a fining-upward succession above the high N:G channels to create the late lowstand systems tract. These units also form the transgressive and highstand systems tracts, as a result of high accommodation space. The maximum flooding surface is identified by tidally influenced strata, which includes current-reversal sedimentary features, clay drapes, rip-up clasts, flaser bedding, and inclined-heterolithic strata.

Bohacs and Suter (1997) studied coal deposition in relation to rates of accommodation and base-level change. For example, a rising ground-water table under stable conditions will quickly produce peat, rapidly filling the accommodation space. Peat will then extend laterally into suitable areas where growth can occur. This results in laterally continuous coal beds. Based on these concepts and examples from four studies, specific systems tracts are concluded to be associated with coal-bed geometries (thickness and lateral extent). Late highstand and early lowstand systems tracts commonly contain isolated and thin (1.6 ft [≤0.5 m]) coal beds. Middle-to-late lowstand and early-to-middle highstand systems tracts commonly contain widespread, moderately thick (3.3 – 9.8 ft [1-3 m]) coal beds. Late lowstand-to-early transgressive and late transgressive-to-early highstand systems tracts commonly contain thick (9.8 ft [≥3 m]), relatively scattered coal beds. Middle transgressive systems tracts are characterized by thin (≤3.3 ft [≤1 m]), restricted, and scattered coal beds. These concepts are developed for alluvial to paralic settings (Bohacs and Suter, 1997).

Plint et al. (2001), identified three depositional sequences, bounded by unconformities within the deltaic deposits of the Upper Cretaceous Dunvegan Formation in Alberta, Canada. Plint et al. (2001) identified three nonmarine systems tracts: (1) A channel-dominated, low-accommodation systems tract, equivalent to the transgressive systems tract; (2) A lacustrine-dominated, high-accommodation systems tract, equivalent to the late transgressive and early highstand systems tract; and (3) Paleosol-dominated, low-accommodation systems tract, equivalent to to the late highstand systems tract. Plint et al. (2001) proposed that marine transgressive and ravinement surfaces can be traced onto the coastal plain where they merge with subaerial unconformities (typically mature paleosols interpreted to represent interfluves).

Fanti and Catuneanu (2010) summarized five depositional sequences in the Upper Cretaceous continental strata of the Wapiti Formation in Alberta, Canada. Stratigraphic units were defined base on bounding unconformities and evaluated in terms of stratigraphic architecture related to changes in accommodation space to apply systems tracts to the strata. Low N:G packages represent high accommodation and deposition within the transgressive and highstand systems tracts. High N:G packages represent low accommodation and deposition within the lowstand systems tract. The maximum flooding surface is represented by a regionally extensive coal.

In the present study, paleogeographic representations are established in order to depict the basic depositional system and its evolution through time. The main purpose of this work is to: (1) establish stratigraphic packages used for correlation into the subsurface; (2) interpret the depositional environments, and their temporal and spatial evolution; (3) apply this knowledge to reservoir characterization; (4) add to the database of outcrop studies used to derive concepts and to better understand coastal-plain reservoir geology and reservoir-scale sequence stratigraphy; and (5) add to the database used for larger-scale sequence-stratigraphic studies in the Piceance Basin.

2. Previous Studies

Several interpretations of the regional-scale sequence-stratigraphic framework are summarized based on previous studies. Crabaugh (2001) and Gomez-Veroiza and Steel (2010) completed studies in the northern Piceance and Sand Wash basins. Patterson et al. (2003), Kirschbaum and Hettinger (2004), and Aschoff and Steel (2011) completed studies in the Uinta and Piceance basins (Fig. 25). Each study used ammonite biostratigraphy established by previous studies to constrain ages (Patterson et al., 2003; Kirschbaum and Hettinger, 2004; Aschoff and Steel, 2011). These studies are useful for correlating strata into the present study to derive a large-scale sequence-stratigraphic framework. The stratigraphic nomenclature for the Piceance, Uinta, and Sand Wash basins is summarized in Figure 26. Piceance Basin nomenclature is used in the present study (Fig. 27).

Masters defined the late, middle, and upper Campanian "Iles clastic wedge" (ICW) in the Sand Wash Basin (Crabaugh, 2001) as a sandstone wedge composed of complex intertonguings of sandstone and mudstone. It is bounded at its base by the Buck Tongue member of the Mancos Shale, which contains *Baculites perplexus,* and at its top by a lithologic contact between the Trout Creek Sandstone and the overlying Williams Fork Formation. Masters subdivided the ICW into segments: lower (largely transgressive) and upper (largely regressive) (Crabaugh, 2001).

Crabaugh (2001) described outcrops of the lower ICW between Craig, Colorado, and Fish Creek, Colorado, along the banks of the Yampa River. Sandstone tongues were described and mapped in the lower ICW. The lower ICW is a 3.3 m.y. wedge (defined by the ammonite biostratigraphy), and is composed of two smaller-scale

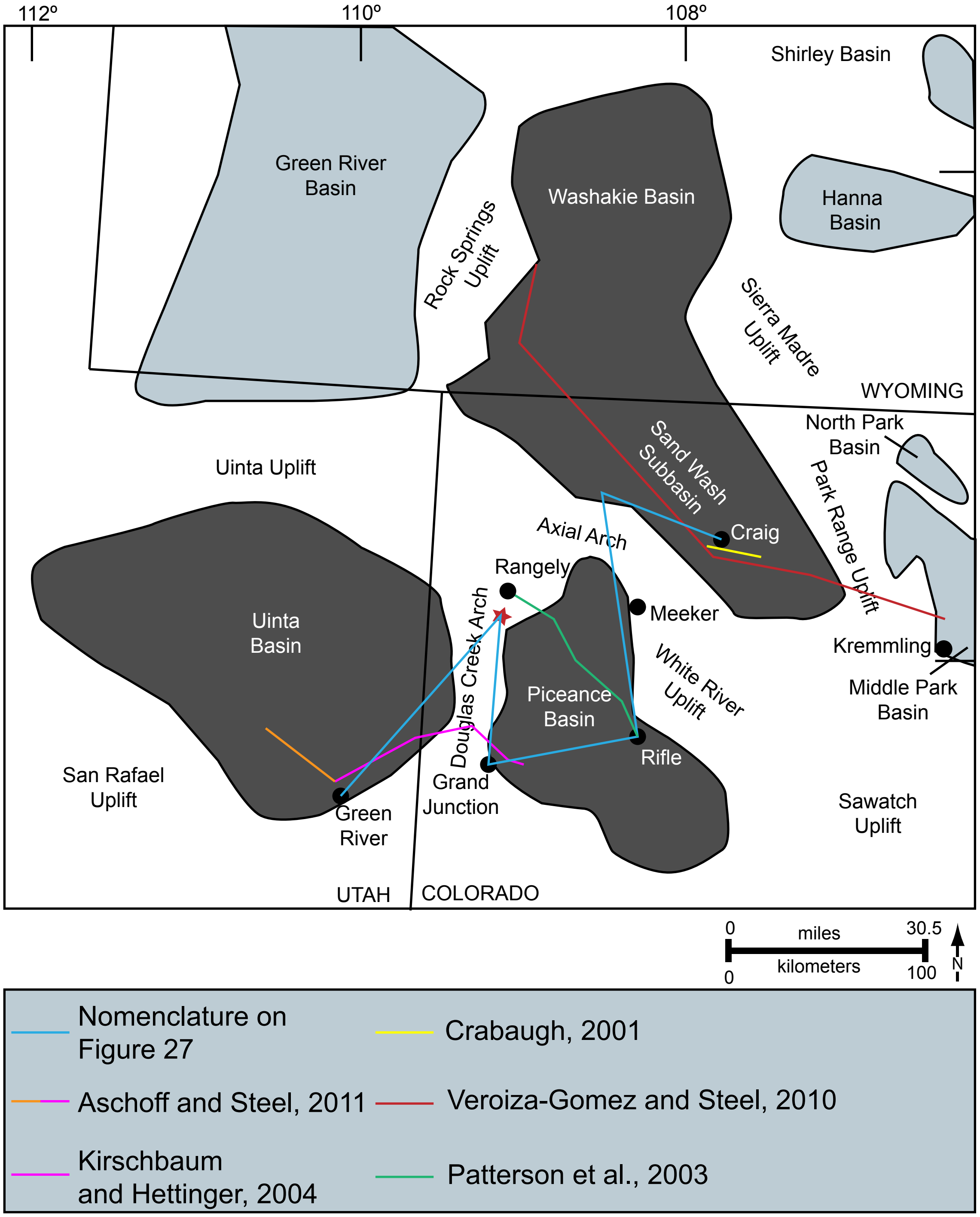

Fig. 25 Map of the Piceance, Uinta, and Sand Wash basins showing study areas discussed in text. Red star shows study area. Modified from Gomez-Veroiza and Steel (2010).

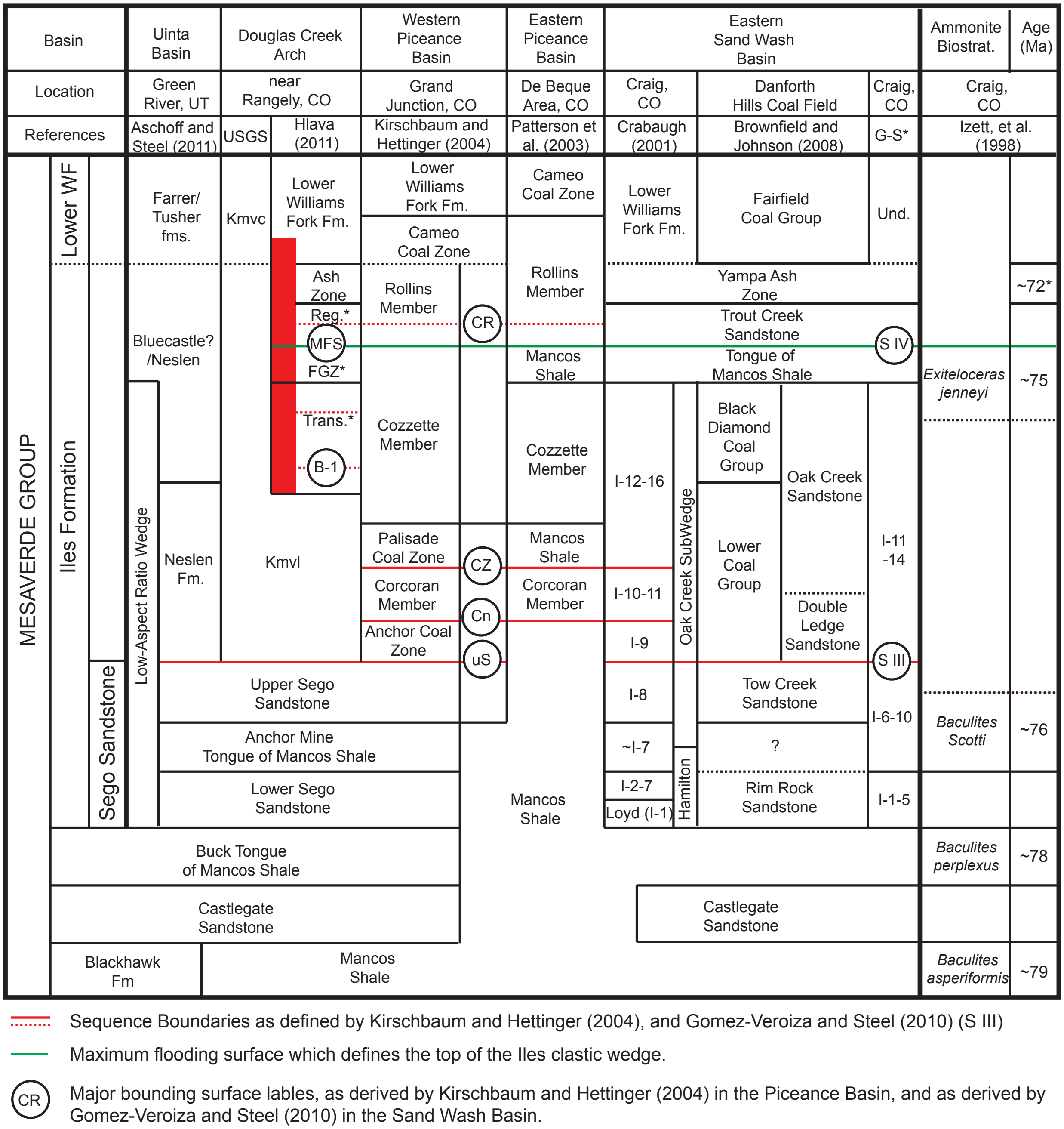

Fig. 26 Nomenclature between the Uinta Basin, the study area, the western and eastern Piceance Basin, and the Sand Wash Basin. Ammonite biostratgraphy and age dates are used to correlate. *The ~72 Ma age date from Brownfield and Johnson (2008) from the Yampa ash bed near Craig, CO; *G-S: Gomez-Veroiza and Steel (2011); *Reg.: Regressive interval; *Trans.: Transgressive interval, *FGZ: fine grained zone. Study interval for the present study within the red bar.

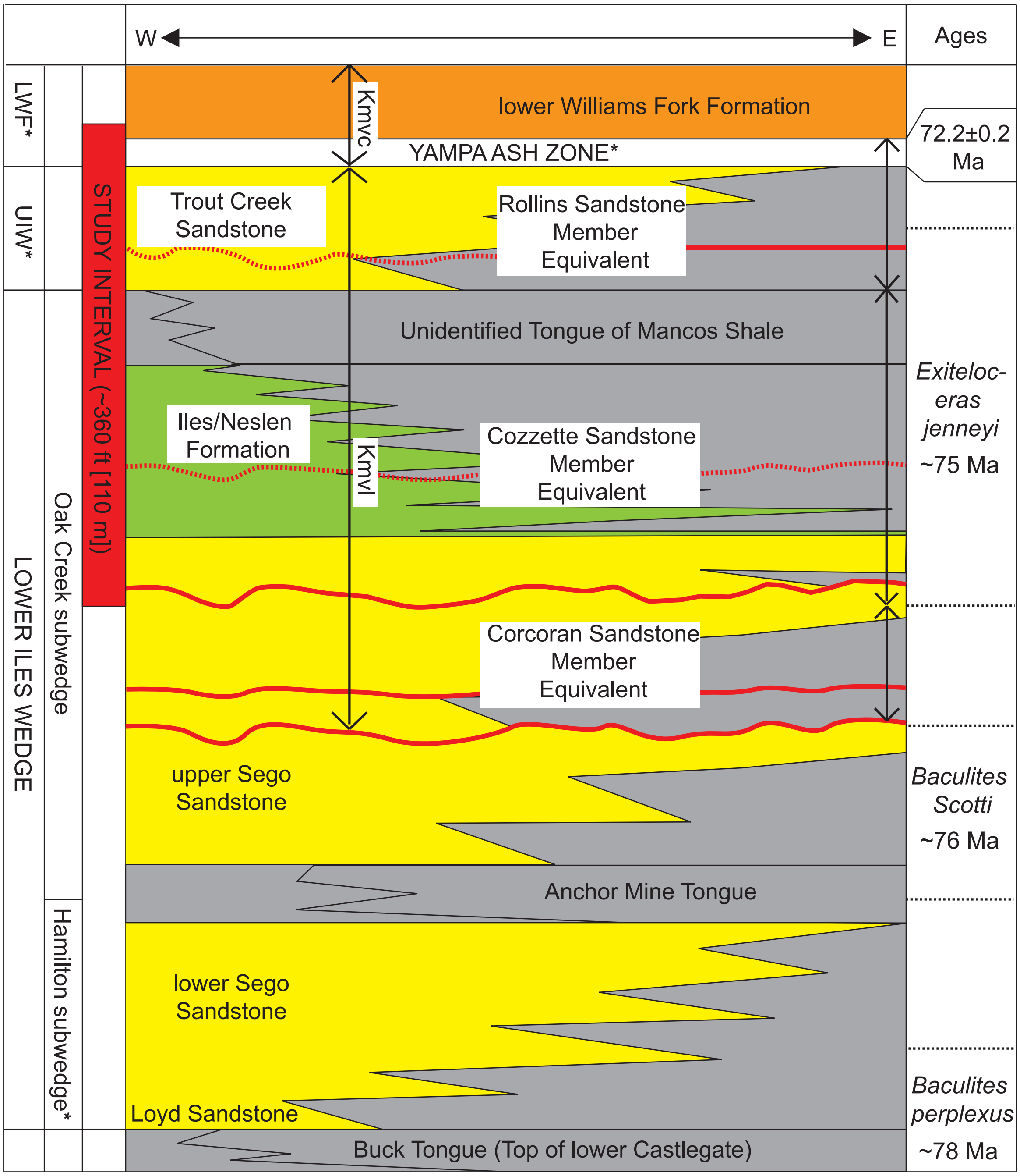

Fig. 27 Stratigraphic intervals using combined nomenclature from the USGS, and the Uinta, Piceance and Sand Wash basins. The study interval lies within the Neslen Formation (Unita), Iles Formation: Corcoran, Cozzette, and Rollins Sandstone members (Piceance). The study interval grades into a Tongue of the Mancos Shale, to the Trout Creek Sandstone (Sand Wash). This is then overlain by the Yampa ash zone, defined by *Brownfield and Johnson (2008), and the lower Williams Fork Formation. *UIW: upper Iles Wedge; *LWF: lower Williams Fork Formation; *Hamilton subwedge, as divided by Crabaugh (2001).

subwedges, the Hamilton subwedge and the Oak Creek subwedge (Figs. 27 and 28). The Hamilton subwedge (1.2 m.y.) is largely regressive, while the Oak Creek subwedge (2.1 m.y.) is largely transgressive. These subwedges are divided by a significant boundary, dated near the *Baculites Scotti* ammonite zone (equivalent to the Anchor Mine Tongue of the Mancos Shale) that represents a large-scale shift from largely regressive to transgressive cycles (Fig. 28). Sixteen smaller-scale shoreline trajectories are recognized within these two subwedges (Iles 1-16). The Hamilton subwedge is composed of Iles-1-7 (1-6 is regressive [lower Sego Sandstone] and 7 is transgressive [Anchor Mine Tongue of the Mancos Shale]). The Oak Creek subwedge is composed of Iles-8-16 (8-9 is regressive [upper Sego Sandstone] and 10-16 is largely transgressive [Iles Formation]). Widespread unconformities and incised valley fills are recognized by Crabaugh (2001) in Iles-3, -6 and -9. The lower ICW is bounded at its top by a tongue of the Mancos Shale, containing *Exiteloceras jenneyi* (Figs. 28 and 29).

Building on Crabaugh (2001), Gomez-Veroiza and Steel (2010) reconstructed the ICW between the Washakie Basin, through the Sand Wash Basin, near Craig, Colorado, to Middle Park Basin, near Kremmling, Colorado, using outcrop data and geophysical logs (Fig. 30). The maximum flooding surfaces were also used to define the lower ICW boundaries: Surface I at the base of ICW, and Surface IV at the top (Figs. 29 and 30). Gomez-Veroiza and Steel (2010) subdivided the lower ICW into 14 zones (Iles 1-14), where Iles 1-10 are largely regressive (lower highstand to forced-regressive systems tract) and Iles 11-14 are largely transgressive (Figs. 29 and 30). The surface separating Iles 10 and 11 is a sequence boundary (Surface III), near the *Baculites Scotti* ammonite zone, and is mappable across the study area. Surface III represents the

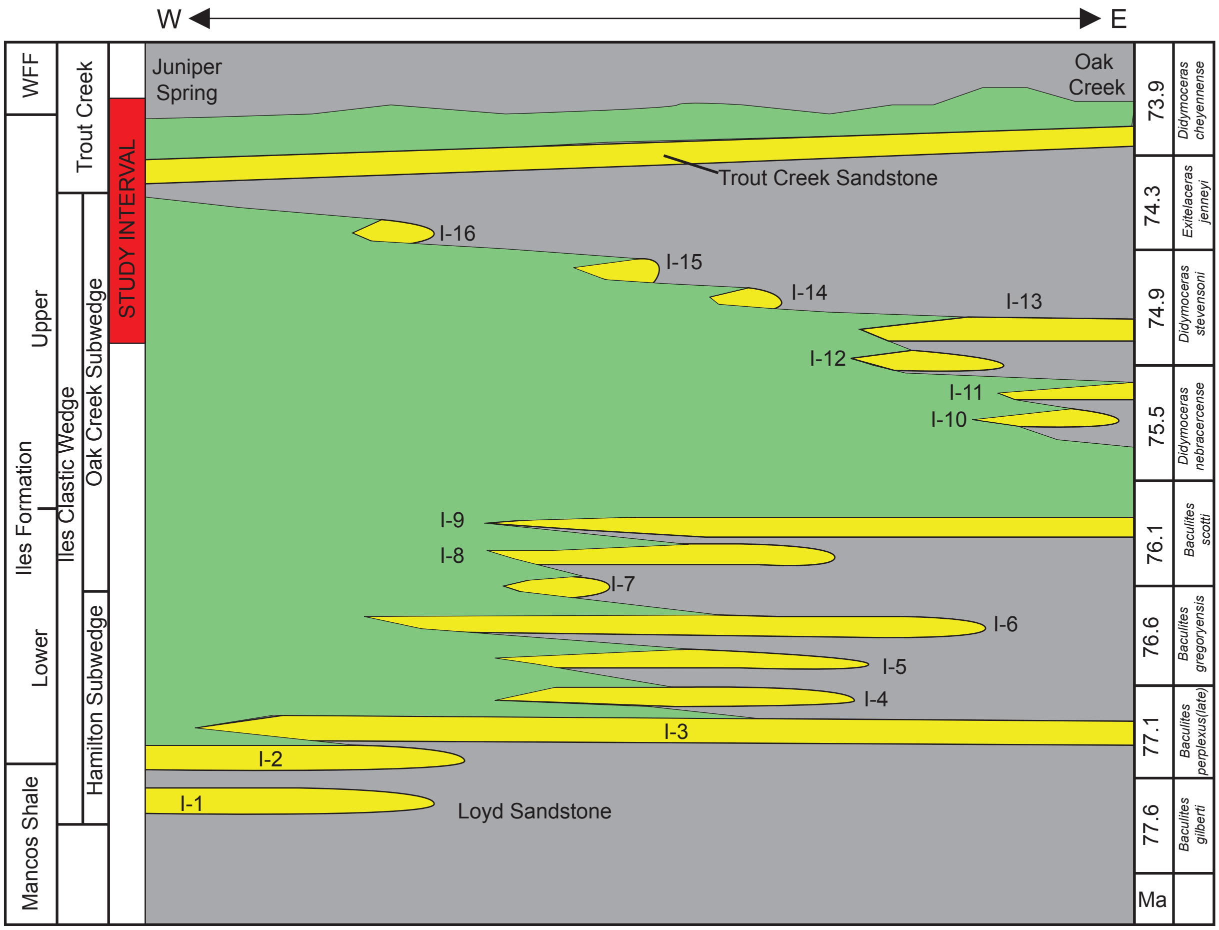

Fig. 28 The study interval (red bar) with respect to the Iles clastic wedge as described by Crabaugh (2001). See Figure 25 for cross-section locations. The present study interval lies within the Iles-12-16 (I-12-16) intervals within the upper portion of the Oak Creek subwedge and the Trout Creek Sandstone. Modified from Crabaugh (2001).

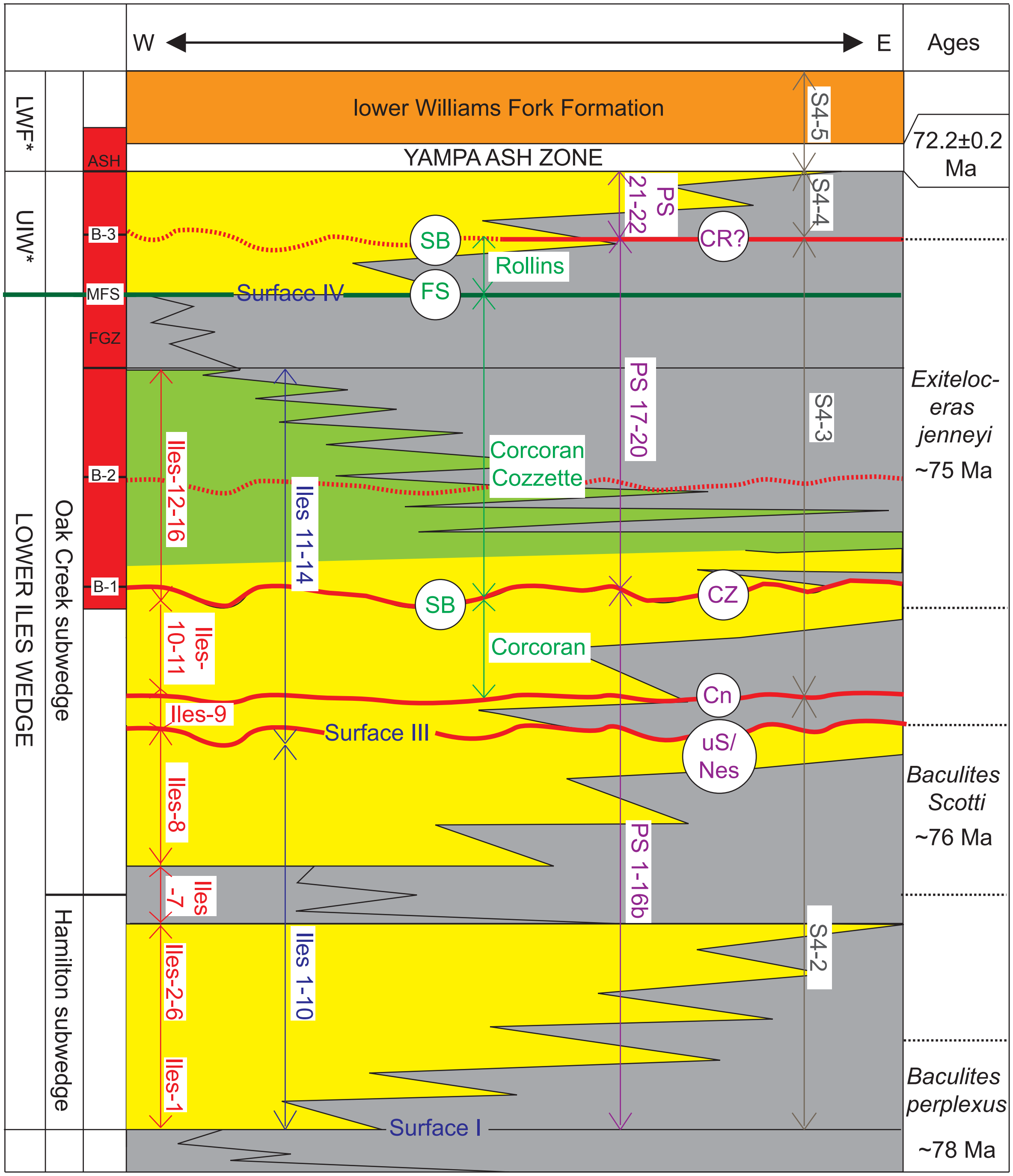

Fig. 29 Diagram showing divisions as described by sequence-stratigraphic analysis in the Iles clastic wedge/Mesaverde Group. Red divisions by Crabaugh (2001). Blue divisions by Gomez-Veroiza and Steel (2010). Green divisions by Patterson et al., (2003). Purple divisions by Kirschbaum and Hettinger (2004). Grey divisions by Aschoff and Steel (2011). Red bar on left represents the study interval. Three ammonite zones are shown (Kirschbaum and Hettinger, 2004), which constrain each of the studies. *UIW: upper Iles wedge; *LWF: lower Williams Fork Formation.

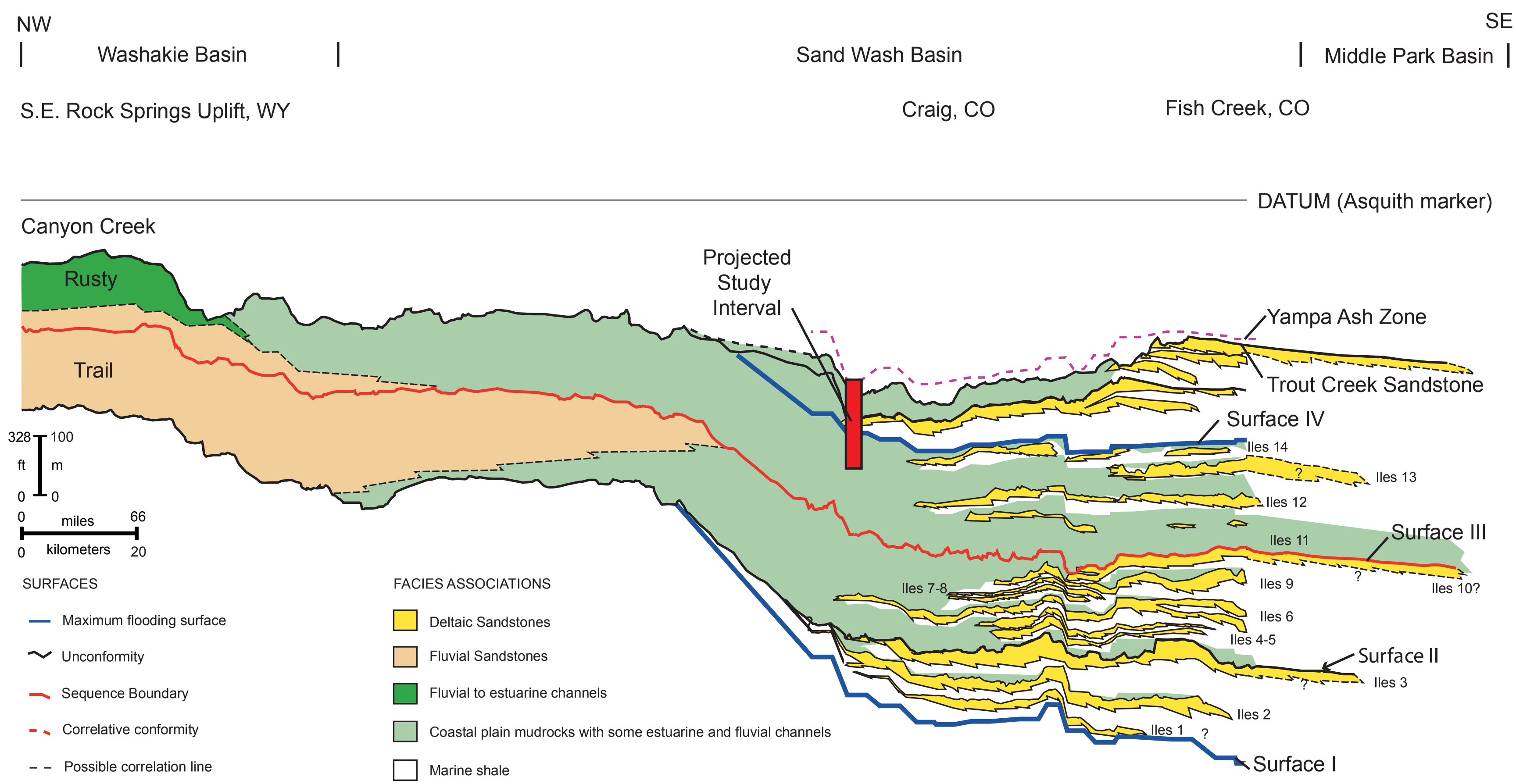

Fig. 30 Generalized cross section and stratigraphy of the Iles clastic wedge as reconstructed by Gomez-Veroiza and Steel (2010). See Figure 25 for cross-section location. Approximate study interval is marked in the red box. Because the cross section is north and west of the study area, thickness and facies associations are not exact. Major correlation zones include the Yampa Ash Zone, Surface IV, and Surface III. The study interval lies approximately within the Iles 12-14 divisions. General facies associations include coastal-plain mudrocks with some estuarine and fluvial channels, marine shale, and potential deltaic sandstones. Modified from Gomez-Veroiza and Steel (2010).

turnaround from regression to transgression, and may correspond to the turnaround that Crabaugh (2001) noted in Iles-9, and is interpreted as an incised valley fill.

Patterson et al. (2003) summarized the sequence stratigraphy between Rangely, Colorado and Rifle Gap, Colorado (Fig. 25). The Castlegate Formation to the lower Corcoran Sandstone Member was interpreted as a part of a highstand systems tract. A regional unconformity truncates the Corcoran Sandstone Member and is overlain by the lowstand to transgressive systems tracts of the upper Corcoran and Cozzette Sandstone members (Fig. 31). The Rollins Sandstone Member forms a highstand systems tract overlain by a sequence boundary and deposits of the Cameo coal zone and the Williams Fork Formation (Patterson et al., 2003).

In multiple studies by Hettinger and Kirschbaum (1998; 2002; 2003) and Kirschbaum and Hettinger (2004), outcrop measured sections, cores, and geophysical logs were used to create a large-scale cross-section through the entire Mesaverde Group in the Piceance and Uinta basins between Coal Basin, Colorado, and Price Canyon, Utah. The 2004 study outlined a high-resolution sequence-stratigraphic framework between the Sego Sandstone and the Mt. Garfield Formation (Iles) (Fig. 32). Six sequences and 23 parasequences were identified. The upper Sego Sandstone sequence represents progradation in a highstand systems tract, followed by an overall lowstand and incision into the top of the upper Sego Sandstone, this is the “uS” sequence boundary, originally described by Van Wagoner (1991) (Fig. 32). Incision into the upper Sego Sandstone was followed by an overall regression of the Iles Formation (Corcoran, Cozzette, and Rollins Sandstone members), separated by numerous sequence boundaries (“Cn”, “CZ”, “CR”) (Fig. 32). Many smaller-scale transgressions

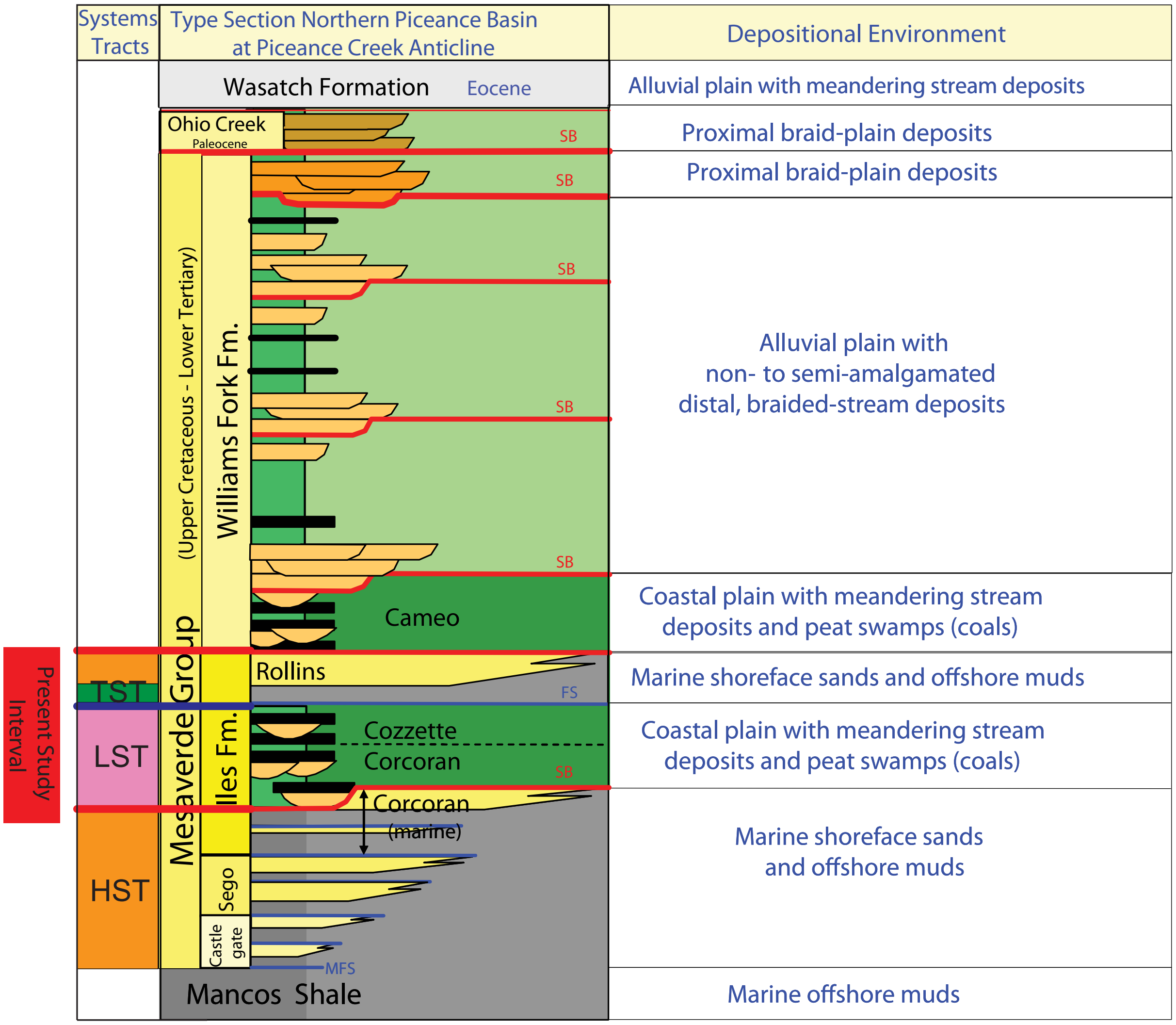

Fig. 31 Interpretation of the shoreface and coastal-plain deposits of the Mesaverde Group in the Piceance Basin by Patterson et al. (2003). To the right are interpreted systems tracts. HST: highstand systems tract (orange); LST: lowstand systems tract (pink); TST: transgressive systems tract (green). The red bar shows the present study interval. Modified from Patterson et al. (2003).

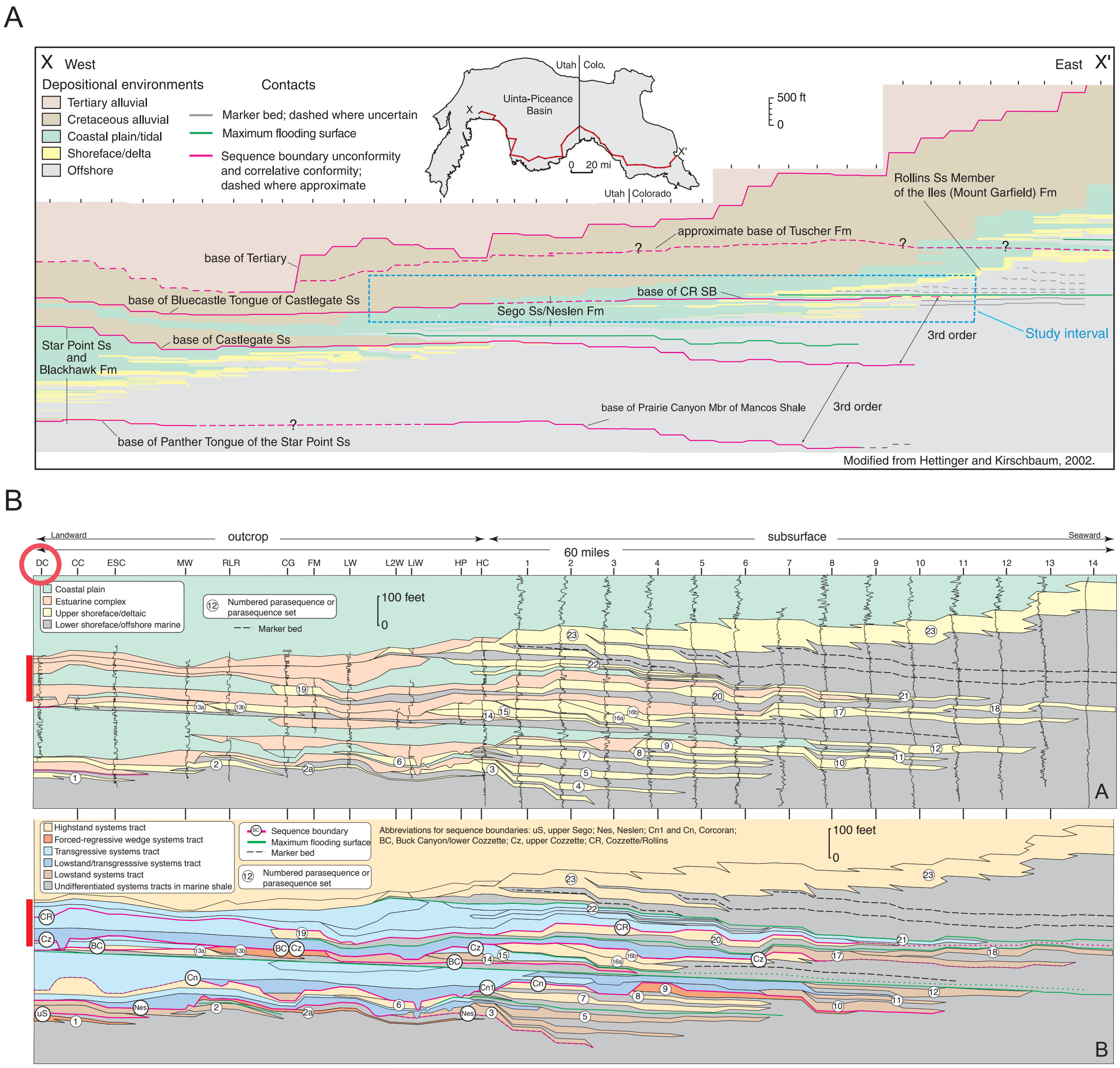

Fig. 32 A) Location map showing location of the cross section. The cross section below shows nomenclature used by Kirschbaum and Hettinger (2004). Blue outline shows the cross-section study area shown in part B. B) Cross sections constructed by Kirschbaum and Hettinger (2004), the red bars to the left of the cross sections show the projected study interval which is roughly equivalent to “DC” (circled in red). Cross section “A” shows parasequences and depositional environments. Cross section “B” shows systems tracts and parasequences. Modified from Kirschbaum and Hettinger (2004).

occurred during the deposition of the Iles Formation, which contrasts with the other sequences in that the preservation of the retrogradational parasequences and the development of large estuaries coincide with maximum flooding, and indicate a relative increase in accommodation during deposition. The retrogradational parasequences are preserved in relatively thick intervals in the Buck Canyon/Cozzette and the Cozzette/Rollins sequences (Fig. 32). Iles Formation deposition was then followed by deposition of the lower Williams Fork Formation in the highstand systems tract. Major surfaces identified by Kirschbaum and Hettinger (2004), are represented in the study area, and may roughly coincide with surfaces identified by Veroiza-Gomez and Steel (2010) and Crabaugh (2001) (Fig. 29). The “uS”/“Nes” sequence boundary is possibly equivalent to “Surface III” of Veroiza-Gomez and Steel (2010). The “CZ” sequence boundary is possibly equivalent to the top of Iles-10 by Crabaugh (2001).

A recent study by Aschoff and Steel (2011), identified sequences within a low-aspect-ratio wedge (identified by an offlapping sequence architecture, which contains basinward extended shoreline tongues that stack with flat to falling trajectories), using ammonite biostratigraphy, detailed measured sections, well logs, and photopans (Fig. 33). This wedge was determined to consist of six depositional sequences (S4-1-S4-6), bounded by regionally extensive unconformities. S4-1 lies below the Sego Sandstone. S4-2 is equivalent to the strata between the Buck Tongue of the Mancos Shale and the upper Sego Sandstone, and was interpreted to represent an overall lowstand sequence set. S4-3 is roughly equivalent to the Corcoran and Cozzette Sandstone members of the Iles Formation, and was interpreted as an overall forced-regressive to lowstand sequence set. S4-4 is roughly equivalent to the Rollins Sandstone Member, and was

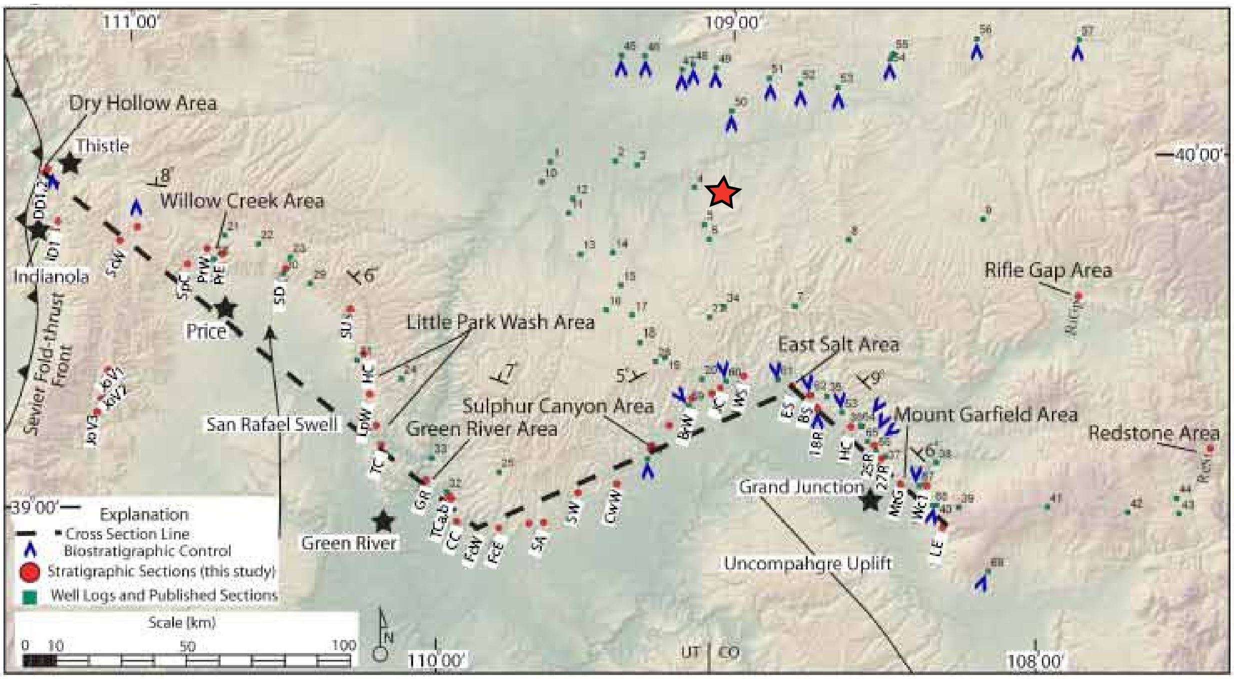

Aschoff and Steel, 2010

B

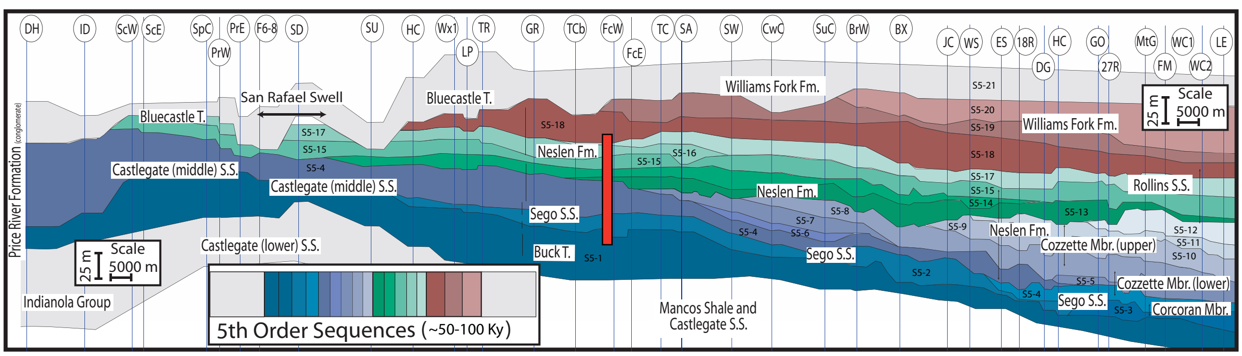

Aschoff and Steel, 2010

Fig. 33 A) Location of cross section pictured in B below. Red star shows approximate projection of the study in relation to the study area, based on southwest to northeast shoreline trajectories. B) Cross section constructed by Aschoff and Steel (2011), which shows higher-order sequences and nomenclature used in the study. Red bar shows approximate position of present study interval in relation to the cross section. Reproduced with permission from Aschoff and Steel (2011).

interpreted as an overall transgressive sequence set. S4-5 corresponds to the Trout Creek Sandstone, and was interpreted as a partial highstand sequence set. S4-6 corresponds to the lower Williams Fork Formation (Figs. 29 and 33). The boundary between S4-2 and S4-3 may be equivalent to the top of Iles 10 of Crabaugh (2001), Surface III of Gomez-Veroiza and Steel (2010), and the “uS/Nes” sequence boundary of Kirschbaum and Hettinger (2004). The boundary between S4-4 and S4-5 may be the equivalent to Surface IV of Gomez-Veroiza and Steel (2010) (Fig. 29).

3. Stratigraphic Placement

With respect to the previous studies, the lower 255 ft (77.7 m) of the present study interval is equivalent to the upper portion of the Oak Creek subwedge and the Corcoran and Cozzette members of the Iles Formation (Fig. 27), and is referred to as the “transgressive interval” for the purposes of this study (Fig. 34). Between 255-280 ft (77.7-85.4 m) is a marked unit of fine-grained strata that is equivalent to the tongue of the Mancos Shale and marks the top of the lower ICW (Fig. 27). This portion of the study interval is referred to as the “fine-grained interval” (Fig. 34). The strata above 280 ft (85.4 m) and below the ash zone at approximately 323 ft (98.5 m) is equivalent to the upper ICW (Rollins Member of the Iles Formation) (Fig. 27) and is referred to as the “regressive interval” (Fig. 34). The regressive interval is bounded at its top by the Yampa Ash Bed, dated at 72.2±0.2 Ma by Brownfield and Johnson (2008), and marks the boundary between the Iles and lower Williams Fork formations near Craig, Colorado (Brownfield and Johnson, 2008). Above 323 ft (98.5 m), the study interval is equivalent to the lower Cameo-Wheeler coal zone (lower Williams Fork Formation) (Fig. 27) and is

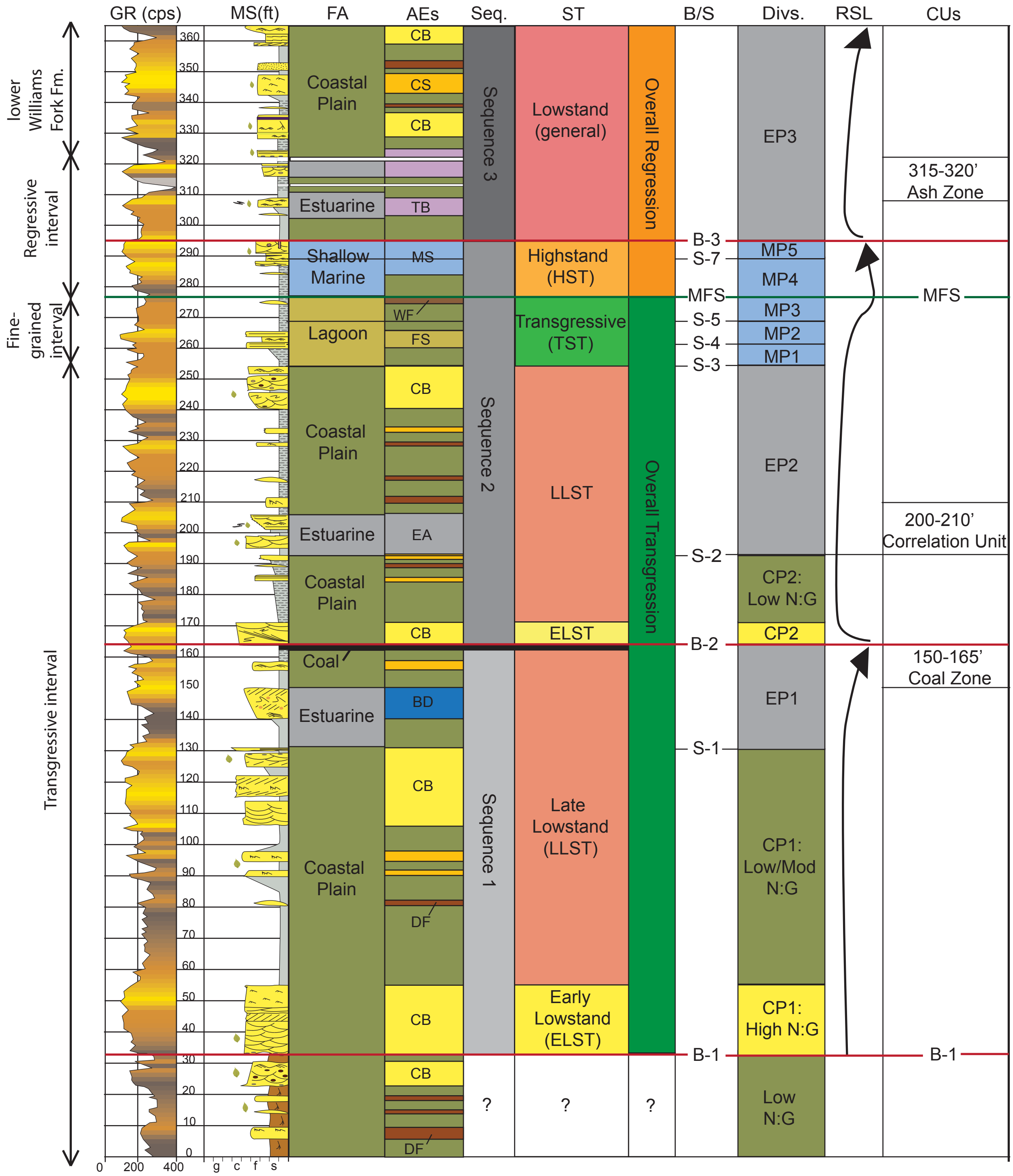

Fig. 34 Stratigraphic placement of facies associations (FA), architectural elements (AEs), sequences (Seq.), systems tracts (ST), boundaries and surfaces (B/S), divisions (Divs.) and a relative sea level curve (RSL), as well as major zones used for correlations (CUs). Stratigraphic variability, as noted in the text, is based on the State Bridge Draw South (SBS) measured section (Appendix A), however, specific interval footage can vary as much as 20 ft (6.1 m) throughout the study area due to structural dip and faulting. See Figure 15 for AE abbreviations.

referred to as the “lower Williams Fork Formation” (Fig. 34). Refer to Figure 26 for detailed nomenclature.

4. Depositional Evolution

Using the observations described previously, measured sections were correlated using Petrel software (Appendix E), and divided into two depositional sequences. A *sequence* is a relatively conformable succession of genetically related strata bounded by unconformities and their correlative conformities (Van Wagoner et al., 1988). Sequences recognized in the present study are composed of multiple "estuarine parasequences” and/or parasequences. In general, these are chronostratigraphic, genetically related intervals of strata bounded by sequence boundaries, estuarine-, or marine-flooding surfaces, which display differing depositional environments in contrast to strata above or below.

An *estuarine parasequence* is defined by packages of estuarine facies associations that record a progradation through time (from estuarine to coastal-plain). These are bounded by estuarine-flooding surfaces at their base. *Estuarine-flooding surfaces* are marked by a sudden deepening from coastal-plain to estuarine facies associations, commonly at a contact between coal and fissile mudrock. A rise in base level will raise groundwater tables, producing poorly drained conditions, resulting in swamp and marsh soils, and lacustrine environments in valleys (Coleman, 1966; Shanley and McCabe, 1994).

Parasequences are relatively conformable successions of genetically related beds or bedsets bounded by marine-flooding surfaces and their correlative surfaces (Van Wagoner et al., 1988). Parasequences are progradational and therefore beds within parasequences shoal upward (Van Wagoner et al., 1990). *Marine flooding surfaces* are defined as the basal-bounding surface of a shallowing-upward succession of lagoon or shallow-marine facies associations. These are commonly marked at a contact between coal and fissile mudrock.

Two sequences are recognized in the study interval, which are each composed of estuarine and/or marine parasequences. Parasequences stack to form parasequence sets. A *parasequence set* is a succession of genetically related parasequences which form a distinctive stacking pattern that is bounded in many cases, by major marine flooding surfaces and their correlative surfaces (Van Wagoner et al., 1988). Parasequence sets can form stacking patterns that are progradational, retrogradational, or aggradational. Coastal-plain facies associations create N:G *packages*. Coastal-plain packages record a change in accommodation through time, where high N:G packages represent low accommodation and low N:G packages represent high accommodation.

Parasequence stacking patterns, coastal-plain packages, major bounding surfaces, and concepts described previously, aid in assigning specific systems tracts within sequences. A *systems tract* is a linkage of contemporaneous depositional systems (Brown and Fisher, 1977). Each sequence is described below, thus, the following presents a sequence-stratigraphic framework proposed for the study interval.

4.1 Sequence One

Sequence one is bounded by interpreted sequence boundaries at the base (B-1) and top (B-2). Sequence one contains one coastal-plain package and one estuarine parasequence. This interval of strata corresponds to the Corcoran/Cozzette members of the Iles Formation. Based on previous studies, the sequence boundary (B-1) interpreted at the base of this sequence may be roughly equivalent to the “CZ” sequence boundary of Kirschbaum and Hettinger (2004) (Fig. 29). Strata above the sequence boundary is referred to as the “transgressive interval” (Fig. 27).

Sequence Boundary (B-1).

Below sequence boundary B-1, a low N:G coastal-plain facies association is recognized at the base of the stratigraphic interval (0-32 ft [0-9.8 m]) (Figs. 34 and 35). Gamma-ray readings in this interval are commonly very high (300-350 cps) in the mudstone with intermittent lower readings in the sandstone (Fig. 34). Lateral thickness variations are unknown because the basal contact is not present (Fig. 35). Paleocurrents average 150º (N=35) (Fig. 36).

The sequence boundary marks a distinct change between the isolated sandstone bodies below to amalgamated sandstone bodies at a sharp and erosional contact containing heterolithic debris (Appendix F). Paleocurrents shift from 150° in the low N:G interval to 86° in the overlying strata (from Fig. 36 to Fig. 38).

Sequence boundaries represent a basinward shift in facies, and are formed when the rate of base-level fall exceeds the rate of subsidence (Van Wagoner et al., 1990). These are recognized by subaerial exposure, sediment bypass, incisement, and a basinward shift in facies. Sequence boundaries in alluvial- and coastal-plain environments are commonly overlain by laterally and vertically amalgamated fluvial complexes that have a high relative proportion of interconnected, coarser-grained, channel-fill sandstone bodies, with less interbedded overbank and mudstone deposits (Shanley and McCabe, 1991; 1994). During a time of relative base-level fall, active fluvial sedimentation would be confined to the valleys, depriving interfluves of fresh

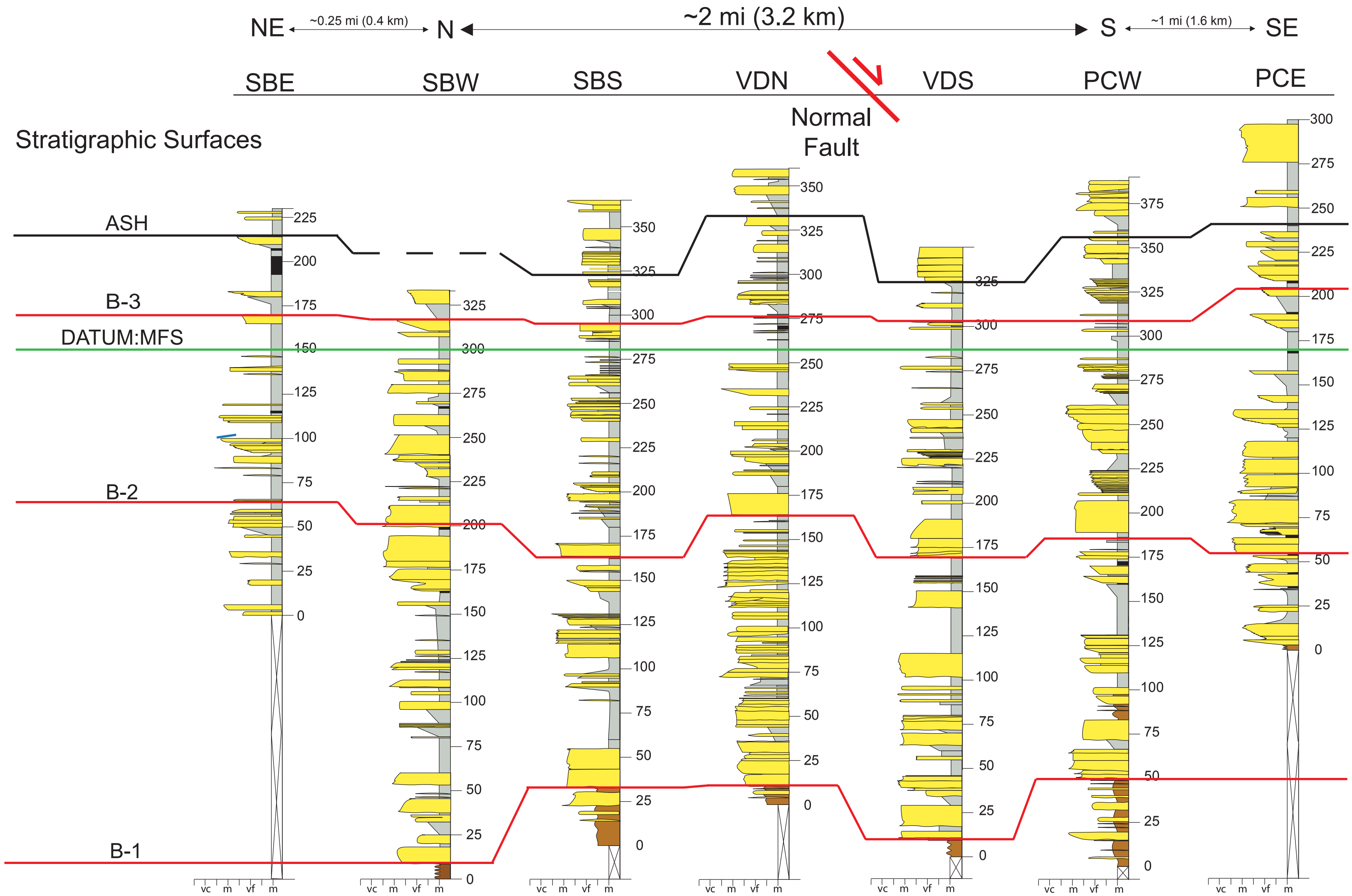

Fig. 35 Cross section of all measured sections (excluding Vandamore Draw West). PCE is a composite section of PCE1 and PCE2. All sections equally spaced. Height in feet. Datum on maximum flooding surface (green line). Measured sections in feet. A normal fault lies between VDS and VDN, structural dip is approximately 2° north. See Appendix A for full measured sections and names. Refer to Figure 7 and Appendix A for locations.

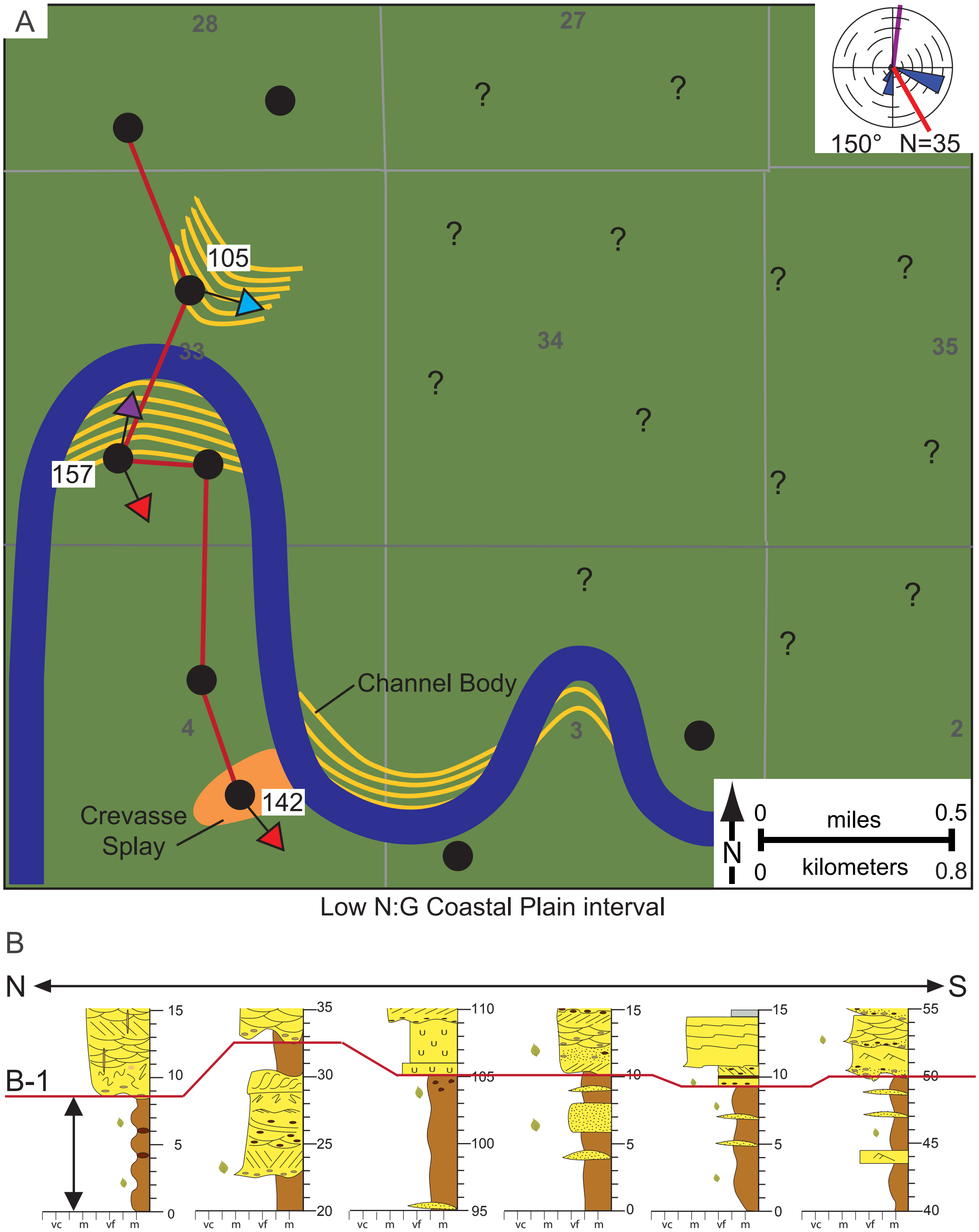

Fig. 36 A) Paleogeographic representation and interpretation of the basal unit of strata (0-33 ft [0-10.1 m]) on Fig. 34) overlain on the study area map (Fig. 7). Paleocurrents averaged 150°. Individual arrows on each measured section show vector mean for the architectural element shown. See Figure 37 for key. B) Cross section showing the upper part of the basal unit, bounded by B-1 at the top.

Paleocurrent Information

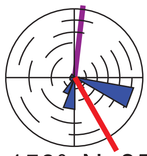

150° N=35

Rose Diagram (in upper right hand corner of all maps). Red line: average paleocurrent orientation. Purple line: vector mean of paleocurrent orientation of inclined heterolithic strata. “150°”: vector mean paleocurrent orientation. “N=35”: number of measurements.

(Red arrow) - Paleocurrents measured on ripple cross stratification

(Green arrow) - Paleocurrents measured on planar cross stratification

(Blue arrow) - Paleocurrents measured on trough cross stratification

(Purple arrow) - Paleocurrents measured on inclined heterolithic strata (no numbers shown)

Map Information

Measured Section Localities

Cross Section Line shown in part B

Fig. 37 Paleocurrent and map key for Figures 36, and 38-53.

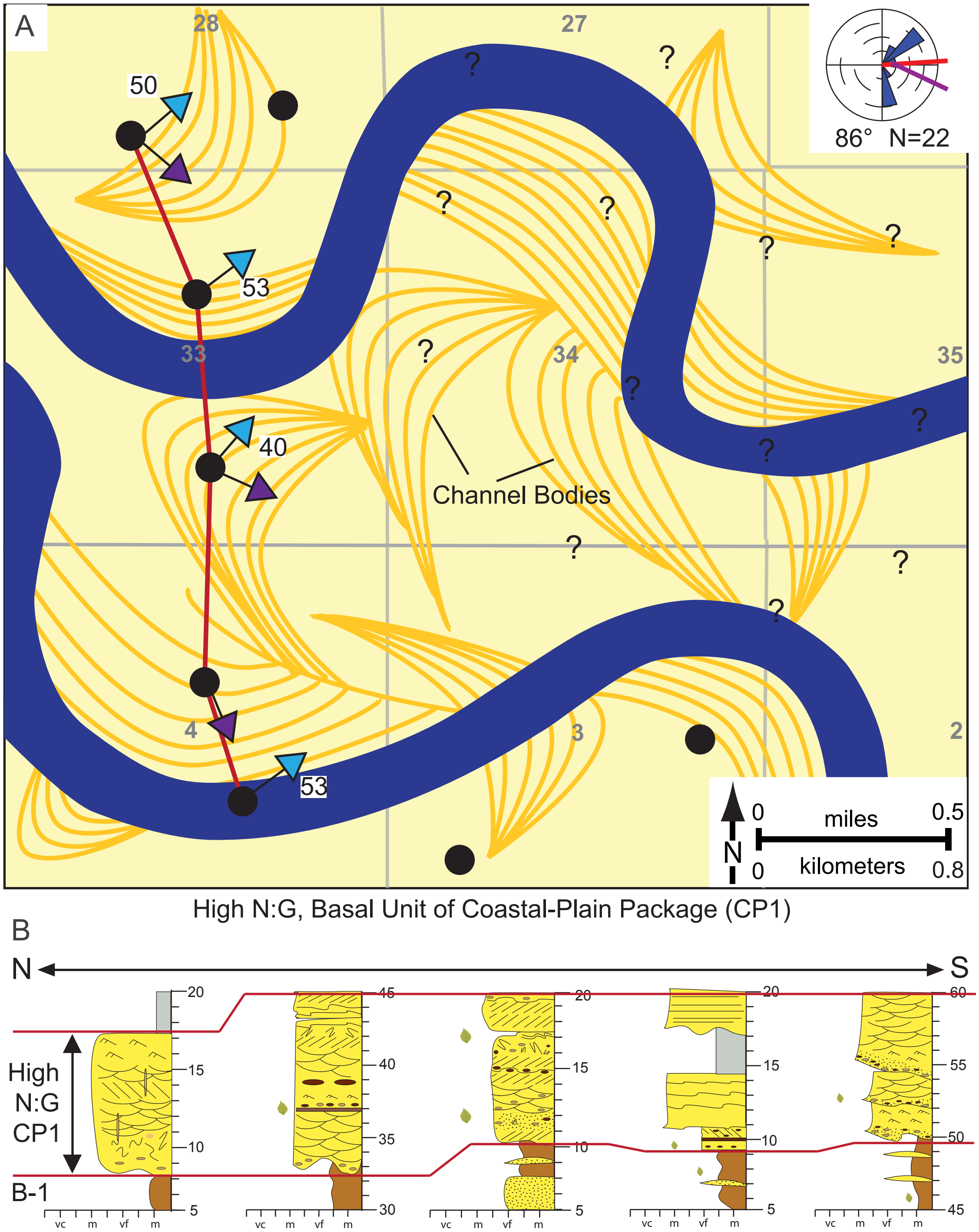

Fig. 38 A) Paleogeographic representation and interpretation of the high N:G (basal unit) of coastal-plain package 1 (CP1) (33-53 ft [10.1-16.2 m] on Fig. 34) overlain on the study-area base map (Fig. 7). Paleocurrents averaged 86°. Individual arrows on each measured section show vector mean for the architectural element shown. See Figure 37 for key. B) Cross section showing the basal unit of CP1, bounded by B-1 at the base.

sediment and leading to the formation of well-developed soil profiles outside the confines of the valley (Blum and Price, 1998; Plint et al., 2001). It is noted that approximately 5 mi (8.0 km) to the north of the State Bridge Draw West measured section the stratigraphic interval contains a thick zone of laterally continuous fine-grained material, and lacks the amalgamated sandstone bodies seen in the study area. This may suggest the presence of an incised valley fill in the study area, which is not present to the north and south.

Early-to-Late Lowstand Systems Tracts: Coastal-Plain Package 1 (CP1)

Coastal-plain package one (CP1) (32-140 ft [9.8-42.7 m]) (Fig. 34) is characterized by a fining-upward succession of coastal-plain facies associations. It is bounded at its base by B-1 and its top by an estuarine flooding surface. Thicknesses are relatively consistent across the interval (125-150 ft [38.1-45.7 m]) but are thinnest in State Bridge Draw South (SBS). Gamma-ray data show a bell-shaped profile associated with increasing gamma-ray values upward. This package is subdivided into to two subunits based on the N:G. The basal subunit (32-55 ft [9.8-16.8 m]) is high N:G with laterally and vertically amalgamated channel bodies. The upper subunit (55-140 ft [16.8-42.7 m]) exhibits a low to moderate N:G with tidally influenced coastal-plain facies associations. The Vandamore Draw North (VDN) measured section contains approximately twice as many channel bodies in this interval than other measured sections in the area (Fig. 35; Appendix A). Channel bodies contain *Teredolites*-bored logs at their bases and occasional borings at their tops (Appendix F). The basal subunit paleocurrent values average 86° (ENE) (N=22), and the upper subunit paleocurrent values average 150° (SE) (N=160) (Figs. 38 and 39)

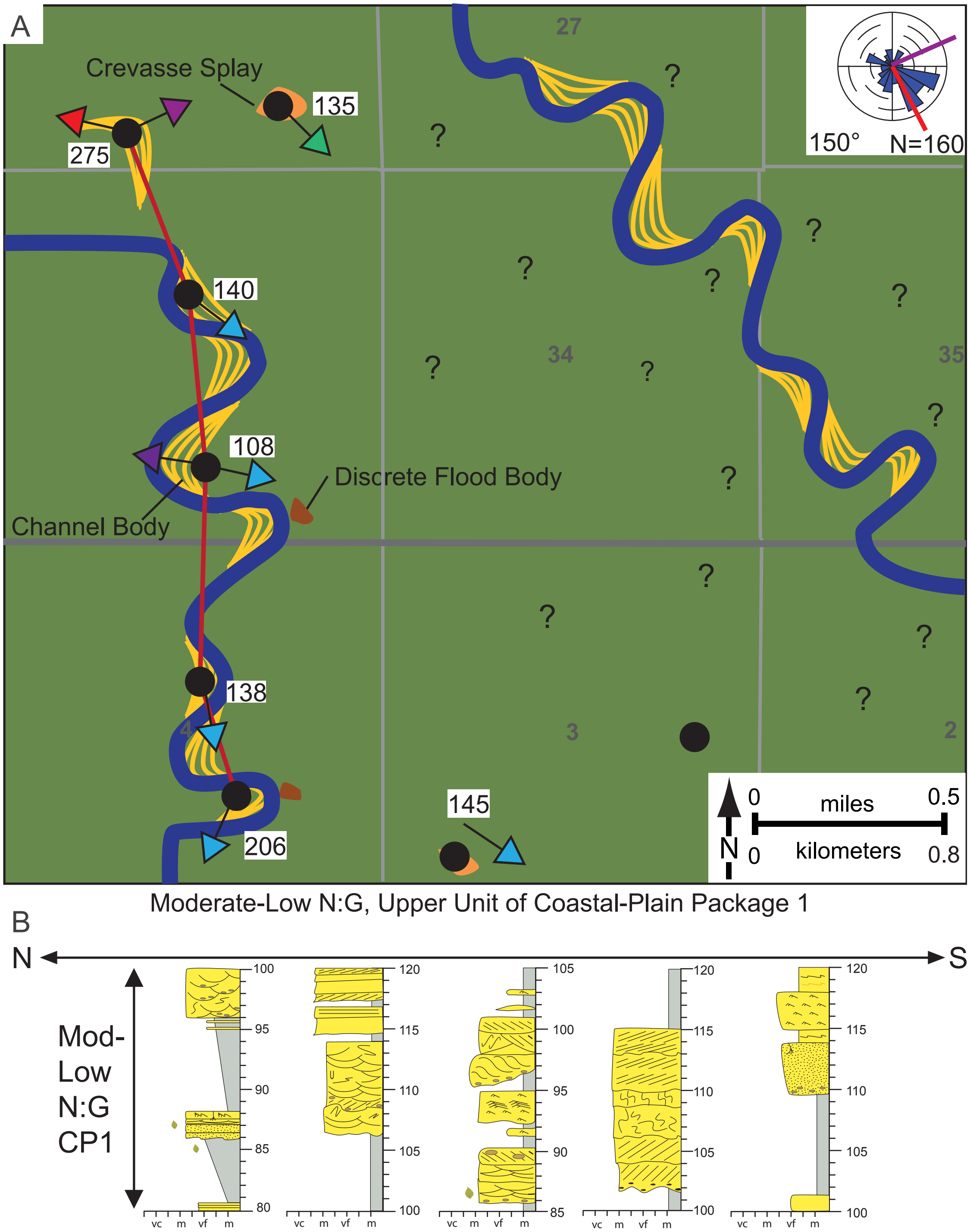

Fig. 39 A) Paleogeographic representation and interpretation of the low to moderate N:G (upper unit) of coastal-plain package 1 (CP1) (53-139 ft [16.2-42.4 m] on Fig. 34) overlain on the study area base map (Fig. 7). Paleocurrents averaged 150°. Individual arrows on each measured section show vector mean for the architectural element shown. See Figure 37 for key. B) Cross section showing strata of the upper unit of CP1, bounded at its top by S-1 (not shown).

The CP1 interval represents coastal-plain deposition, possibly within an incised valley (Fig. 35). Above a sequence boundary, laterally and vertically amalgamated, fluvial channel sandstone bodies exist, which are often overlain by more isolated meander-belt sandstone bodies and an increased proportion of mudstone (Shanley and McCabe, 1991; 1994). The change from amalgamated to isolated sandstone bodies also occurs due to changes in accommodation rates. Amalgamated sandstone bodies are related to periods of minimal accommodation, whereas isolated sandstone bodies are related to increases in accommodation (Holbrook, 1996; Rogers 1998; Plint et al, 2001). Because the CP1 interval lies directly atop the sequence boundary, and below the first major marine-flooding surface (or local flooding surface), the amalgamated sandstone bodies of the basal subunit are interpreted to represent an early lowstand systems tract (ELST) (Fig. 34). An ELST occurs during a time of rapid eustatic fall (Van Wagoner et al., 1988; 1990). The tidally influenced strata, thick mudstone units, coals, and isolated sandstone bodies of the upper subunit are interpreted to represent late lowstand (LLST) or transgressive (TST) systems tracts and a time of early to rapid eustatic rise (Van Wagoner et al., 1988; 1990). Because of the limited extent of the study area, it is not known if a LLST or TST is represented. If these units are confined within an incised valley, a LLST would interpreted for the units and if they are not, they would be interpreted as a TST. For the purposes of this study, the units are interpreted as LLST (Fig. 34).

Late Lowstand Systems Tract: Estuarine Parasequence 1 (EP1)

Estuarine parasequence one (EP1) (140-165 ft [42.7-50.3 m]) (Fig. 34) is bounded at its base by an estuarine flooding surface (S-1) and at its top by a laterally continuous coal. The entire package has a fining-upward grain-size trend. Gamma-ray data has a funnel- to variable-shaped profile (Fig. 34). It contains two subunits, which record a progradation from a bayhead delta (subunit 1) to the coastal plain (subunit 2). The bayhead delta contains deeper water facies and an increased proportion of mudstone to the south, and shallow-water facies and a higher proportion of sandstone to the north (Fig. 40). Bayhead delta paleocurrent values average 177° (SSE) (N=17), and are separated into northward-orientations in the south, which are possibly due to landward currents from the flood-tidal currents, and southward-orientations to the north, which are possibly due to basinward currents from the bayhead delta. Coastal-plain deposits similar to CP1 overlie the bayhead delta and record progradation of EP1 (Fig. 41). Paleocurrent values of the coastal-plain deposits average 130° (SE) (N=12).

This estuarine parasequence is interpreted to be a part of the LLST or TST (dependent on whether it is confined or not). According to Plint et al. (2001), during the time of maximum flooding, tidally influenced, lacustrine, and brackish-water deposits, and coal development are common. Plint et al., 2001 also states that the latest stages of valley filling may occur under tidally influenced conditions, and the uppermost part of the valley fill is sometimes defined by a bioturbated, coarsening- upward trend, interpreted to be a small bayhead delta. Lacustrine-dominated deposits are produced when accommodation is generated faster than filling, resulting in standing bodies of water (Hampson et al, 1989; Plint et al., 2001). The laterally continuous coal atop EP1, which forms the upper bounding surface, might represent a coastal-plain flooding surface (Fig. 34).

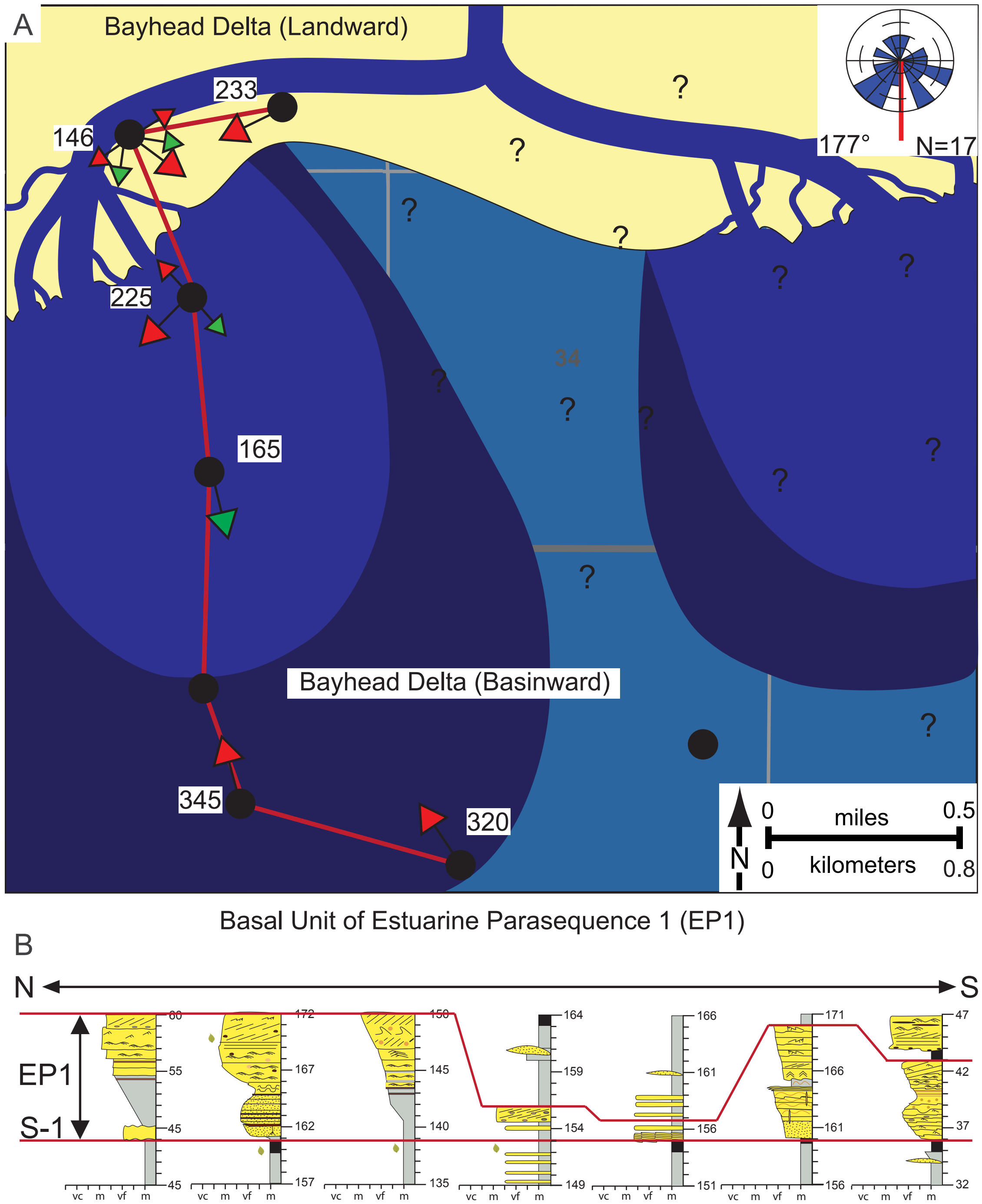

Fig. 40 A) Paleogeographic representation and interpretation basal unit (bayhead delta) of estuarine parasequence 1 (EP1) (139-150 ft [42.4-45.7 m] on Fig. 34) overlain on the study-area base map (Fig. 7). Paleocurrents averaged 177°. Large individual arrows on each measured section show vector mean for the architectural element shown. Small arrows show individual measurements. Note the planar cross-stratification is directed basinward and the southern ripple cross-stratification is directed landward. See Figure 37 for key. B) Cross section showing strata of the basal unit of EP1, bounded at its base by S-1. Note the thickness and facies changes from north to south (explained in text).

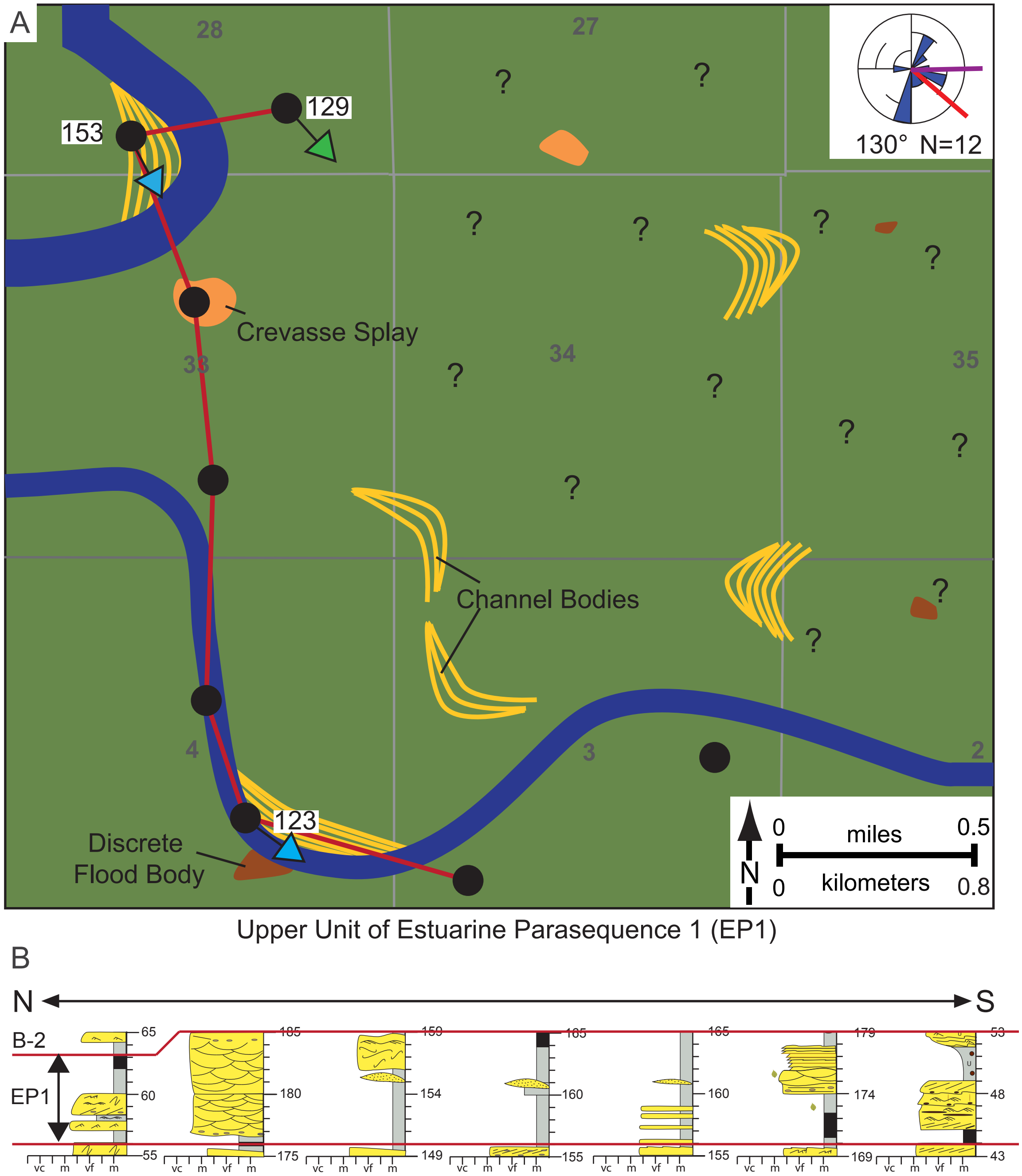

Fig. 41 A) Paleogeographic representation and interpretation of the low N:G coastal-plain strata (upper unit) of estuarine parasequence 1 (EP1) (150-164 ft [45.7-50 m] on Fig. 34) overlain on the study-area base map (Fig. 7). Paleocurrents averaged 130°. Individual arrows on each measured section show vector mean for the architectural element shown. See Figure 37 for key. B) Cross section showing strata of the upper unit of EP1, bounded at its top by B-2.

4.3 Sequence Two

Sequence two is bounded by sequence boundaries (B-2 and B-3). Sequence two is composed of one coastal-plain package, two estuarine parasequences, five marginal-marine parasequences, and a maximum flooding surface (MFS). Deposits below the MFS are considered to be part of the ‘transgressive interval” (Fig. 34). The MFS may correspond to Surface IV of Veroiza-Gomez and Steel (2010) (Fig. 29) based on its stratigraphic placement and surrounding facies. The MFS lies within the interval referred to as the “fine-grained interval” (Fig. 34). Deposits above the MFS may be equivalent to the Rollins Sandstone Member (Fig. 28) based on previous studies and stratigraphic placement. Deposits above the MFS are referred to as the lower part of the “regressive interval.”

Sequence Boundary (B-2).

Sequence boundary B-2 is marked by a distinct change from the coal at the top of EP1 to amalgamated channel bodies (Fig. 34). The surface contains high-energy facies of medium-to-coarse-grained sandstone and localized heterolithic debris.

Similar to B-1, B-2 is a candidate for a sequence boundary. The evidence for this interpretation is: 1) there is an abrupt change upward in depositional architecture and N:G; (2) the overlying amalgamated sandstone bodies can be correlated across the study area; and (3) paleocurrent orientations change dramatically (from SE to W) above B-2.

Early-to-Late Lowstand: Coastal-Plain Package 2 (CP2)

Coastal-plain package two (CP2) (165-192 ft [50.3-58.5 m]) (Fig. 34) is bounded at its base by B-2 and at its top by a thick unit of floodplain strata. This unit has an overall fining-upward grain-size trend, with variable gamma-ray profiles (Fig. 34). It has a relatively consistent thickness of approximately 25 ft [7.6 m]) and thins to the southeast (e.g. the Philadelphia Creek East measured section, Fig. 35). This interval contains two subunits based on N:G. The basal subunit (165-172 ft [20.3-52.4 m]) is characterized by a high N:G, large, amalgamated channel bodies, which contain heterolithic debris and can be up to 20 ft (6.1 m) thick (Fig. 42). The upper subunit (172-192 ft [52.4-58.5 m]) exhibits low N:G coastal-plain strata (Fig. 43). Paleocurrent orientation of the basal subunit average 277° (W) (N=48) and the upper subunit paleocurrents average 127° (N=11).

Similar to CP1, this interval was deposited in a coastal-plain setting (Figs. 36 and 42), possibly within an incised valley. The amalgamated channel bodies of the basal subunit are interpreted to represent an ELST. The upper subunit represents the LLST (Figs. 34 and 43).

Late Lowstand/Transgressive Systems Tract: Estuarine Parasequence 2 (EP2)

Estuarine parasequence two (EP2) is bounded at its base by an estuarine-flooding surface (S-2) and overlain by a marine-flooding surface (192-252 ft [58.5-76.8 m]) (Fig. 34). EP2 is characterized by a coarsening- to fining-upward grain-size trend, similar to EP1 (Fig. 34). This interval is generally 40-50 ft (12.2-15.2 m) thick, but is thinnest in the Vandamore Draw North measured section (Fig. 35), which may relate to the abundance of channel bodies seen in CP1. It contains two subunits. The basal

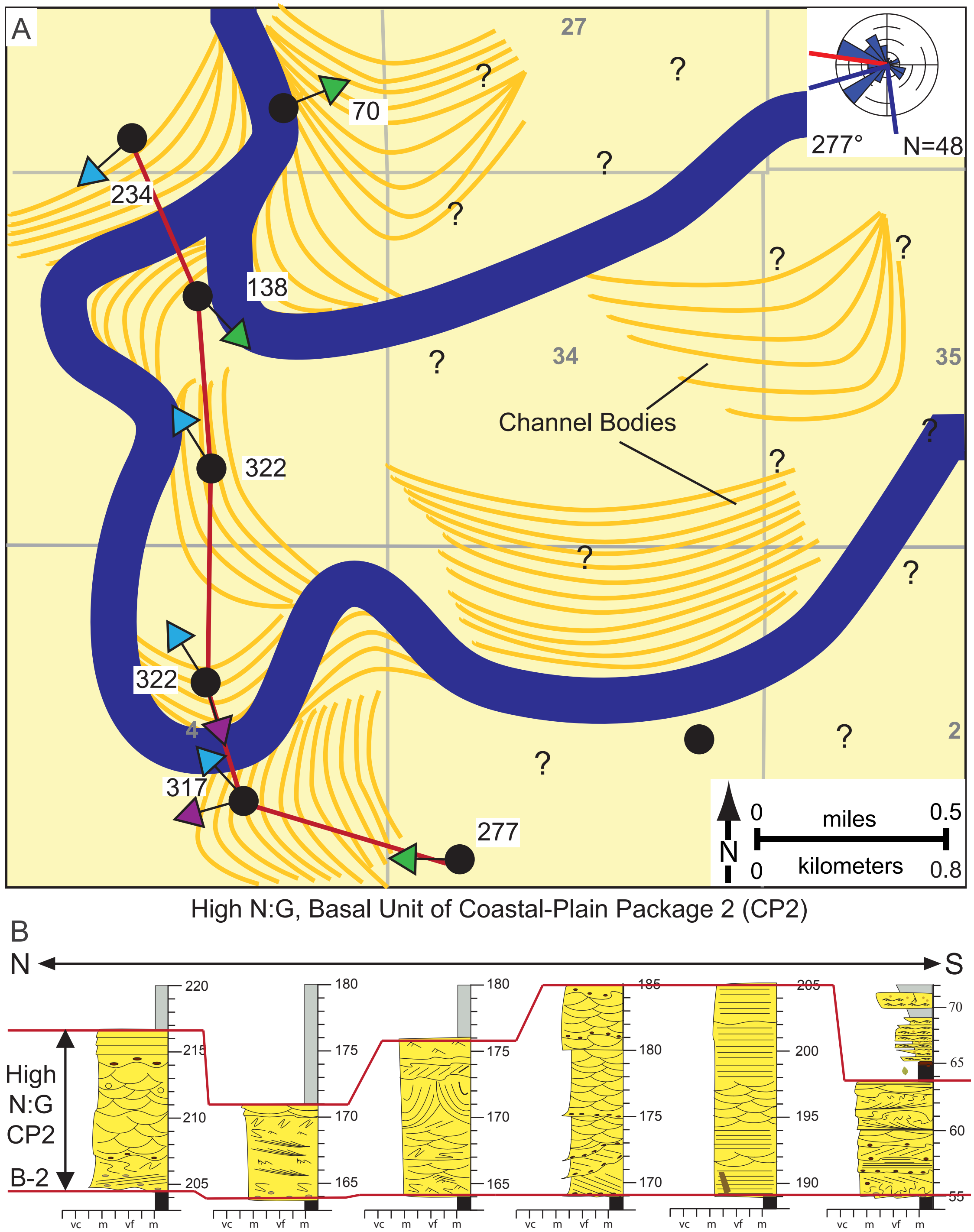

Fig. 42 A) Paleogeographic representation and interpretation of the high N:G (basal unit) of coastal-plain package 2 (CP2) (164-171 ft [50.0-52.1 m] on Fig. 34, overlain on the study-area base map (Fig. 7). Paleocurrents averaged 277°. Individual arrows on each measured section show vector mean for the architectural element shown. See Figure 37 for key. B) Cross section showing strata of the basal unit of CP2, bounded at its base by B-2.

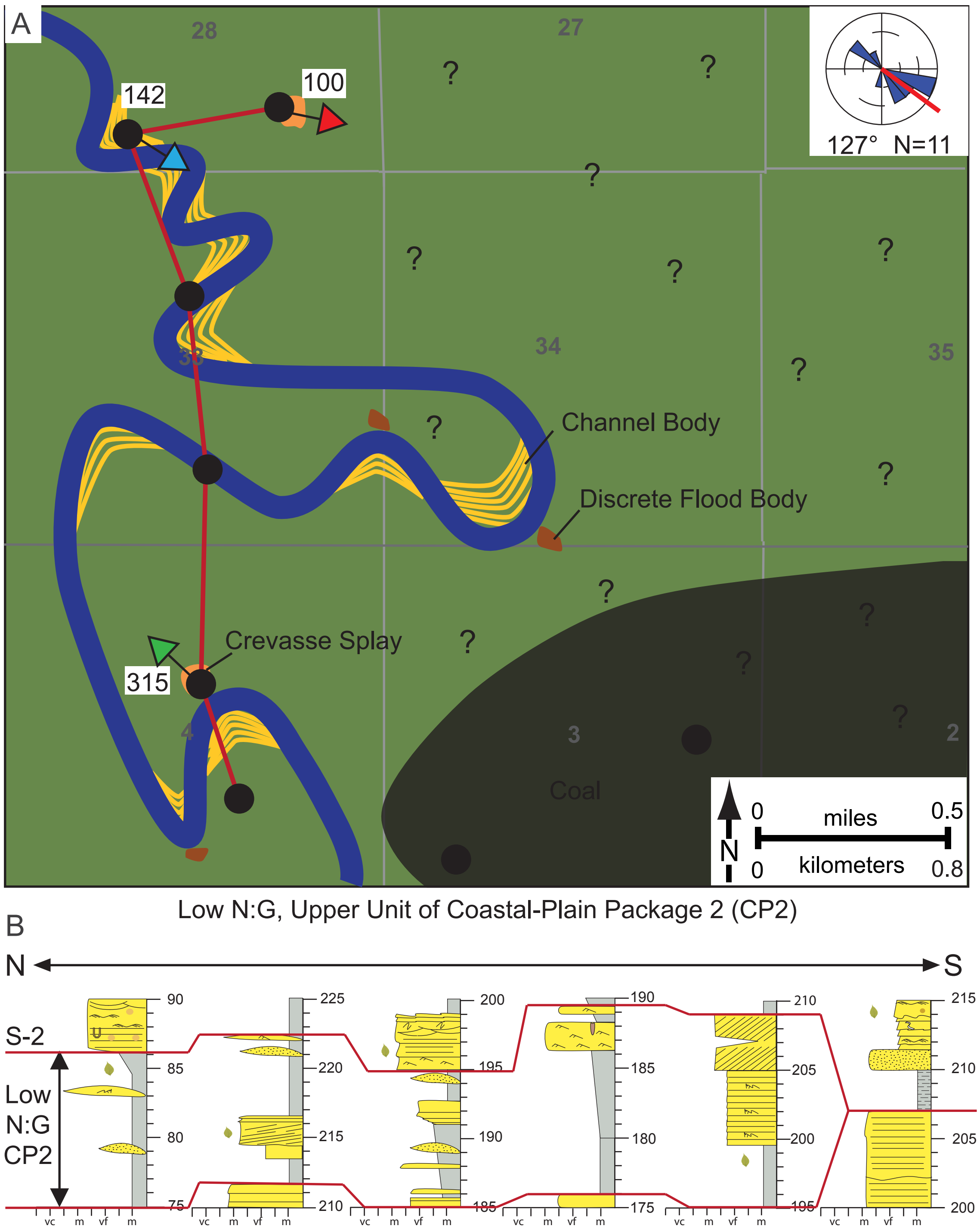

Fig. 43 A) Paleogeographic representation and interpretation of the low N:G (upper unit) of coastal-plain package 2 (CP2) (171-195 ft [52.1-59.5 m] on Fig. 34) overlain on the study-area base map (Fig. 7). Paleocurrents averaged 127°. Individual arrows on each measured section show vector mean for the architectural element shown. See Figure 37 for key. B) Cross section showing strata of the upper unit of CP2, bounded at its top by S-2.

subunit is composed of the estuarine assemblage architectural element (Fig. 44), and the upper subunit is composed of low N:G coastal-plain strata (Figs. 34 and 45). Paleocurrent values of the basal subunit average 170° (N=31) and upper subunit average 278° (N=31).

The entire succession represents estuarine filling with additional progradation of the coastal-plain in the upper subunit. Basinward is believed to be southeast based on lateral thickness variations and paleocurrent values. EP2 is believed to represent the LLST or TST (depending on lateral extent) (Fig. 34).

Transgressive Systems Tract: Parasequences 1-3 (Parasequence Set 1)

Parasequences one through three represent a parasequence set (PS1) which is bounded at its base by a marine flooding surface (S-3) and the top by a maximum flooding surface (252-280 ft [76-85 m]) (Fig. 34). Each parasequence has a coarsening-upward grain-size trend. The parasequence set has an overall fining-upward grain-size trend into a thick unit of fissile mudstone. Gamma-ray data show a bell-shaped profile (Fig. 34). Parasequence set one is relatively consistent in thickness throughout the study interval (approximately 50 ft [15.2 m]) (Fig. 35), and contains lagoon facies associations composed of three parasequences (MP1, MP2, and MP3, Fig. 34). MP1 and MP2 contain foreshore architectural elements (Figs. 46 and 47). MP3 contains the washover fan to the north and grades into middle shoreface facies to the southeast (Fig. 48). Paleocurrent values average 85° (N=33).

Because of the juxtaposition of the lagoon deposits of MP1 over the coastal-plain deposits of CP2, S-3 represents a marine-flooding surface. Because these deposits are very similar to shallow marine, the traditional concepts of sequence stratigraphy can be

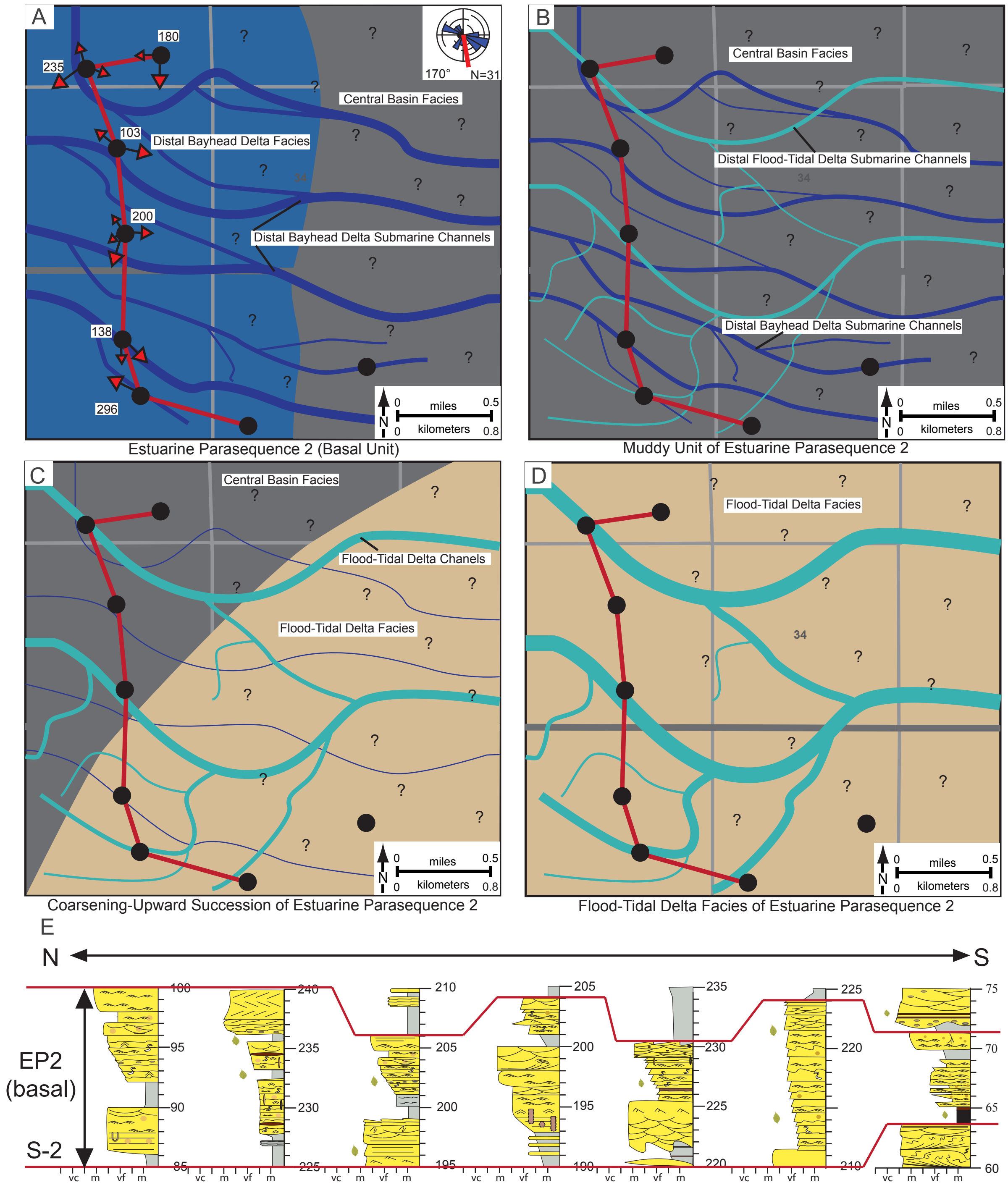

Fig. 44 Entire paleogeographic representation and interpretation of the evolution of the estuarine assemblage of estuarine parasequence 2 (EP2) (195-206 ft [59.5-62.8 m] on Fig. 34) overlain on the study-area base map (Fig. 7). Paleocurrents averaged 170° for the entire unit. A) Bayhead-delta facies. Large arrows show average paleocurrent orientation for each measured section. Smaller arrows show individual measurements (to show variance). See Figure 37 for key. B) Central-basin facies. C) Southward approach of flood-tidal-delta facies. D) Flood-tidal delta facies. E) Cross section showing strata of the estuarine assemblage strata of EP2, bounded at its base by S-2.

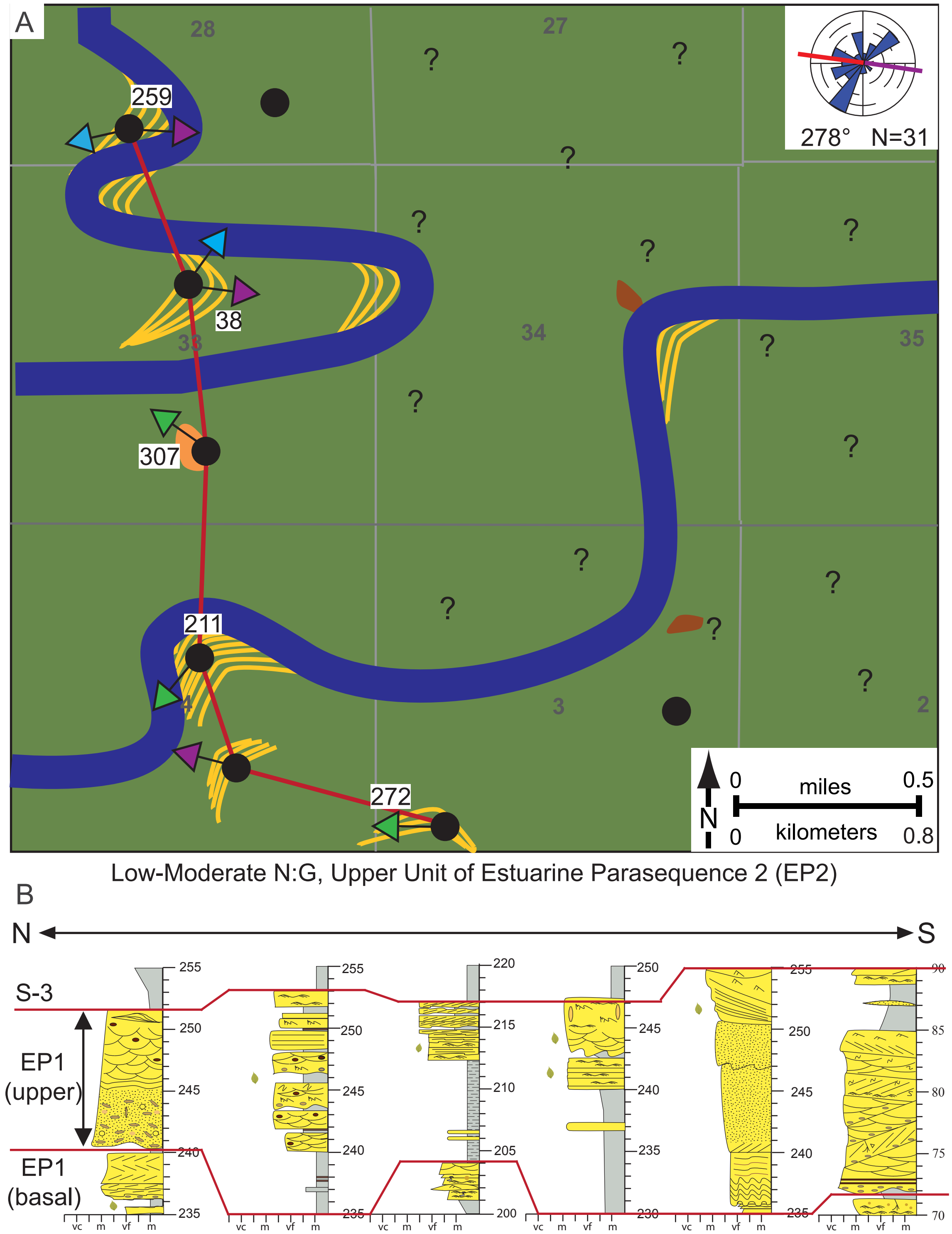

Fig. 45 A) Paleogeographic representation and interpretation of the low to moderate N:G (upper unit) of estuarine parasequence 2 (EP2) (206-253 ft [62.8-77.1 m] on Fig. 34) overlain on the study area base map (Fig. 7). Paleocurrents averaged 278°. Individual arrows on each measured section show vector mean for the architectural element shown. See Figure 37 for key. B) Cross section showing strata of the upper unit of EP2, bounded at its top by S-3.

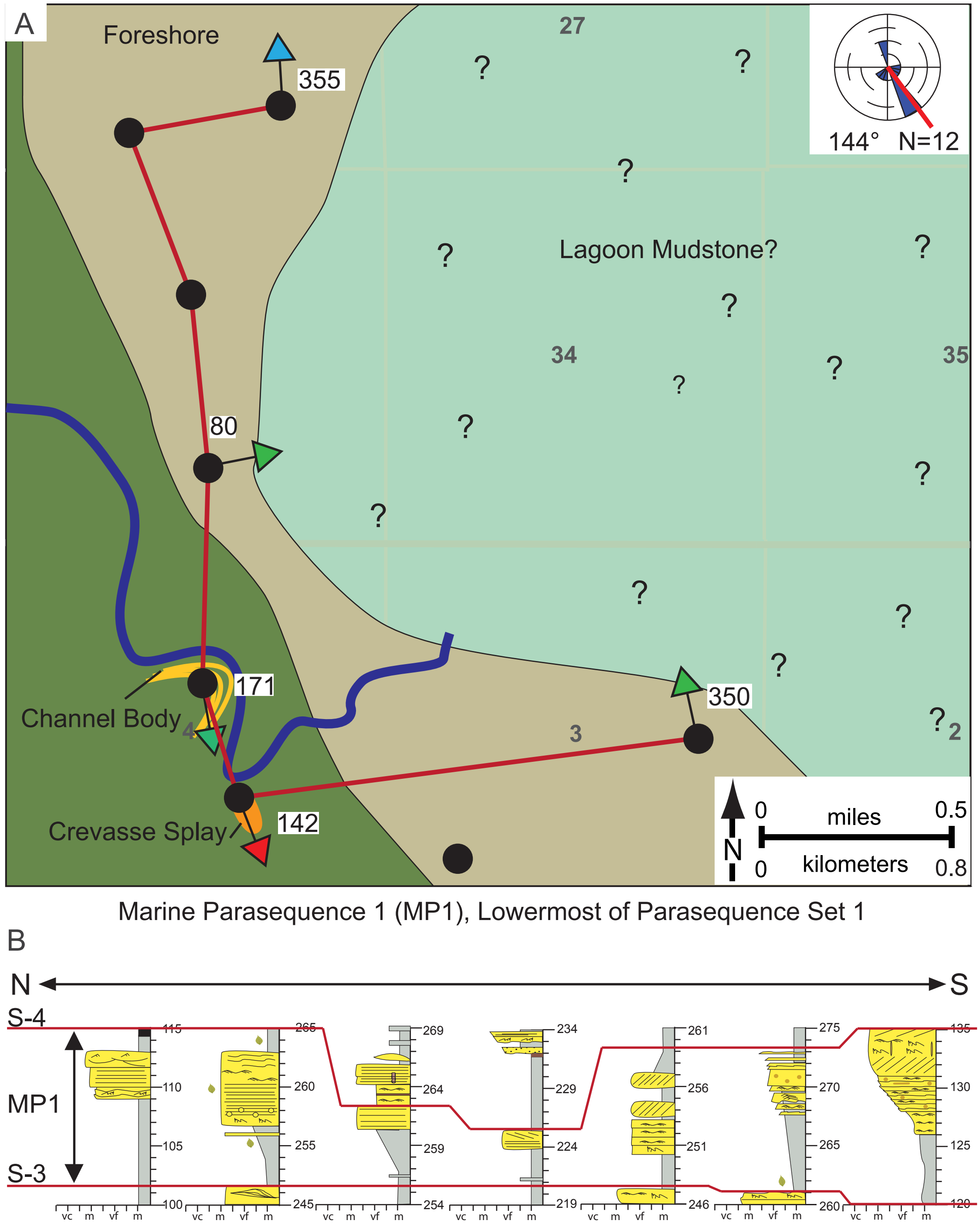

Fig. 46 A) Paleogeographic representation and interpretation of the lagoon foreshore strata of marine parasequence 1 (MP1), which forms the basal unit of parasequence set 1 (255-262 ft [77.7-79.9 m] on Fig. 34) overlain on the study-area base map (Fig. 7). Paleocurrents averaged 144°. Individual arrows on each measured section show vector mean for the architectural element shown. See Figure 37 for key. B) Cross section showing strata of MP1, bounded at its base by S-3 and its top by S-4.

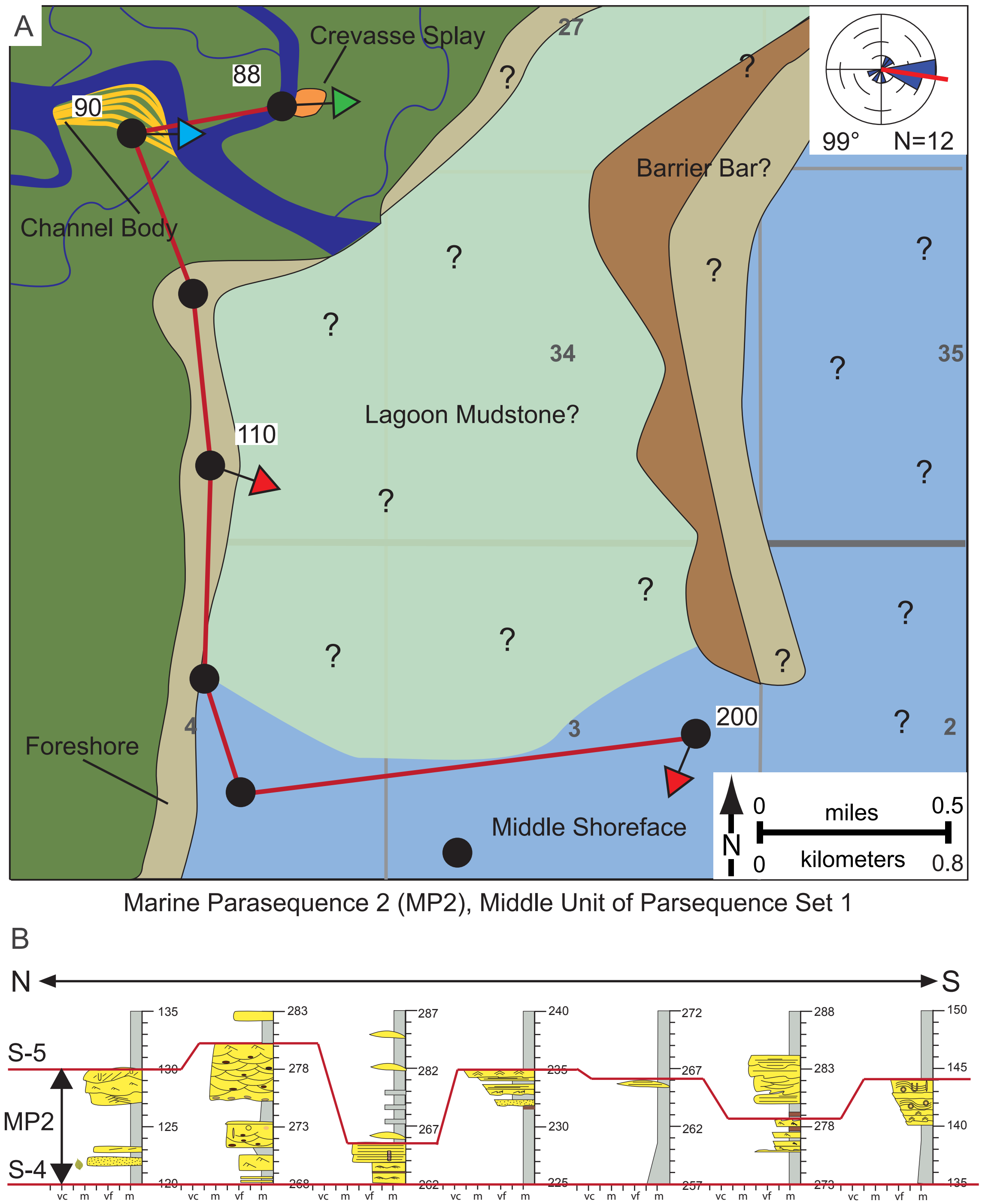

Fig. 47 A) Paleogeographic representation and interpretation of the lagoon strata of marine parasequence 2 (MP2), which forms the middle unit of parasequence set 1 (263-266 ft [80.2-81.1 m] on Fig. 34) overlain on the study-area base map (Fig. 7). Paleocurrents averaged 99°. Individual arrows on each measured section show vector mean for the architectural element shown. See Figure 37 for key. B) Cross section showing strata of MP2, bounded at its base by S-4 and its top by S-5.

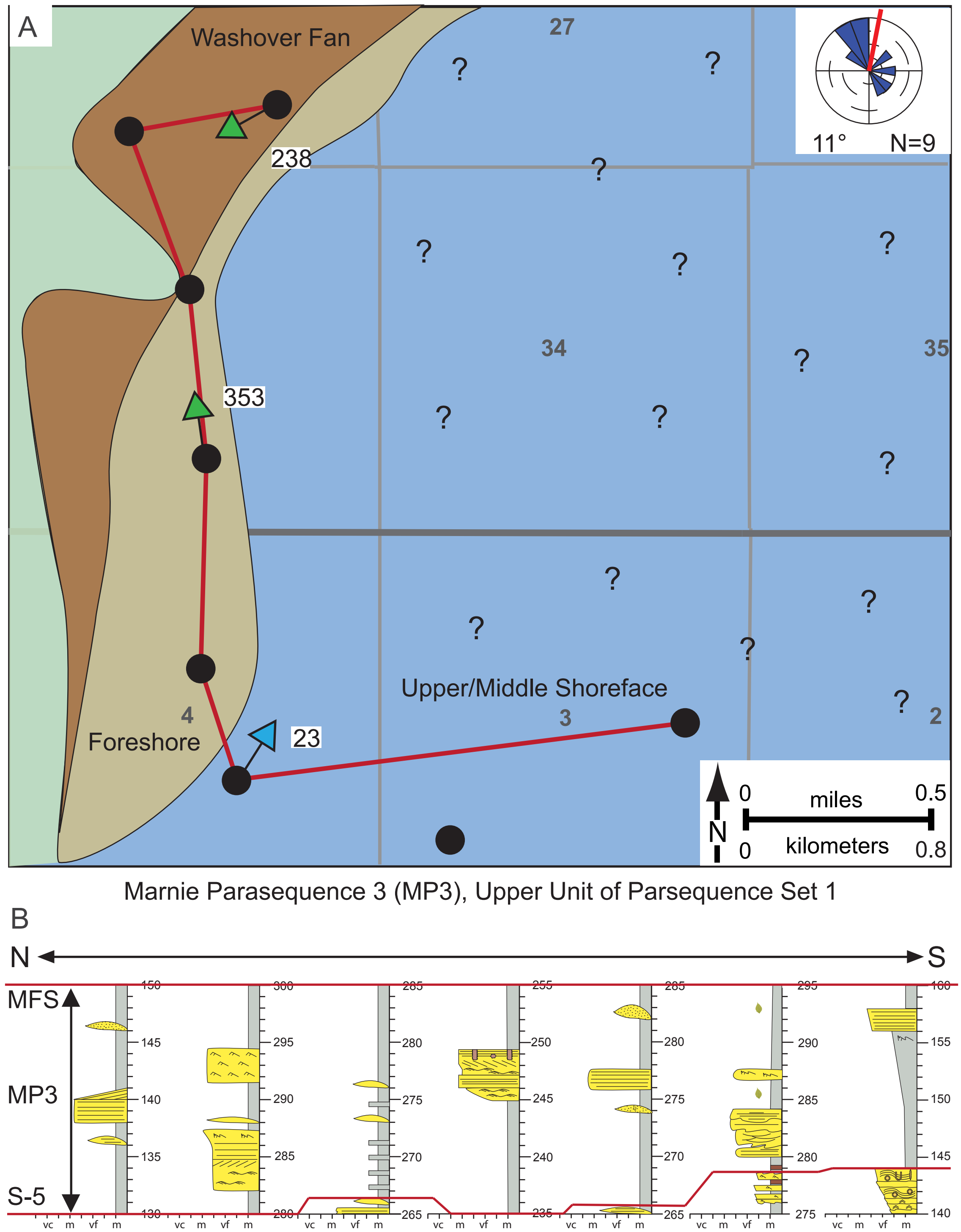

Fig. 48 A) Paleogeographic representation and interpretation of the barrier bar and marine strata of marine parasequence 3 (MP3), which forms the upper unit of parasequence set 1 (266-285 ft [81.1-86.9 m] on Fig. 34) overlain on the study-area base map (Fig. 7). Paleocurrents averaged 11°. Individual arrows on each measured section show vector mean for the architectural element shown. See Figure 37 for key. B) Cross section showing strata of MP3, bounded at its base by S-5 and at the top by the maximum flooding surface (MFS).

applied. Three parasequences are interpreted on the basis that each shoals and coarsens upward. These parasequences form a retrogradational parasequence set, on the basis that each parasequence thins and fines upward. Three flooding surfaces are present (S-3, S-4, and S-5). The depositional environment changes from the foreshore strandplain of a lagoon to the washover fans of the inland-migrating barrier-bar complex. The basinward direction is interpreted to be to the south based on lateral thicknesses, facies, and paleocurrent data. Parasequence set one is interpreted to be the TST based on: (1) the retrogradational stacking pattern and (2) the overall fining-upward nature of the unit. Flooding surface (S-3) represents a marine-flooding surface and a transgressive surface.

Maximum Flooding Surface (MFS).

A unit of thick, fissile mudstone exists at 276 ft (84.1 m) between PS1 and the next interval of strata. The gamma-ray readings are relatively high to very high (~300 cps) (Fig. 34). Mudstone intervals are black to dark-grey in color (Appendix F). This unit is laterally continuous, beyond the confines of the study area.

This unit of mudstone is believed to represent the maximum transgression, and contains a maximum-flooding surface (MFS) on the basis of: (1) the lateral continuity, (2) the high-gamma ray readings, (3) the retrogradational stacking of the facies below, and (4) the overlying facies, which suggest aggradational stacking. Thus, this unit indicates a turnaround in the depositional environment. Facies directly above this unit represent the deepest-water facies for the sandstone bodies, indicating that the maximum-water level occurred during this time. Exact stratigraphic placement of the

MFS is unknown, due to the lack of subdivision of the mudstone facies; however, it is believed to be located at the highest gamma-ray reading in the interval.

Highstand Systems Tract: Parasequences 4-5 (Parasequence Set 2)

Parasequences MP4 and MP5 represent a parasequence set (PS2) (280-303 ft [85.4-92.4 m]) (Fig. 34) which is bounded at its base by the MFS and at its top by a sequence boundary (B-3). It contains two parasequences separated by one flooding surface (S-7) of middle shoreface architectural elements (Figs. 49 and 50). Occasional coals are present (Appendix F). Gamma-ray data shows a very high reading at the base followed by funnel-shaped profile, with variable readings at the top (Fig. 34). This interval has a relatively consistent thickness (approximately 20 ft [6.1 m]), thickens to the north and southeast, and thins to the southwest (Fig. 35). Paleocurrent values averaged 260°, however, data are limited (N=3).

This interval was deposited in a shallow-marine environment, which consists of two parasequences. The stacking pattern suggests an aggradational parasequence set. The basinward direction is interpreted to be to the south and southeast using thicknesses and facies types (deeper-water facies to the southeast). This interval is bounded at its base by the MFS, thus, deposits above the MFS are within the highstand systems tract (HST) (Fig. 34). The highstand systems tract occurs during the late part of a relative sea-level rise, a stillstand, and the early part of a relative sea-level fall (Van Wagoner et al., 1988; 1990).

Sequence Three

Sequence three is bounded at its base by B-2 and continues upward to the top of the section, where it is eroded. Sequence three is composed of one estuarine

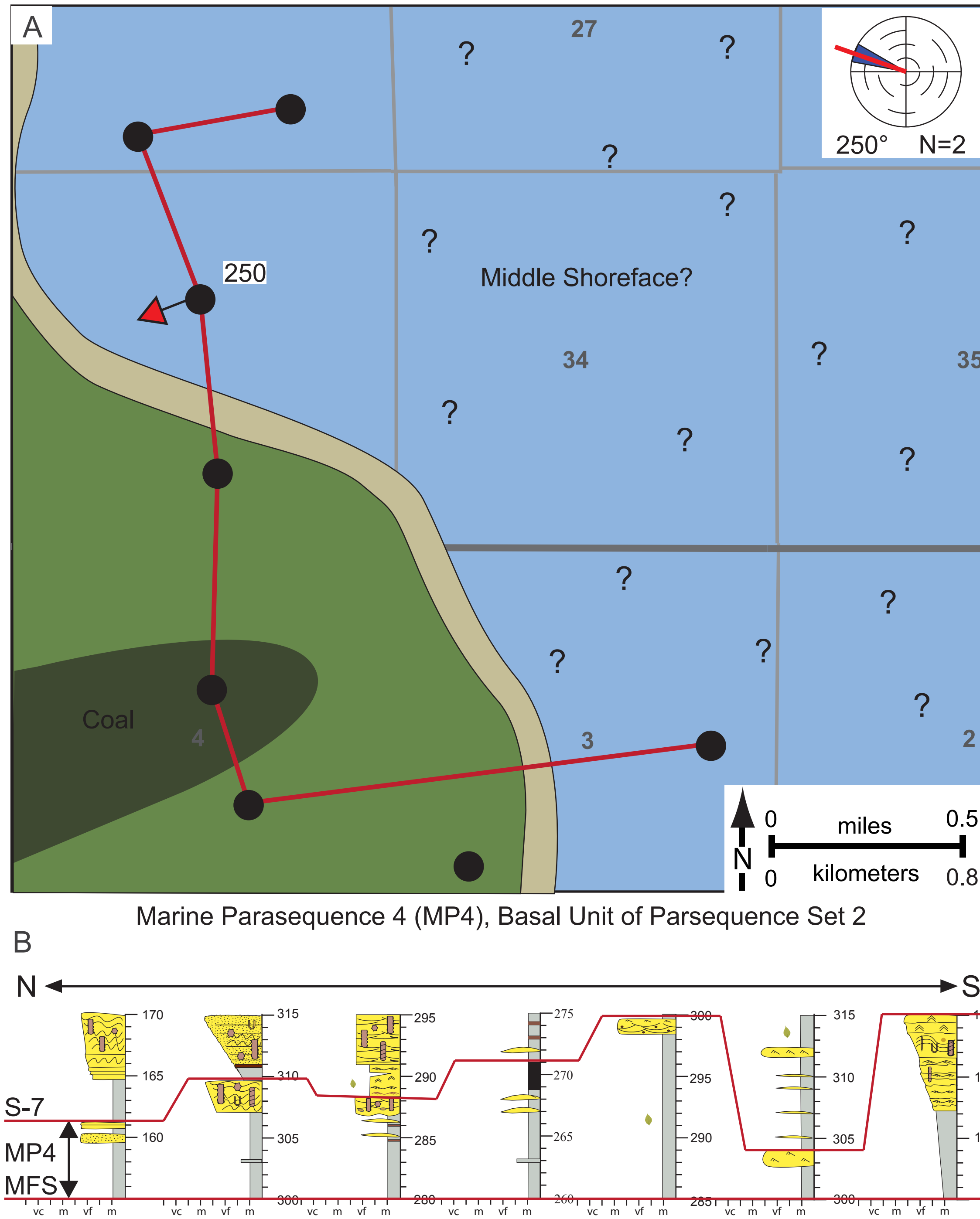

Fig. 49 A) Paleogeographic representation and interpretation of the marine strata of marine parasequence 4 (MP4), which forms the basal unit of parasequence set 2 (280-288 ft [85.4-87.8 m] on Fig. 34) overlain on the study-area base map (Fig. 7). Paleocurrents averaged 250°. Individual arrows on each measured section show vector mean for the architectural element shown. See Figure 37 for key. B) Cross section showing strata of MP4, which is bounded at its base by the MFS and its top by S-7.

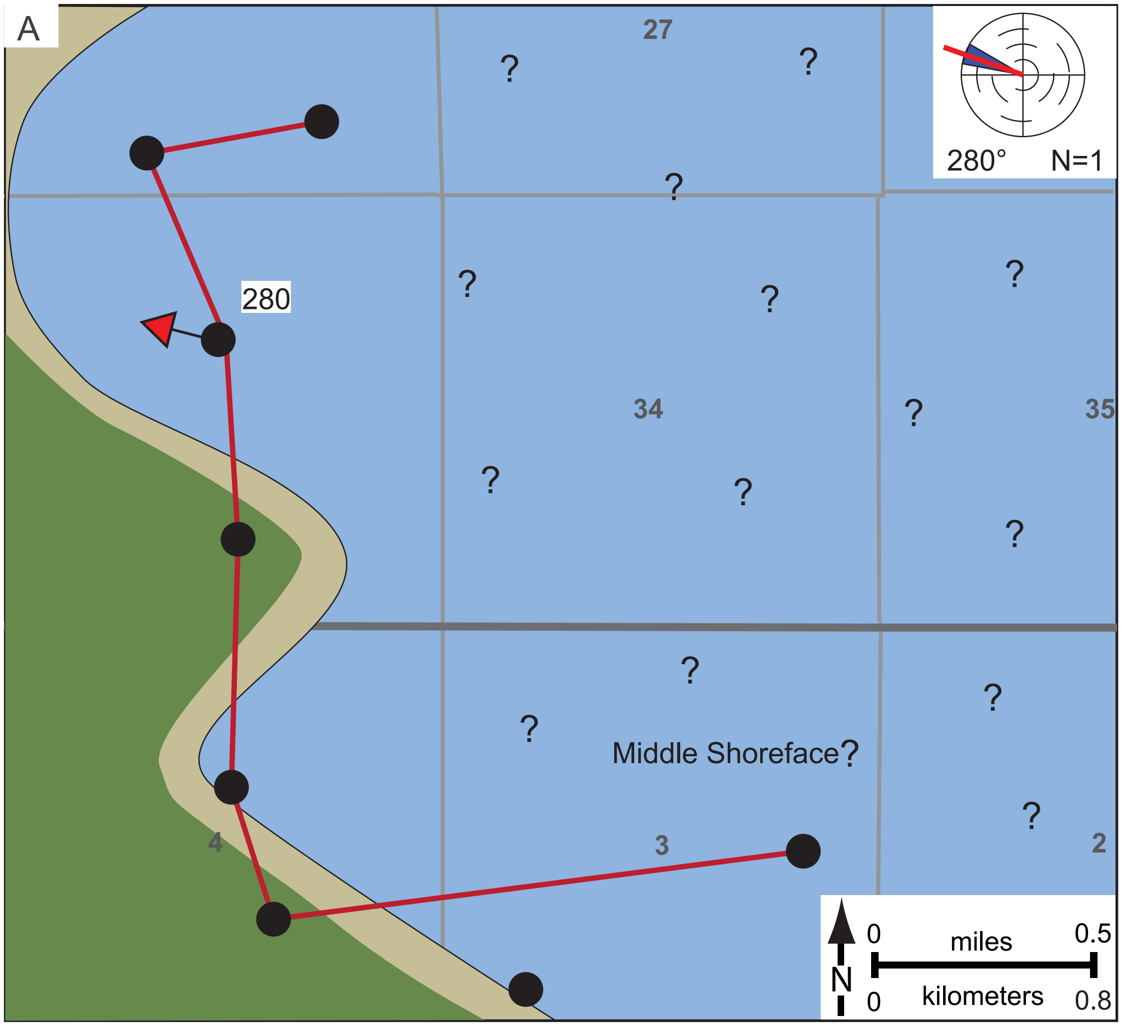

Marine Parsequence 5 (MP5), Upper Unit of Parsequence Set 2

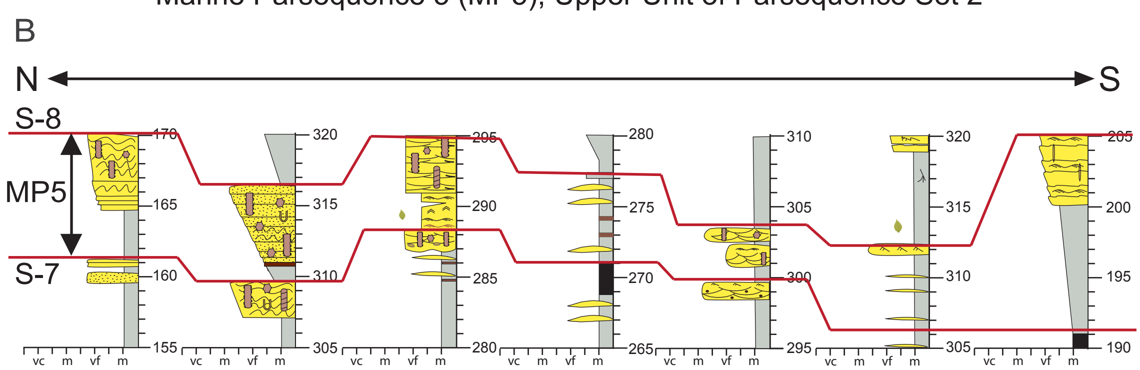

Fig. 50 A) Paleogeographic representation and interpretation of the marine strata of marine parasequence 5 (MP5), which forms the upper unit of parasequence set 2 (288-295 ft [87.8-89.9 m] on Fig. 34) overlain on the study-area base map (Fig. 7). One paleocurrent value is 280°. Individual arrows on each measured section show vector mean for the architectural element shown. See Figure 37 for key. B) Cross section showing strata of MP5, which is bounded at its base by S-7 and its top by S-8.

parasequence (EP3). These deposits overlie the ash zone and form the upper part of the “regressive interval”. Deposits of this interval may be equivalent to the Cameo Coal Zone of the lower Williams Fork Formation.

Sequence Boundary 3 (B-3)

Sequence boundary B-3 is marked by a distinct change from heavily bioturbated middle shoreface sandstone of PS2 to coal and associated mudrock of estuarine parasequence 3 (EP3). The surface is subtle, marked by a basinward shift in facies.

Lowstand Systems Tract: Estuarine Parasequence 3 (EP3)

Estuarine parasequence three (EP3) (303-325 ft [92.4-99.1 m]) (Fig. 34) is bounded by an estuarine flooding surface (S-8) at its base. There is no top because erosion has removed the overlying strata. This interval has variable thicknesses (25-50 ft [7.6-15.2 m]) (Fig. 35). This interval lies within the lower part of the ash zone, which has high gamma-ray values (sometimes >450 cps) (Appendix A). It contains two subunits: 1) basinward migrating tidal barforms of EP3 (Figs. 51 and 52); and 2) additional progradation of tidally influenced coastal-plain strata (Fig. 53). Paleocurrent values of tidal barforms averaged 320° (NW) (N=28). Gamma-ray data varied (Fig. 34). Paleocurrent values of the coastal-plain strata averaged 1°, (N=62). Total thicknesses are unknown.

The basinward direction is interpreted to be toward the southeast. Many of the paleocurrent values have a strong flood-tide influence, which is opposite (180°) from the tidal barform IHS. Overall, this interval demonstrates progradation, and is interpreted as the early and late lowstand systems tracts (Fig. 34).

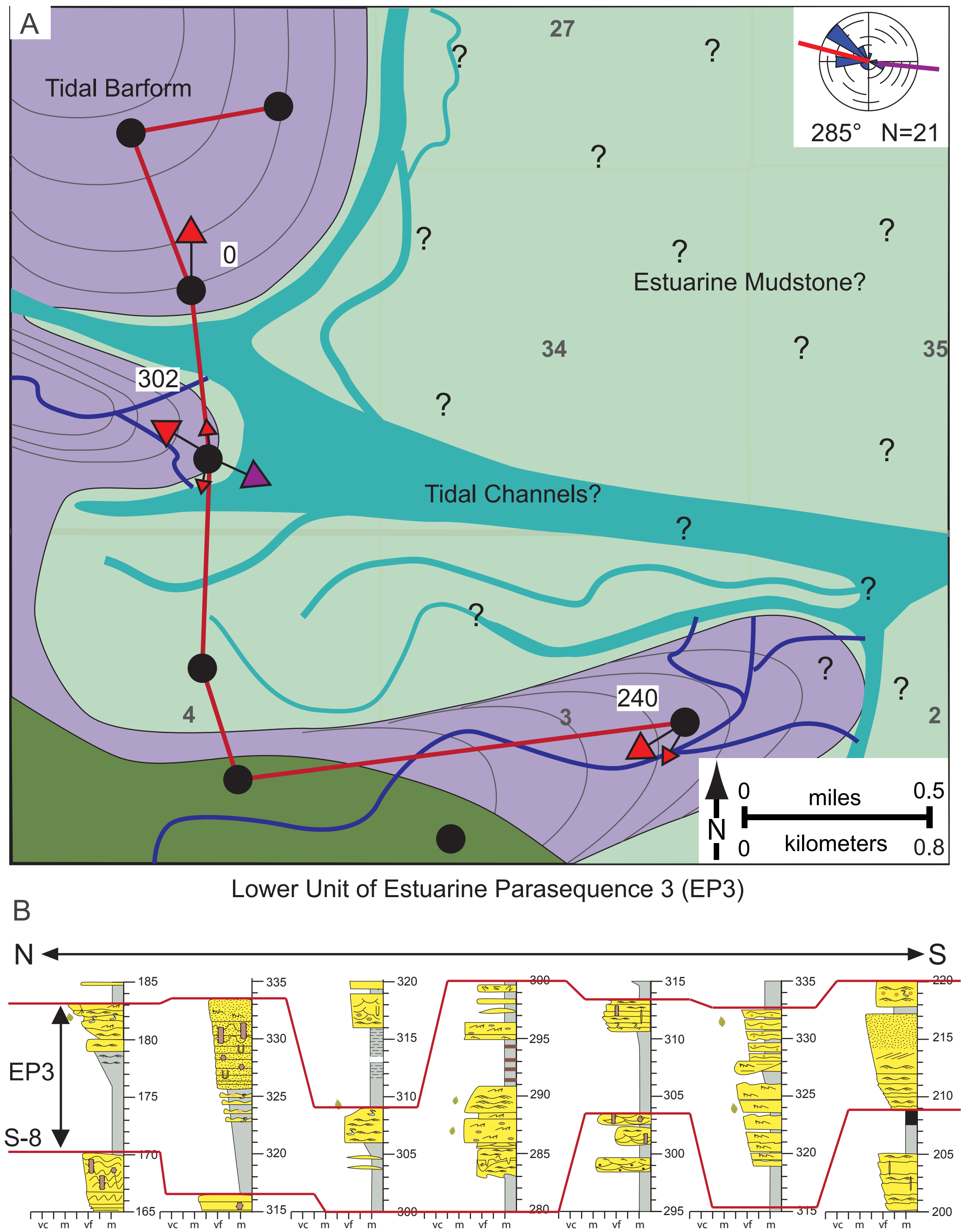

Fig. 51 A) Paleogeographic representation and interpretation of the estuarine strata (tidal barforms) of estuarine parasequence 3 (EP3) (295-309 ft [89.9-92.4 m] on Fig. 34 overlain on the study-area base map (Fig. 7). Paleocurrents averaged 285°. Individual arrows on each measured section show vector mean for the architectural element shown. See Figure 37 for key. B) Cross section showing strata of EP3, which is bounded at its base by S-8.

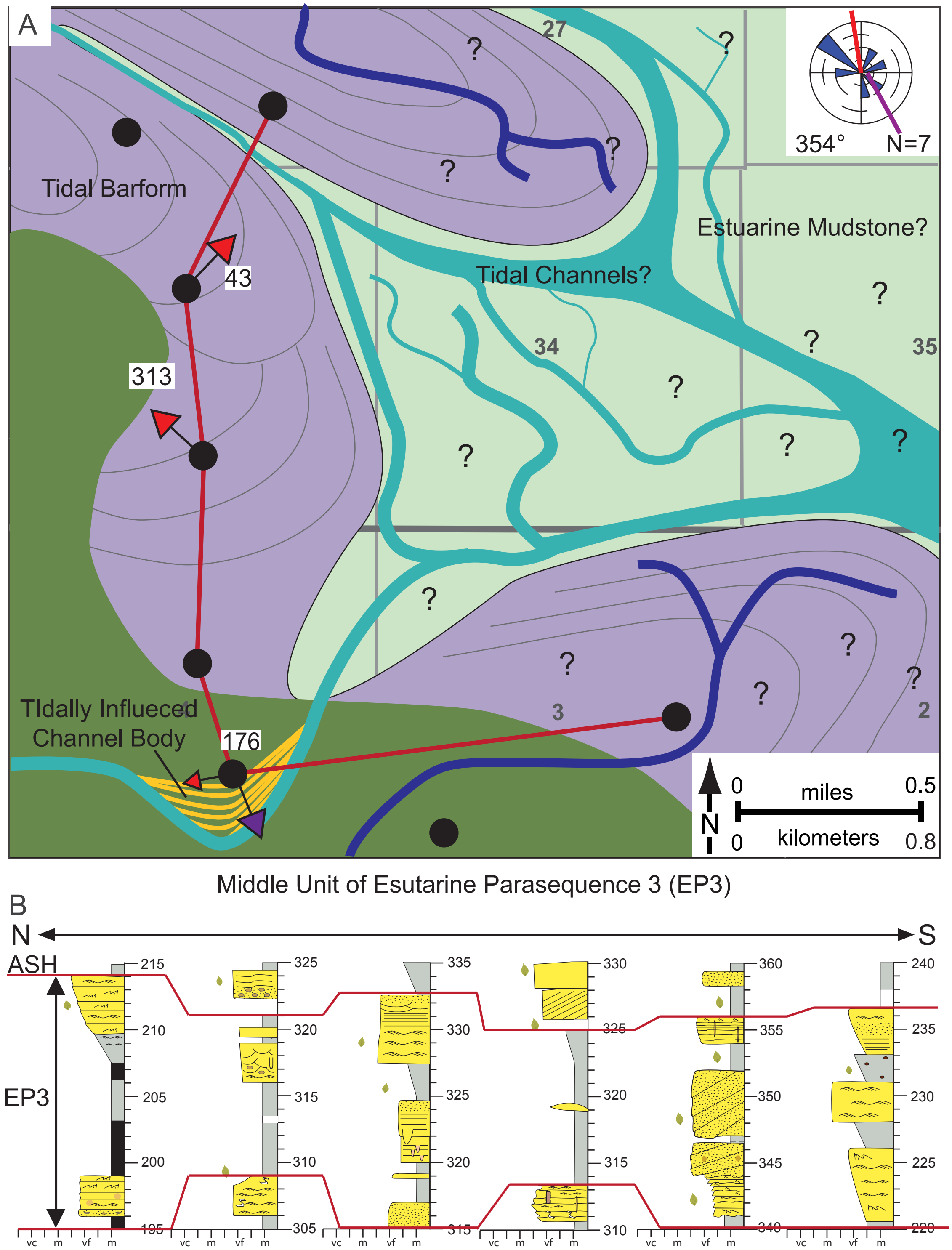

Fig. 52 A) Paleogeographic representation and interpretation of the estuarine strata (tidal barforms) of middle estuarine parasequence 3 (EP3) (309-333 ft [94.2-101.5 m] on Fig. 34) overlain on the study area base map (Fig. 7). Paleocurrents averaged 354°. Individual arrows on each measured section show vector mean for the architectural element shown. See Figure 37 for key. B) Cross section showing strata of EP3, which is bounded at its top by the ash.

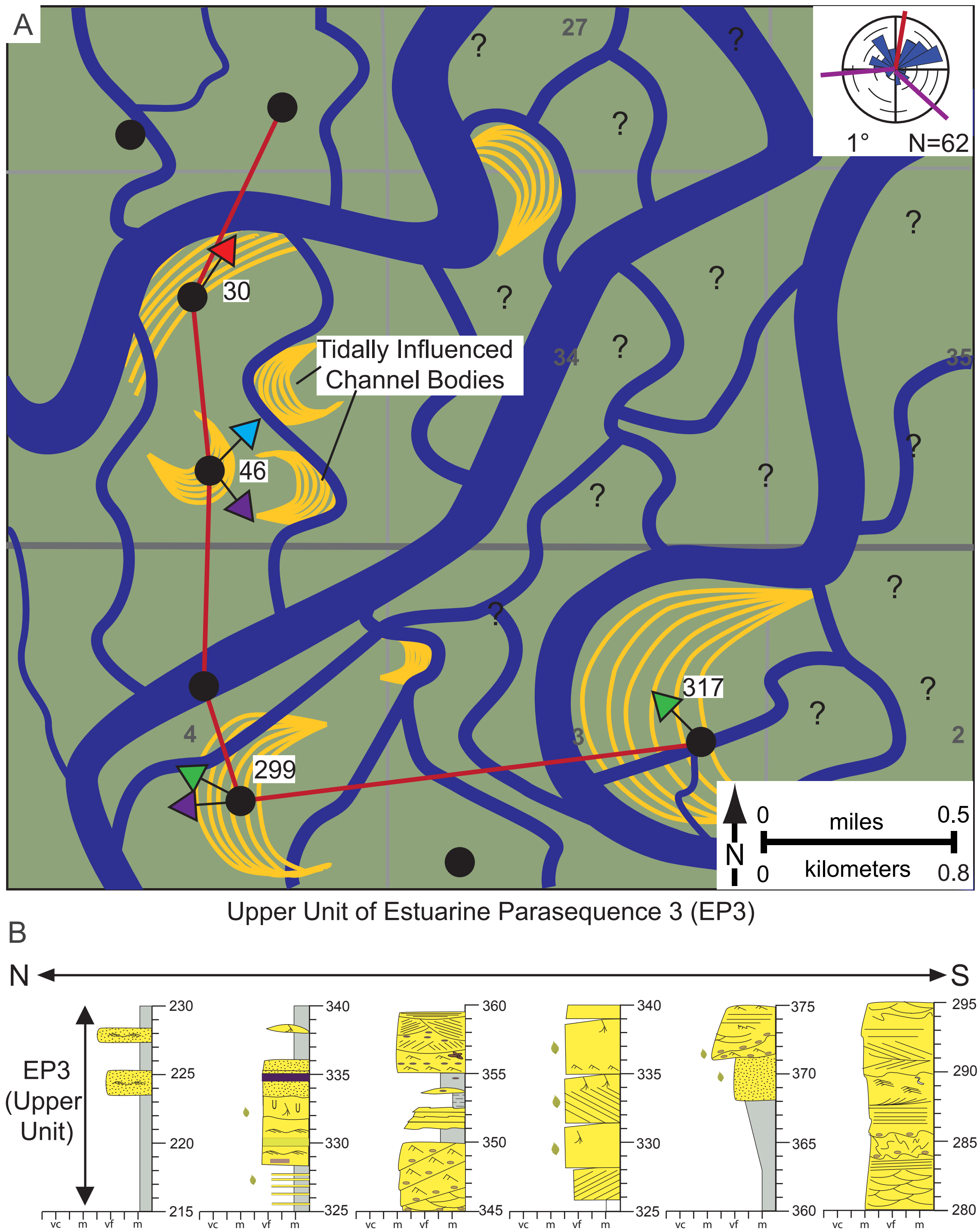

Fig. 53 A) Paleogeographic representation and interpretation of the tidally influenced coastal-plain strata of estuarine parasequence 3 (EP3) (333-360 ft [101.5-109.8 m] on Fig. 34) overlain on the study-area base map (Fig. 7). Paleocurrents averaged 1°. Individual arrows on each measured section show vector mean for the architectural element shown. See Figure 37 for key. B) Cross section showing the coastal-plain strata of EP3, which is bounded at its base by the ash (not shown) and is eroded at the top of the interval.

Alternate Interpretation

Allen and Posamentier (1993) outlined the sequence stratigraphy of estuarine deposits of the Gironde estuary within a fluvial-incised valley. The sequence is composed of lowstand, transgressive, and highstand systems tracts and associated bounding surfaces. A sequence boundary at the base of the study interval is expressed by an unconformity, which separates lowstand fluvial deposits from underlying Tertiary carbonates. The lowstand systems tract is composed of a continuous unit of relatively thin fluvial gravel and coarse sand. The TST is composed of estuarine point bars, tidal bars, and tidal flats, which onlap the alluvial plain. The transgressive surface underlies these deposits and is characterized by onlap onto the lowstand fluvial deposits. The MFS is where the regressive highstand estuarine muds prograde over transgressive tidal-estuarine muddy sands or estuary-mouth sands. In the landward end of the estuary, the maximum flooding surface would be very difficult to identify because it separates identical facies (tidal-estuarine point bars). In the seaward end of the estuary, the maximum flooding surface is recognized by a contact between estuarine muds and the underlying estuary mouth sands. The highstand systems tract forms a bayhead delta consisting of prograding tidal sand bars, tidal flats, and upper-estuary point bars.

The present study interval has many similarities with the study by Allen and Posamentier (1993). Using the ideas outlined in Allen and Posamentier (1993), the interval would be one full sequence. Strata above B-1 (CP1, high N:G) would form the amalgamated fluvial sandstone bodies of the ELST and LLST. Overlying this unit would be the transgressive surface and estuarine and coastal-plain strata of the TST. The MFS would be identified within the fine-grained strata between PS2 and PS3. In this case, the estuary-mouth sands described in Allen and Posamentier (1993) would be synonymous with the middle shoreface sandstone bodies described in the present study. The estuarine (tidal barforms) strata above the MFS would represent prograding tidal sand bars of the HST.

5. Limitations to the Sequence-Stratigraphic Interpretation

Sequence-stratigraphic concepts take into account rates of changes in sea level/base level, climactic conditions, subsidence, sediment supply, and tectonism (allocyclic), but not local changes within the system (autocyclic). Autocyclic controls include the slope of the coastal plain, slope of the shelf, vegetation, stream power, stream discharge, sediment load, coal and mud compaction (local subsidence), and lateral shifts in facies, channel belts, or depositional zones. Because strata studied in this interval are primarily coastal plain and the study area has a limited areal extent (2 mi^2 [3.2 km^2]), applying sequence stratigraphy to the study area is challenging. Additionally, strata in the study interval are a part of a foreland basin system of the Sevier orogenic belt to the west. Strata in this interval were heavily influenced by the foreland basin development in terms of accommodation space and sediment supply.

A study by Hickson et al. (2005) found that the 2-D variation in alluvial architecture is controlled very strongly by externally forced facies migrations such as changes in sediment supply, base level, or subsidence. Coastal-plain fluvial deposits are meandering, which mean avulsions occur frequently. The high N:G deposits in this study could be associated with channel avulsion and a subsequent lateral shift of a channel belt. In general, aggradation and degredation of channels reflect the balance between stream power and sediment supply (Blum and Törnqvist, 2000). Generally, channels aggrade when the sediment supply exceeds transport capacity of the discharge. Channels incise when transport capacity exceeds sediment supply. Additionally, both of these elements act on both a local and basinwide scale. Many of these processes also act on different time scales, therefore, determining exact cause of channel architecture is difficult to discern (Miall, 2006).

Friend et al. (1979) identified four controlling factors in channel-belt lateral migration vs. stability: (1) river mean flow strength; (2) bank strength; (3) flood periodicity and duration; and (4) vertical movement of the alluvial strata. Gibling (2006) also discussed the controlling factors in producing differing channel-body geometries and dimensions. As the bank migration rate increases relative to the channel aggradation rate, lateral accretion occurs. Conversely, if the channel aggradation rate increases with respect to the bank migration rate, a fixed channel pattern with vertical accretion occurs. If the area is reoccupied by channels frequently, a resulting pattern of amalgamation results.

The limited extent of the study area does not allow for lateral correlations from marine to coastal-plain strata. Additionally, correlation of the major bounding surfaces (sequence boundaries, flooding surfaces, and the maximum flooding surface) is limited. With a wider study area, these surfaces could be identified or modified, thus, changing the interpretation presented in this study. The presence of tidally influenced facies and marine facies indicates an overall transgression; however, placement of exact surfaces is unknown.

6. Summary

Based on previous basin-scale studies, the lower two-thirds of the study interval (Kmvl) is equivalent to the lower Corcoran, Cozzette, and Rollins Sandstone members of the Iles Formation in the Piceance Basin. The upper one-third of the study interval (Kmvc) is equivalent to the lower Williams Fork Formation of the Piceance Basin. The entire study interval is also equivalent to the Iles clastic wedge, as defined in the Sand Wash Basin.

Three sequences are identified and divided into systems tracts on the basis of proposed major boundaries and overall stacking patterns of estuarine or marine parasequences or coastal-plain packages. Sequence one contains CP1 and EP1 and represents the ELST to LLST bounded by sequence boundaries (B-1 and B-2). Sequence one is composed of coastal-plain and estuarine deposits believed to be within a local incised valley. Sequence two contains CP2, EP2, PS1, and PS2 and is bounded by B-2 and B-3. It contains four systems tracts: ELST, LLST, TST and HST. Between the TST and the HST lies the maximum flooding surface. Sequence two is composed of coastal-plain, estuarine, lagoon, and marine deposits. Sequence three contains EP3 and represents the early-to-late lowstand systems tracts. Sequence three is composed of estuarine tidal bars and tidally influenced coastal-plain deposits. In general, the entire study interval represents a transgressive-to-regressive cycle. Changes in depositional environment through time are represented on Figure 54.

There are multiple ways to interpret the strata observed in the study interval. Sequence-stratigraphic concepts derived by established studies in continental and marine settings are used as guidelines for interpretation. Continental settings are

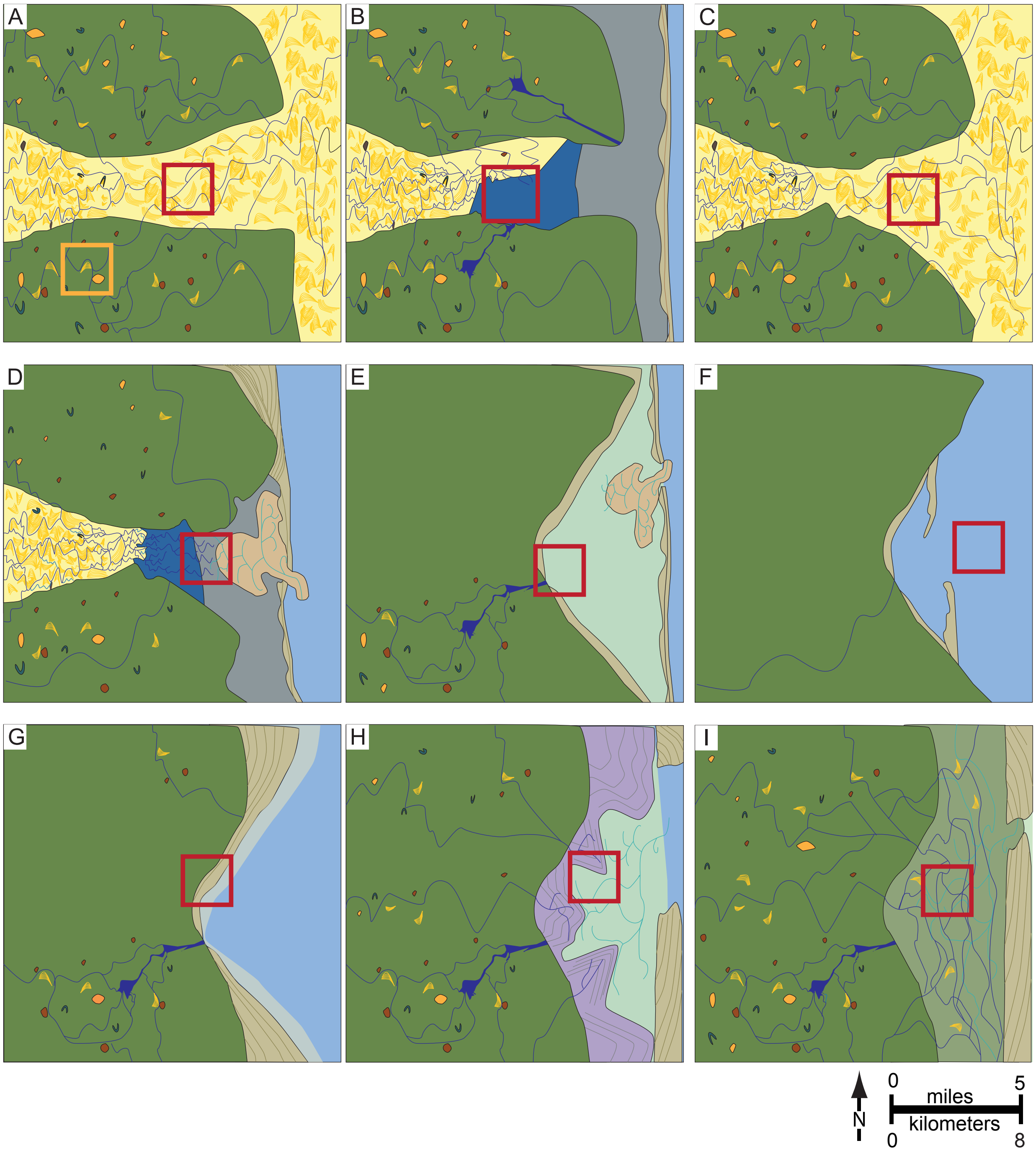

Fig. 54 Diagrams representing the depositional environments for each stratigraphic unit. A) Orange box shows basal unit of strata. Red box shows basal unit of coastal-plain package 1. B) Red box shows basal unit of estuarine parasequence 1. C) Red box shows basal unit of coastal-plain package 2. D) Red box shows basal unit of estuarine parsequence 2. E) Red box shows the lagoon of parasequence set 1. F) Red box shows maximum flooding. G) Red box shows shallow-marine parasequence set 2. H) Red box shows estuarine parsequence 3. I) red box shows additonal progradation of estuarine parasequence 3 (upper unit). See Figures 37-61 for more detailed information and see Figure 10B for key.

complex. Many factors can control sedimentation distributions including slope, vegetation, stream power, stream discharge, sediment load, local subsidence, and lateral shifts in facies, channel belts, or depositional zones. These controls are autocyclic, and may have no relation to relative changes in sea level.

CHAPTER FOUR

APPLICATIONS TO RESERVOIR CHARACTERIZATION

1. Introduction

Architectural elements are evaluated in terms of their dimensions, geometries, reservoir quality, and spatial distributions. Dimensions include apparent width and thickness. Apparent width is the linear distance between sandstone-body terminations in outcrop. This is related to the preserved size of the sandstone body at the time of deposition, the orientation of the sandstone body with respect to the canyon wall, and the degree of present day erosion (Cole and Cumella, 2005; Pranter et al., 2009). Geometries include two-dimensional (cross-sectional) shapes observed in outcrops and photopans. Coastal-plain architectural-element characteristics, dimensions, and geometries of this study are compared to outcrop-based data for the lower Williams Fork Formation in Coal Canyon, Colorado (Cole and Cumella, 2005; Panjaitan, 2006; Pranter et al., 2009). Facies type and distribution, dimensions, and geometries of each architectural element as well as petrographic analysis of thin sections determine relative reservoir quality of architectural elements. Relative reservoir quality is based on the potential porosity and permeability distribution, and potential baffles and barriers to flow for each architectural element analyzed in this study. Spatial distribution analysis includes architectural-element stratigraphic placement in terms of N:G packages within a sequence-stratigraphic framework. The study interval is divided into packages based on N:G, which includes: high (>80% sandstone), moderate (50-80% sandstone), and low (<50% sandstone).

2. Dimensions, Geometries, and Controlling Factors of Coastal-Plain Strata

2.1 Previous Studies

Anderson (2005) characterized five sandstone bodies (four point bars and one crevasse splay) in Iles Formation outcrops north of Rangely, Colorado. Both types of sandstone bodies have similar N:G, rock volume, facies, and average thickness. The distribution and architecture of the two types, however, are different. Point bars are isolated and less connected where as crevasse splays are laterally continuous and connected. Anderson (2005) determined that point bars have mounded 3-D shapes, with an average thickness of 18 ft (5.5 m). Crevasse splays have teardrop 3-D shapes with average thicknesses of 19 ft (5.8 m).

Caldes (2005) characterized fluvial sandstone bodies within Iles Formation outcrops east of Rangely, Colorado. Four main types of sandstone bodies were characterized: (1) isolated channel bodies; (2) amalgamated channel bodies; (3) low-angle crevasse splays; and (4) high-angle crevasse splays. The amalgamated channels have sand-on-sand contacts, are composed of trough cross-stratified sandstone, and lack any internal accretion surfaces. The lateral continuity of amalgamated channel bodies (as a whole) is 4,600 ft (1,402.4 m). Sandstone bodies could be larger, however, due to erosion and structural dip, could not be measured. A single channel body within the amalgamated channel bodies is 25 ft (7.6 m) thick and 700 ft (213.4 m) in length. Amalgamated channel bodies are highly connected and have lenticular 2-D geometries. Isolated channel bodies have abundant large-scale accretion surfaces, with abundant fine-grained material, and have a diverse facies assemblage. An individual sandstone body is 600 ft (182.9 m) in width and up to 35 ft (10.7 m) thick. Isolated channel bodies have lenticular 2-D geometries with no lateral connectivity to adjacent channel bodies. The low-angle crevasse splay is characterized by flat, horizontal bedding composed of a low-diversity facies assemblage embedded in floodplain strata. The low-angle crevasse splay has an average thickness of 8 ft (2.4 m) and an average length of 750 ft (228.7 m). The high-angle crevasse splay is characterized by high-angle bedding and a diverse facies assemblage embedded in floodplain strata. It has an average thickness of 30 ft (9.1 m) and an average length of 550 ft (167.7 m).

Caldes (2005) evaluated channel and crevasse splay facies associations in terms of their controlling factors: accommodation and sedimentation, or the accommodation-sedimentation ratio (A/S). Caldes (2005) proposed that a low A/S ratio suggests highly connected, amalgamated, low-diversity channel sandstone bodies, where as a high A/S ratio suggests low-connectivity, isolated, high-diversity channel sandstone bodies.

As mentioned previously, Shanley and McCabe (1991; 1993; 1994; 1995) evaluated depositional sequences in terms of depositional architecture, sandstone connectivity, sandstone-mudstone ratios, coal-bed geometry, and degree of shoreface and foreshore preservation. A balance between the rate of change in base level, sediment supply, and accommodation results in changes of these elements. High N:G ratios are commonly deposited due to low accommodation space, a high sediment supply, or low subsidence. Low N:G ratios are commonly deposited by high accommodation space, low sediment supply, or high subsidence.

Gibling (2006) summarized the dimensions (width and thickness) of more than 1,500 Quaternary fluvial bodies in various basins around the world. Three major groups of deposits are recognized: (1) mobile-channel belts (braided and low-sinuosity); (2) fixed channels and poorly channelized systems (distributaries, avulsion, and crevasse systems); and (3) valley fills (deep incision). Each of these groups produces differing channel-body dimensions and geometries. Fixed channels produce thick and laterally discontinuous channel deposits compared to mobile channels, which produce thin, laterally continuous channel deposits.

2.2 Data Collection Methods

In the present study, sandstone bodies (N=38) were measured by mapping sandstone-body pinchouts using global positioning systems (GPS; horizontal accuracy = 3 ft [1 m]) to obtain an apparent width measurement. Apparent width was calculated by finding the straight-line distance between the two pinch-out points mapped for each sandstone body. Sandstone-body thickness was measured every 20-30 ft (6.1-9.1 m) laterally (N=120) and averaged for each sandstone body (Appendix C). Measured architectural elements include discrete flood bodies (N=6), crevasse splays (N=9), and channel bodies (N=24). Dimensions of sandstone bodies are limited to those in which a lateral pinch-out point could be easily recognized. Therefore, measurements were all within low and moderate N:G intervals. Sandstone bodies are characterized by field descriptions (mini-measured sections; Appendix A), gamma-ray response (Appendix B), and paleocurrent values (Appendix D).

In the following discussion, coastal-plain architectural elements are evaluated in terms of geometries and dimensions (apparent width and thickness). Stratigraphic architecture of channel bodies is addressed in terms of mobile versus fixed-channel belts.

2.3 Discrete Flood Bodies

Discrete flood bodies consist of a single bed of asymmetric-ripple cross-stratified or structureless sandstone facies embedded in floodplain strata (Fig. 13). Discrete flood bodies are the smallest architectural element. The average apparent width is 61.5 ft (18.8 m) (N=6), and the average thickness is 1.6 ft (0.5 m) (N=10) (Table 4). Discrete flood bodies range from 20.0 ft (6.1 m) to 117.6 ft (35.8 m) in apparent width and from 1 ft (0.3 m) to 4.5 ft (1.4 m) in thickness. Average width-to-thickness ratio (W/T) is 39.3 (Fig. 55; Table 4). Two-dimensional (2-D) geometries are symmetrically lenticular (Fig. 56).

2.4 Crevasse Splays

Crevasse splays consist of coarsening-upward bedsets composed of asymmetrical-ripple cross-stratified, structureless sandstone, and muddy sandstone facies embedded in floodplain strata (Fig. 16). Crevasse splays are the second-smallest architectural element. The average apparent width is 90.5 ft (27.6 m) (N=9), and the average thickness is 1.8 ft (0.5 m) (N=18) (Table 4). Crevasse splays range from 30.0 ft (9.1 m) to 347.4 ft (105.9 m) in apparent width and from 1.0 ft (0.3 m) to 3.4 ft (1.0 m) in thickness. Average W/T is 44.9 (Fig. 55; Table 4). Crevasse splays are broadly lenticular, with some asymmetry in 2-D (Fig. 56).

2.5 Channel Bodies

Channel bodies include multiple lateral-accretion deposits composed of cross-stratified, ripple-cross stratified, and structureless sandstone facies. Channel bodies commonly fine upward and are either isolated or amalgamated (Fig. 17). The average apparent width is 287.7 ft (87.7 m), and the average thickness is 4.9 ft (1.5 m) (Table 4).

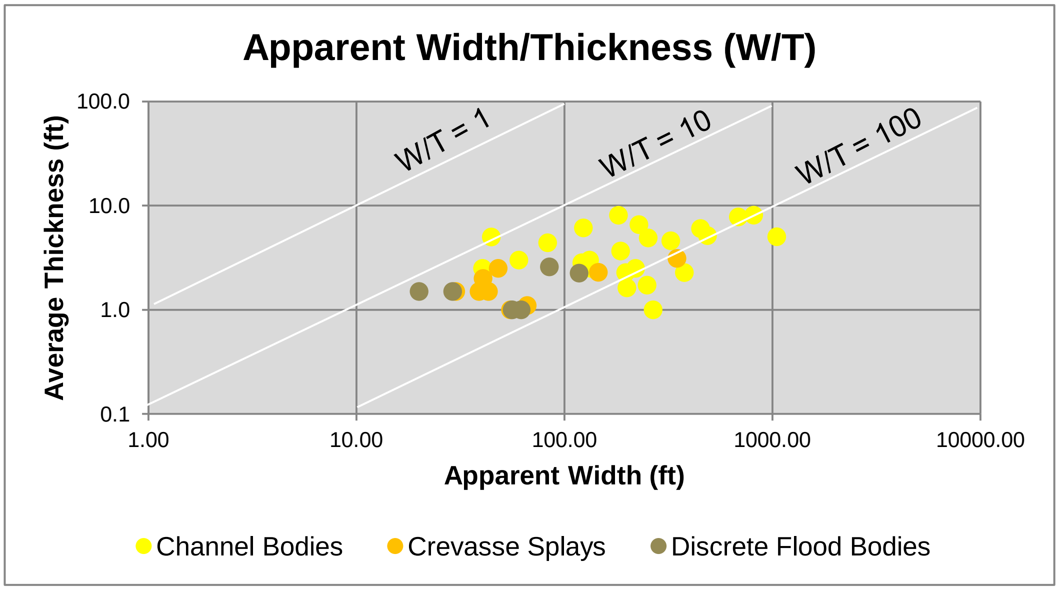

Fig. 55 Apparent-width to thickness (W/T) plot for the study area. Sandstone bodies include channel bodies (N=24) in yellow, crevasse splays (N=9), in orange, and discrete flood bodies (N=6), in brown. W/T ratios are shown on the white lines.

Architectural Element	N	Minimum	Mean	Median	Maximum	Standard Deviation
Discrete Flood Body	6					
Thickness (ft)	10	1.0	1.6	1.5	3.4	0.4
Apparent width (ft)		20.0	61.5	59.0	117.6	36.0
W:T ratio		13.3	39.3	45.5	61.9	20.4
Crevasse Splay	9					
Thickness (ft)	18	1.0	1.8	3.2	4.5	0.7
Apparent width (ft)		30.0	90.5	55.0	347.4	102.3
W:T ratio		19.2	44.9	20.3	111.6	30.9
Channel Body	24					
Thickness (ft)	92	1.0	4.9	4.1	30.0	3.5
Apparent width (ft)		40.4	287.7	199.6	1048.1	251.3
W:T ratio		8.9	72.5	59.9	266.7	61.7

Table 4 Summary of statistics for measured architectural elements. N = Number of measurements.

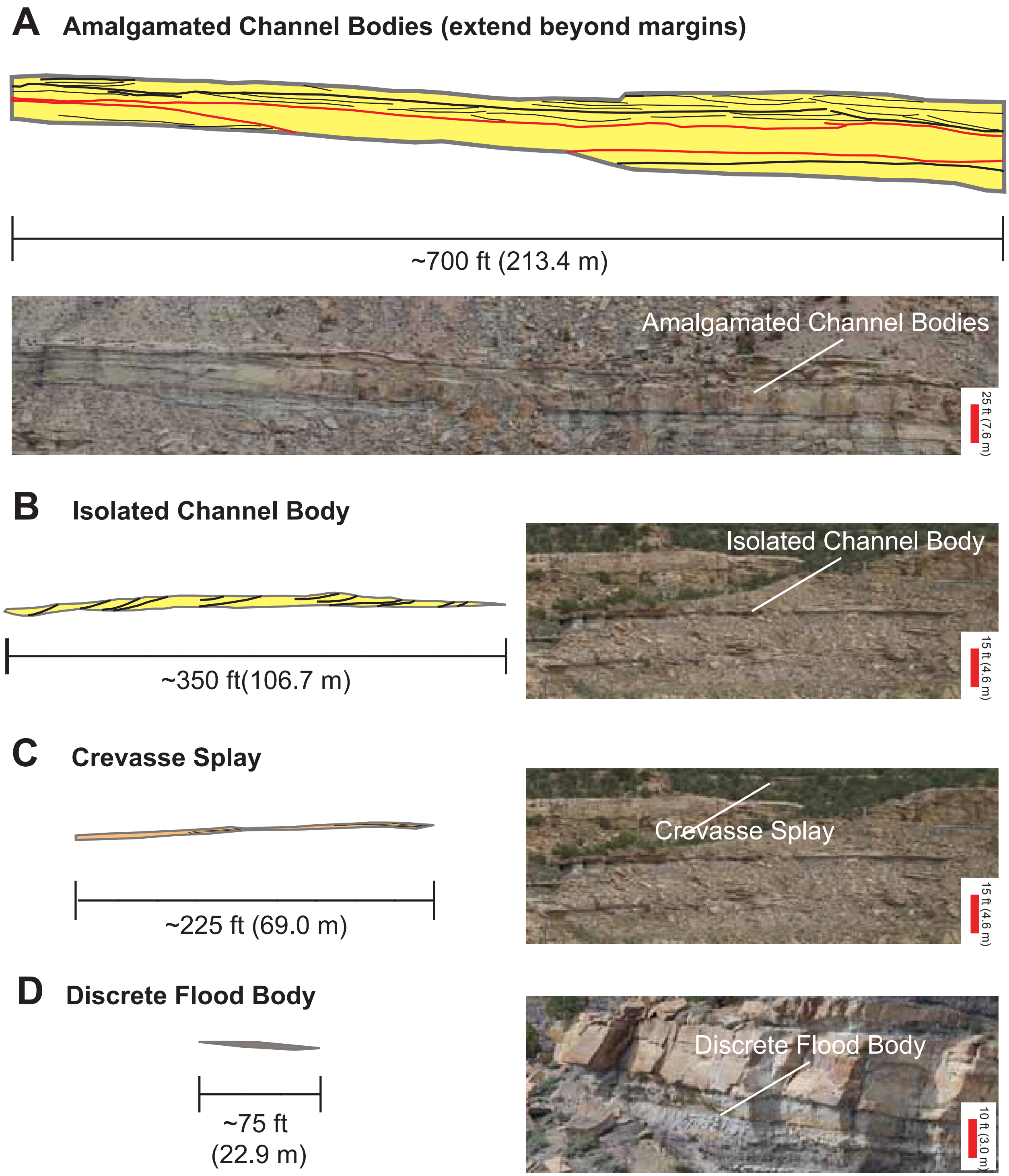

Fig. 56 Diagrammatic size-comparison and geometries chart showing internal and external geometries of coastal-plain architectural elements. A) Amalgamated channnel bodies, which contain multiple laterally and vertically stacked channel bodies. A single identified channel body is outlined in red to show a size comparison to the isolated channel body in part B. B) Isolated channel body. C) Crevasse splay. D) Discrete flood body.

Channel bodies range from 40.4 ft (12.3 m) to 1,048.1 ft (319.5 m) in width (N=24) and from 1 ft (0.3 m) to 30.0 ft (9.1 m) in thickness (N=92). Average W/T is 72.5 (Fig. 55; Table 4). From photopan and outcrop observations, individual channel bodies within the amalgamated, high N:G intervals are more laterally continuous (>1,000 ft [304.9 m]) than those in the low N:G intervals (Fig. 56). Some channel bodies, however, are much smaller in terms of apparent width and thickness due to erosion from overlying channels. In this case, the amalgamated sandstone bodies suggest mobile-channel-belt deposition. Conversely, the isolated sandstone bodies suggest fixed-channel-belt deposition.

2.6 Comparison to Coal Canyon

Cole and Cumella (2005) characterized 136 lenticular-to-channel-form sandstone bodies in 700 ft (213.4 m) of strata within the lower Williams Fork Formation in Coal Canyon, Colorado (Table 5). Sandstone bodies were traversed with a Trimble GeoExplorer differential GPS receiver. During mapping, sedimentological characteristics, thickness measurements, and paleocurrent measurements were recorded. Fourteen lithofacies were identified which included alluvial, floodplain, fluvial channel, splay, and lacustrine depositional environments. Five types of sandstone bodies were identified: (1) narrow; (2) simple sinuous; (3) compound sinuous; (4) crevasse-channel; and (5) crevasse-splay (Cole and Cumella, 2005). Narrow sandstone bodies have poorly defined lateral-accretion surfaces and well-developed levees and splays. Simple-sinuous sandstone bodies are characterized by well-developed lateral-accretion surfaces. Compound-sinuous sandstone bodies are characterized by multiple internal scours, lateral-accretion surfaces and amalgamation. Crevasse-channel

	COAL CANYON		THIS STUDY		
Architectural Element	Channel Body	Crevasse Splay	Channel Body	Crevasse Splay	Discrete Flood Body
# Measured	N=389	N=279	N=24	N=9	N=6
Min. Thickness (ft)	3.9	0.5	1.0	1.0	1.0
Max. Thickness (ft)	47.1	15.0	30.0	4.5	3.5
Avg. Thickness (ft)	10.4	5.1	4.9	1.8	1.6
Min. Apparent Width (ft)	44.1	40.1	40.4	30.0	20.0
Max. Apparent Width (ft)	2791.1	843.3	1148.1	347.4	117.6
Avg. Apparent Width (ft)	460.8	231.1	287.7	90.5	61.5
Avg. W/T Ratio	45.5	94.6	72.5	44.9	39.3

Table 5 Statistics comparing sandstone bodies measured in Coal Canyon, Colorado, and those measured in the present study (Cole and Cumella, 2005; Panjaitan, 2006; Pranter et al., 2009).

sandstone bodies are characterized by thin, narrow bodies with no distinct channel-form cross section. Crevasse-splay deposits are characterized by broadly lenticular geometries. Average sandstone-body thickness ranges between 0.5 ft (0.2 m) and 29 ft (8.8 m), with an average of 9 ft (2.7 m). Sandstone-body apparent width ranges between 40 ft (12.2 m) to 2,791 ft (850.9 m), with an average of 528 ft (161.0 m).

Studies by Panjaitan (2006) and Pranter et al. (2009) address the abundance, stratigraphic position, apparent width, thickness, and connectivity of sandstone bodies in the lower Williams Fork Formation in Coal Canyon, Colorado. A combination of field descriptions, global positioning system (GPS) traverses, and high-resolution aerial light detection and ranging (LiDAR) data, digital orthophotography, and ground-based photomosaics were used to map and document the abundance, stratigraphic position, and dimensions of single-story and multistory channel bodies and crevasse splays. Deposits include isolated, lenticular sandstone bodies deposited by meandering river systems. Sandstone bodies (N=688) were measured (including the 136 from the Coal and Cumella [2005] study) and included three main types: (1) single-story channels (N=116); (2) multistory channels (N=273); and (3) crevasse splays (N=279). Average single-story channel thickness is 12.3 ft (3.8 m) and average apparent width is 339.5 ft (103.5 m) (Pranter et al., 2009). Average multistory-channel thickness is 19.1 ft (5.8 m) and average apparent width is 512.3 ft (156.2 m). Crevasse-splay average thickness is 5.1 ft (1.6 m) and average apparent width is 231.1 ft (70.5 m).

In the present study, sandstone bodies (N=38) are characterized and included channel bodies, comparable to the single-story channels of Pranter et al. (2009). The crevasse-splays are comparable to those defined by Pranter et al. (2009). Discrete flood bodies are indentified only in this study. In the following discussion, the results of the present study are compared to those completed in Coal Canyon, Colorado.

Coal Canyon sandstone bodies are part of a coastal-plain facies association, where as the present study interval includes estuarine, lagoon, and shallow-marine facies associations. Sandstone bodies in the present study interval are compared to those of Coal Canyon in terms of dimensions in Table 5. The sandstone bodies of this study area tend to be smaller, approximately by 50%, than those of Coal Canyon. Width-to-thickness ratios in Coal Canyon are comparable to those in the present study (Fig. 57). Sandstone bodies of this study have similar geometrical forms of those in Coal Canyon, including broadly lenticular shapes in crevasse splays and lenticular forms in channel bodies. Single-story and multistory channels have been noted in both areas.

Because Coal Canyon exposes outcrops of the lower Williams Fork Formation (Kmvc interval) and is approximately 40 mi (64.4 km) south of the present study area, there can be a wide range of possibilities to explain the differences between the study areas. The present study area lies within the Kmvl interval, which contains shallow-marine and tidally influenced strata, unlike the Kmvc (Coal Canyon study interval). Additionally, outcrop exposures with relation to paleocurrent orientation can highly affect to the apparent dimensions of a sandstone body. For both study areas, large sandstone bodies, which were eroded by modern processes, are not included into the dataset.

3. Qualitative Reservoir Characteristics of Architectural Elements

A qualitative assessment of architectural-element reservoir quality is described. It is important to note that the reservoir quality assigned to each architectural element is given with respect to the others within this study. Reservoir quality is not assigned

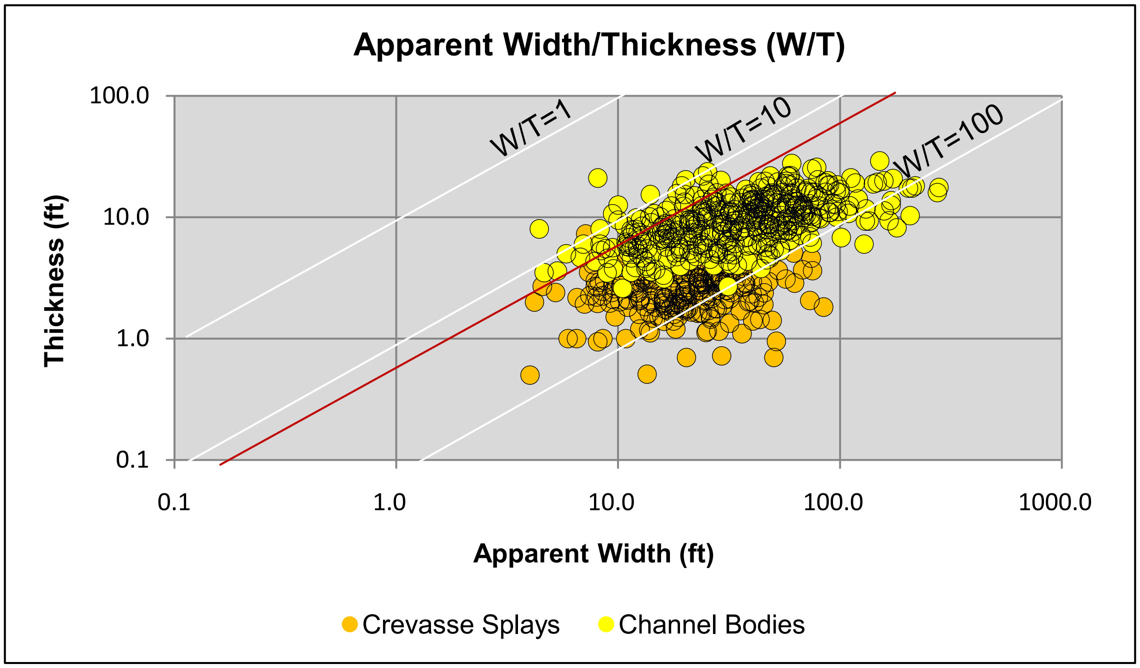

Fig. 57 Apparent width-to-thickness (W/T) plot for the Coal Canyon, Colorado study area. Sandstone bodies include channel bodies (N=389) in yellow and crevasse splays (N=279), in orange. W/T ratios are shown on the white lines (Cole and Cumella, 2005; Panjaitan, 2006; Pranter et al., 2009).

based on previous studies or subsurface data. Each architectural element is addressed in terms of lithology, facies, frequency of occurrence, dimensions, geometries, spatial distributions, and petrographic properties. Petrographic properties include point counts (N=100) of grain composition and grain, porosity, and cement percentages (Appendix G). However, diagenesis and cementation are directly impacted by outcrop weathering, therefore these values are not interpreted.

Lithologies and the facies present within an architectural element have a direct impact on reservoir recovery. For example, well-sorted sandstone bodies are commonly better reservoirs than poorly sorted muddy sandstone bodies. Internal lithologies and facies can also create internal compartments (i.e., mudrock drapes on lateral-accretion deposits) (Pranter et al., 2007). As stated previously, percentages of architectural elements are based on total footage represented by each architectural element on the measured sections divided by the total footage of all architectural elements combined. Dimensions and 2-D geometries are evaluated based on photopans and ground measurements. The cross-sectional area was calculated by multiplying the apparent width and average thickness for each architectural element. Suggested 3-D geometries are proposed for each architectural element based on present-day plan-view images as viewed from Google Earth. Spatial distribution directly relates to a particular architectural element’s placement within a lateral or vertical extent. Thin sections were evaluated in terms of framework composition (based on 100 point counts), grain textures, cement, sorting, and relative porosity (Appendix G; Table 6). Figure 58 shows a summary the architectural-element analysis.

Sample #/AE*	Textures	Framework Composition (%)	Grains/Cement/Porosity	Comments	4x Photo - uncrossed polars
PC6/Crevass eSplay	**Grain Size:** Upper fine- Lower Medium **Roundess:** subangular- subrounded **Sorting:** Well	**Quartz:** 68 **Chert:** 16 **B/M*:** <1 **Feldspar:** 6 **Chalcedony:** <1 **RG/MCC*:** 10 **Calcite:** <1	**Grains:** 66% **Cement:** 19% - kaolinite **Porosity:** 15%	grain replacement, some sutured grains, some unknown grains - possible organisms, no bioturbation	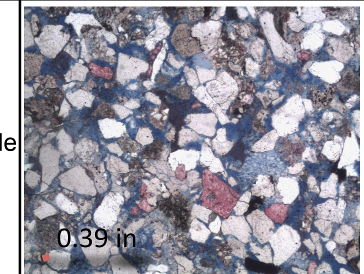
PC22 /Channel Body	**Grain Size**: Lower fine **Roundness:** subangular - subrounded **Sorting:** Poor	**Quartz:** 58 **Chert:** <1 **B/M*:** 2 **Feldspar:** 24 **RG/MCC*:** 16	**Grains:** 61% **Cement:** 22% - hematite **Porosity:** 17%	some grains aligned within the hematite stained area, hematite creates lining, grains are aligned - bimodal distribution, moderate bioturbation	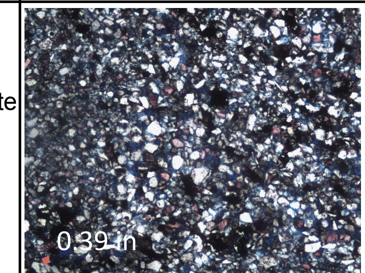
PC40/Delta Front	**Grain Size:** Upper Very Fine **Roundness:** angular - subrounded **Sorting:** Moderate-poor	**Quartz:** 74 **Chert:** 3 **B/M*:** 1 **Feldspar:** 18 **RG/MCC:** 3 **Zircon:** <1 **Unknown:** 1	**Grains:** 82% **Cement:** 0% **Porosity:** 18%	patchy clay,graded with some abrupt grain-size contacts, grain dissolution, cryptic bioturbation	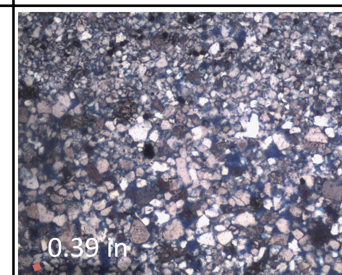
PC70/Flood-Tidal Delta	**Grain Size:** Lower Medium **Roundness**: subrounded- round **Sorting:** Poor	**Quartz:** 59 **Chert:** 16 **B/M*:** <1 **Feldspar:** 8 **SRF*:** 6 **RG*:** 10 **Unknown:** 1 **Zircon:** <1	**Grains:** 56% **Cement:** 28% - kaolinite, opaques, clays, quartz overgrowth **Porosity:** 16%	bedded, grain alignment, and in bands, partially dissolved grains, chert has ghosting - remnants of halimeda, grain that had dolomite in it - since dissolved away, rare bioturbation	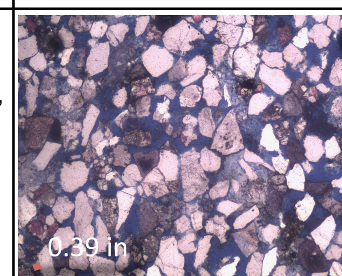

Sample #/AE*	Textures	Frameowrk Composition (%)	Grains/Cement/Porosity	Comments	4x Photo - uncrossed polars
PC80/Point Bar	**Grain Size:** Lower Medium **Roundness:** subangular - subrounded **Sorting:** Moderate	**Quartz:** 69 **Chert:** 12 **B/M*:** 2 **Feldspar:** 8 **RG*:** 7 **Unknown:** 2	**Grains:** 72% **Cement:** 22% - quartz overgrowth, calcite, illite and smectite, opaques, kaolinite **Porosity:** 6%	grain dissolution, cements abundant, no bioturbation	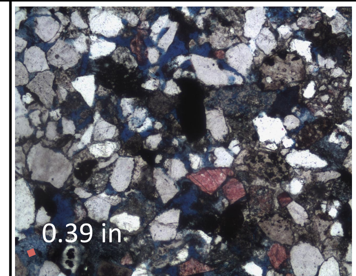
PC110/Point Bar	**Grain Size:** Upper fine **Roundness:** angular - rounded **Sorting:** Moderate -poor	**Quartz:** 57 **Chert: 2** **B/M*:** 1 **Feldspar:** 20 **RG*:** 19 **In Situ Mud:** 1	**Grains:** 74% **Cement:** 10% - opaques, quartz overgrowth, calcite, kaolinite **Porosity:** 16%	grain alignment, fine layers, drapes of mud, no bioturbation	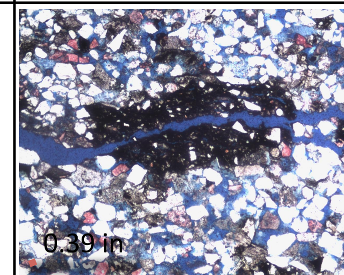
PC130/Middle Shoreface	**Grain Size:** Upper fine **Roundness:** subangular - subrounded **Sorting:** Moderate	**Quartz:** 68 **Chert:** 10 **B/M*:** 2 **Feldspar:** 12 **RG*:** 8	**Grains:** 68% **Cement:** 6% - opaques, kaolinite, quartz overgrowth **Porosity:** 26%	chert ghosting, unknown organism, grain dissolution, not as much grain replacement, rare bioturbation	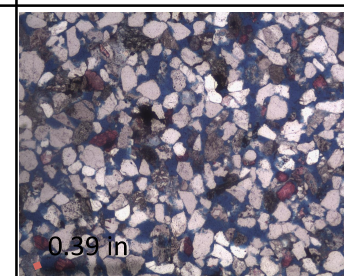
PC140/Middle Shoreface	**Grain Size:** Fine Lower **Roundness:** subangular - subrounded **Sorting:** Moderate - well	**Quartz:** 65 **Chert:** 13 **B/M*:** 1 **Feldspar:** 17 **RG*:** 3 **Unknown:** 1	**Grains:** 71% **Cement:** 6% - opaque rims around grains, quartz overgrowth **Porosity:** 23%	kaolinite rare, laminated with grain alignment, rare bioturbation	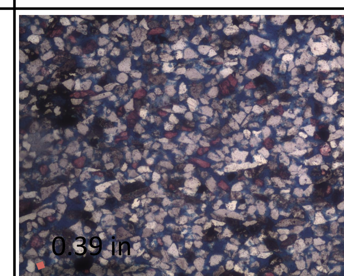

Sample #/AE*	Textures	Framework Composition (%)	Grains/Cement/Porosity	Comments	4x Photo - uncrossed polars
PC206/Tidal Barform	**Grain Size:** Middle Very Fine **Roundness:** angular -rounded **Sorting:** Moderate - well	**Quartz:** 78 **Chert:** 3 **B/M*:** 0 **Feldspar:** 6 **In Situ Mud:** 13 **Zircon:** <1	**Grains:** 69% **Cement:** 8% - opaques, clay, calcite, quartz overgrowth **Porosity:** 23%	simple composition, no kaolinite, grain dissolution, muddy patches, hard to see grains, moderate bioturbation	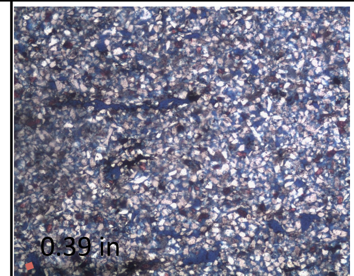
PC220/Tidal Barform	**Grain Size:** Very Fine Upper **Roundness**: angular - subrounded **Sorting:** Moderate - well	**Quartz:** 70 **Chert:** 8 **B/M*:** 0 **Feldspar:** 12 **Unknown:** 4	**Grains:** 66% **Cement:** 8% - opaques, quartz overgrowth **Porosity:** 26%	moderate bioturbation with hematite rims around burrow edge grains hard to see, muddy patches, very little kaolinite	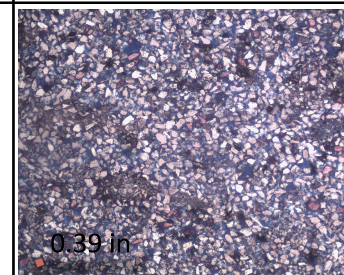
PC230/Tidal Barform	**Grain Size:** Fine Lower **Roundness:** angular - subrounded **Sorting:** Moderate - well	**Quartz:** 72 **Chert:** 8 **B/M*:** 0 **Feldspar:** 15 **In Situ Mud:** 4	**Grains:** 74% **Cement:** 4% - quartz overgrowth **Porosity:** 22%	simple composition,little hematite staining, rare to no kaolinite, grain dissolution common, moderate bioturbation causes muddy patches	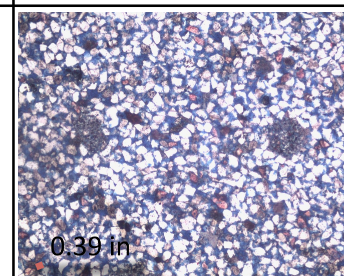
PC235/Tidal Barform	**Grain Size:** Lower Fine **Roundness:** subangular - subrounded **Sorting:** Moderate	**Quartz:** 40 **Chert:** 10 **B/M*:** 0 **Feldspar:** 10 **Opaques:** 10 **RG*:** 30	**Grains:** 76% **Cement:** 24% - clays, opaques, calcite **Porosity:** <1%	unknown grain type, contains lots of mud, laminated, grain alignment, very little kaolinite, lots more feldspar, orange looking replacement, rare bioturbation	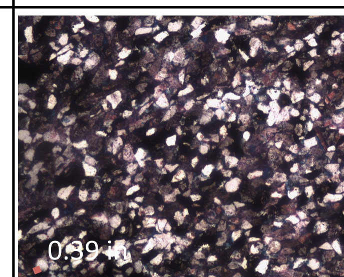

Sample #/AE*	Textures	Framework Composition (%)	Grains/Cement/Porosity	Comments	4x Photo - uncrossed polars
PC251/Point Bar	**Grain Size:** Upper Fine **Roundness:** subangular - rounded **Sorting:** Moderate - well	**Quartz:** 68 **Chert:** 16 **B/M*:** 0 **Feldspar:** 10 **RG/MCC*:** 2 **Opaques:** 2 **In Situ Mud:** 2	**Grains:** 67% **Cement:** 16% - calcite, clays, quartz overgrowth **Porosity:** 17%	reworked calcite cement, rounded grains, no kaolinite, lots of opaquesm coaly mudchips, moderate bioturbation	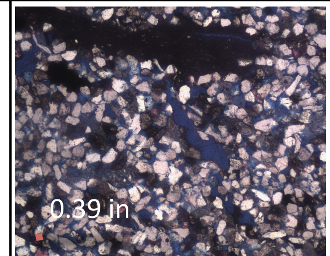
PC345/Point Bar	**Grain Size:** Lower Fine **Roundness:** angular - subangular **Sorting:** Poor	**Quartz:** 74 **Chert:** 10 **B/M*:** 0 **Feldspar:** 12 **RG*:** 4	**Grains:** 57% **Cement:** 38% - calcite **Porosity:** 5%	very little mud, mostly calcite cement, no bioturbation	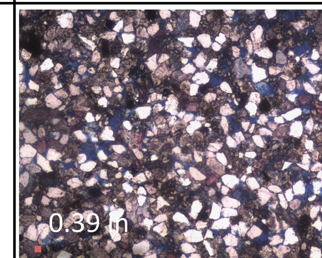
SBS 200/Middle Shoreface	**Grain Size:** Upper Very Fine **Roundness:** subrounded - rounded **Sorting:** Moderate - well	**Quartz:** 84 **Chert:** 8 **B/M*:** <1 **Feldspar:** 2 **Opaques:** 4	**Grains:** 71% **Cement:** 22% - calcite, quartz overgrowth, opaques **Porosity:** 7%	very little mud, but patchy , laminated with opaques, no kaolinite, rare bioturbation in thin section, but hand sample contains large *Ophiomorpha* burrows.	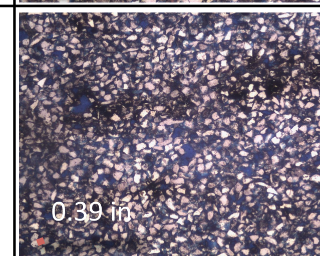
SBW 165/Lower Delta Front	**Grain Size:** Lower Medium **Roundness:** angular - rounded **Sorting:** poor	**Quartz:** 58 **Chert:** 4 **B/M*:** <1 **Feldspar:** 6 **RG*:** 24 **Carbonaceous Debris:** 10	**Grains:** 45% **Cement:** 0% **Porosity:** <1% **Mud**: 55%	laminated with coal, no bioturbation	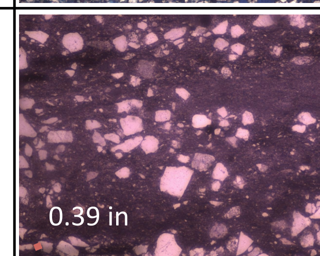

Table 6 Photomicrographs of selected samples, see Appendix A for collection locations. *B/M: Biotite/Muscovite, RG: replaced grains, RG/MCC: replaced grains/mud-chip clasts, AE: Architectural Element. Red bar on photographs is 0.39 inches (1 mm)

3.1 Discrete Flood Bodies

Discrete flood bodies are moderately to poorly sorted and contain very fine-to fine-grained sandstone and mudrock (Table 2). No thin sections were collected for analysis. Because a discrete flood body is a single bed, no internal compartments exist. Discrete flood bodies constitute only 1.3% of the composite stratigraphic interval (Fig. 11) and are common in low N:G coastal-plain intervals (Fig. 34). Gamma-ray profiles are variable (Fig. 13). Based on apparent width and thickness measurements, discrete-flood body cross-sectional area averages 98.4 ft^2 (30.0 m^2) and are the least laterally continuous (Fig. 58) of the architectural elements (Table 4). Two-dimensional geometries are symmetrically lenticular (Fig. 56), and proposed 3-D geometries are lobes. Based on these properties, relative reservoir quality is poor (Table 7; Fig. 58).

3.2 Crevasse Splays

Crevasse splays contain very fine-to-medium-grained, subangular-to-subrounded, moderately sorted sandstone, muddy sandstone, and siltstone (Table 2; Table 6). Crevasse splays also have internal bedding, which are typically draped with mudrock and create small-scale internal heterogeneities and vertical compartments (Fig. 16). Crevasse splays comprise 8.6% of the composite stratigraphic interval (Fig. 11), and are most common in low N:G coastal-plain intervals (Fig. 34). Gamma-ray profiles are funnels, which are typically <5 ft (<1.5 m) thick (Fig. 16). Based on apparent-width and thickness measurements, crevasse splay cross-sectional area averages ~162.9 ft^2 (49.7 m^2). Crevasse splays are thin (1-4.5 ft [0.3-1.4 m]) and laterally discontinuous (Table 4; Fig. 58). Similar to discrete flood bodies, 2-D

	Architectural Element								
Parameter	Discrete Flood Body	Crevasse Splay	Channel Body	Bayhead Delta	Estuarine Assemblage	Tidal Barform	Foreshore	Washover Fan	Middle Shoreface
% of interval	1.3	8.6	29	2.1	3.9	4	2	0.4	2.6
score	2	8	9	4	6	7	3	1	4
grain size	vf - f	vf - m	f - m	vf - f	vf - m	vf - f	vf - m	vf - f	vf - f
score	5	4	5	5	4	5	4	5	5
roundness	NA	subang - subround	subang - subround	NA	NA	subang - subround	NA	NA	subround
score	0	0	0	0	0	0	0	0	0
sorting	mod-poor	moderate	moderate-good	mod - poor	variable	variable	well - very well	well - very well	mod - well
score	2	3	4	2	3	3	5	5	4
average thickness	1.6	1.8	4.9	5	11.6	9	4	4	6
score	1	2	4	5	8	7	3	3	6
apparent width	61.5	90.5	287.7	NA	NA	NA	NA	NA	NA
score	0	0	0	0	0	0	0	0	0
cross-sectional area	98.4	162.9	1179.6+	~5,000	>122,496	~3,500	~31,680	~2,000	~6,000
score	1	2	4.00	6	9	5	8	3	7
continuity	low	mod - low	mod - high	mod - high	high	low - mod	moderate	low - mod	moderate
score	1	2	3	3	5	3	4	3	4
compartments	None	vertical	vertical and horizontal	vertical and horizontal	vertical	vertical and horizontal	None	None	Vertical
score	5	4	3	3	4	3	5	5	4
Total Score	17	25	32	28	39	33	32	25	34
Rank	9	7/8	4/5	6	1	3	4/5	7/8	2
Relative Quality	poor	poor	good	moderate	excellent	good	good	poor	excellent

Table 7 Parameters used for each architectural element to evaluate the relative reservoir quality. Most scores are given based on ranks. A "0" score means that parameter was not evaluated for each architectural element, and is not used in the final score. Scores for grain size are higher if grains are bigger and vice versa. Scores for sorting are higher if sorting is better and vice versa. Scores for compartments are higher if less compartments exist and vice versa.

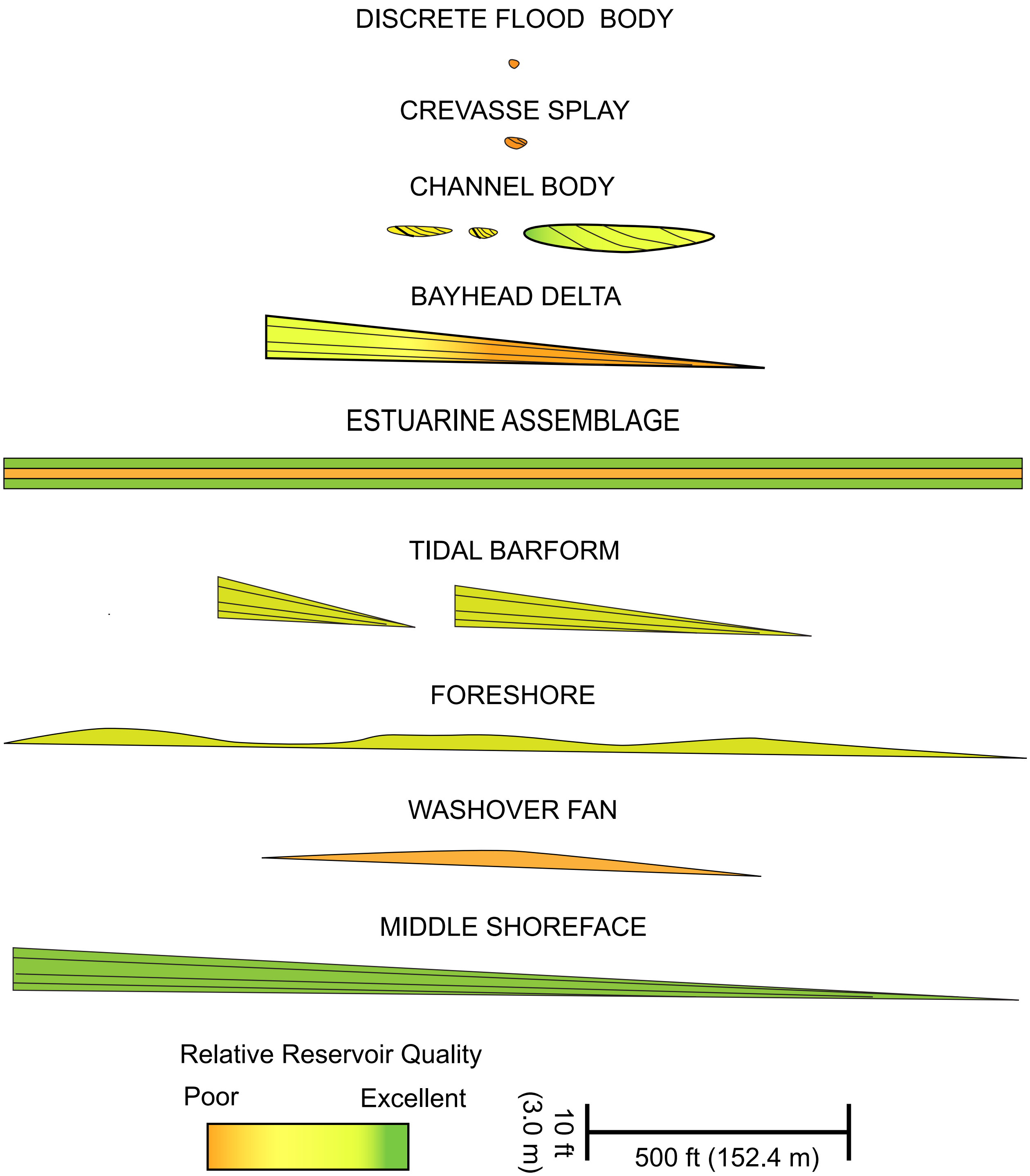

Fig. 58 Relative sizes, geometries, relative reservoir quality, and potential compartments associated with architectural elements in the study interval are shown. The estuarine assemblage extends beyond scale of the figure.

geometries are broadly lenticular (Fig. 56). Potential 3-D geometry is a lobe. Relative reservoir quality is poor (Table 7; Fig. 58).

3.3 Channel Bodies

Point bars are composed of fine-to-medium-grained, moderately sorted, sandstone (Table 2; Table 6). Point bars (depending on the amalgamation) contain IHS and cut-and-fill geometries, which may be locally draped by mudrock, creating small-scale vertical and horizontal compartments, especially in tidally influenced channel bodies. Tidally influenced channel bodies have mudrock draped between lateral accretion deposits, therefore, are likely to be compartmentalized between bedsets. Amalgamated channel bodies have more sand-on-sand contacts, so compartments have higher potentials to communicate both laterally and vertically. Gamma-ray data consist of bell- or cylindrical-shaped profiles (Fig. 17). Based on measured apparent-width and thickness, isolated channel-body cross-sectional area averages ~1,179.6 ft^2 (359.6 m^2). Based on photopan estimations, amalgamated point bar (cross-sectional) areas are at least 15,000 ft^2 (4,573.1 m^2), and possibly greater. Channel bodies are moderately thick (4-30 ft [1.2-9.1 m]) and laterally discontinuous to highly continuous (Table 4). Channel bodies are common throughout the entire study area, however, are more common in ELST, LST, and HST intervals (Fig. 34). The TST is almost completely void of channel bodies. Two-dimensional geometries are lenticular with scoured, irregular bases, and flat tops (Fig. 56). Proposed 3-D geometries are possibly crescents or ellipsoids. Channel bodies comprise 29% of the composite stratigraphic interval (Fig. 11). Overall relative reservoir quality is good (Table 7; Fig. 58).

3.4 Bayhead Delta

The bayhead delta contains abundant interbedded very fine-to-fine-grained, subrounded, moderately to poorly sorted sandstone and mudrock (Table 2; Table 6). Internal vertical compartmentalization is likely within the lower one-half of the bayhead delta, where mudrock is interbedded with sandstone in horizontal bedsets (Fig. 19). The bayhead delta comprises 2.1% of the composite stratigraphic interval (Fig. 11), but is laterally continuous. The single bayhead delta in this study is present in the uppermost interval of the LLST (Fig. 34). The gamma-ray profile consists is a funnel, which is >5ft (>1.5 m) thick (Fig. 19). Based on photopan estimations, the bayhead delta has a cross-sectional area of 5,000 ft^2 (1,524.4 m^2). Two-dimensional geometries are sheets or large wedges. Presumed 3-D geometry is a lobe. Relative reservoir quality is moderate depending on location (Table 7; Fig. 58). Downdip (VDS, PCW measured sections; Appendix A), muddy sandstone facies are common and the bayhead delta thins; therefore has poor reservoir quality. Updip (SBW, SBE measured sections; Appendix A), sandstone facies are common and the bayhead delta thickens; therefore has moderate reservoir quality (Table 7; Fig. 58).

3.5 Estuarine Assemblage

The estuarine assemblage consists of very fine-to-medium-grained, poorly to well-sorted sandstone, muddy sandstone, and mudrock (Table 2; Table 6). Because of the tripartite facies distribution, vertical internal compartmentalization is likely. Facies tend to be laterally continuous; therefore, horizontal compartmentalization is unlikely. The estuarine assemblage consumes 3.9% of the composite stratigraphic interval (Fig. 11), but is laterally continuous. The gamma-ray profile has an hourglass shape (Fig.

20). The estuarine assemblage is located near the middle of the stratigraphic study interval (Fig. 34). Based on apparent width and thickness data, flood-tidal delta cross-sectional area averages ~122,496 ft^2 (37,346 m^2) (within the study area), and most likely extends outside the study area. Two-dimensional geometry is tabular and the proposed 3-D geometry is a sheet. Overall relative reservoir quality is excellent, however, due to compartmentalization, relative reservoir quality is poor in the muddy central unit and excellent in the lower and upper sandy units (Table 7; Fig. 58).

3.6 Tidal Barforms

Tidal barforms have variable sorting and consist of subrounded-to-subangular, very fine-to-fine-grained sandstone and muddy sandstone (Table 2; Table 6). Mudrock-filled burrows are abundant. Tidal barforms may be compartmentalized due to the presence of muddy sandstone facies draping IHS, similar to tidally influenced point bars (Fig. 21). Tidal barforms consume 4.0% of the composite stratigraphic interval (Fig. 11) and are only present in the top of the stratigraphic interval, in the LST (Fig. 34). Gamma-ray profiles have a funnel shape, and may be confused with a crevasse splay (Fig. 21). Based on observed widths from photopans and thicknesses from measured sections, tidal barform cross-sectional area averages ~3,500 ft^2 (1,067.1 m^2), similar to channel bodies. Tidal barforms can be thick (2-18 ft [0.6-5.5 m]), and moderately to highly continuous. Two-dimensional geometry is a wedge, whereas possible 3-D geometries are elongated lobes. Relative reservoir quality is good (Table 7; Fig. 58).

3.7 Foreshores

The Foreshore contains moderately well-to-well-sorted, very fine-to-medium-grained sandstone and muddy sandstone (Table 2). No thin sections were collected for analysis. The foreshore is not internally compartmentalized. Foreshores comprise 2% of the composite stratigraphic interval (Fig. 11), and are common in moderate N:G intervals, in the TST (Fig. 34). Gamma-ray profiles show a funnel shape, and are similar to the bayhead delta, washover fan, and middle shoreface architectural elements (Fig. 22). Based on apparent-width values from photopans and thicknesses from measured sections, foreshore cross-sectional area averages ~31,680 ft^2 (9,658.5 m^2). Foreshores are relatively thin (1-5 ft [0.3-1.5 m]). Two-dimensional geometries may be lenticular to tabular, and the suggested 3-D geometries are sheets. Relative reservoir quality is good (Table 7; Fig. 58).

3.8 Washover Fans

The washover fan consists of well-to-very well-sorted, very fine-to-fine-grained sandstone (Table 2). No thin sections were collected for analysis. The washover fans observed in this study are not internally compartmentalized. Washover fans are the least common architectural element, and comprise 0.4% of the composite stratigraphic interval (Fig. 11). Gamma-ray profiles have a funnel shape and may be easily confused with other coarsening-upward profiles (Fig. 23). Average width is estimated at ~500 ft (152.4 m) based on a single photopan. Washover fans are relatively thin (1-5 ft [0.3-1.5 m]), and likely not laterally continuous. Based on the apparent-width value from a photopan and thicknesses from measured sections, washover fan cross-sectional area averages ~2,000 ft (~609.8 m). Washover fans are only present near the top of the stratigraphic study interval in the TST (Fig. 34). Two-dimensional geometries are lenticular, and suggested 3-D geometries are half-circles. Relative reservoir quality is poor (Table 7; Fig. 58).

3.9 Middle Shorefaces

The middle shoreface sandstone body consists of very fine-to-fine-grained, moderately to-well-sorted, subrounded, bioturbated sandstone and muddy sandstone facies (Table 2; Table 6). The middle shoreface sandstone body lacks internal compartmentalization. Middle shorefaces comprise 2.6% of the composite stratigraphic interval (Fig. 11) and are only present near the top of the study interval (upper Kmvl) (Fig. 34). Gamma-ray profiles have funnel shape and may be easily confused with other coarsening-upward profiles, however, tend to have lower gamma-ray values (70-90 API) than the other architectural elements (Fig. 24). Based on observed width values from photopans and thicknesses from measured sections, middle shoreface cross-sectional area averages ~6,000 ft^2 (1,829.3 m^2) (within the study area). Middle shoreface architectural elements are 1-9 ft (0.3-2.7 m), thick on average, but can be moderately to highly continuous. Two-dimensional geometry is tabular to wedge-shaped, and suggested 3-D geometry is a sheet. Relative reservoir quality is excellent (Table 7; Fig. 58).

4. Net-to-Gross Packages: Relation to Sequence Stratigraphy and Reservoir Characterization

Net-to-gross (N:G) ratio is evaluated in this study and is directly related to architectural-element occurrence, dimensions, and geometries. The study interval is divided into packages based on N:G, which includes: high (>80% sandstone), moderate (50-80% sandstone), and low (<50% sandstone). The predictability and occurrence of the N:G packages directly relates to the interpreted sequence-stratigraphic framework and is described in the following discussion.

4.1 High Net-to-Gross Packages

High N:G packages (basal subunits of CP1 and CP2) are composed of amalgamated channel-body architectural elements (Fig. 59). Based on properties discussed, these deposits are likely to have good-to-excellent relative reservoir quality (Fig. 58) and are associated with the ELST. The ELST is correlated by tracing the sequence boundary (B-1) at the base of an incised valley. A sequence boundary may be expressed on a gamma-ray log by a sudden change from low N:G to high N:G units, which are laterally continuous (Appendix F). Sequence boundaries may be located in FMI logs by a significant change in paleocurrent orientation, such as between EP1 and CP2. A sequence boundary in core may be recognized by an abrupt grain-size change and heterolithic debris overlain by thick (>20 ft [6.1 m]), amalgamated sandstone bodies.

4.2 Moderate Net-to-Gross Packages

A moderate N:G package (PS2 and PS3) is present in the TST and HST, and is composed primarily of estuarine assemblage, tidal barform, foreshore, washover fan, and middle shoreface architectural elements (Fig. 59). Based on properties discussed, these deposits could have moderate-to-excellent relative reservoir quality (Fig. 58). In general, these packages are recognized by a funnel-shaped gamma-ray profile resting on coal-bearing mudrock or coal. Architectural elements are moderately to highly continuous (0.5-2 mi [0.8-3.2 km]). The base of the funnel-shaped profile may represent a marine- or estuarine-flooding surface. These units can be correlated and constrained across distances using the estuarine- or marine-flooding surface as a base and the top of the funnel-shaped profile to bound the upper surface. Paleocurrent data derived from FMI logs could be used to locate the updip and downdip directions. Cores can be used

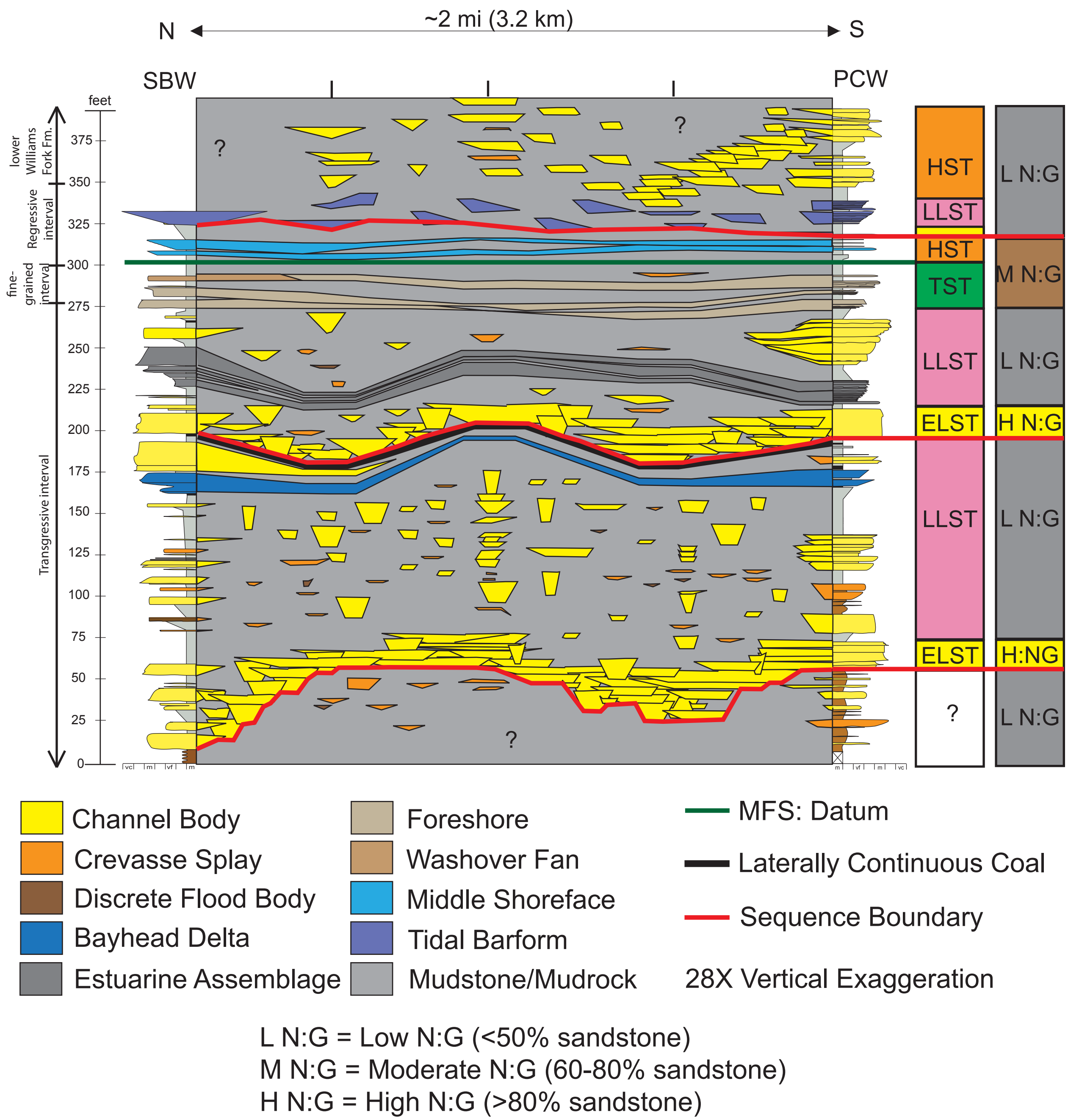

Fig. 59 Schematic cross section between State Bridge Draw West and Philadelphia Creek West measured sections to represent spatial distribution of architectural elements and placement of major bounding surfaces. Diagram also shows nomenclature divisions used in this study (to left). Sandstones more abundant and amalgamated just above sequence boundaries. Measurements in feet. Datum on the Maximum Flooding Surface (MFS). The columns to the right show interpreted systems tracts: early lowstand (ELST, yellow); late lowstand (LLST, pink); transgressive (TST, green); and highstand (HST, orange), and net-to-gross (N:G) intervals.

to confirm an architectural-element trend by evaluating the vertical facies (higher energy facies upward). Systems tracts are defined based on vertical stacking patterns.

The TST (PS1) is characterized by a rapid relative sea-level rise and retrogradational parasequences. The MFS (top of PS1) marks a change from a retrogradational parasequence set to aggradational or progradational parasequence sets. The MFS is recognized by high (>300 cps), "hourglass shape" gamma-ray profile within thick interval of fissile mudstone. In core, the MFS is represented by a thick (10-20 ft [3.0-6.1 m]) unit of intensely bioturbated, fissile mudrock which may be sparsely interbedded with thin sandstone. The maximum-flooding surface provides a datum for local correlations because it commonly represents the flattest depositional surface. The HST (PS2) lies above the MFS, and is characterized by an aggrading-to-prograding parasequence set. The HST is correlated and constrained using the maximum-flooding surface at the base.

4.3 Low Net-to-Gross Packages

Low N:G packages (upper units of CP1 and CP2) are composed of isolated channel-body, discrete flood-body, and crevasse-splay architectural elements (Fig. 59). Based on discussed properties, these deposits could have poor to good relative reservoir quality (Fig. 58). Many of these deposits are interpreted as LLST. The LLST represents a relative sea-level rise following a relative sea-level lowstand. These intervals are recognized on gamma-ray data by thin, fining-upward profiles within coals and coal-bearing mudrock, and the associated sandstone being less than 500 ft (152.4 m) wide. Thin, coarsening-upward gamma-ray profiles may represent crevasse splays. No identifying features may be present in FMI logs. In core, these units contain a low-energy facies, mudrock, and coal, and may contain tidal indicators with abundant bioturbation and rooting.

5. Summary

Based on collected dimensional data from coastal-plain architectural elements, channel bodies are the largest, with an average apparent width of 287.7 ft (87.7 m) and an average thickness of 4.9 ft (1.5 m). Discrete flood bodies are the smallest architectural element, with an average apparent width of 61.5 ft (18.8 m) and an average thickness of 1.6 ft (0.5 m). Facies, facies associations, and architectural elements are more diverse in the study interval (Kmvl-lower Kmvc) as compared to studies done in Coal Canyon, Colorado, which is in the lower Kmvc interval approximately 40 mi (64.4 km) to the south. Sandstone bodies are larger in Coal Canyon by almost 50%.

Nine architectural elements are identified and assigned a specific relative reservoir quality based primarily on sedimentological properties, frequency of occurrence, geometries, and dimensions. Middle-shoreface, foreshore, and channel-body architectural elements provide good-to-excellent relative-reservoir quality because they contain abundant well-sorted sandstone facies and the sandstone bodies are relatively large. Crevasse splays and discrete flood bodies likely provide poor relative reservoir quality due to their small sizes and low frequency of occurrence.

The study interval presents a complex assemblage of facies associations, which are summarized in terms of N:G ratios. In general, high and low N:G intervals are represented by coastal-plain facies assemblages and laterally discontinuous sandstone bodies. Moderate N:G intervals commonly contain estuarine, lagoon, and shallow-marine facies associations which are laterally continuous. High N:G intervals are related to the ELST, and overlie sequence boundaries. These interval can be expected to fine upward into a low N:G interval of the LLST.

CHAPTER FIVE

CONCLUSIONS AND RECOMMENDATIONS

1. Conclusions

The reservoir-scale architecture, sequence-stratigraphic framework, and paleogeography of the Kmvl (upper lower Iles clastic wedge) through the Kmvc (lower Williams Fork Formation) intervals in the Douglas Creek Arch was completed by defining facies, facies associations, and architectural elements based on detailed outcrop descriptions, paleocurrent data, and gamma-ray data. Coastal-plain packages, estuarine, and shallow-marine parasequences were identified and correlated across the study area to determine lateral relationships and vertical stacking patterns, so as to define major sequence-stratigraphic boundaries and systems tracts. The stratigraphic controls on potential reservoir parameters are addressed. The conclusions of this study are the following:

Seventeen facies and four facies associations are observed and characterized in the 365-ft (111.3-m) thick stratigraphic interval. Facies associations include: the coastal plain (76.1%), estuarine (12.5%), lagoon (4.8%), and shallow marine (6.6%). The variability in facies and architectural elements displays the complex nature of these deposits.

Nine architectural elements are identified and characterized in terms of dimensions, spatial variability, geometries, facies-stacking patterns, ichnofacies, and internal and external bounding surfaces. Architectural elements include: discrete flood body, crevasse splay, channel body, bayhead delta, estuarine assemblage, washover fan, foreshore, middle shoreface, and tidal barform. The most common architectural element is the channel body (54.0%) and the least common is the washover fan (0.7%).

Based on previous basin-scale studies, the lower two-thirds of the study interval (Kmvl) is equivalent to the lower Corcoran, Cozzette, and Rolllins Sandstone members of the Iles Formation in the Piceance Basin. The upper one-third of the study interval (Kmvc) is equivalent to the lowermost Williams Fork Formation of the Piceance Basin. The entire study interval is also equivalent to the Iles clastic wedge, as defined in the Sand Wash Basin.

The stratigraphic study interval records an overall transgressive-regressive cycle. The strata retrograde from coastal-plain to shallow-marine facies associations and prograde from shallow-marine to coastal-plain facies associations.

Two sequences are identified and divided into lowstand, transgressive, and highstand systems tracts bounded by sequence boundaries. Sequence one contains one coastal-plain package and one estuarine parasequence. Sequence two contains one coastal-plain package, two estuarine parasequences, and two parasequence sets. A maximum flooding surface is identified between the transgressive and highstand systems tracts in sequence two.

Based on collected dimensional data from coastal-plain architectural elements, channel bodies are the largest, with an average apparent width of 287.7 ft (87.7 m) and an average thickness of 4.1 ft (1.3 m). Discrete flood bodies are the smallest architectural element, with an average apparent width of 61.5 ft (18.8 m) and an average thickness of 2.0 ft (0.6 m).

Facies, facies associations, and architectural elements are more diverse in the study interval (Kmvl-lower Kmvc) as compared to studies done in Coal Canyon, Colorado within the lower Kmvc interval approximately 40 mi (64.4 km) to the south. Coastal-plain, tidal, and shallow-marine strata are present in the study interval where as Coal Canyon contains only coastal-plain strata. Sandstone bodies are larger in Coal Canyon, by almost 50%.

Channel-body, middle-shoreface, and foreshore architectural elements have good to excellent relative reservoir quality, where as crevasse splays and discrete flood bodies have poor relative reservoir quality.

Large-scale net-to-gross (N:G) packages are identified in the study interval and are directly related to the sequence-stratigraphic framework. High N:G intervals lie above sequence boundaries in the early lowstand systems tract and contain laterally and vertically amalgamated channel bodies. Moderate N:G intervals contain laterally continuous estuarine, lagoon, and shallow-marine facies associations within the transgressive and early highstand systems tracts. Low N:G intervals commonly lie within the late lowstand systems tract and contain isolated, laterally discontinuous coastal-plain facies associations.

2. Recommendations

Recommendations for future work include:

In this study, poor outcrop exposures of mudrock hindered the ability to subdivide mudrock facies. Additional study and trenching on the measured sections to subdivide mudrock facies would be very beneficial. Mudrock facies subdivisions will provide better constraints on marine flooding surfaces and the maximum flooding surface, plus test the overall sequence-stratigraphic framework.

Additional study on the measured sections to collect spectral gamma-ray data, to better relate to the data collected in the subsurface. For example, potassium division will show feldspar in sandstone that reads unusually high. Uranium spikes will show organic-rich intervals, possibly related to the maximum flooding surface.

Extending the study area beyond the 2 mi^2 (3.2 km^2) in which it was confined. Extension would allow for: (1) additional dimensional information on units, which were laterally continuous beyond the confines of the study area; (2) correlation of major sequence-stratigraphic surfaces; (3) the ability to define the limits of the incised valley; and (4) to test the sequence-stratigraphic framework given.

Regional correlation into the subsurface using well logs, cores, and FMI logs to test the overall sequence-stratigraphic framework.

Conduct ammonite and/or microfossil biostratgraphy within the study interval to test the age of the maximum flooding surface to better constrain the study interval.

Radiometric dating and/or geochemical fingerprinting on the ash beds within the ash zone, to better constrain the age, and to determine if the they correlate to the Yampa Ash beds described near Craig, CO.

A more thorough evaluation of trace fossils may help determine depositional environments.

REFERENCES

Allen, J.R.L., 1965, A review of the origin and characteristics of recent alluvial sediments: Sedimentology, v. 5, p. 89-191.

Allen, G.P., and Posamentier, H.W., 1993, Sequence stratigraphy and facies model of an incised valley fill: The Gironde Estuary, France: Journal of Sedimentary Petrology, v. 63, n. 3, p. 378-391.

Anderson, D.S., 2005, Architecture of crevasse splay and point-bar bodies of the nonmarine Iles Formation north of Rangely, Colorado; implications for reservoir description; Cretaceous sand body geometries in the Piceance Basin area of northwest Colorado: The Mountain Geologist, v. 42, p. 109-122.

Arnott, R.W.C., and Southard, J.B., 1990, Exploratory flow-duct experiments on combined-flow bed configurations, and some implications for interpreting storm-event stratification: Journal of Sedimentary Petrology, v. 60, p. 211-219.

Aschoff, J.L., and Steel R.J., Anatomy and Development of a Low-Accommodation Clastic Wedge, Upper Cretaceous, Cordilleran Foreland Basin, USA: Sedimentary Geology (2010), doi. 10.1016/j.sedgeo.2010.10.006.

Bader, J.W., 2009, Structural and tectonic evolution of the Douglas Creek arch, the Douglas Creek fault zone, and environs, northwestern Colorado and northeastern Utah: Implication for petroleum accumulation in the Piceance and Uinta basins: Rocky Mountain Geology, v. 44, n. 2, p. 121-145.

Barnum, B.E., Scott, R.W., Jr., and Pantea, M.P., 1997, Geologic map of the Texas Mountain quadrangle, Rio Blanco County, Colorado: U.S. Geological Survey Miscellaneous Field Investigations Series Map MF-2321, 1:24,000, 1 sheet.

Bates, Charles C., 1953, Rational Theory of Delta Formation: American Association of Petroleum Geologists Bulletin, v. 37, n. 9, p. 2119-2162.

Beynon, B.M., and Pemberton, G.S., 1992, Ichnological Signature of a Brackish Water Deposit: An Example from the Lower Cretaceous Grand Rapids Formation, Cold Lake Oil Sands Area, Alberta *in* Pemberton, G.S., ed., Applications of Ichnology to Petroleum Exploration, A Core Workshop, Society for Sedimentary Geology Core Workshop n. 17: Society for Sedimentary Geology, p. 199-222.

Bhattacharya, J.P., and Walker, R.G., 1992, Deltas, *in* Walker, R.G., and James, N.P., eds., Facies Models Response to Sea Level Change: Waterloo, Ontario: Geological Association of Canada, p. 157-177.

Binford, B., 2009, Stratigraphic architecture and connectivity of high-sinuosity fluvial sandstone bodies in Coal Canyon, Colorado, with subsurface comparison to Grand Valley: Unpublished M.S. Thesis, University of Colorado, Boulder, CO, 128 p.

Blakey, R.C., 2004; 2009, Paleogeography and Geologic Evolution of North America, http://jan.ucc.nau.edu/~rcb7/namK75.jpg: Accessed February, 2010.

Blum, M.D., and Price, D.M., 1998, Quaternary example from the Colorado River, Gulf coastal plain of Texas, *in* Shanley, K.M. and McCabe, P.J. eds., Relative role of eustasy, climate and tectonism in continental rocks: Society for Sedimentary Geology Special Publication 59, p. 31-48.

Blum, M.D., and Törnqvist, T.E., 2000, Fluvial responses to climate and sea-level chane: a review and look forward: Sedimentology, v. 47 (Supplement 1), p. 2-48.

Bohacs, K., and Suter, J., 1997, Sequence Stratigraphic Distribution of Coaly Rocks: Fundamental Controls and Paralic Examples: American Association of Petroleum Geologists Bulletin, v. 81, n. 10, p. 1612-1639.

Boyd, R., Dalrymple, R., and Zaitlin, B.A., 1992, Classification of clastic coastal depositional environments: Sedimentary Geology, v. 80, p. 139-150.

Bridge, John S., 1984, Large-Scale Facies Sequences in Alluvial Overbank Environments: Journal of Sedimentary Petrology, v. 54, n. 2, p. 583-588.

Bridges, P.H., 1976, Lower Silurian transgressive barrier islands, southwest Wales: Sedimentology, v. 23, p. 374-362.

Bromley, Richard G., S. George Pemberton, and Ray A. Rahmani, 1984, A Cretaceous woodground; the Teredolites ichnofacies: Journal of Paleontology, v. 58, n. 2, p. 488-498.

Brown, L.F. Jr., and Fisher, W.L., 1977, Seismic-stratigraphic interpretation of depositional systems: examples from Brazilian rift and pull-apart basins, *in* Payton, C.E. ed., Seismic Stratigraphy-Applications to Hydrocarbon Exploration: American Association of Petroleum Geologists Memoir 26, p. 213-248.

Brownfield, M.E., and Johnson, E.A., 2008, The Yampa Bed – A Regionally Extensive Tonstein in the Williams Fork Formation, Northwestern Piceance Creek and Southern Sand Wash Basins, Colorado: United States Geological Survey Scientific Investigations Report 2008-5033, 32 p.

Burst, J.F., 1965, Subaqueously formed shrinkage cracks in clay: Journal of Sedimentary Petrology, v. 35, p. 348-355.

Cant, D.J., 1998, Sequence stratigraphy, subsidence rates, and alluvial facies, Mannville Group, Alberta foreland basin, *in* Shanley, K.W. and McCabe, P.J. eds., Relative role of eustasy, climate an tectonism in continental rocks: Society for Sedimentary Geology Special Publication 59, p. 49-63.

Caldes, B.A., 2005, Attribute Variation within fluvial sand bodies of the Iles Formation, East of Rangely, Colorado: The Mountain Geologist, v. 42, p. 123-139.

Carroll, Christopher James, 2003, Fractures in the Mesaverde Group at Somerset Coal Field, Delta and Gunnison Counties, Colorado, *in* Peterson, K.M. Olson, T.M. and Anderson, D.S. eds., Piceance Basin 2003 guidebook: Rocky Mountain Association of Geologists, p. 205-217.

Clifton, H.E., 1976, Wave-formed sedimentary structures – A conceptual model, *in* Davis, R.A., Jr., and Ethington, R.L. eds., Beach and Nearshore Sedimentation: Society for Sedimentary Geology, Special Publication 24, p. 126-148.

Coleman, J.M., 1966, Ecological changes in a massive fresh-water clay sequence: Transactions Gulf Coast Association of Geological Societies, v. 16, p. 159-174.

Cole, R, and Cumella, S.P., 2003, Stratigraphic architecture and reservoir characteristics of the Mesaverde Group, southern Piceance Basin, Colorado, *in* Peterson, K.M., Olson, T.M., and Anderson, D.S., eds., Piceance Basin 2003 guidebook: Rocky Mountain Association of Geologists, p. 385-442.

Cole, R., and Cumella, S., 2005, Sand-body architecture in the lower Williams Fork Formation (Upper Cretaceous), Coal Canyon, Colorado, with comparison to the Piceance Basin subsurface: The Mountain Geologist, v. 42, no. 3, p. 85-108.

Cole, R.D., and Pranter, M.J., 2008, From Rocks to Models: Outcrop-based analysis and statistics for subsurface characterization of fluvial reservoir geometry and connectivity, Williams Fork Formation, Piceance Basin, Colorado: Williams Fork Consortium-Phase IV 2008 Sponsor Field Trip Guidebook, 79 p.

Collinson, J.D., 1969, The sedimentology of the Grindslow Shales and the Kinderscout Grit: a Deltaic Complex in the Namurian of Northern England: Journal of Sedimentary Petrology, v. 39, p. 194-221.

Collinson J.D., 1970, Bedforms of the Tana River, Norway: Geografiska Annaler. Series A, Physical Geography, v. 53, n. 1, p. 31-56.

Collinson, J.D., and Thompson D.B., 1989, Sedimentary Structures, 2nd ed., Unwin Hyman: London: p. 60-84.

Crabaugh, J.P., 2001, Nature and growth of nonmarine-to-marine clastic wedges: Examples from the Upper Cretaceous Iles Formation, Western Interior (Colorado) and the Lower Paleogene Wilcox Group of the Gulf of Mexico Basin (Texas), Dissertation, The University of Wyoming, Laramie, WY.

Cumella, Stephen P., and Douglas B. Ostby, 2003, Geology of the Basin-Centered Gas Accumulation, Piceance Basin, Colorado, *in* Peterson, K.M. Olson, T.M. and Anderson, D.S. eds., Piceance Basin 2003 guidebook: Rocky Mountain Association of Geologists, p. 171-193.

Cumella, Stephen P., 2006, Overview of a Giant Basin-Centered Gas Accumulation, Mesaverde Group, Piceance Basin, Colorado: The Rocky Mountain Association of Geologists, The Mountain Geologist, v. 43, n. 3, p. 219-224.

Cumella, S.P., and Scheevel J., 2008, The influence of stratigraphy and rock mechanics and Mesaverde gas distribution, Piceance Basin, Colorado: The American Association of Petroleum Geologists, pg. 137-155.

Dalrymple, R.W., Zaitlin, B.A., and Boyd, R., 1992, Estuarine Facies Models: Conceptual Basis and Stratigraphic Implications: Journal of Sedimentary Petrology, v. 62, n. 6, p. 1130-1146.

Dalrymple, R.W., 1992, Tidal Depositional Systems *in* Walker, R.G., and James, N.P., eds., Facies Models Response to Sea Level Change: Waterloo, Ontario: Geological Association of Canada, p 195-218.

Dalrymple, Mark, 2001, Fluvial reservoir architecture in the Statfjord Formation (northern North Sea) augmented by outcrop analogue statistics: Petroleum Geoscience, v. 7, p. 115-122.

De Boer, R.L., Oost, A.P., and Visser, M.J., 1989, The diurnal inequality of the tide as a parameter for recognizing tidal influences: Journal of Sedimentary Petrology, v. 59, p. 912-921.

DeCelles, P.G., and Currie, B.S., 1996, Long-term sediment accumulation in the Middle Jurassic-early Eocene Cordilleran retroarc foreland-basin system: Geology, v. 24, n. 7, p. 591-594.

DeCelles, P.G., 2004, Late Jurassic to Eocene Evolution of the Cordilleran Thrust Belt and Foreland Basin System, Western U.S.A.: American Journal of Science, v. 304, p. 105-168.

Dott, R.J. and Bourgeois, J., 1982, Hummocky stratification: Significance of its variable bedding sequences: Geological Society of America Bulletin, v. 93, p. 663-680.

Dumas, S., and Arnott, W.R.C., 2006, Origin of hummocky and swaley cross-stratification – The controlling influence of unidirectional current strength and aggradation rate: Geological Society of America: Geology, v. 34, n. 12, p. 1073-1076.

Edwards, M.B., Eriksson, K.A., and Kier, R.S., 1983, Paleochannel Geometry and Flow Patterns Determined from Exhumed Permian Point Bars in North-Central Texas: Journal of Sedimentary Petrology, v. 53, n. 4, p. 1261-1270.

Fanti, F., and O. Catuneanu, 2010, Fluvial sequence stratigraphy: The Wapiti Formation, west-central Alberta, Canada: Journal of Sedimentary Research, v. 80, no. 4, p. 320-338.

Finzel, E.S., Ridgway, K.D., Reifenstuhl, R.R., Blodgett, R.B., White, J.M., and Decker, P.L., 2009, Stratigraphic framework and estuarine depositional environments of the Miocene Bear Lake Formation, Bristol Bay Basin, Alaska: Onshore equivalents to potential reservoir strata in a frontier gas-rich basin: American Association of Petroleum Geologists Bulletin, v. 93, n. 3, p. 379-405.

Franczyk, K.J., 1989, Depositional controls on the Late Campanian Sego sandstone and implications for associated coal-forming environments in the Uinta and Piceance basins, *in* Evolution of sedimentary basins – Uinta and Piceance basins, ch. F: U.S. Geological Survey bulletin, 1787-F.

Fraser, G.S., 1989, Estuarine Coasts *in* Clastic Depositional Sequences: Processes of Evolution and Principles of Interpretation: Prentice-Hall Inc., Englewood Cliffs, New Jersey, p. 231-250.

Frey, R.W., and Pemberton, S.G., 1984, Trace fossil facies models, *in* Walker, R.G. ed., Facies Models (2nd ed.): Geoscience Canada, Reprint Series 1, p.189-207.

Frey, R.W. and Pemberton, S.G., 1985, Biogenic structures in outcrops and cores. I. Approaches to ichnology: Bulletin of Canadian Petroleum Geology, v. 33, p. 72-115.

Friend, P.F., M.J. Slater, and R.C. Williams, 1979, Vertical and lateral building of river sandstone bodies, Ebro Basin, Spain: The Geological Society, v. 136, p. 39-46.

Gautier, D.L, 1982, Siderite concretions: Indicators of early diagenesis in the Gammon Shale (Cretaceous): Journal of Sedimentary Petrology, v. 52, p. 859-871.

Gibling, Martin R., 2006, Width and thickness of fluvial channel bodies and valley fills in the geological record: A literature compilation and classification: Journal of Sedimentary Research, v. 76, p. 731-770.

Gomez-Veroiza C.A., and Steel, R.J., 2010, Iles clastic wedge development and sediment partitioning within a 300-km fluvial to marine Campanian transect (3 m.y.), Western Interior seaway, southwestern Wyoming and northern Colorado: American Association of Petroleum Geologists Bulletin, v. 94, n. 9, p. 1349-1377.

Hampson, G., Stollhofen, H., and Flint, S., 1999, A sequence stratigraphic model for the Lower Coal Measures (Upper Carboniferous) of the Ruhr district, north-west Germany: Sedimentology, v. 46, p. 1199-1231.

Hayes, M.O., 1975, Morphology of sand accumulations in estuaries: an introduction to the symposium, *in* Cronin, L.E. ed., Estuarine Research, Vol. II: New York: Academic Press: p. 3-22.

Hettinger, R.D., McCabe, P.J., and Shanley, K.W., 1993, Detailed facies anatomy of transgressive and highstand systems tracts from the Upper Cretaceous of southern Utah, U.S.A., *in* Weimer, P., and Posamentier, H.W., eds., Siliciclastic sequence stratigraphy – Recent development and applications: American Association of Petroleum Geologists Memoir 58, ch.9 , p. 325-257.

Hettinger, R.D. and Kirschbaum, M.A., 2002, Stratigraphy of the Upper Cretaceous Mancos Shale (upper part) and Mesaverde Group in the southern part of the Uinta and Piceance Basins, Utah and Colorado: United State Geological Survey Geologic Investigation Series I-2674, 21 p.

Hettinger, R.D., and Kirschbaum, M.A., 2003, Statigraphy of the Upper Cretaceous Mancos Shale (upper part) and Mesaverde Group in the southern part of the Uinta and Piceance Basins, Utah and Colorado (Chapter 12), *in* Petroleum Systems and geologic assessment of oil and gas in the Uinta-Piceance Province, Utah and Colorado: United State Geological Survey Digital Data Series DDS-69-B, 25 p.

Heward, A.P., 1981, A Review of Wave-Dominated Clastic Shoreline Deposits *in* Earth Science Reviews: Elsevier Scientific Publishing Company: Amsterdam: v.17, p. 223-276.

Hewlett, A.C., 2010, Analysis and modeling of the fluvial architecture and static connectivity of the Williams Fork Formation, central Mamm Creek Field, Piceance Basin, Colorado: Master's thesis, University of Colorado, Boulder, CO.

Hickson, T.A., Sheets, B.A., Paola, C. and M Kelberer, M., 2005, Experimental test of tectonic controls on three-dimensional alluvial facies architecture: Journal of Sedimentary Research, v. 75, p. 710-722.

Hoak T.E., and Klawitter. A.L., 1997, Prediction of fractured reservoir production trends and compartmentalization using an intergrated analysis of basement structures in the Piceance Basin, western Colorado, *in* Hoak, T.E., Klawitter, A.L., and Blomquist, P.K., eds., Fractured reservoirs: characterization and modeling: Rocky Mountain Association of Geologists Guidebook, p. 67-102.

Holbrook, J.M., 1996, Complex fluvial response to low gradients at maximum regression: a genetic link between smooth sequence boundary morphology and architecture of overlying sheet sandstone: Journal of Sedimentary Research, v. 66, p. 713-722.

Howard, J.D., and Frey, R.W., 1984, Characteristic trace fossils in nearshore to offshore sequences, Upper Cretaceous of east-central Utah: Canadian Journal of Earth Sciences, v. 21, p. 200-219.

Izett, G.A., Cobban, W.A., Dalrymple, G.B., and Obradovich, J.D., 1998, $^{40}Ar/^{39}Ar$ age of the Manson impact structure, Iowa, and correlative impact ejecta in the Crow Creek Member of the Pierra Shale (Upper Cretaceous), South Dakota and Nebraska: Geological Society of America Bulletin, v. 110, p. 361-376.

Johnson, R.C., 1989, Geologic history and hydrocarbon potential of Late Cretaceous-age, low-permeability reservoirs, Piceance Basin, Western Colorado, Evolution of Sedimentary Basins-Unita and Piceance Basins: U.S. Geological Survey Bulletin 1787-E, 51 p.

Johnson, R.C., and Smith, M.C., 1993, Geologic Map of the Philadelphia Creek Quadrangle: U.S. Department of the Interior: Reston, Virginia: Geological Survey.

Johnson, R. C., and Flores, R.M., 2003, History of the Piceance Basin from Latest Cretaceous Through Early Eocene and the Characterization of Lower Tertiary Sandstone Reservoirs, *in* Peterson, K.M., Olson, T.M., and Anderson, D.S. eds., Piceance Basin 2003 Guidebook: Rocky Mountain Association of Geologists, p. 21-61.

Kirschbaum, M.A., and Hettinger, R.D., 1998, Stratigraphy and depositional environments of the Late Campanian coal-bearing Neslen/Mount Garfield Formations, eastern Book Cliffs, Utah and Colorado: U.S. Geological Survey Open-File Report 98-43, 1 pl.

Kirschbaum, M.A., and Hettinger, R.D., 2004, Facies Analysis and Sequence Stratigraphic Framework of Upper Campanian Strata (Neslen and Mount Garfield Formations, Bluecastle Tongue of the Castelgate Sandstone, and Mancos Shale), Eastern Book Cliffs, Colorado and Utah: U.S. Department of the Interior, Report DDS-69-G, 46 p.

Ke, X., Evans, G., and Collins, M.B., 1996, Hydrodynamics and sediment dynamics of The Wash Embayment, eastern England: Sedimentology, v. 43, p. 137-174.

Komar, P.D., 1976, Beach processes and sedimentation: Englewood Cliffs, New Jersey: Prentice Hall, 429 p.

Kreisa, R.D. and Moiola, R.J., 1986, Sigmoidal tidal bundles and other tide-generated sedimentary structures of the Curtis Formation, Utah: Geological Society of America Bulletin, v. 97, p. 381-387.

Leckie, D.A. and Walker, R. G., 1982, Storm- and tide-dominated shorelines in Cretaceous Moosebar-Lower Gates interval – Outcrop equivalents of deep basin gas trap in Western Canada: American Association of Petroleum Geologists Bulletin, v. 66, p. 138-157.

Lowe, D.R., 1975, Water escape structures in coarse-grained sediments: Sedimentology, v. 22, p. 157-204.

MacEachern, J.A., and Pemberton, G.S., 1992, Ichnological Aspects of Cretaceous Shoreface Successions and Shoreface Variability in the Western Interior Seaway of North America, *in* Pemberton, S.G. ed., Applications of Ichnology to Petroleum Exploration, A Core Workshop, Society for Sedimentary Geology Core Workshop No. 17: Society for Sedimentary Geology, p. 57-84.

Male, W.H., 1992, The Sedimentology and Ichnology of the Lower Cretaceous (Albian) Bluesky Formation in the Karr Area of West-Central Alberta, *in* Pemberton, S.G. ed., Applications of Ichnology to Petroleum Exploration, A Core Workshop, Society for Sedimentary Geology Core Workshop No. 17: Society for Sedimentary Geology, p. 33-56.

McCabe, P.J., 1984, Depositional environments of coal and coal-bearing strata, *in* Rahmani, R.A. and Flores, R.M. eds., Sedimentology of coal and coal–bearing sequences: International Association of Sedimentologists Special Publication 32, p. 51-66.

Mccabe, P.J., 1991, Geology of coal; environments of deposition, *in* Gluskoter, H.J., Rice, D.D., and Taylors, R.B., eds., Economic geology, U.S.: GSA, The Geology of North America, v. P-2.

Mclaurin, B.T., and Steel, R.J., 2000, Fourth-order nonmarine to marine sequences, middle Castlegate Formation, Book Cliffs, Utah: Geology, v. 28, p. 359-362.

Miall, A.D., 1985, Architectural-Element Analysis: A New Method of Facies Analysis Applied to Fluvial Deposits: Earth-Science Reviews, v. 22, p. 261-308.

Miall, A.D., 1992, Alluvial Deposits *in* Walker, R.G., and James N.P., eds., Facies Models Response to Sea Level Change: Waterloo, Ontario: Geological Association of Canada, p. 119-142.

Miall, A.D., 2006, Reconstructing the architecture and sequence stratigraphy of the preserved fluvial record as a tool for reservoir development: A reality check: American Association of Petroleum Geology Bulletin, v. 90, p. 989-1002.

Myrow, P.M., and Southard, J.B., 1991, Combined-flow model for vertical stratification sequence in shallow marine storm-deposited beds: Journal of Sedimentary Research, v. 61, p. 202-210.

Noe, D.C., 1984, Variations in Shoreline Sandstones from a Late Cretaceous interdeltaic embayment, Sego Sandstone (Campanian), Northwestern Colorado: Master's thesis, The University of Texas at Austin, TX, 64 p.

O'Brien, P.E., and Wells, A.T., 1986, A Small, Alluvial Crevasse Splay: Journal of Sedimentary Petrology, v. 56, n. 6, p. 876-879.

Olsen, T., Steel, R.J., Høgseth, K Skar, T., and Røe, S.L.,1995, Sequential architecture in a fluvial succession – sequence stratigraphy in the Upper Cretaceous Mesaverde Group, Price Canyon, Utah: Journal of Sedimentary Research, v. 65, n. 2, p. 265-280.

Panjaitan, H., 2006, Sand-body dimensions in outcrop and subsurface, lower Williams Fork Formation, Piceance Basin, Colorado: Master's thesis, Colorado School of Mines, CO, 170 p.

Patterson, P.E., Kronmueller, K., and Davies, T.D., 2003, Sequence Stratigraphy of the Mesaverde Group and Ohio Creek Conglomerate, Northern Piceance Basin, Colorado, *in* Peterson, K.M., Olson, T.M., and Anderson, D.S., eds., Piceance Basin 2003 guidebook: Rocky Mountain Association of Geologists, p. 115-128.

Pattison, Simon A.J., 1992, Recognition and interpretation of estuarine mudstones (central basin mudstones) in the tripartite valley-fill deposits of the Vikinig Cormation, Central Alberta, *in* Pemberton, S.G. ed., Applications of Ichnology to Petroleum Exploration, A Core Workshop, Society for Sedimentary Geology Core Workshop No. 17: Society for Sedimentary Geology, p. 223-249.

Pemberton, G.S., MacEachern, J.A., and Frey, R.W., 1992, Trace Fossil Facies Models: Environmental and Allostratigraphic Significance in Walker, R.G. and James N.P., eds., Facies Models Response to Sea Level Change: Waterloo, Ontario: Geological Association of Canada, p. 47-72.

Plint, A.G., 1991, High frequency relative sea level oscillations in Upper Cretaceous shelf clastics of the Alberta foreland basin - possible evidence of a glacio-eustatic control?, *in* MacDonald, D.I.M., ed., Sedimentation, tectonics and eustasy: International Association of Sedimentologists Special Publication, n. 12, p. 409-428.

Plint A.G., McCarthy, P.J., and Faccini, U.F., 2001, Nonmarine sequence stratigraphy: Updip expression of sequence boundaries and systems tracts in a high-resolution framework, Cenomanian Dunvegan Formation, Alberta foreland basin, Canada: American Association of Petroleum Geologists Bulletin, v. 85, n. 11, p. 1967-2001.

Plummer, P.S. and Gostin, V.A., 1981, Shrinkage cracks: dessication or synaeresis?: Journal of Sedimentary Petrology, v. 51, p. 1147-1156.

Posamentier, H.W., and Vail, P.R., 1988, Eustatic controls on clastic deposition II – sequence and systems tract models, *in* C.K. Wilgus, B.S. Hatings, C.G. St. C. Kendall, H.W. Posamentier, C.A. Ross, and J.C. Van Wagoner, eds., Sea level changes – an integrated approach: Society for Sedimentary Geology Special Publication 42, p. 125-154.

Posamentier, H.W., Jervey, M.T., and Vail, P.R., 1988, Eustatic controls on clastic deposition. I. Conceptual framework, *in* Wilgus, C.K., Hastings. B.S., Kendall. C.G.St.C., Posamentier, H.W., Ross. C.A., and Van Wagoner, J.C., eds., Sea Level Changes – An integrated Approach: Society for Sedimentary Geology Special Publication, v. 42, p. 110-124.

Posamentier, H.W., and Allen, G.P., 1993, Variability of the sequence stratigraphic model: effects of local basin factors: Sedimentary Geology, v. 86, p. 91-109.

Pranter, M.J., Ellison, A.I., Cole, R.D., and Patterson, P.E., 2007, Analysis and modeling of intermediate-scale reservoir heterogeneity based on a fluvial point-bar outcrop analog, Williams Fork Formation, Piceance Basin, Colorado: American Association of Petroleum Geologists Bulletin, v. 91, no. 7, p. 1025-1051.

Pranter, M.J., Vargas, M.F., and Davis, T.L., 2008, Characterization and 3-D reservoir modeling of fluvial sandstones of the Williams Fork Formation, Rulison Field, Piceance Basin, Colorado, U.S.A: Journal of Geophysics and Engineering, v. 5, p. 158-172.

Pranter, M.J., Cole, R.D., Panjaitan H., and Sommer, N.K., 2009, Sandstone-body dimensions in a lower coastal-plain depositional setting: Lower Williams Fork Formation, Coal Canyon, Piceance Basin, Colorado: American Association of Petroleum Geologists, v. 93, n. 10, pp. 1379-1401.

Reineck, H-E., and Wunderlich, F., 1968, Classification and Origin of Flaser and Lenticular Bedding: Sedimentology, v. 11, p. 99-104.

Reinson, G.E., 1992, Transgressive Barrier Island and Estuarine Systems *in* Walker R.G., and James N.P. eds., Facies Models Response to Sea Level Change: Waterloo, Ontario: Geological Association of Canada, p 179-194.

Rogers, R.R., 1998, Sequence analysis of the Upper Cretaceous Two Medicine and Judith River formation, Montana: nonmarine response to the Claggett and Bearpaw marine cycles: Journal of Sedimentary Research, v. 68, p. 615-631.

Sanders, J.E., 1960, Origin of Convoluted Laminae: Geological Magazine, v. 97, p. 409-421.

Saunders, T.D.A., and Pemberton, S.G., 1988, Trace fossils and sedimentology of a Late Cretaceous progradational barrier island sequence: Bearpaw-Horseshoe Canyon Formation transition: Dorothy, Alberta: Canadian Society of Petroleum Geologists, Field trip guide, Sequences, Stratigraphy, Sedimentology: Surface and Subsurface, 166 p.

Schwartz, R.K., 1982, Bedforms and stratification characteristics of some modern small-scale washover sand bodies: Sedimentology, v. 29, p. 835-850.

Shaak, R.V., 2010, Stratigraphic architecture of shallow-marine to coastal-plain parasequences: lower Williams Fork Formation, Southeastern Piceance Basin, Colorado: Master's thesis, University of Colorado, Boulder, CO, 176 p.

Shanley, K.W., and McCabe, P.J., 1991, Predicting facies architecture through sequence stratigraphy – an example from the Kaiparowitz Plateau, Utah: Geology, v. 19, p. 742-745.

Shanley, K.W., McCabe, P.J., and Hettinger, R.D., 1992, Tidal influence in Cretaceous fluvial strata from Utah, USA: a key to sequence stratigraphic interpretation: Sedimentology, v. 39, p. 905-930.

Shanely, K.W., and McCabe, P.J., 1993, Alluvial architecture in a sequence stratigraphic framework: a case history from the Upper Cretaceous of southern Utah, U.S.A., *in* S.S. Flint and I.D. Bryant, eds., The geological modeling of hydrocarbon reservoirs and outcrop analogues: International Association of Sedimentologists Special Publication 15, p. 21-56.

Shanley, K.W., and McCabe, P.J., 1994, Perspectives on the Sequence Stratigraphy of continental strata: American Association of Petroleum Geologists Bulletin, v. 78, p. 544-568.

Shanley, K.W., and McCabe, P.J., 1995, Sequence stratigraphy of Turonian-Santonian strata, Kaiparowitz Plateau, southern Utah, U.S.A.: implications for regional correlation and foreland basin evolution, *in* J.C. Van Wagoner and G.T. Bertram, eds., American Association of Petroleum Geologists Memoir 64, p. 103-136.

Sommer, N. K., 2007, Sandstone-body connectivity in a meandering-fluvial system: An example from the Williams Fork Formation, Piceance Basin, Colorado: Master's thesis, University of Colorado, Boulder, CO, 193 p.

Soliman, S.M., 1964, Primary structures in part of the Nile delta sand beach, *in* L.M.J.U. van Straaten ed., Deltaic and Shallow Marine Deposits: Amsterdam: Elsevier p. 379-387.

Southard, J.B., 1982, Bed Configurations, in J.C. Harms, J.B. Southard, and R.G. Walker eds., Structures and sequences in clastic rocks: Society of Economic Paleontologists and Mineralogists, Short Course Notes 9, p. 1-24.

Thomas, R.G., Smith, D.G., Wood, J.M., Visser, J., Calverley-Range, E.A., and Koster, E.H., 1987, Inclined Heterolithic Stratification – Terminology, Description, Interpretation and Significance: Sedimentary Geology, v. 53, p. 123-179.

Vail, P.R., Mitchum, R.M., and Thompson, S. III, 1977, Seismic stratigraphy and global changes of sea level, Part 4: Global cycles of relative changes in sea level, *in* Payton, C.E. ed., Seismic stratigraphy – Applications to hydrocarbon exploration: American Association of Petroleum Geologists Memoir 26, p. 83-97.

Van Wagoner, J.C., Posamentier, H.W., Mitchum, R.M., Vail. P.R., Sarg, J.F., Loutit T.S., and Hardenbol, J., 1988, An overview of the fundamentals of sequence stratigraphy and key definition, *in* Wilgus, C.K., Hastings, B.S., Kendall, C.G.St.C., Posamentier, H.W., Ross, C.A., and Van Wagoner, J.C., eds, Sea-Level Changes: An Integrated Approach: Society for Sedimentary Geology Special Publication 42, p. 39-45.

Van Wagoner, J.C., 1991, High-frequency sequence stratigraphy and facies architecture of the Sego Sandstone in the Book Cliffs of western Colorado and eastern Utah, *in* Van Wagoner, J.C., Nummedal, D., Jones, C.R., Taylor, D.R., Jennette, D.C., and Riley, G.W., eds., Sequence stratigraphy – Applications to shelf sandstone reservoirs: American Association of Petroleum Geologists Field Conference, p. 1-10.

Van Wagoner, J.C., Mitchum, R.M., Campion, K.M., and Rahmanian, V.D., 1990, Siliciclastic sequence stratigraphy in well logs, cores, and outcrops – Concepts for high-resolution correlation of time and facies: American Association of Petroleum Geologists Methods in Exploration Series, no. 7, 55 p.

Vargas, M.F., 2004, Characterization and modeling of fluvial sandstone distribution and static connectivity, Williams Fork Formation, Rulison Field, Piceance Basin, Colorado: Master's thesis, University of Colorado, Boulder, CO, 136 p.

Walker, R.G., 1992, Facies, facies models and modern stratigraphic concepts, *in* Walker, R.G., and James, N.P., eds., Facies Models Response to Sea Level Change: Waterloo, Ontario: Geological Association of Canada, p, 1-14.

Walker, R.G., and Plint, A.G., 1992, Wave- and Storm-Dominated Shallow Marine Systems, *in* Walker, R.G., and James N.P., eds., Facies Models Response to Sea Level Change: Waterloo, Ontario: Geological Association of Canada, p 219-238.

Wightman, D.M., Pemberton, G.S., and Singh, C., 1987, Depositional modeling of the Upper Mannville (Lower Cretaceous) central Alberta: Implications for the recognition of brackish water deposits, *in* Tillman, R.W. and Weber, K.J. eds., Reservoir Sedimentology: Society of Economic Paleontologists and Mineralogists, Special Publication 40, p. 189-220.

Willis, B.J., and Gabel, S.L., 2003, Formation of Deep Incisions into Tide-Dominated River Deltas: Implications for the Stratigraphy of the Sego Sandstone, Book Cliffs, Utah, W.S.A.: Society for Sedimentary Geology Journal of Sedimentary Research, v. 73, p. 246-263.

Yoshida, S., Willis, A., and Miall, A.D.,1996, Tectonic control of nested sequence architecture in the Castlegate Sandstone (Upper Cretaceous), Book Cliffs, Utah: Journal of Sedimentary Research, v. 66, p. 737-748.

Yoshida, S., Miall, A.D., and Willis, A., 1998, Sequence stratigraphy and marine to nonmarine facies architecture of foreland basin strata, Book Cliffs, Utah, U.S.A. – Discussion: American Association of Petroleum Geologists, v. 82, p. 1596-1606.

Yoshida, S., Johnson, H.D., Pye, K., and Dixon, R.J., 2004, Transgressive changes from tidal estuarine to marine embayment depositional systems: The Lower Cretaceous Woburn Sands of southern England and comparison with Holocene analogs: American Association of Petroleum Geologists, v. 88, n. 10, p. 1433-1460.

APPENDIX A

1. **Locations of measured sections**
2. **Photopans of measured sections**
3. **Measured sections**
4. **Mini-measured sections**
5. **Sampled Interval**

ID	Name	N	W	Elevation (ft)	Sandstone Body ID
SBW	State Bridge Draw West	39°55'53"	108°44'39"	5835	NA
SBS	State Bridge Draw South	39°55'07"	108°44'26"	5833	NA
SBE	State Bridge Draw East	39°55'37"	108°43'49"	5823	NA
VDN	Vandamore Draw North	39°54'41"	108°44'19"	5889	NA
VDW	Vandamore Draw West	39°54'50"	108°44'26"	5733	NA
VDS	Vandamore Draw South	39°54'29"	108°44'22"	5901	NA
PCW	Philadelphia Creek West	39°53'59"	108°44'10"	5863	NA
PCE1	Philadelphia Creek East 2	39°54'15"	108°42'43"	6035	NA
PCE2	Philadelphia Creek East 1	39°54'00"	108°43'19"	6035	NA
MS8	State Bridge Draw West	4422069.513	692863.270	5811	CB13
MS7	State Bridge Draw West	4422067.675	692782.659	5790	CB15
MS6	State Bridge Draw West	4422058.871	692922.534	5796	CB17
MS9	State Bridge Draw West	4422058.146	692811.172	5824	CB14, 1
MS10	State Bridge Draw West	4422010.413	692769.676	5826	CB14, 2
MS3	State Bridge Draw West	4422127.395	693032.939	5964	CB8 and CS3
MS4	State Bridge Draw West	4422125.504	693019.506	5966	CB8 and CS3
MS5	State Bridge Draw West	4422271.996	693077.541	5937	NA
MS1	State Bridge Draw West	4422096.024	692968.515	5883	CB18 and CB19
MS2	State Bridge Draw West	4422073.153	693081.140	5882	CB18 and CB19
MS1	Vandamore Draw South	4419917.851	693295.927	5892	CB5 and CB4
MS2	Vandamore Draw South	4419903.287	693354.979	6006	CB6

Appendix A1 Latitude and Longitude coordinates taken with a Garmin GPS with 30 ft (10 m) accuracy at the base of each measured section and mini-measured section.

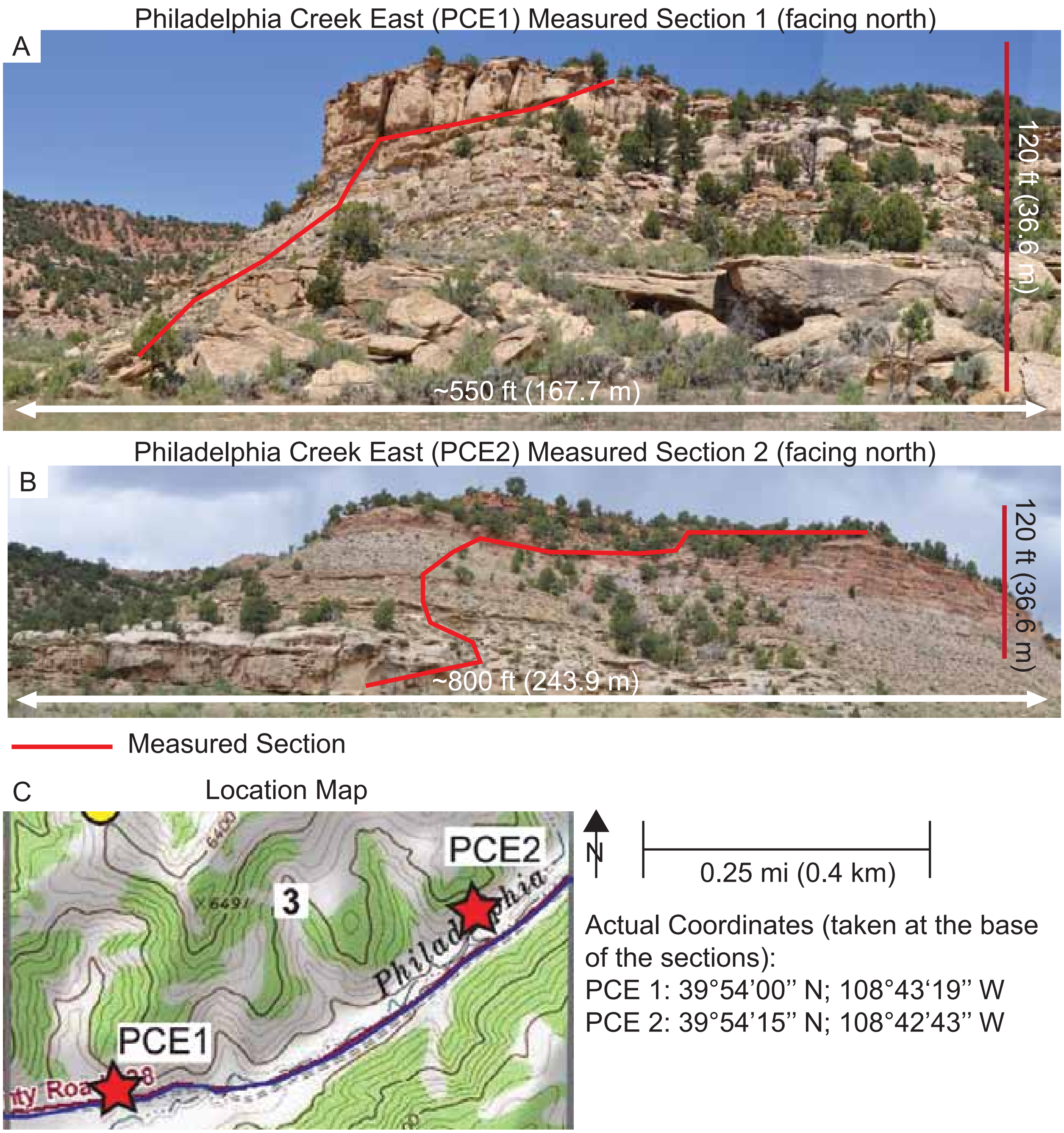

Appendix A2: Measured section photopans for A) PCE 1 and B) PCE 2. C) Location map for parts A and B. See Appendix A4 for measured sections.

Philadelphia Creek West (PCW) Measured Section (facing north)

Vandamore Draw South (VDS) Measured Section (facing east)

Measured Section

C Location Map

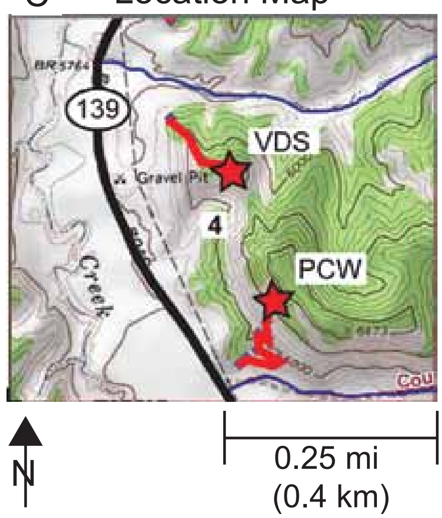

Actual Coordinates:
PCW: 39°53'59'' N; 108°44'10'' W
VDS: 39°54'29'' N; 108°44'22'' W

Appendix: Measured section photopans for A) PCW and B) VDS. C) Location map for parts A and B. See Appendix for measured sections.

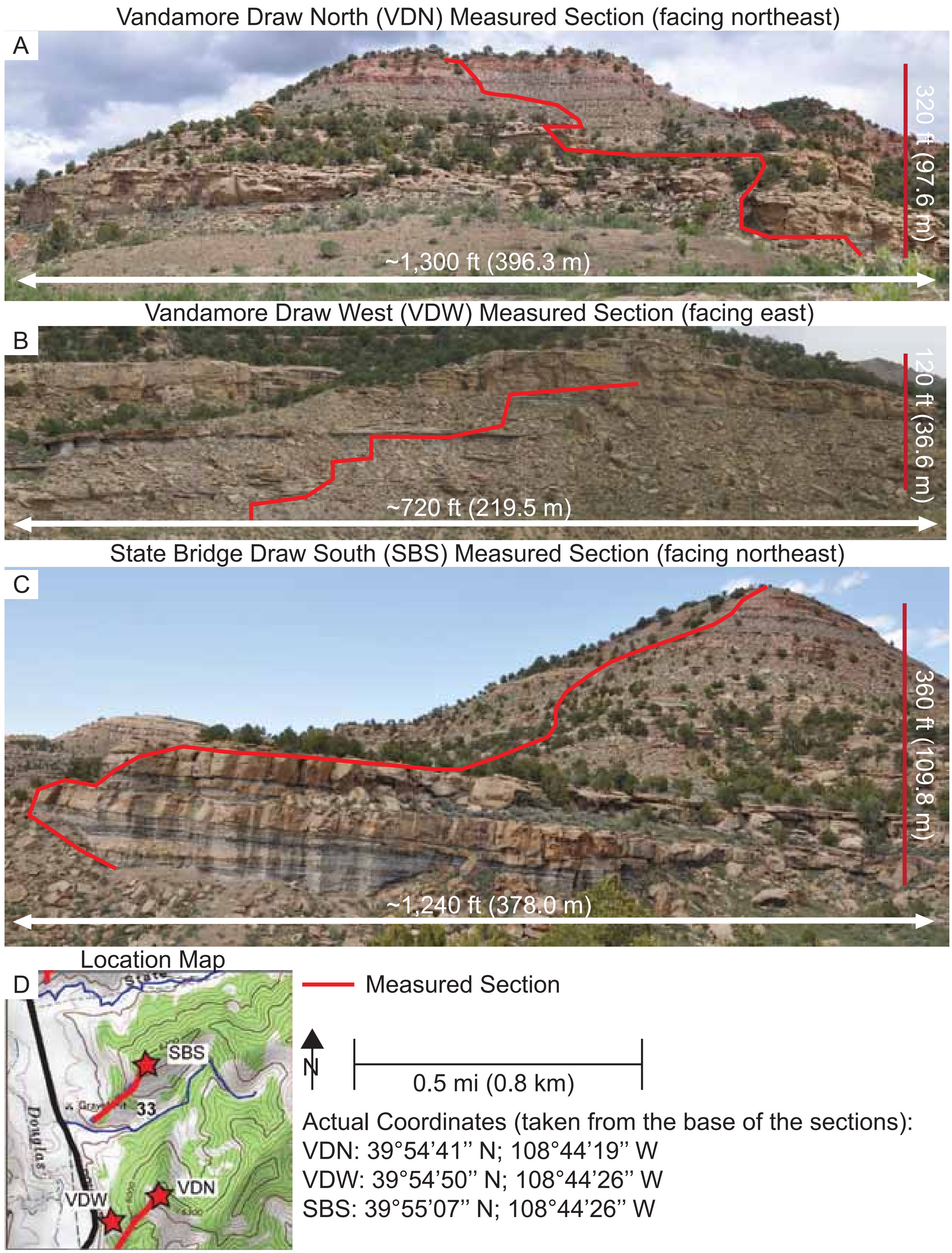

Appendix A2: Measured section photopans for A) VDN, B) VDW, and C) SBS. D) Location map for parts A, B and C. See Appendix A3 for measured sections.

State Bridge Draw West (SBW) Measured Section (facing north)

State Bridge Draw East (SBE) Measured Section (facing north)

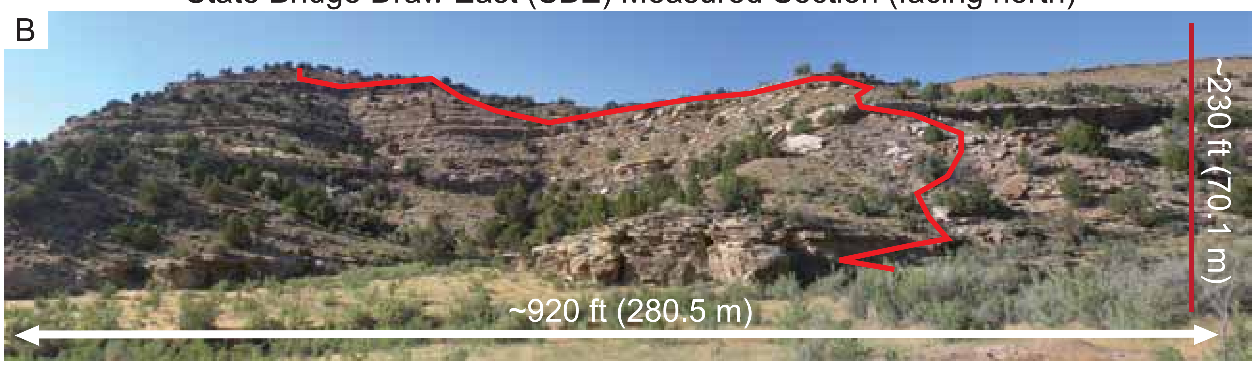

Measured Section

Location Map

Actual Coordinates (taken at the base of sections):
SBW: 39°55’53’’ N; 108°44’39’’ W
SBE: 39°55’37’’ N; 108°43’49’’ W

Appendix A2: Measured section photopans for A) SBW and B) SBE. C) Location map for parts A and B. See Appendix A3 for measured sections.

Appendix A3

Key to all Measured Sections

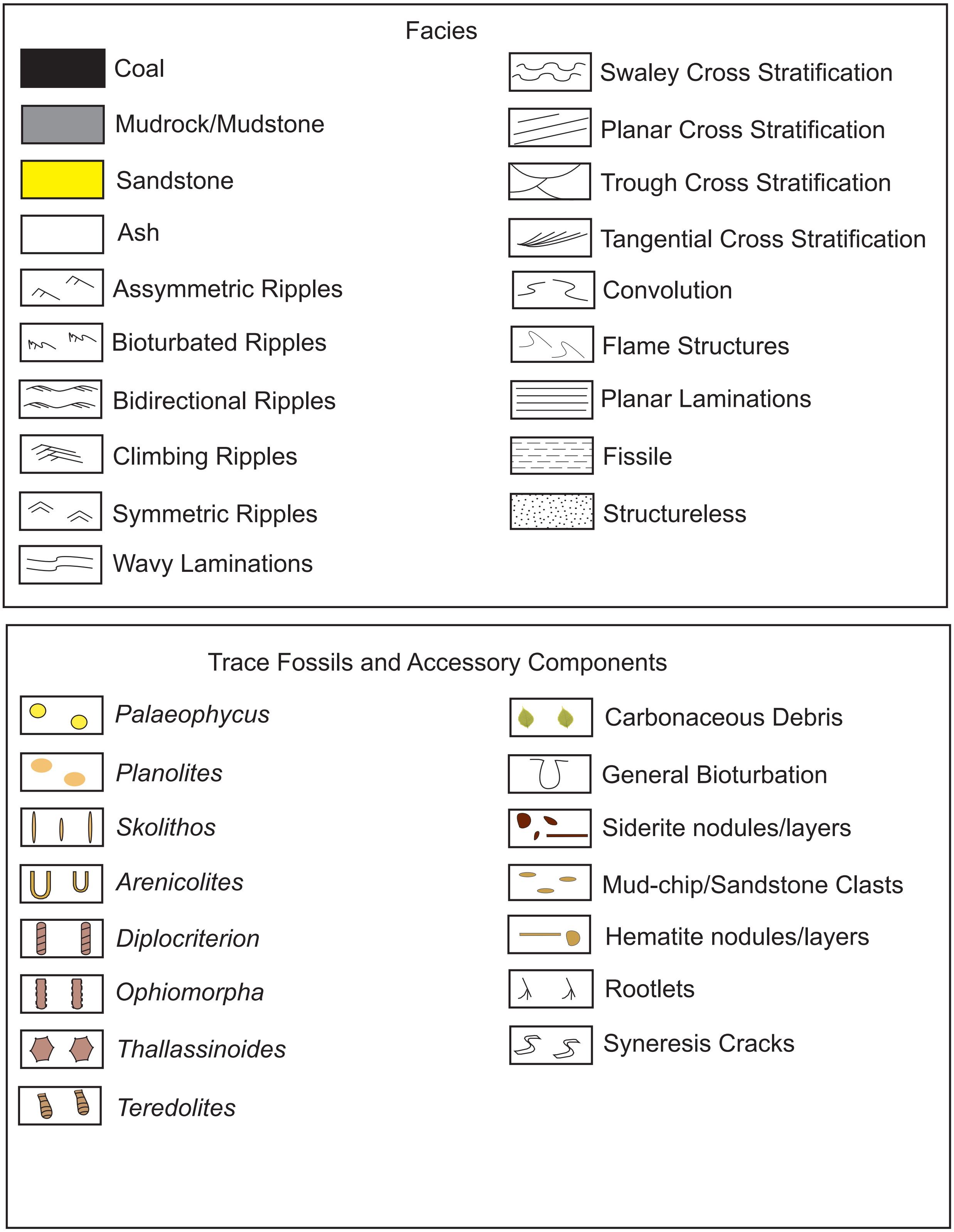

Appendix A3 Key for measured sections.

Appendix A3

Philadelphia Creek East (PCE) Measured Section

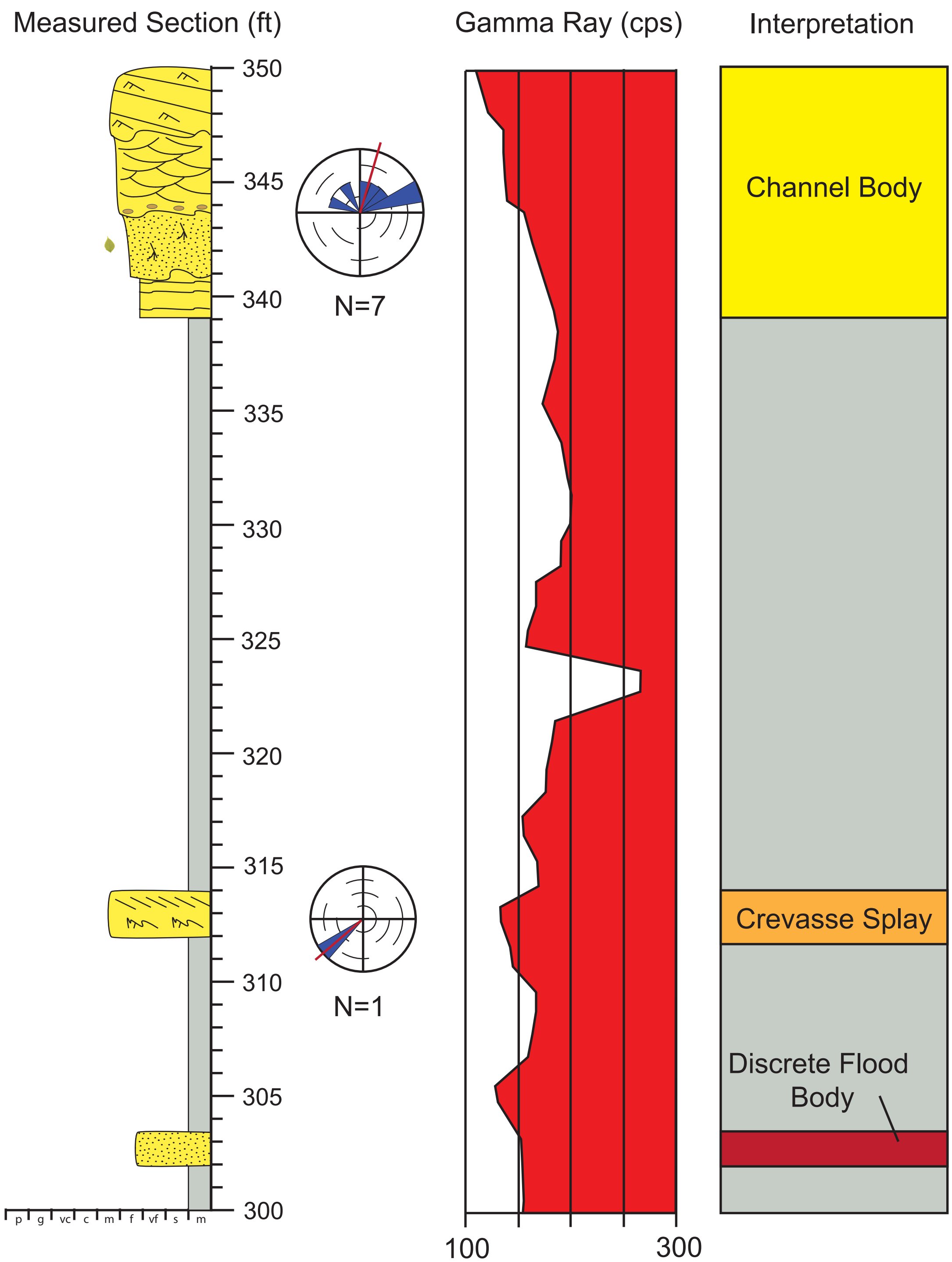

Measured Section (ft)
Gamma Ray (cps)
Interpretation
350
345
340
335
330
325
320
315
310
305
300
p g vc c m f vf s m
N=7
N=1
100
300
Channel Body
Crevasse Splay
Discrete Flood Body

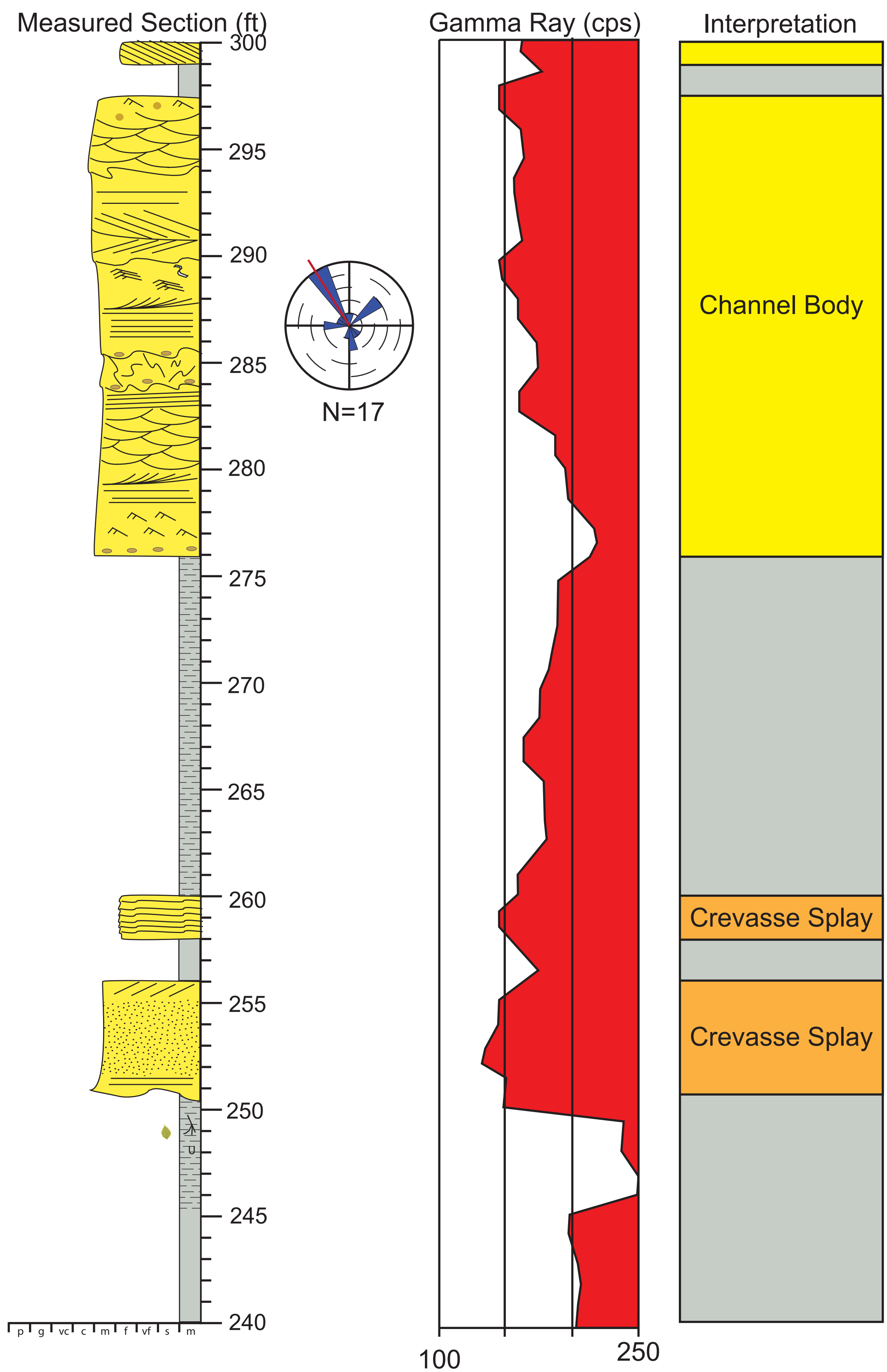
Measured Section (ft)
300
295
290
285
280
275
270
265
260
255
250
245
240
p g vc c m f vf s m
N=17
Gamma Ray (cps)
100
250
Interpretation
Channel Body
Crevasse Splay
Crevasse Splay

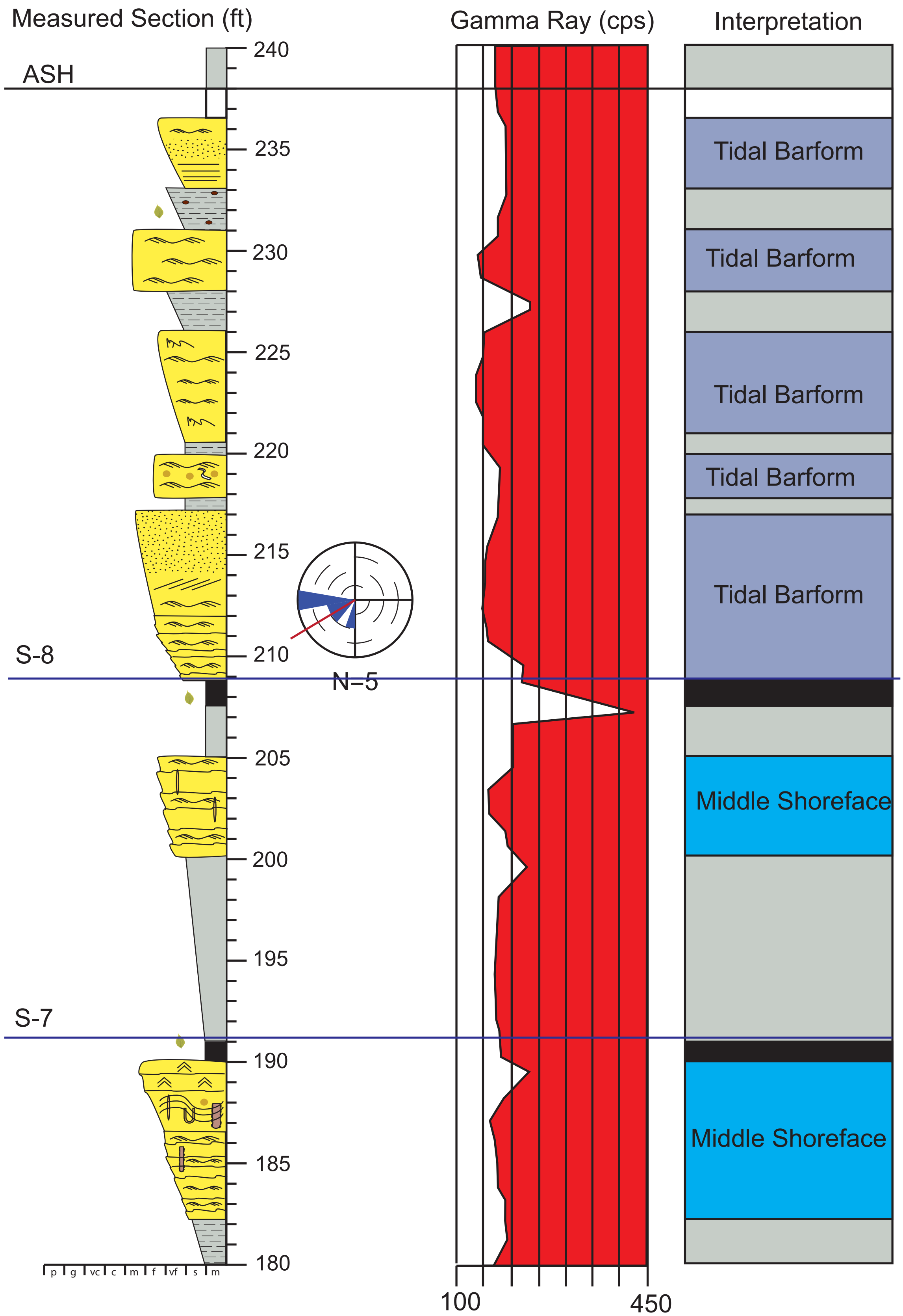

Measured Section (ft)
Gamma Ray (cps)
Interpretation
ASH
240
235
230
225
220
215
210
205
200
195
190
185
180
S-8
S-7
N–5
p g vc c m f vf s m
100
450
Tidal Barform
Tidal Barform
Tidal Barform
Tidal Barform
Tidal Barform
Middle Shoreface
Middle Shoreface

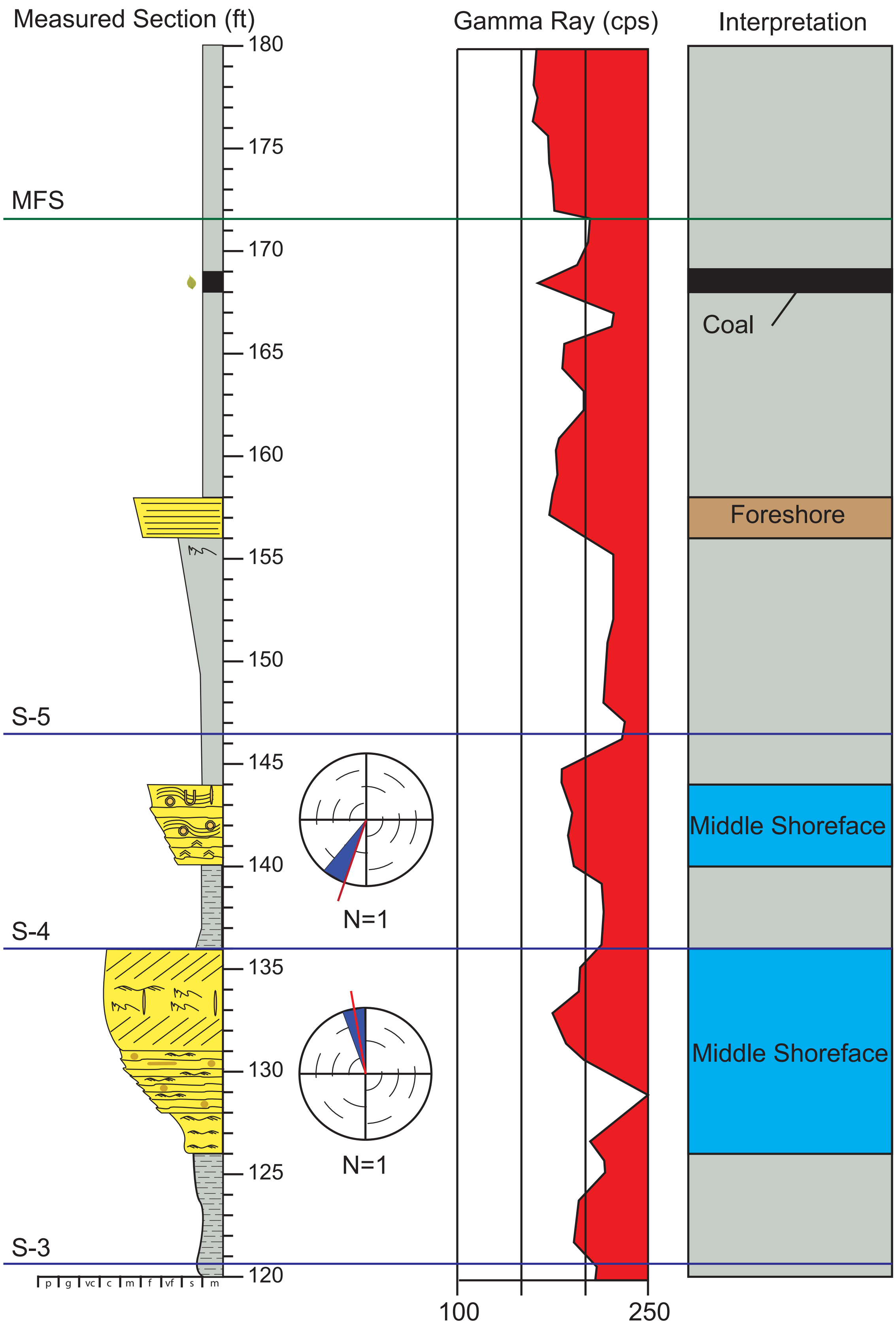

Measured Section (ft)
Gamma Ray (cps)
Interpretation
180
175
170
165
160
155
150
145
140
135
130
125
120
MFS
S-5
S-4
S-3
p g vc c m f vf s m
N=1
N=1
100
250
Coal
Foreshore
Middle Shoreface
Middle Shoreface

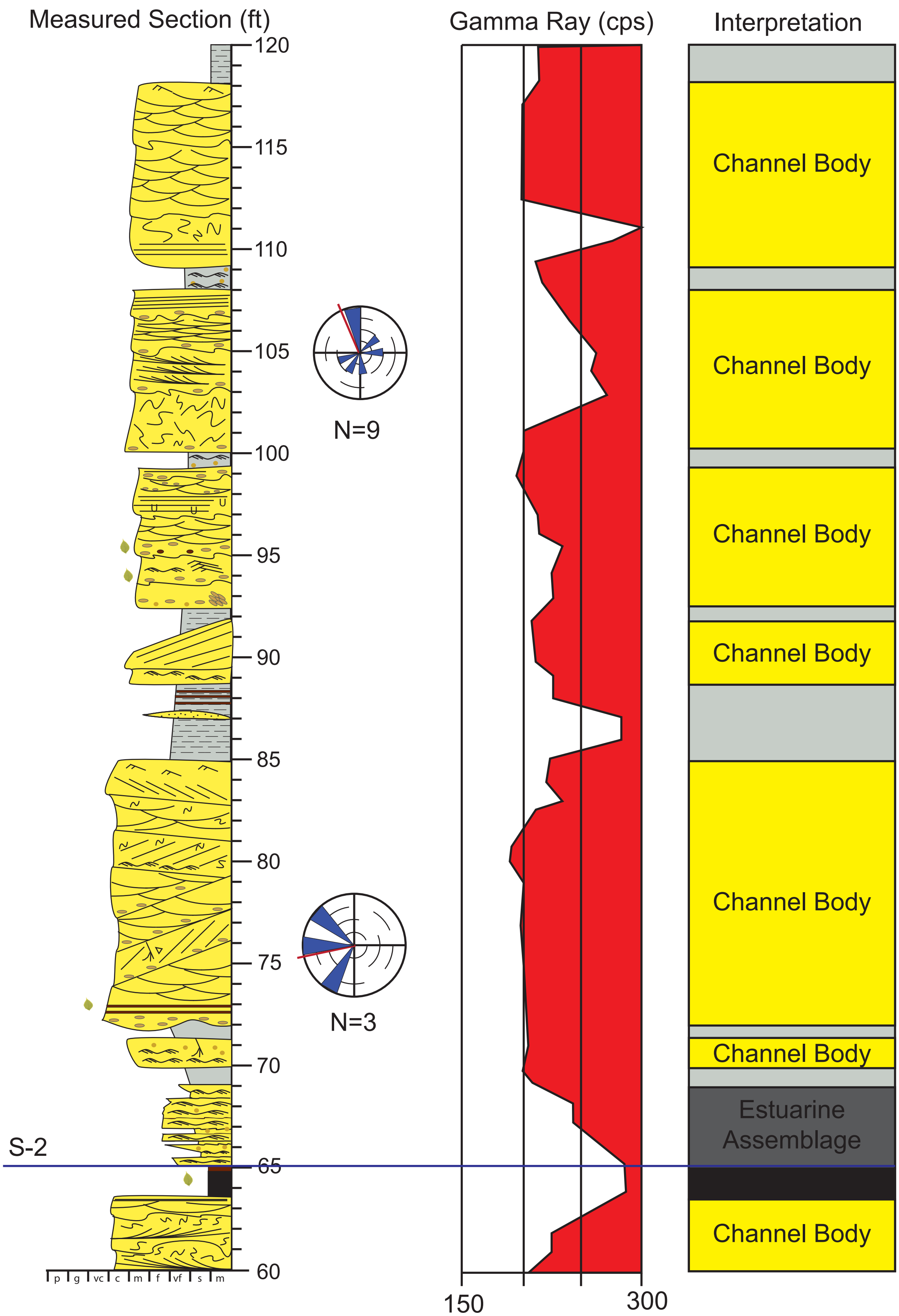

Measured Section (ft)
120
115
110
105
100
95
90
85
80
75
70
65
60
p g vc c m f vf s m
S-2
N=9
N=3
Gamma Ray (cps)
150
300
Interpretation
Channel Body
Channel Body
Channel Body
Channel Body
Channel Body
Channel Body
Estuarine Assemblage
Channel Body

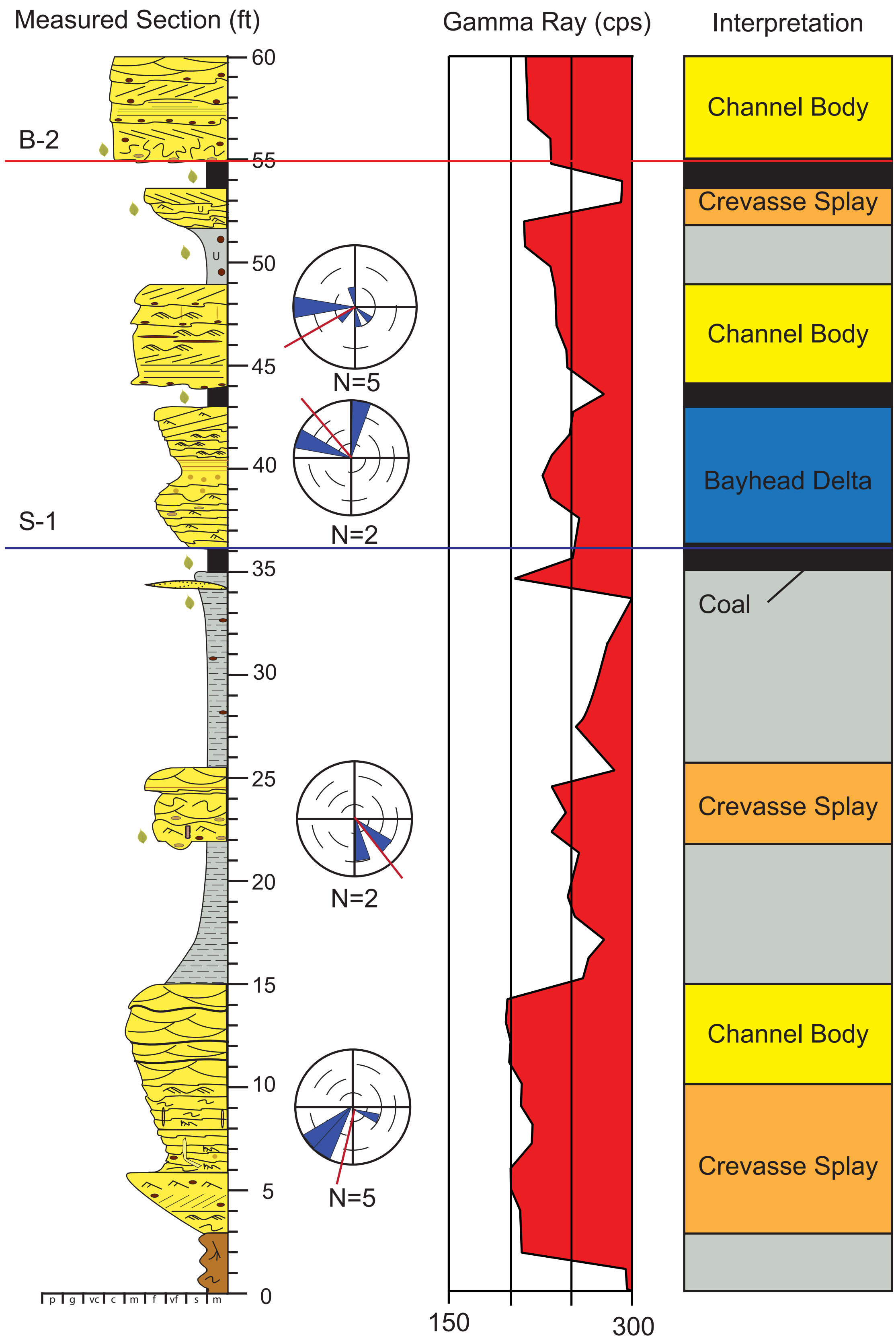

Measured Section (ft)
Gamma Ray (cps)
Interpretation
B-2
S-1
60
55
50
45
40
35
30
25
20
15
10
5
0
p g vc c m f vf s m
N=5
N=2
N=2
N=5
150
300
Channel Body
Crevasse Splay
Channel Body
Bayhead Delta
Coal
Crevasse Splay
Channel Body
Crevasse Splay

Appendix A3

Philadelphia Creek West (PCW) Measured Section

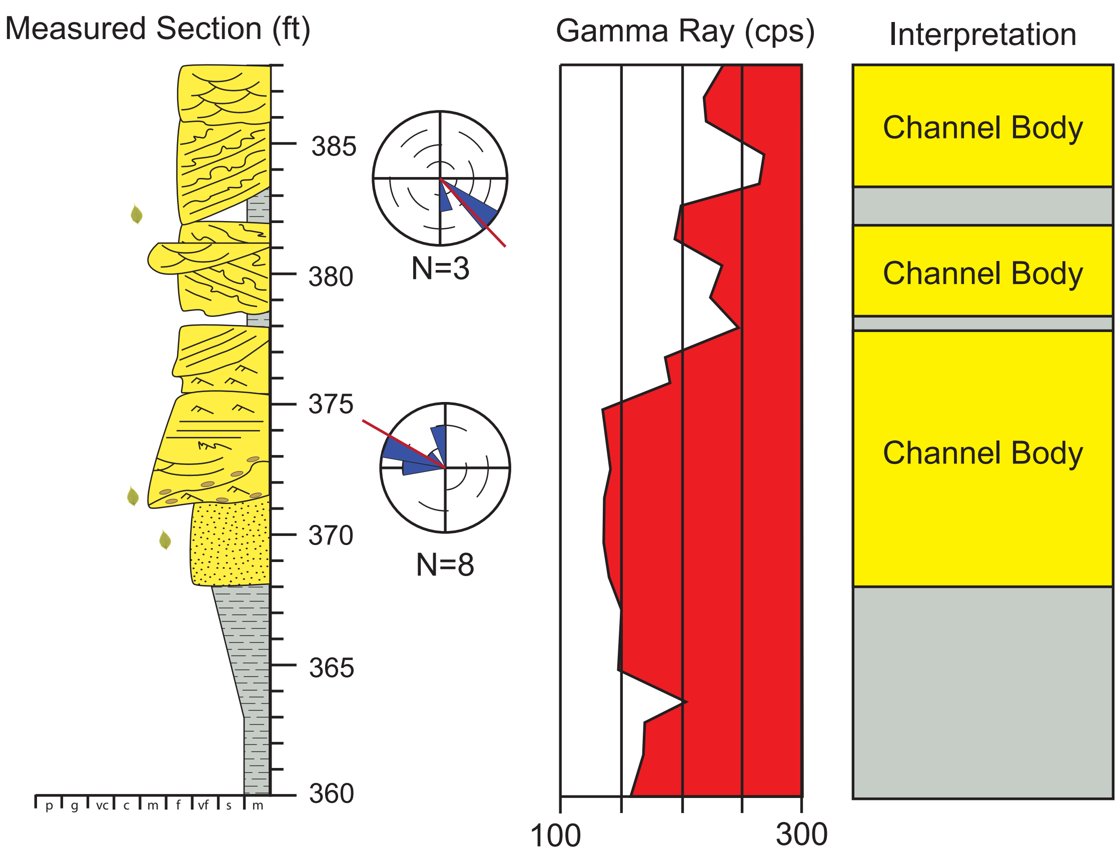

Measured Section (ft)
385
380
375
370
365
360
p g vc c m f vf s m
N=3
N=8
Gamma Ray (cps)
100
300
Interpretation
Channel Body
Channel Body
Channel Body

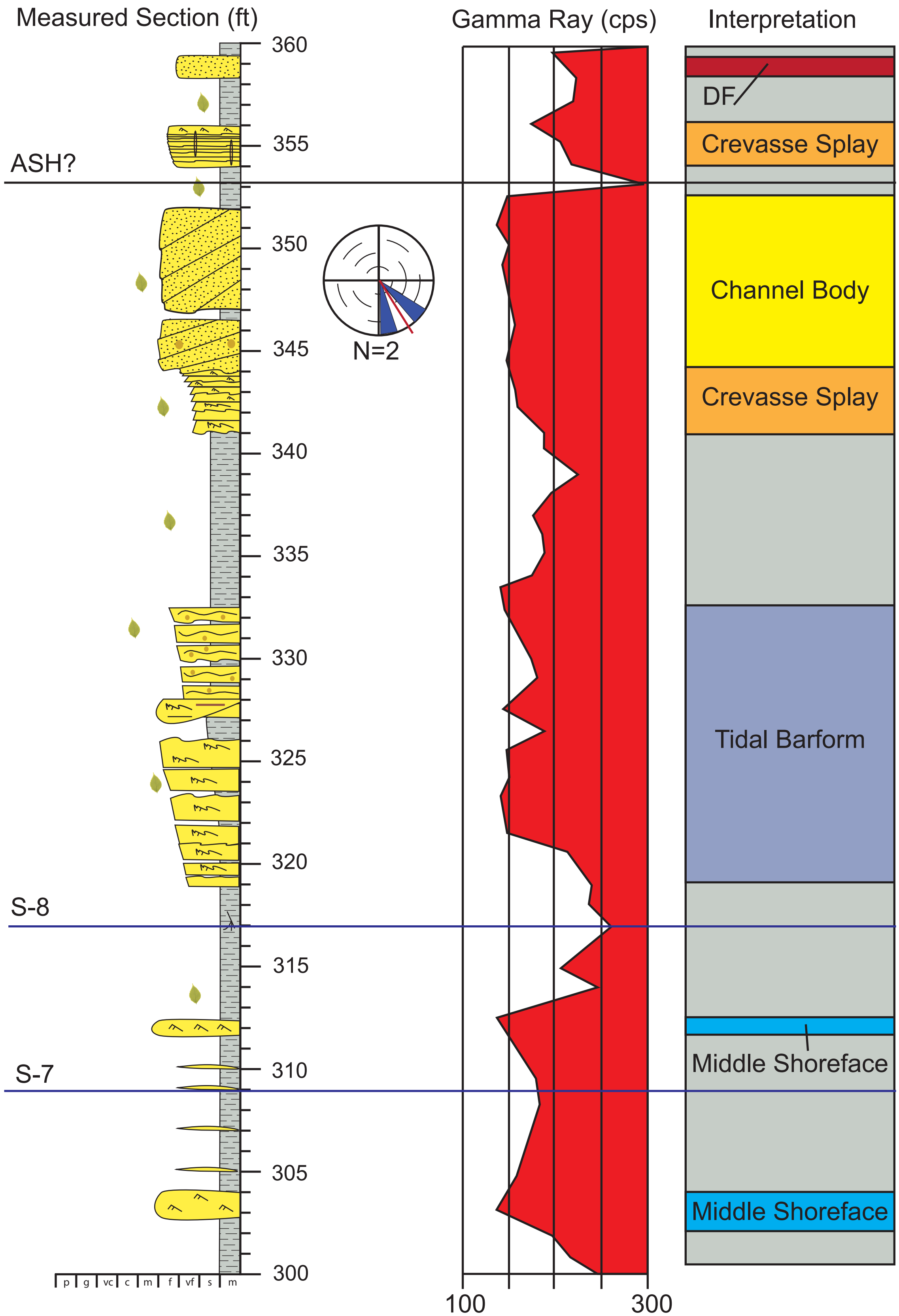

Measured Section (ft)
Gamma Ray (cps)
Interpretation
360
355
350
345
340
335
330
325
320
315
310
305
300
ASH?
S-8
S-7
N=2
p g vc c m f vf s m
100
300
DF
Crevasse Splay
Channel Body
Crevasse Splay
Tidal Barform
Middle Shoreface
Middle Shoreface

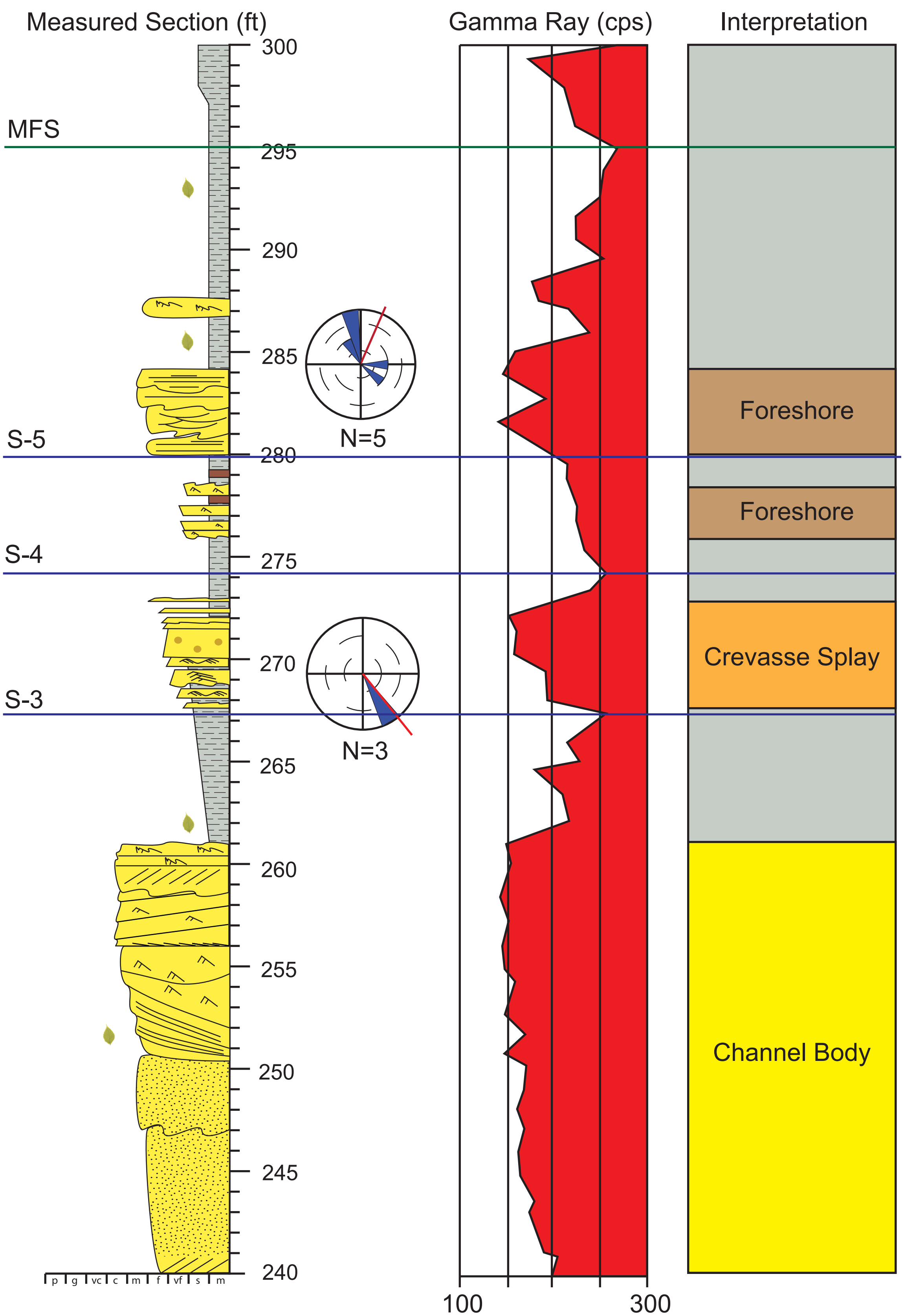

Measured Section (ft)
Gamma Ray (cps)
Interpretation
MFS
S-5
S-4
S-3
300
295
290
285
280
275
270
265
260
255
250
245
240
N=5
N=3
p g vc c m f vf s m
100
300
Foreshore
Foreshore
Crevasse Splay
Channel Body

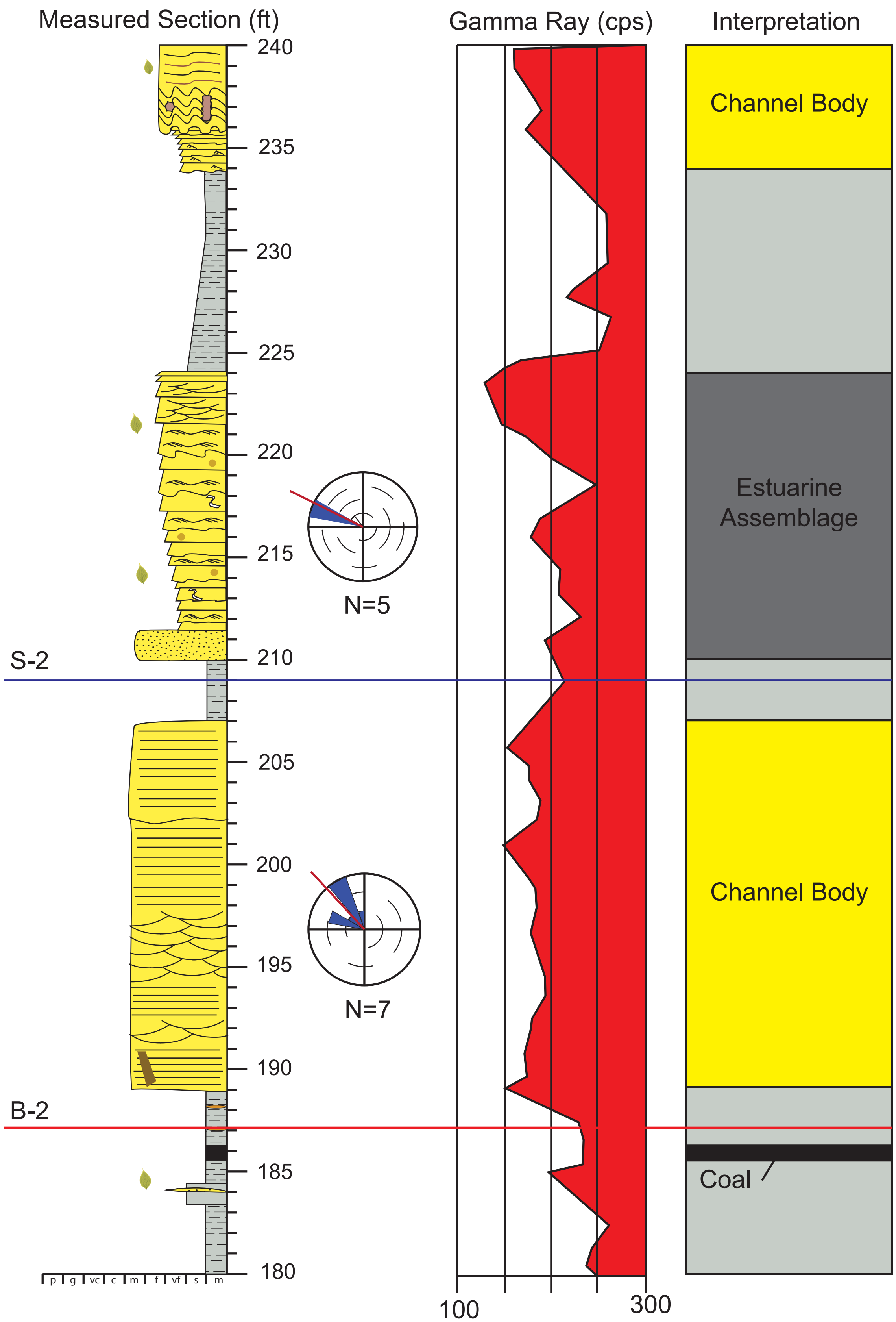

Measured Section (ft)
240
235
230
225
220
215
210
205
200
195
190
185
180
p g vc c m f vf s m
S-2
B-2
N=5
N=7
Gamma Ray (cps)
100
300
Interpretation
Channel Body
Estuarine Assemblage
Channel Body
Coal

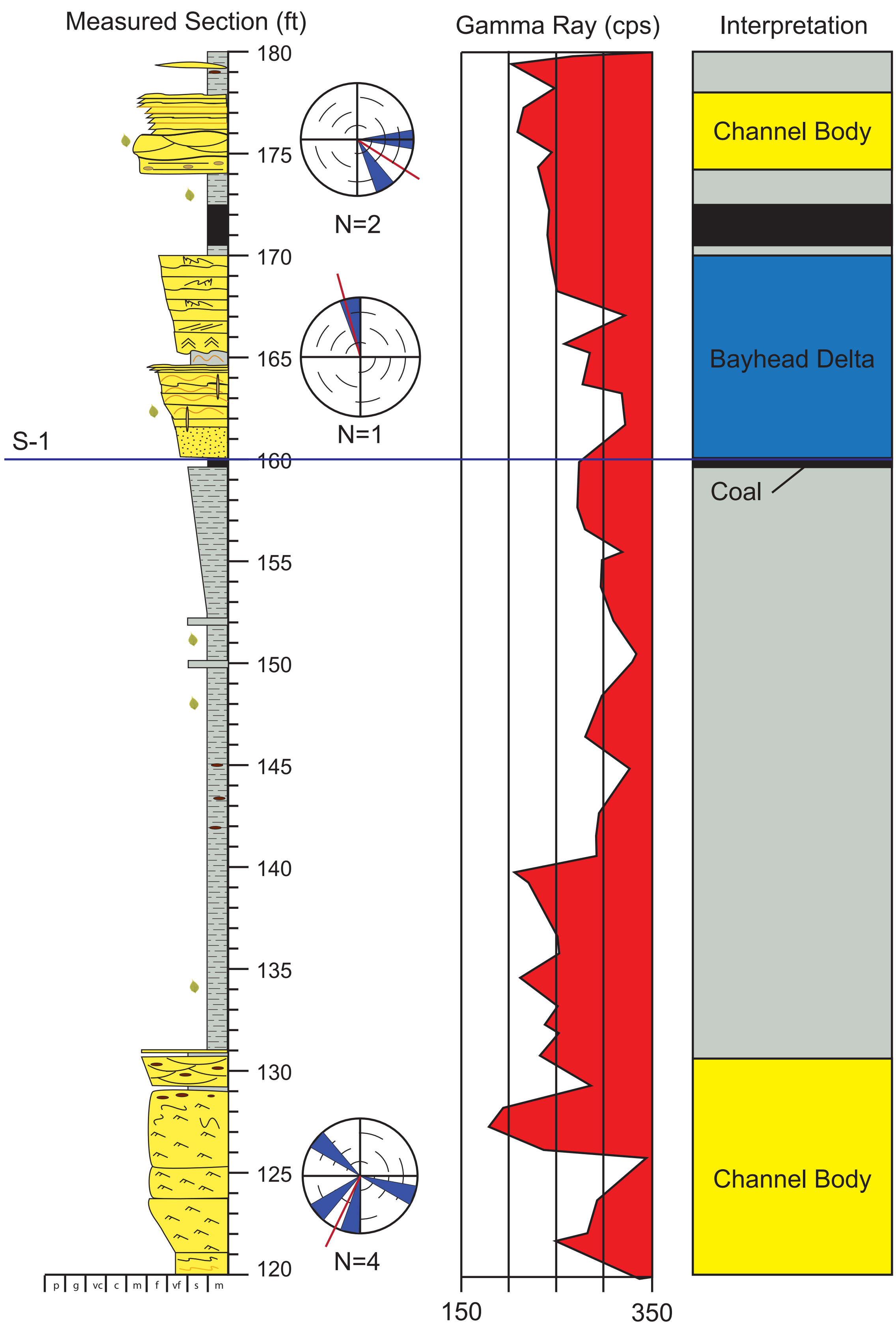
Measured Section (ft)
Gamma Ray (cps)
Interpretation
180
175
170
165
160
155
150
145
140
135
130
125
120
S-1
N=2
N=1
N=4
p g vc c m f vf s m
150
350
Channel Body
Bayhead Delta
Coal
Channel Body

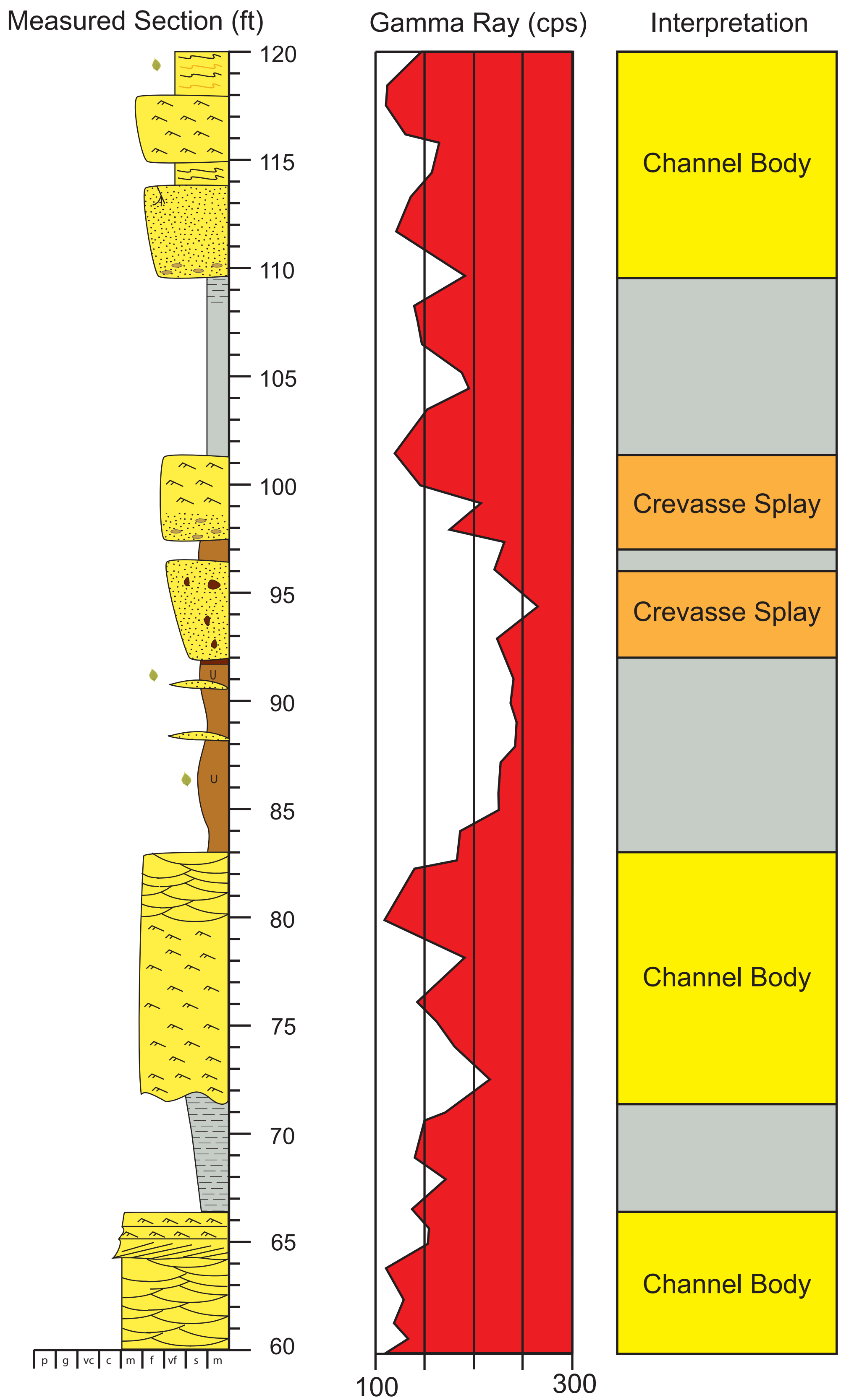
Measured Section (ft)
Gamma Ray (cps)
Interpretation
120
115
110
105
100
95
90
85
80
75
70
65
60
p
g
vc
c
m
f
vf
s
m
100
300
Channel Body
Crevasse Splay
Crevasse Splay
Channel Body
Channel Body

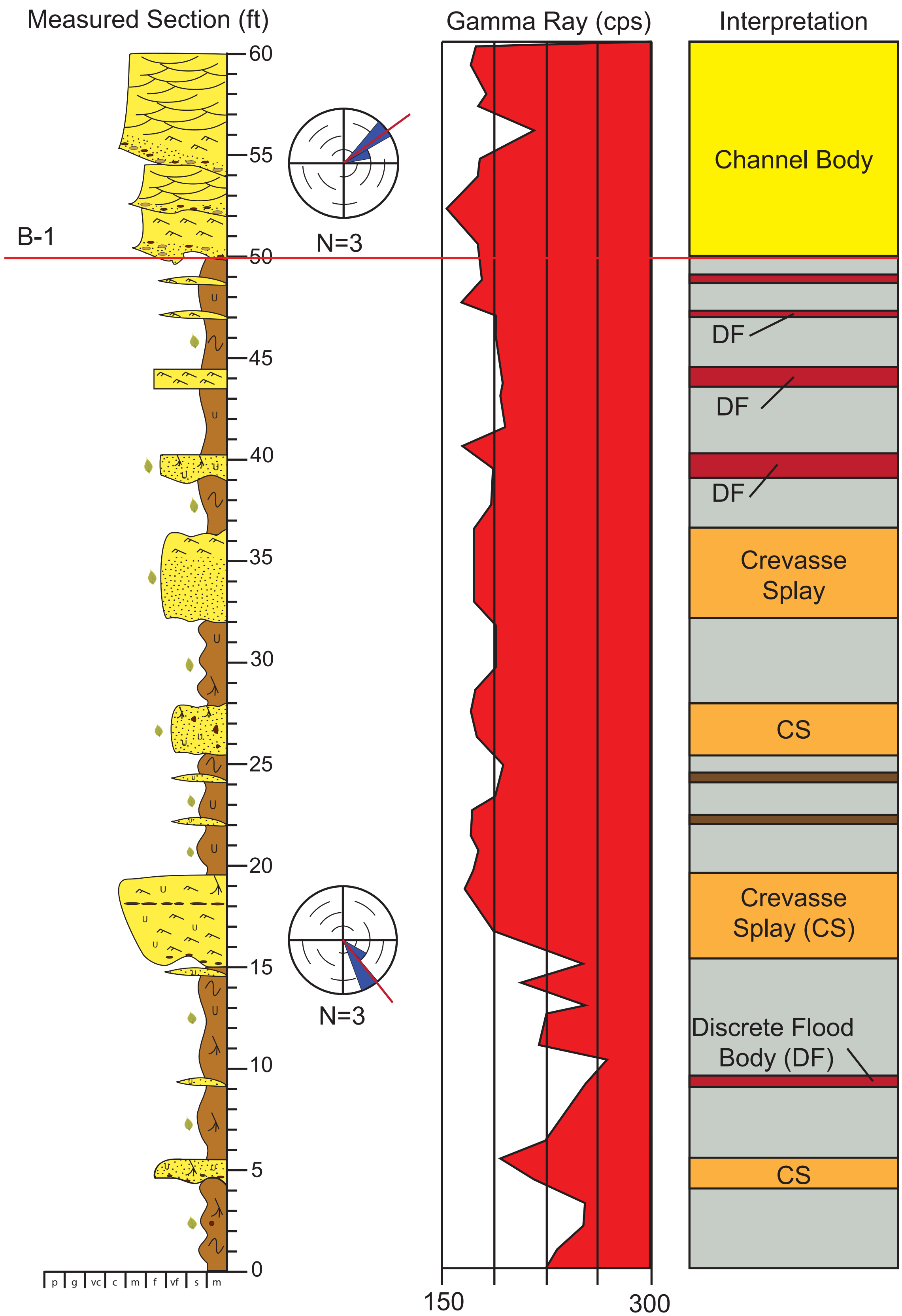
Measured Section (ft)
Gamma Ray (cps)
Interpretation
60
55
50
45
40
35
30
25
20
15
10
5
0
B-1
N=3
N=3
p g vc c m f vf s m
150
300
Channel Body
DF
DF
DF
Crevasse Splay
CS
Crevasse Splay (CS)
Discrete Flood Body (DF)
CS

Appendix A3

Vandamore Draw South (VDS) Measured Section

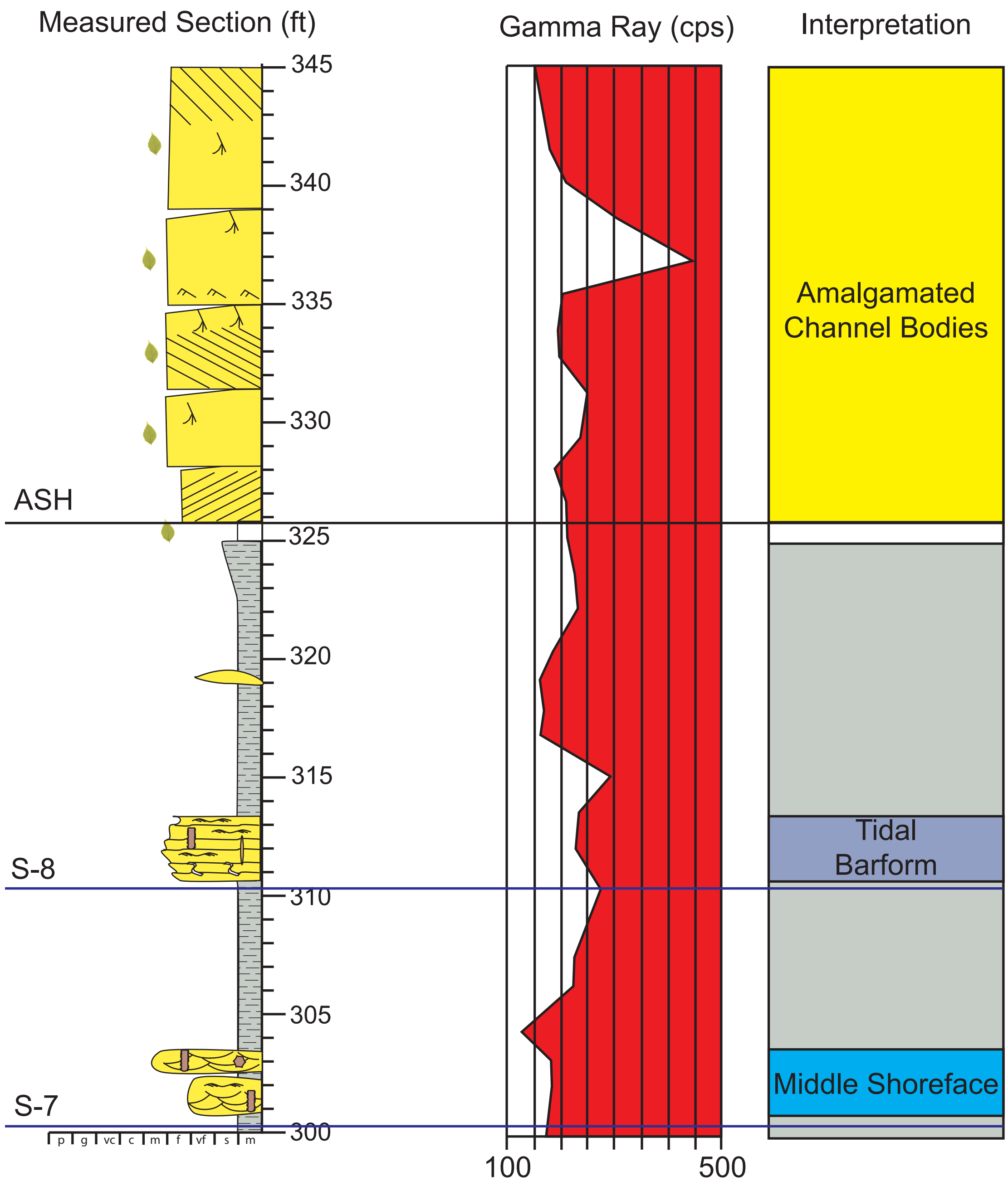
Measured Section (ft)
Gamma Ray (cps)
Interpretation
345
340
335
330
325
320
315
310
305
300
ASH
S-8
S-7
p
g
vc
c
m
f
vf
s
m
100
500
Amalgamated Channel Bodies
Tidal Barform
Middle Shoreface

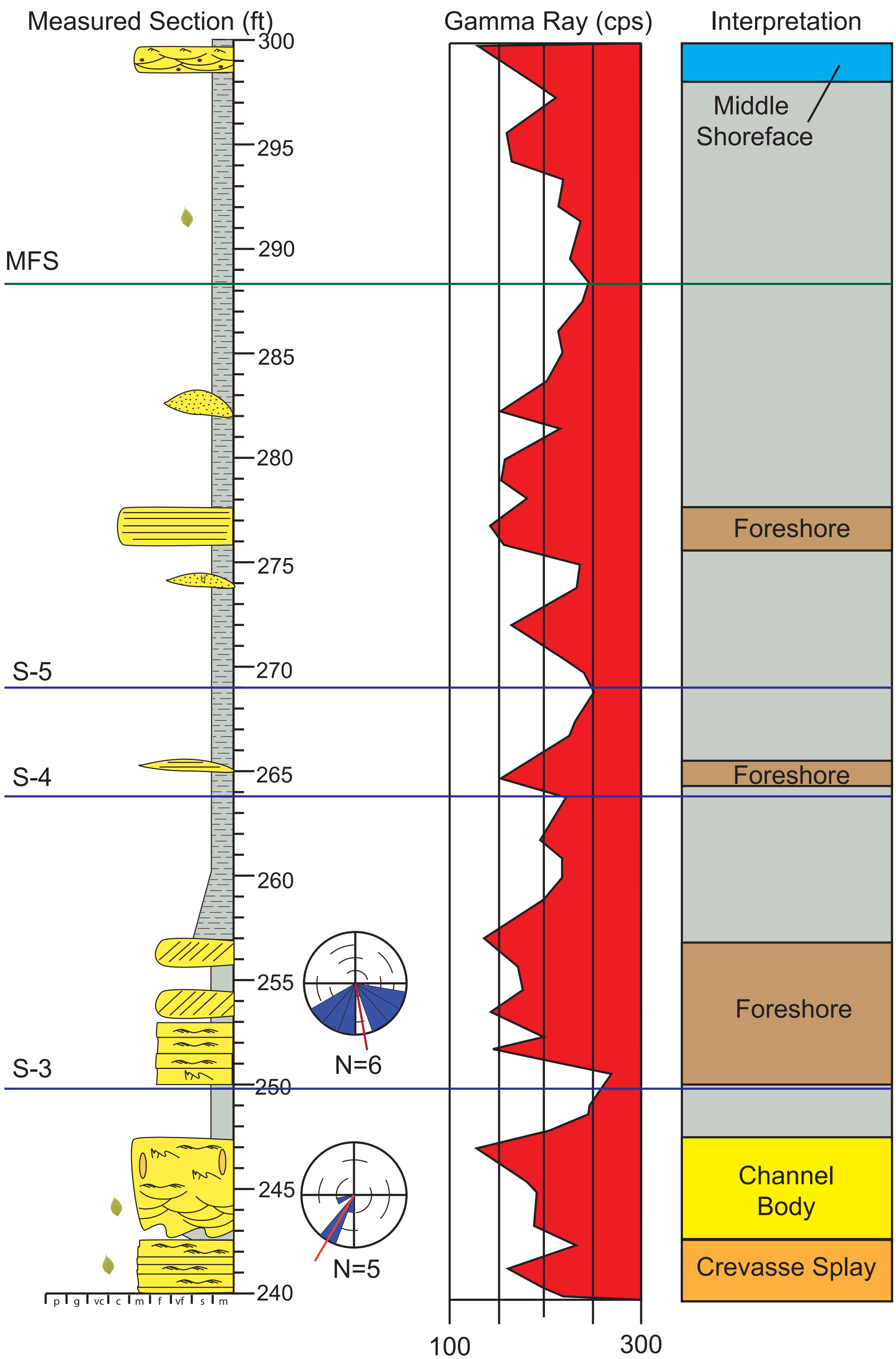
Measured Section (ft)
Gamma Ray (cps)
Interpretation
300
295
290
285
280
275
270
265
260
255
250
245
240
MFS
S-5
S-4
S-3
N=6
N=5
p g vc c m f vf s m
100
300
Middle Shoreface
Foreshore
Foreshore
Foreshore
Channel Body
Crevasse Splay

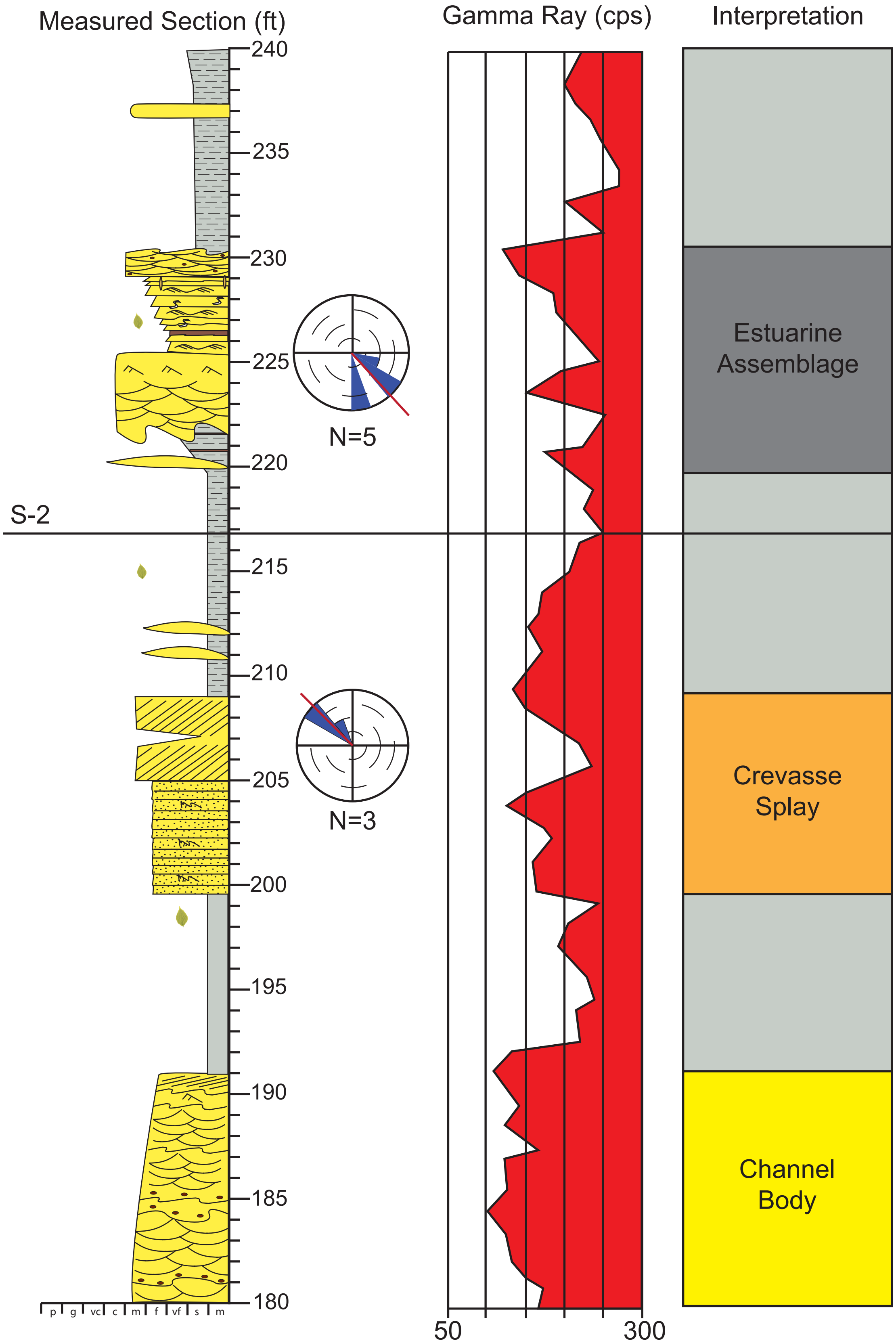

Measured Section (ft)
240
235
230
225
220
215
210
205
200
195
190
185
180
p g vc c m f vf s m
N=5
N=3
S-2
Gamma Ray (cps)
50
300
Interpretation
Estuarine Assemblage
Crevasse Splay
Channel Body

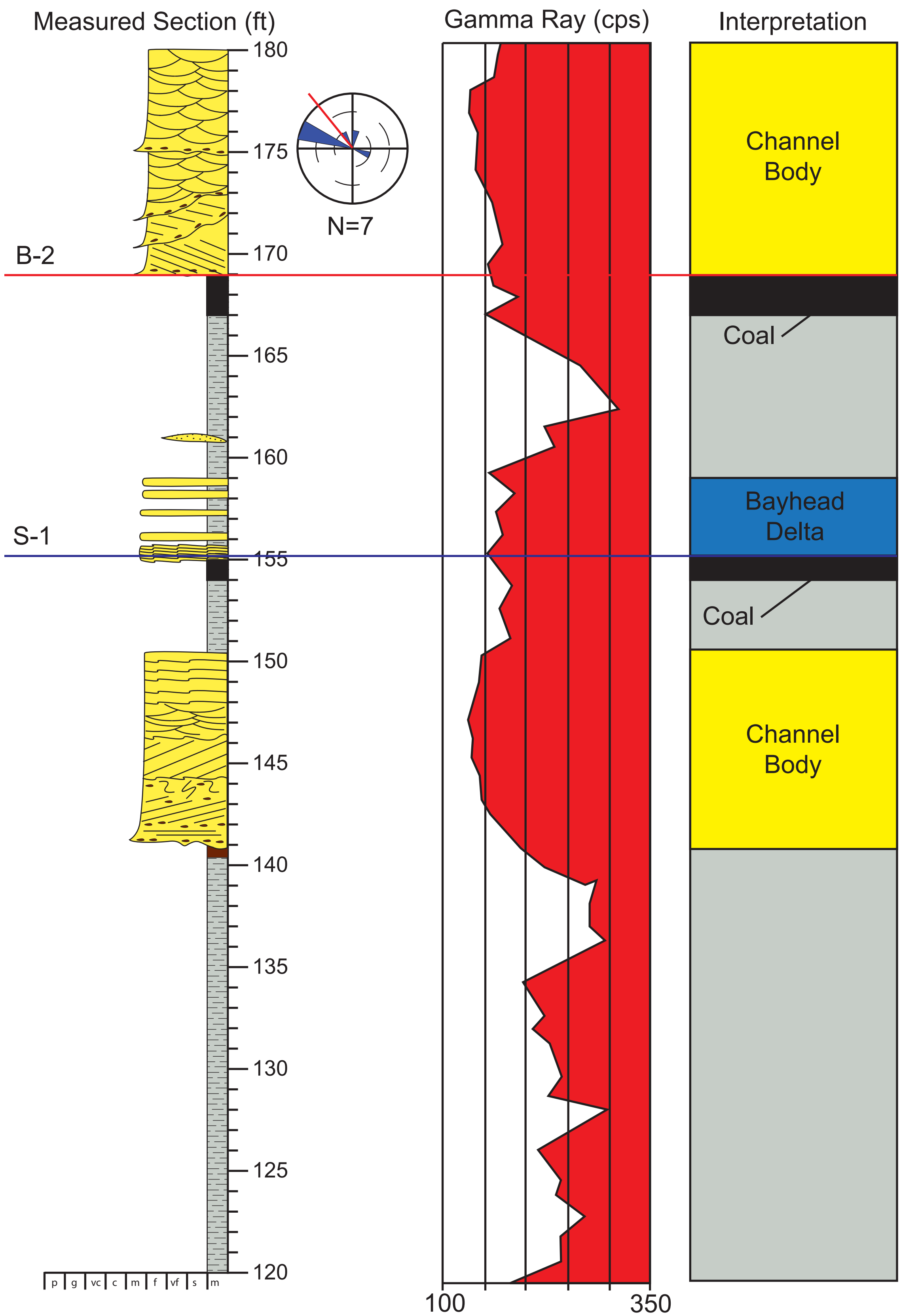
Measured Section (ft)
Gamma Ray (cps)
Interpretation
180
175
170
165
160
155
150
145
140
135
130
125
120
B-2
S-1
N=7
p g vc c m f vf s m
100
350
Channel Body
Coal
Bayhead Delta
Coal
Channel Body

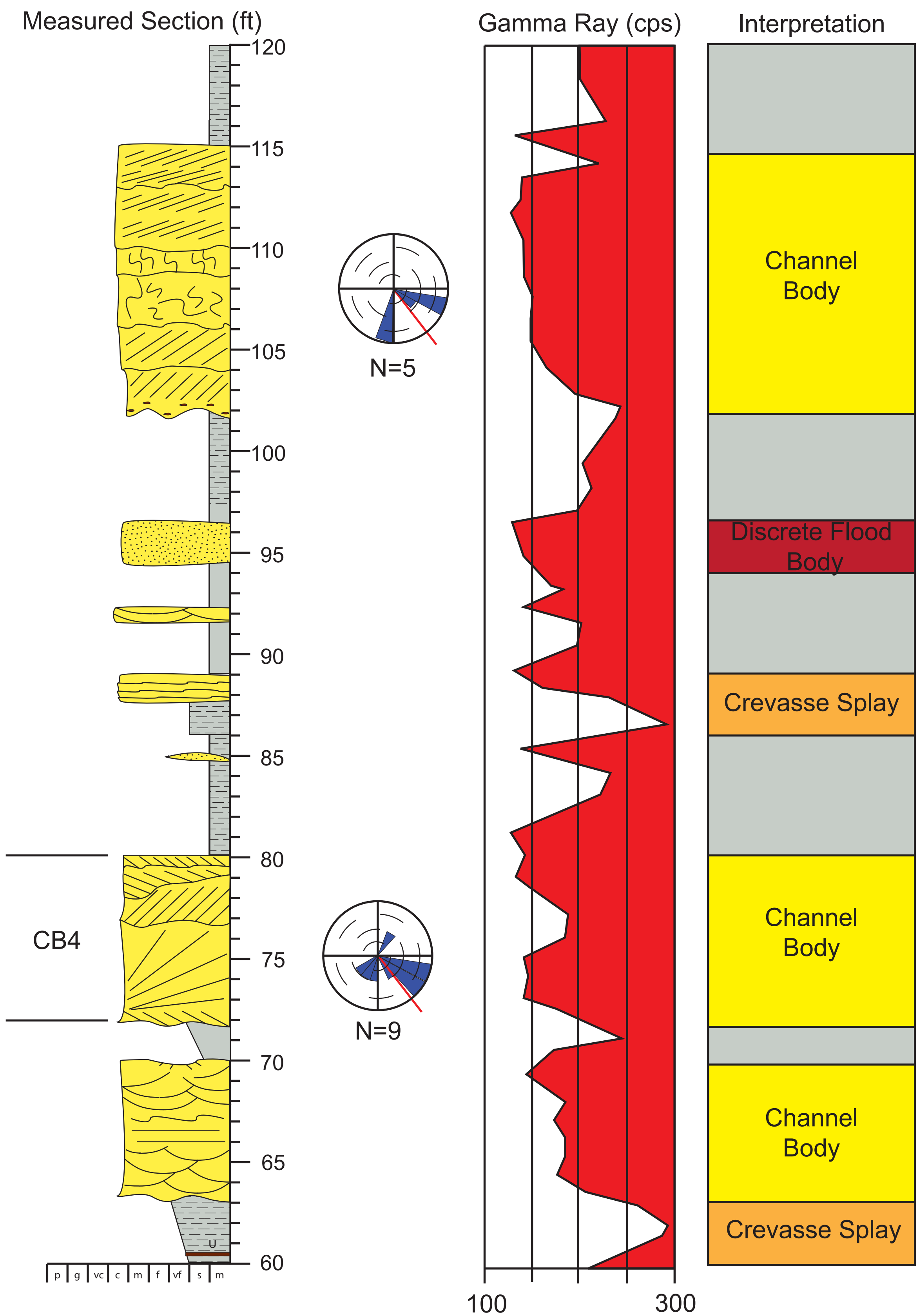

Measured Section (ft)
120
115
110
105
100
95
90
85
80
75
70
65
60
CB4
p
g
vc
c
m
f
vf
s
m
N=5
N=9
Gamma Ray (cps)
100
300
Interpretation
Channel Body
Discrete Flood Body
Crevasse Splay
Channel Body
Channel Body
Crevasse Splay

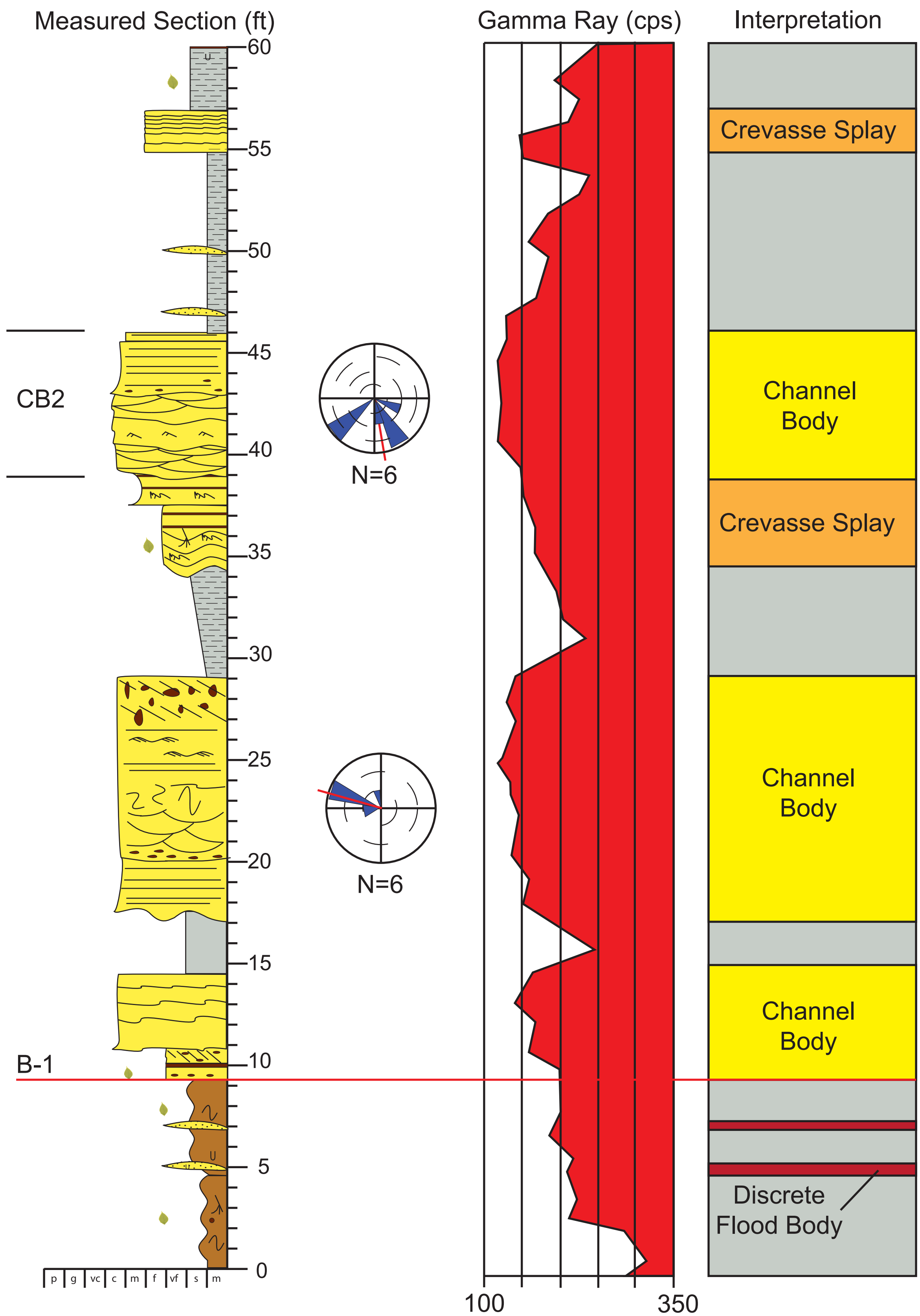
Measured Section (ft)
Gamma Ray (cps)
Interpretation
60
55
50
45
40
35
30
25
20
15
10
5
0
CB2
B-1
N=6
N=6
p g vc c m f vf s m
100
350
Crevasse Splay
Channel Body
Crevasse Splay
Channel Body
Channel Body
Discrete Flood Body

Appendix A3

Vandamore Draw North (VDN) Measured Section

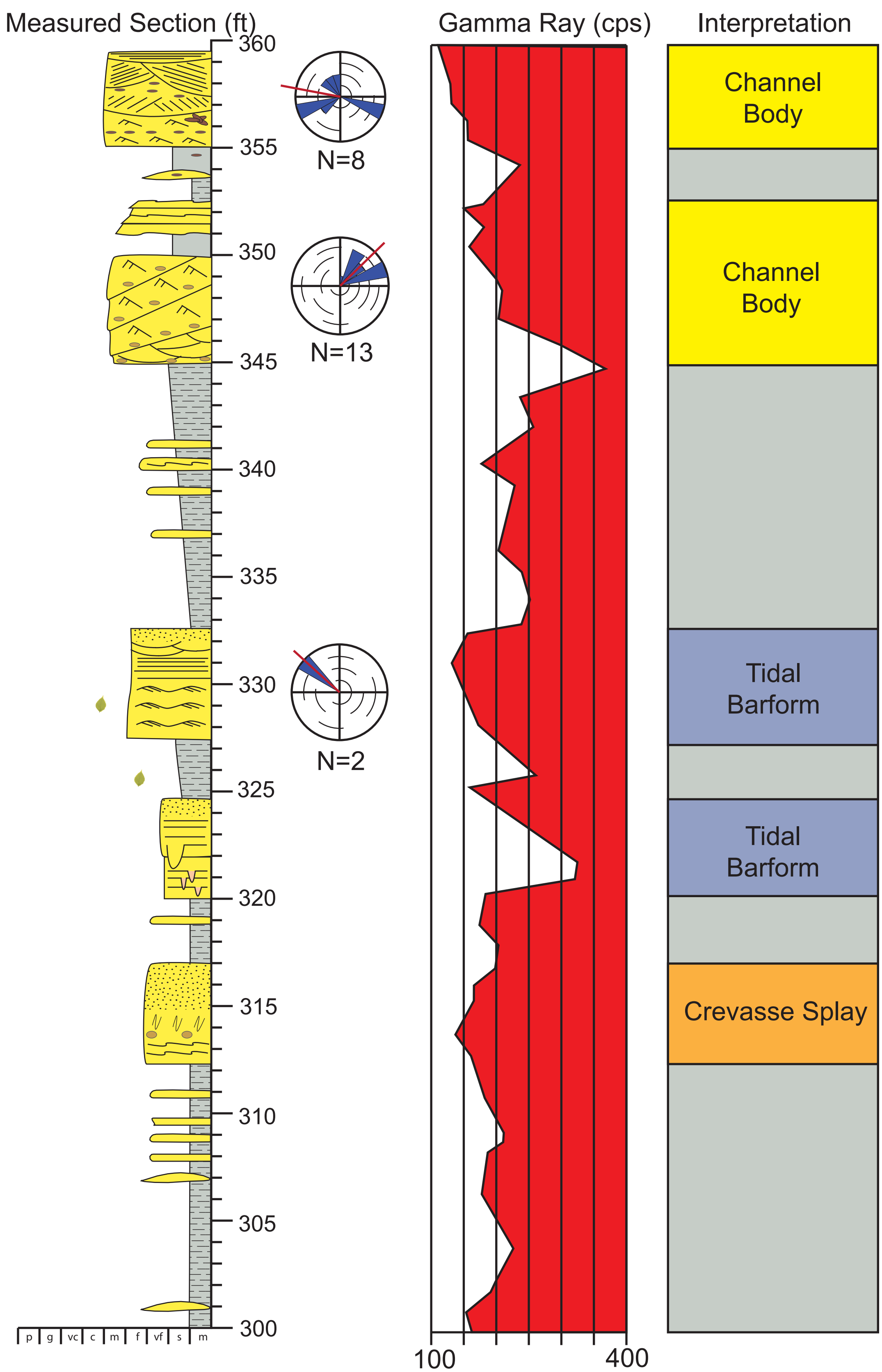
Measured Section (ft)
Gamma Ray (cps)
Interpretation
360
355
350
345
340
335
330
325
320
315
310
305
300
p g vc c m f vf s m
N=8
N=13
N=2
100
400
Channel Body
Channel Body
Tidal Barform
Tidal Barform
Crevasse Splay

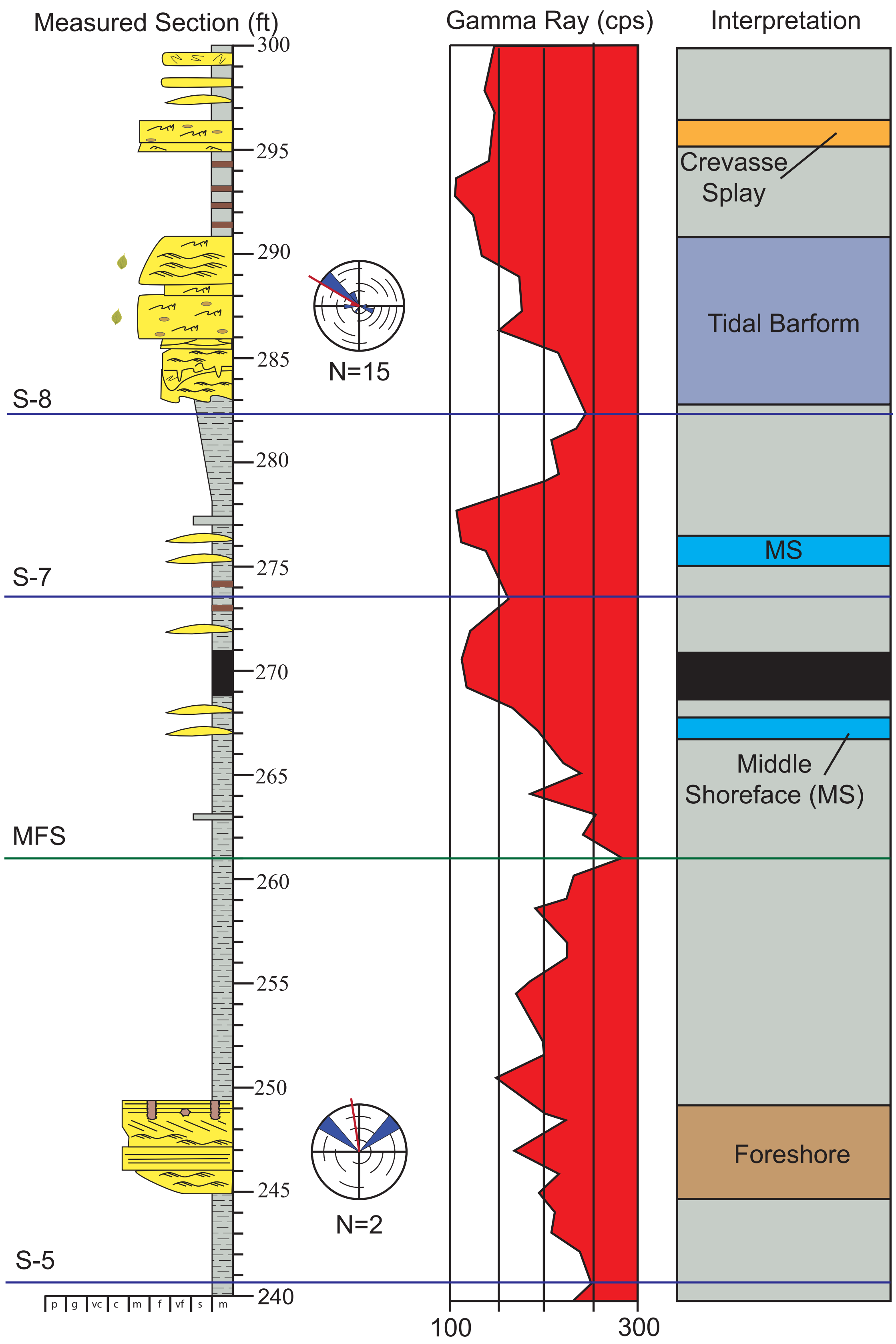

Measured Section (ft)
Gamma Ray (cps)
Interpretation
300
295
290
285
280
275
270
265
260
255
250
245
240
S-8
S-7
MFS
S-5
N=15
N=2
p g vc c m f vf s m
100
300
Crevasse Splay
Tidal Barform
MS
Middle Shoreface (MS)
Foreshore

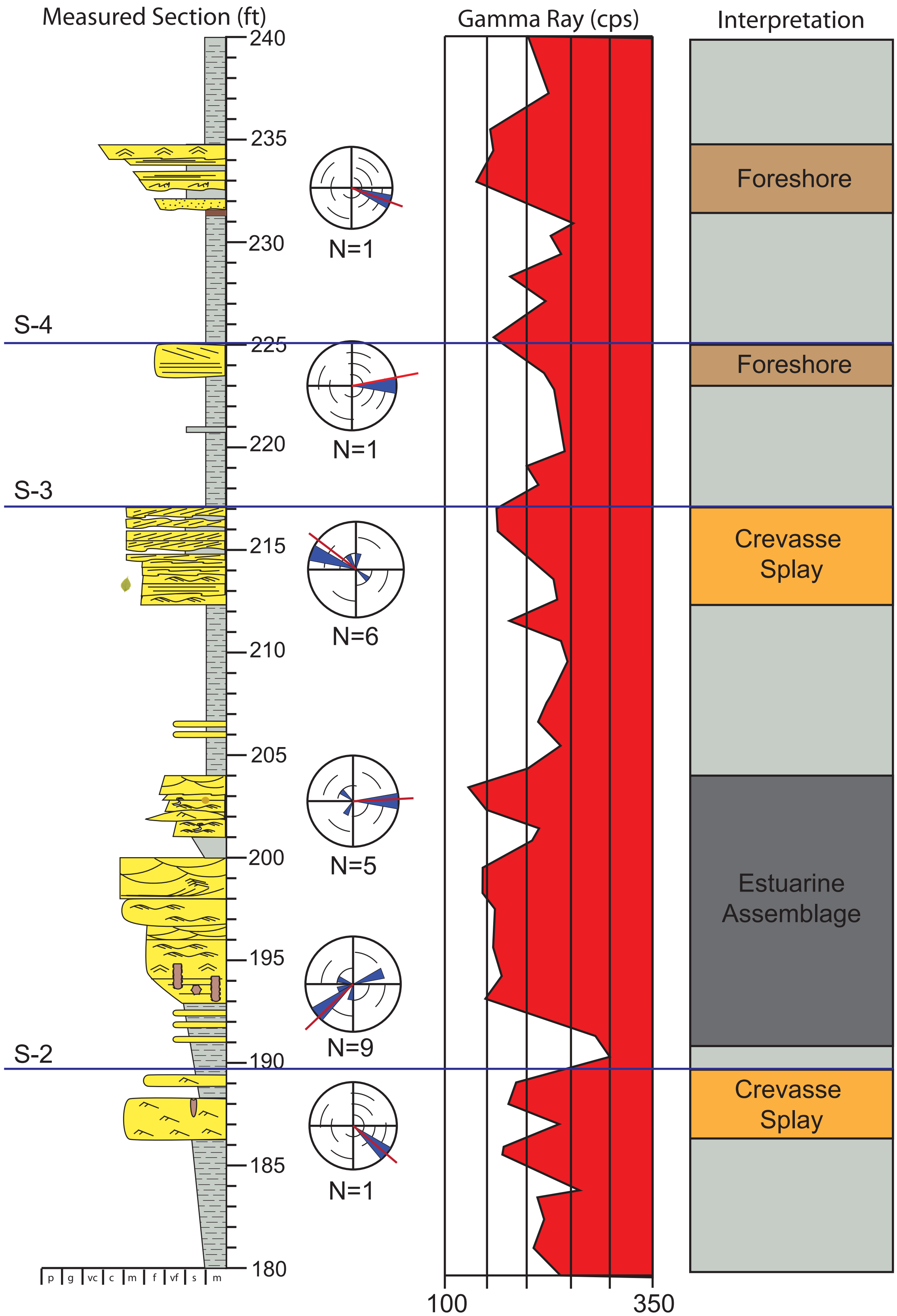
Measured Section (ft)
Gamma Ray (cps)
Interpretation
240
235
230
225
220
215
210
205
200
195
190
185
180
S-4
S-3
S-2
N=1
N=1
N=6
N=5
N=9
N=1
100
350
p g vc c m f vf s m
Foreshore
Foreshore
Crevasse Splay
Estuarine Assemblage
Crevasse Splay

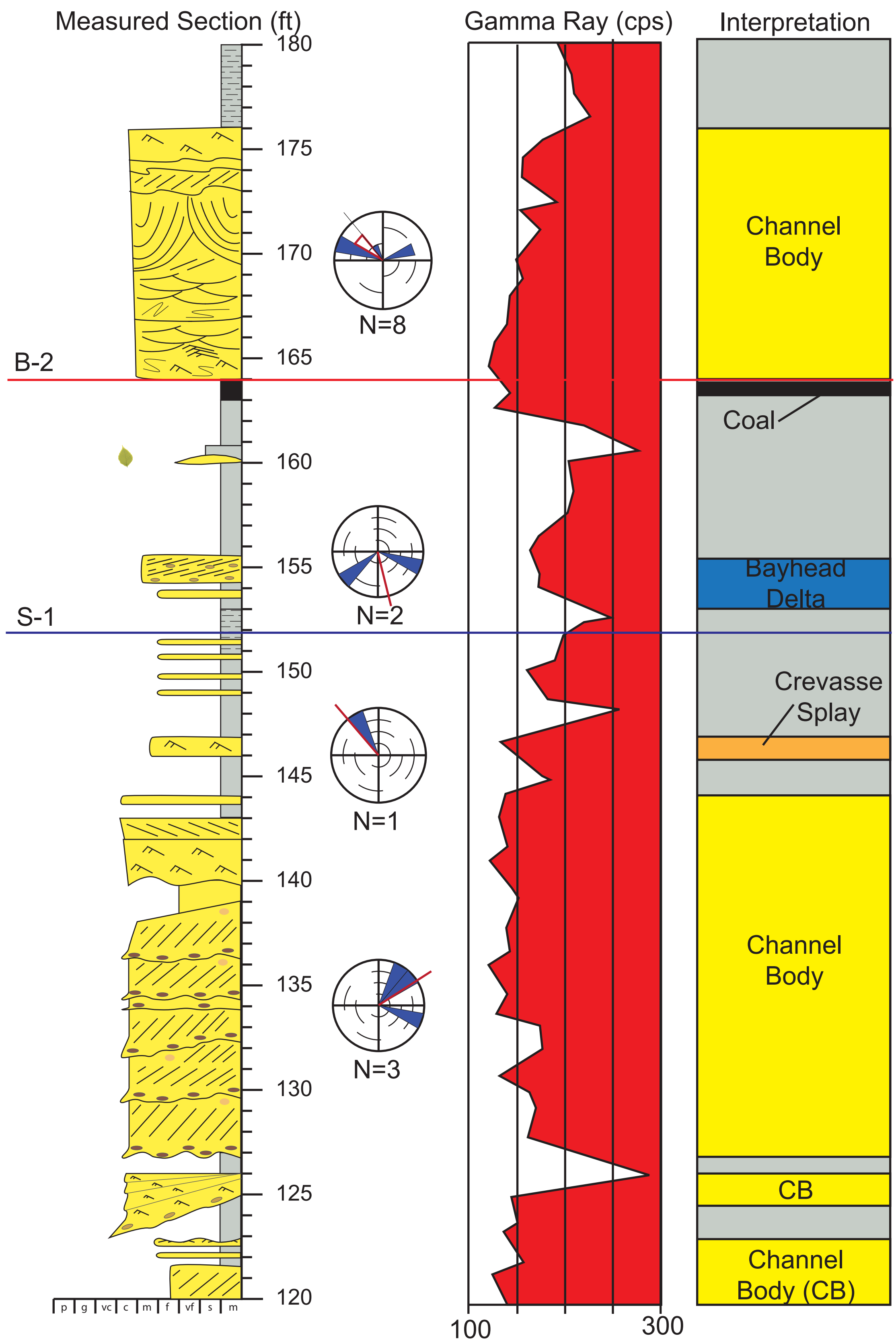

Measured Section (ft)
180
175
170
165
160
155
150
145
140
135
130
125
120
B-2
S-1
N=8
N=2
N=1
N=3
p g vc c m f vf s m
Gamma Ray (cps)
100
300
Interpretation
Channel Body
Coal
Bayhead Delta
Crevasse Splay
Channel Body
CB
Channel Body (CB)

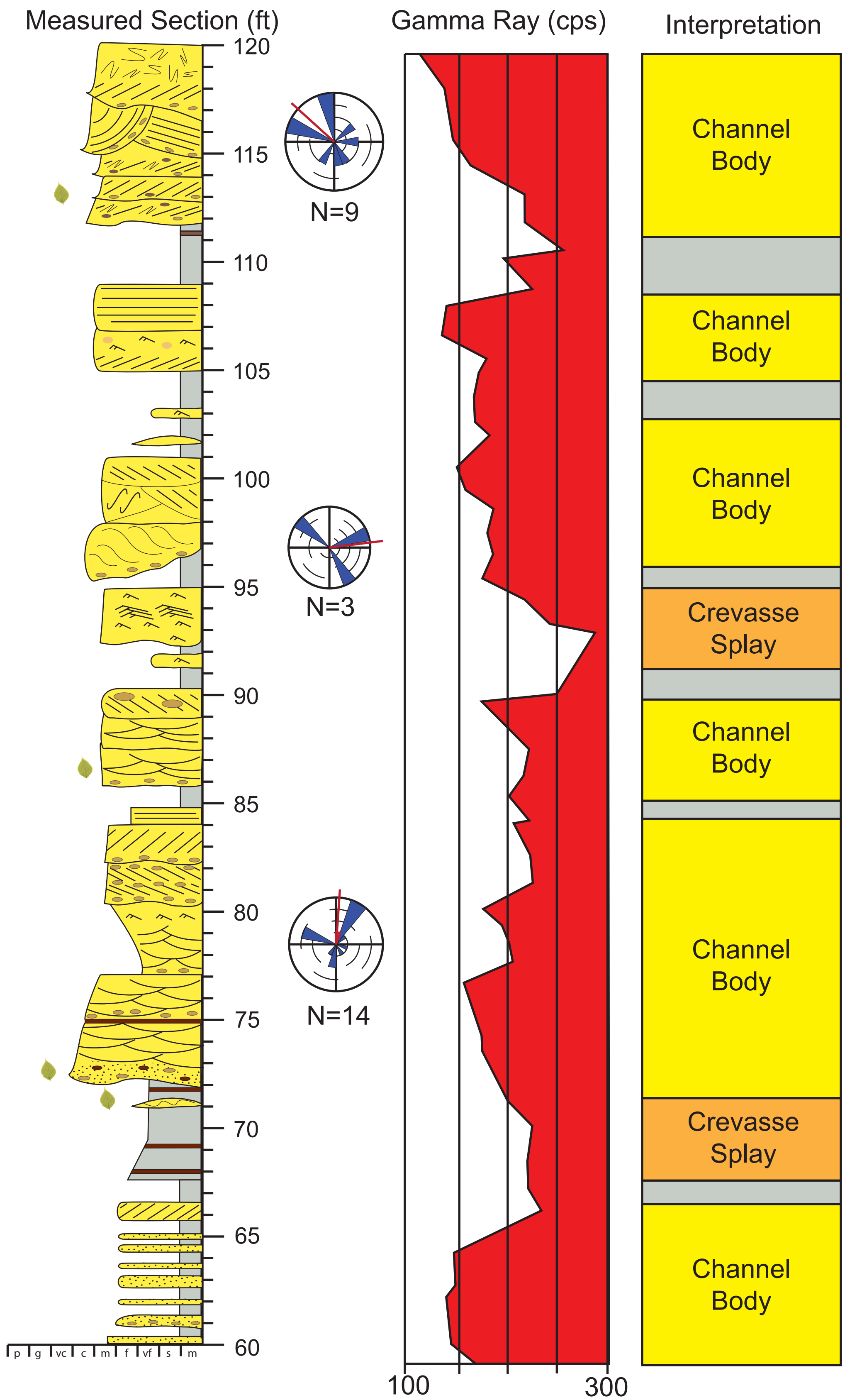

Measured Section (ft)
Gamma Ray (cps)
Interpretation
120
115
110
105
100
95
90
85
80
75
70
65
60
p g vc c m f vf s m
N=9
N=3
N=14
100
300
Channel Body
Channel Body
Channel Body
Crevasse Splay
Channel Body
Channel Body
Crevasse Splay
Channel Body

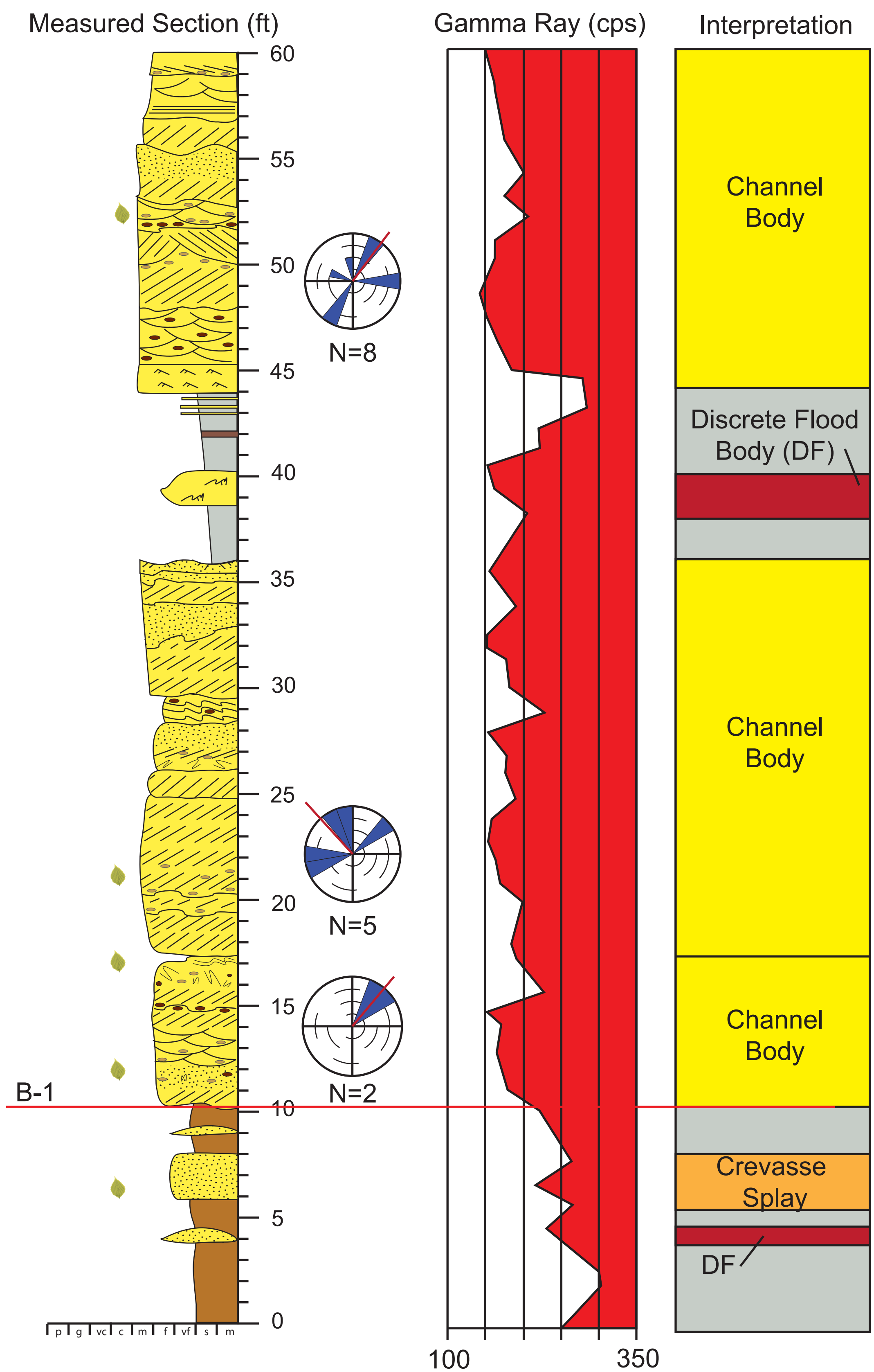

Measured Section (ft)
60
55
50
45
40
35
30
25
20
15
10
5
0
p g vc c m f vf s m
B-1
N=8
N=5
N=2
Gamma Ray (cps)
100
350
Interpretation
Channel Body
Discrete Flood Body (DF)
Channel Body
Channel Body
Crevasse Splay
DF

Appendix A3

Vandamore Draw West (VDW) Measured Section

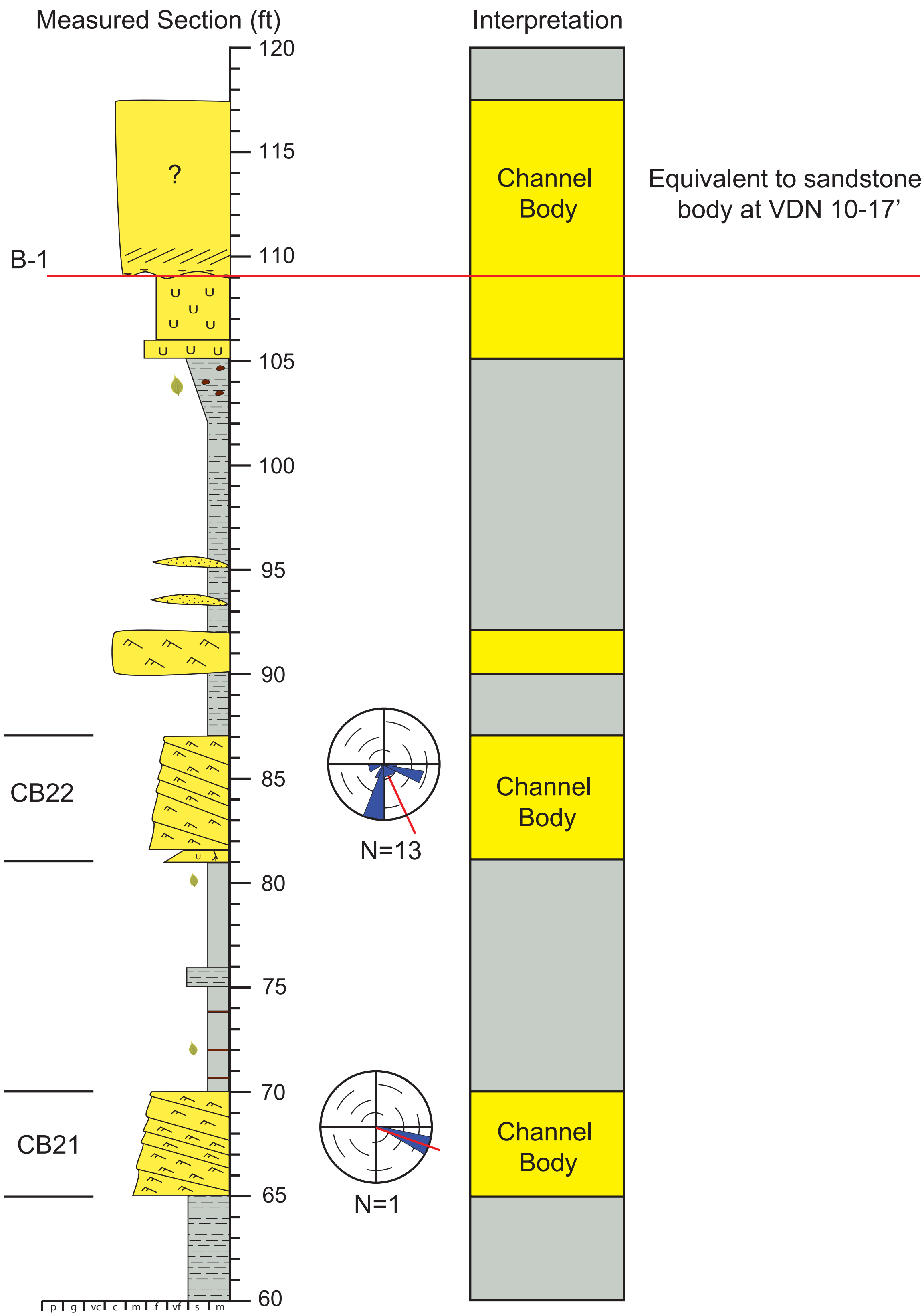

Measured Section (ft)
Interpretation
120
115
110
105
100
95
90
85
80
75
70
65
60
B-1
?
CB22
CB21
N=13
N=1
Channel Body
Channel Body
Channel Body
Equivalent to sandstone body at VDN 10-17'
p g vc c m f vf s m

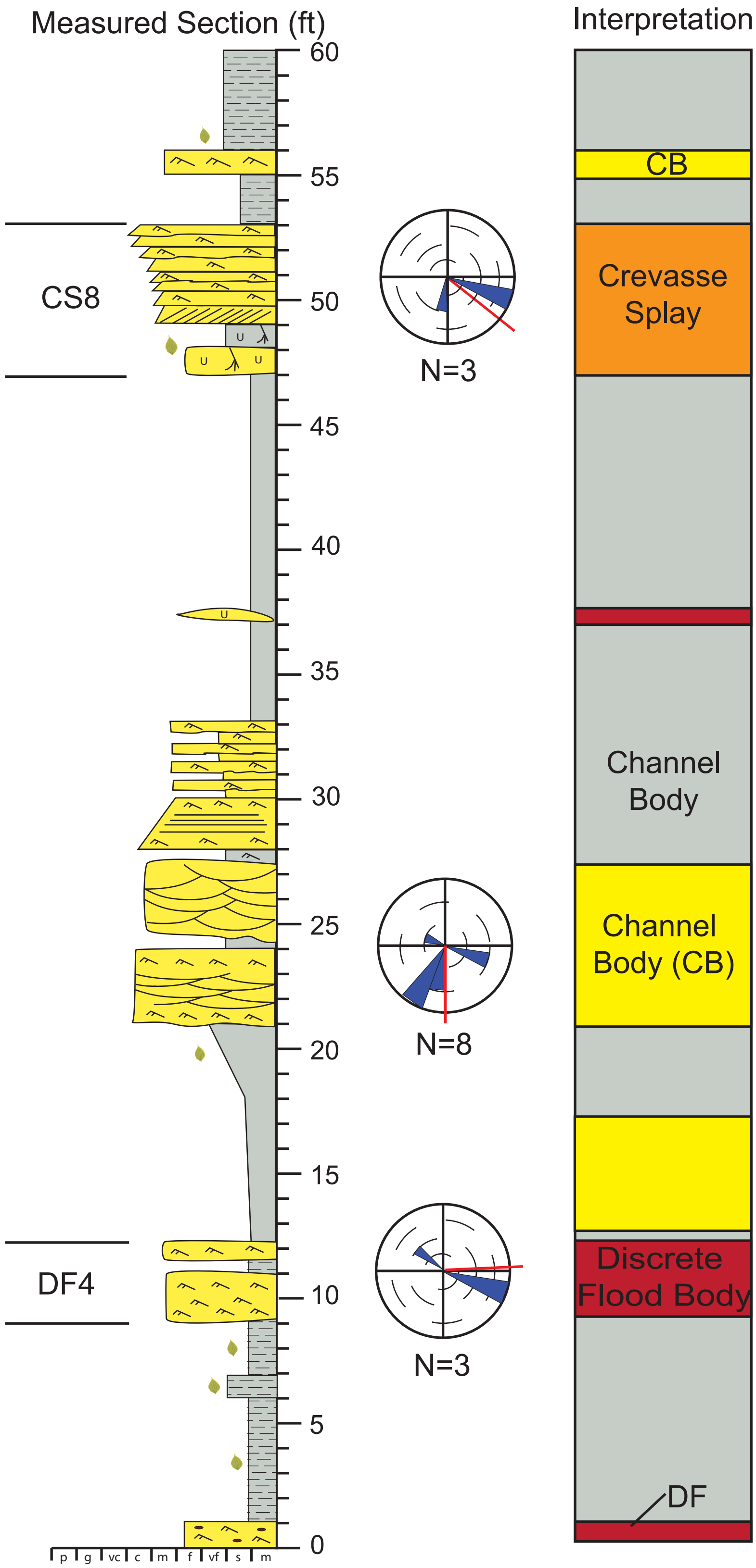
Measured Section (ft)
Interpretation
60
55
50
45
40
35
30
25
20
15
10
5
0
CS8
DF4
N=3
N=8
N=3
p g vc c m f vf s m
CB
Crevasse Splay
Channel Body
Channel Body (CB)
Discrete Flood Body
DF

Appendix A3

State Bridge Draw South (SBS) Measured Section

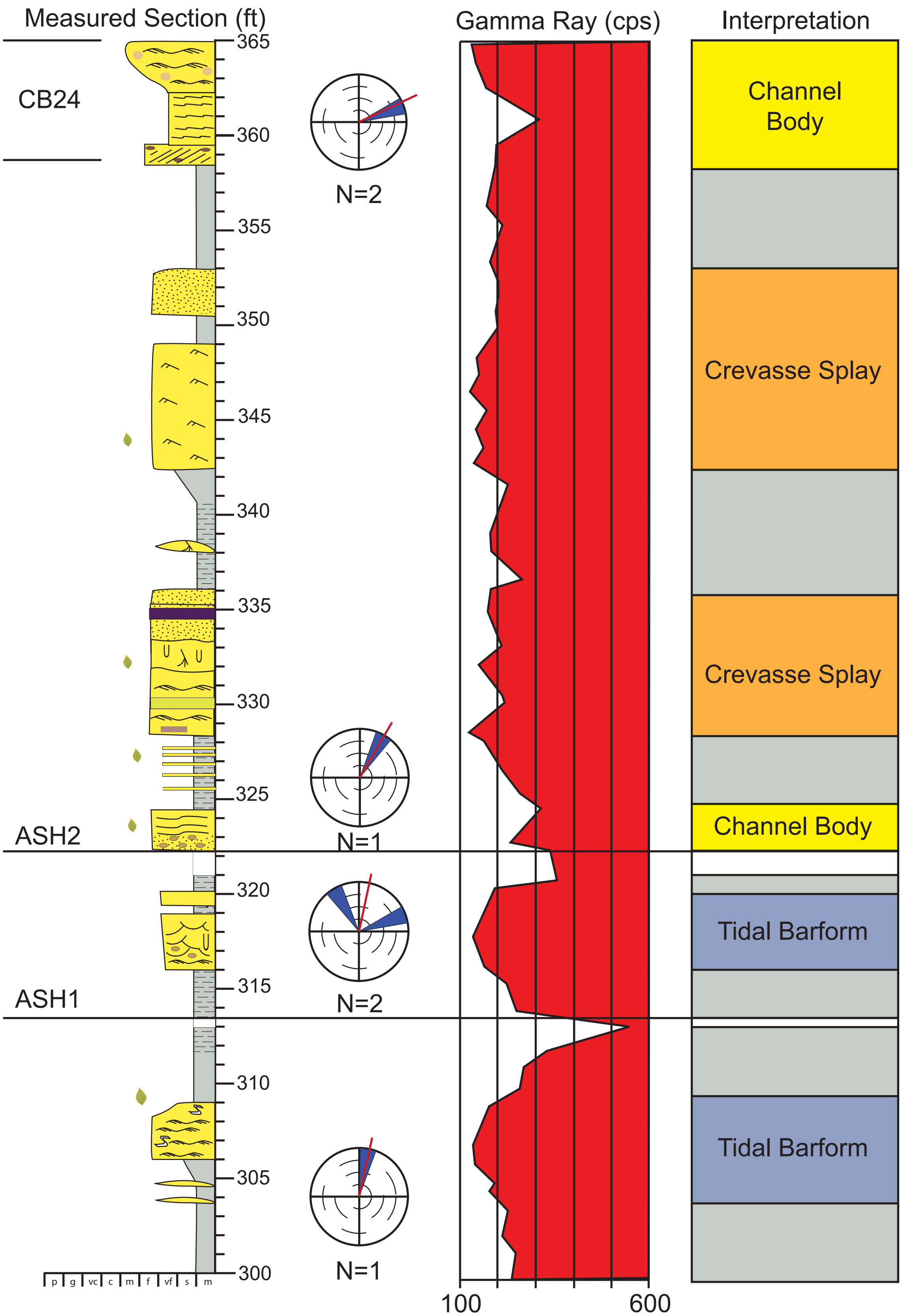
Measured Section (ft)
Gamma Ray (cps)
Interpretation
CB24
ASH2
ASH1
365
360
355
350
345
340
335
330
325
320
315
310
305
300
p g vc c m f vf s m
N=2
N=1
N=2
N=1
100
600
Channel Body
Crevasse Splay
Crevasse Splay
Channel Body
Tidal Barform
Tidal Barform

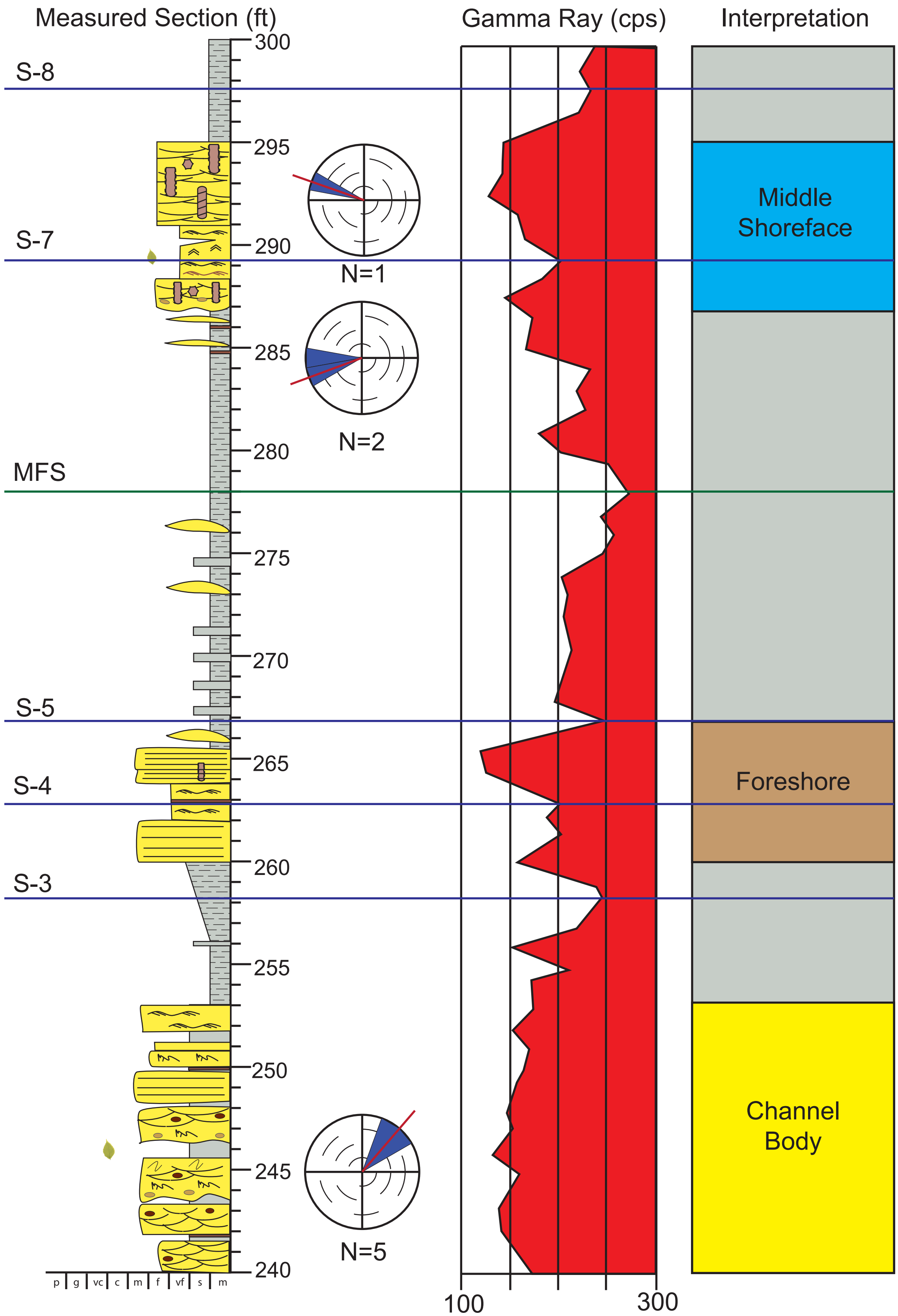

Measured Section (ft)
Gamma Ray (cps)
Interpretation
S-8
S-7
MFS
S-5
S-4
S-3
300
295
290
285
280
275
270
265
260
255
250
245
240
p g vc c m f vf s m
N=1
N=2
N=5
100
300
Middle Shoreface
Foreshore
Channel Body

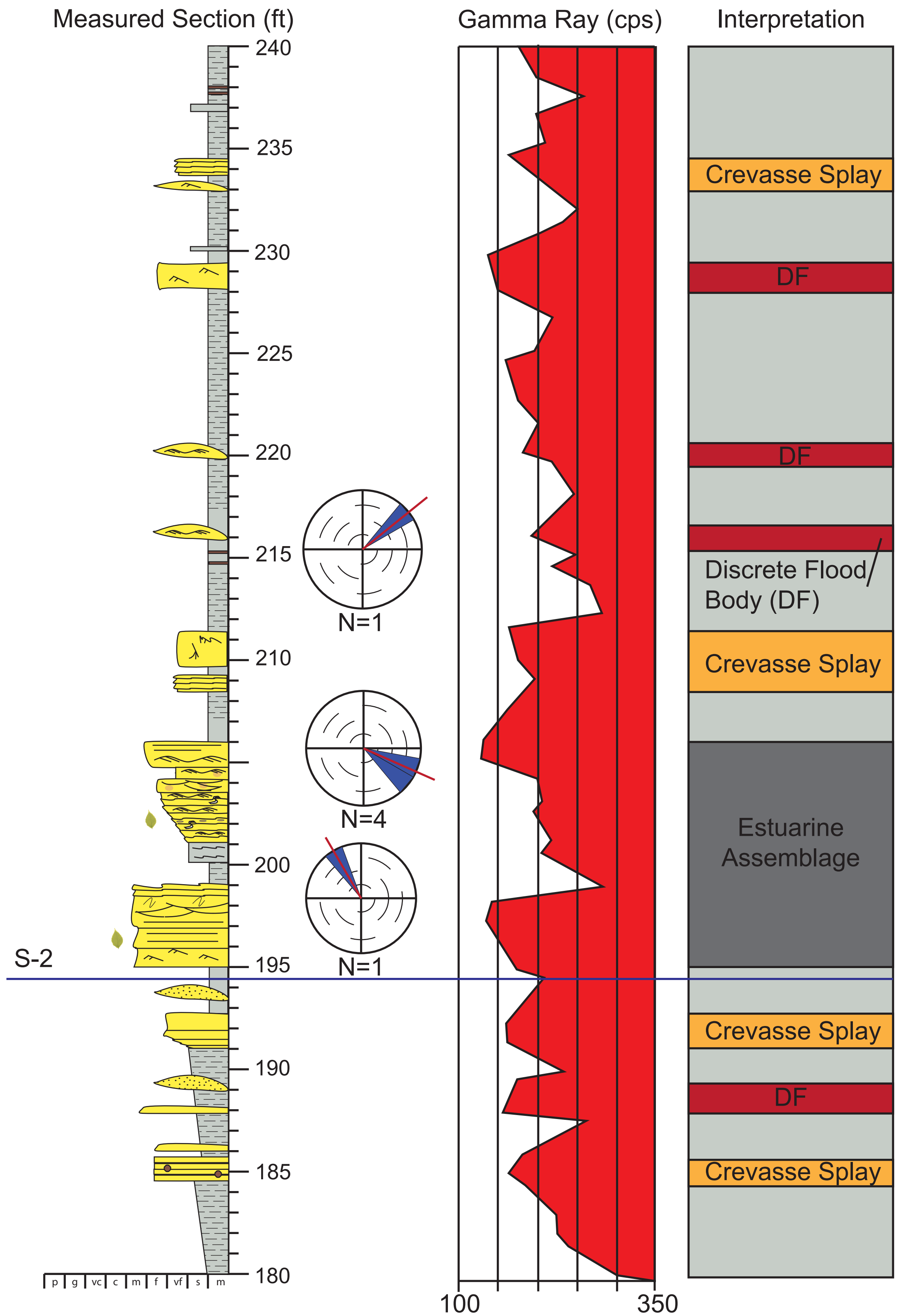

Measured Section (ft)
Gamma Ray (cps)
Interpretation
240
235
230
225
220
215
210
200
195
190
185
180
p
g
vc
c
m
f
vf
s
m
N=1
N=4
N=1
S-2
100
350
Crevasse Splay
DF
DF
Discrete Flood Body (DF)
Crevasse Splay
Estuarine Assemblage
Crevasse Splay
DF
Crevasse Splay

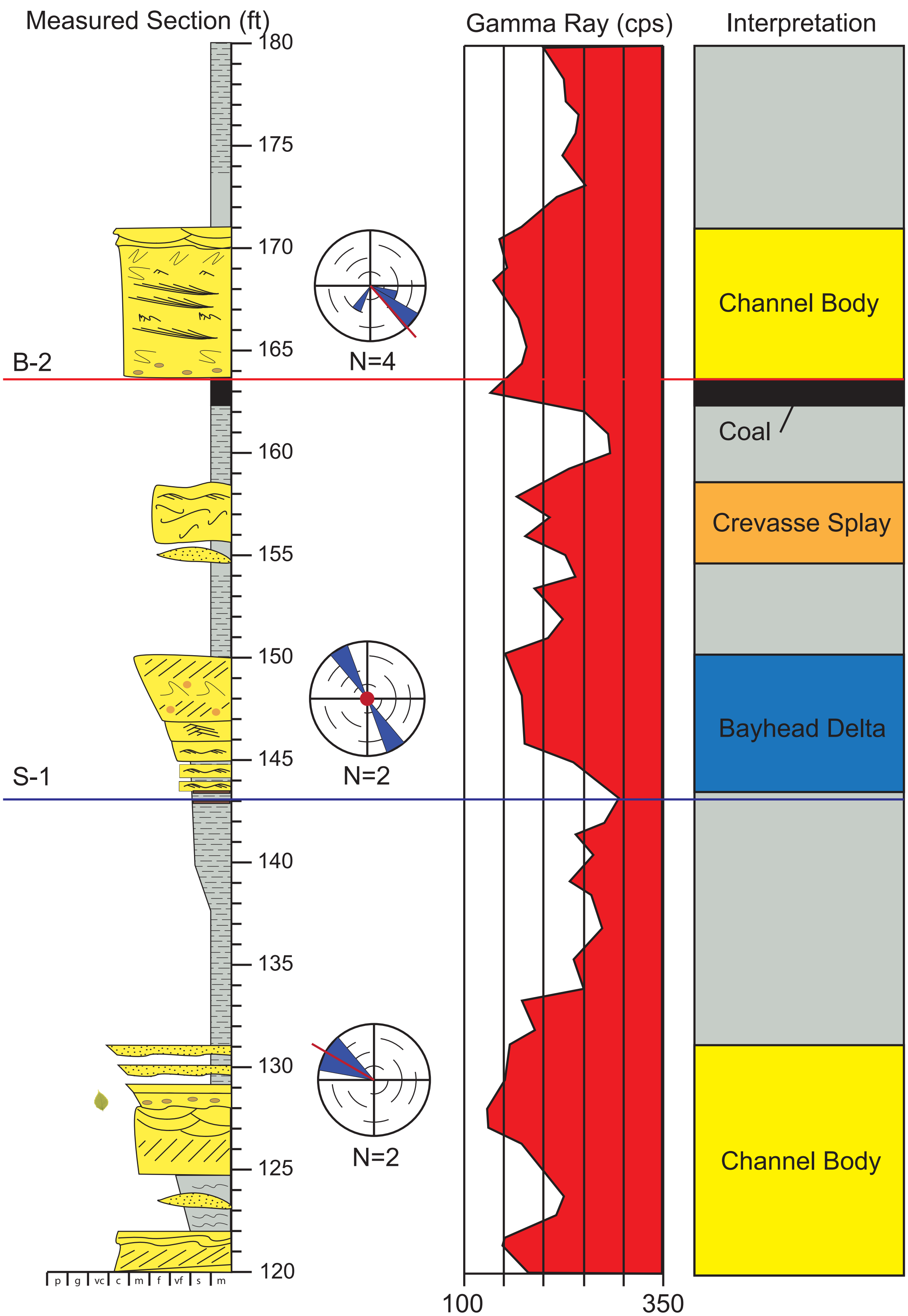

Measured Section (ft)
180
175
170
165
160
155
150
145
140
135
130
125
120
B-2
S-1
p g vc c m f vf s m
N=4
N=2
N=2
Gamma Ray (cps)
100
350
Interpretation
Channel Body
Coal
Crevasse Splay
Bayhead Delta
Channel Body

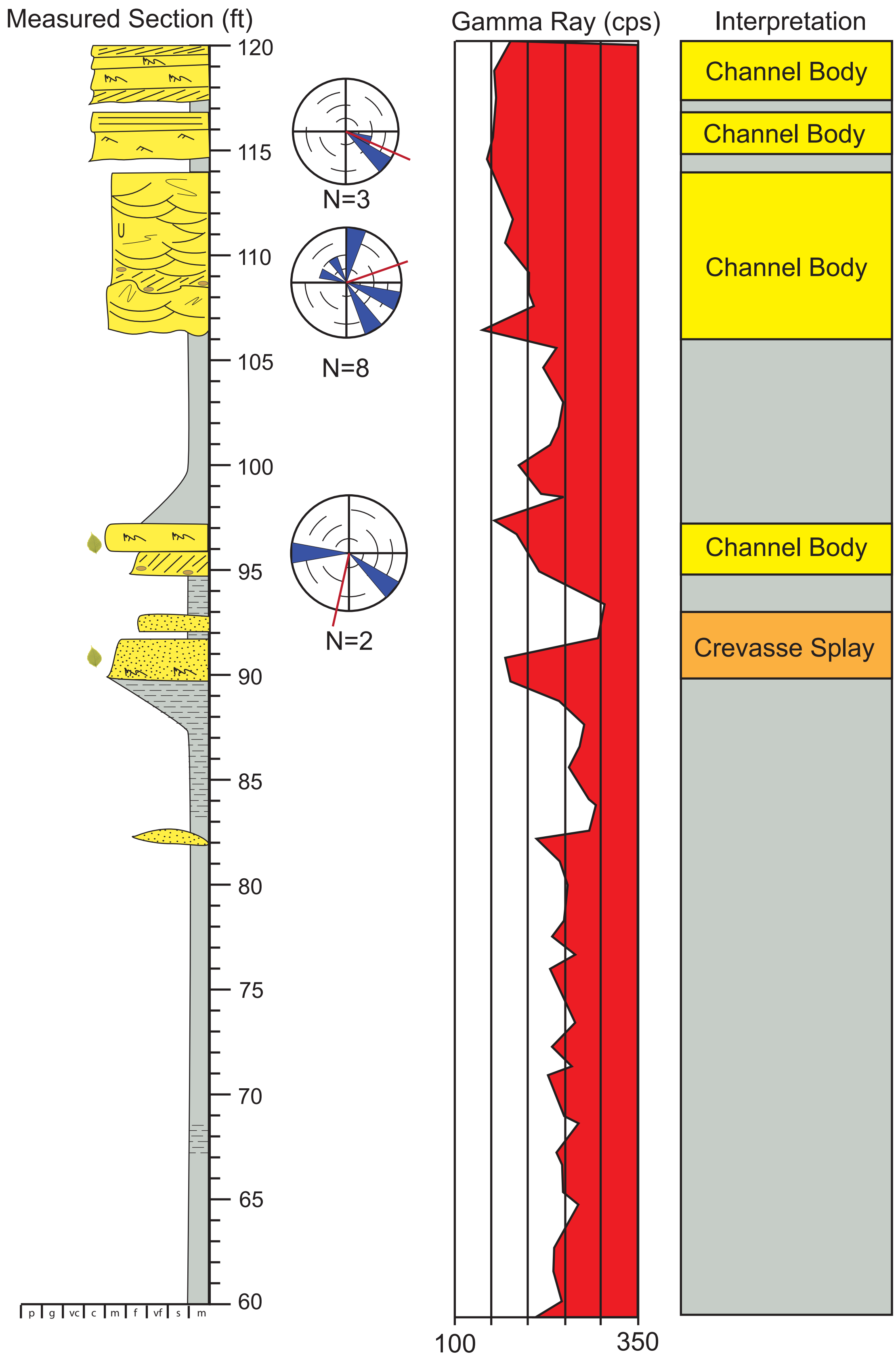

Measured Section (ft)
120
115
110
105
100
95
90
85
80
75
70
65
60
p g vc c m f vf s m
N=3
N=8
N=2
Gamma Ray (cps)
100
350
Interpretation
Channel Body
Channel Body
Channel Body
Channel Body
Crevasse Splay

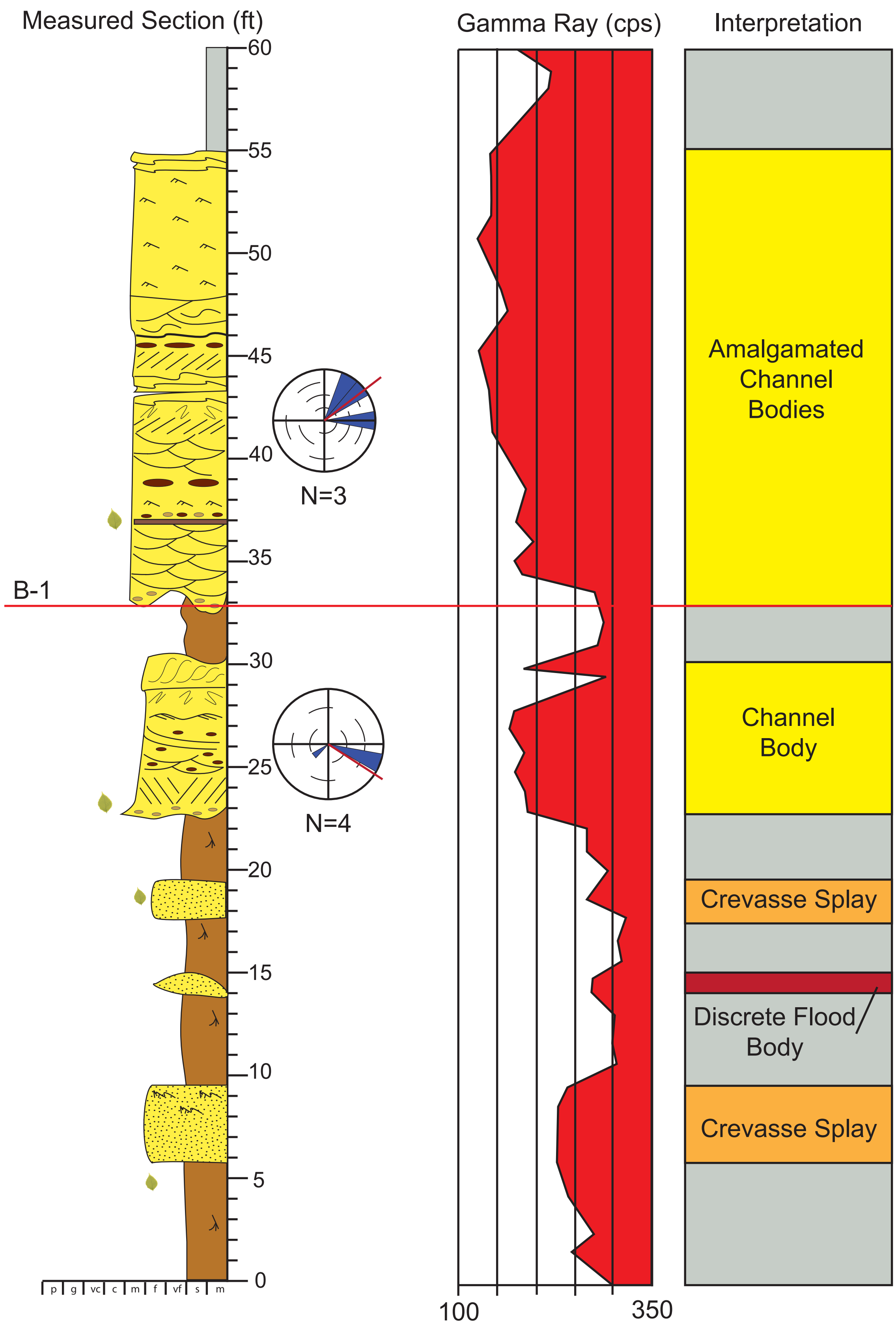

Measured Section (ft)
60
55
50
45
40
35
30
25
20
15
10
5
0
B-1
N=3
N=4
p g vc c m f vf s m
Gamma Ray (cps)
100
350
Interpretation
Amalgamated Channel Bodies
Channel Body
Crevasse Splay
Discrete Flood Body
Crevasse Splay

Appendix A3

State Bridge Draw West (SBW) Measured Section

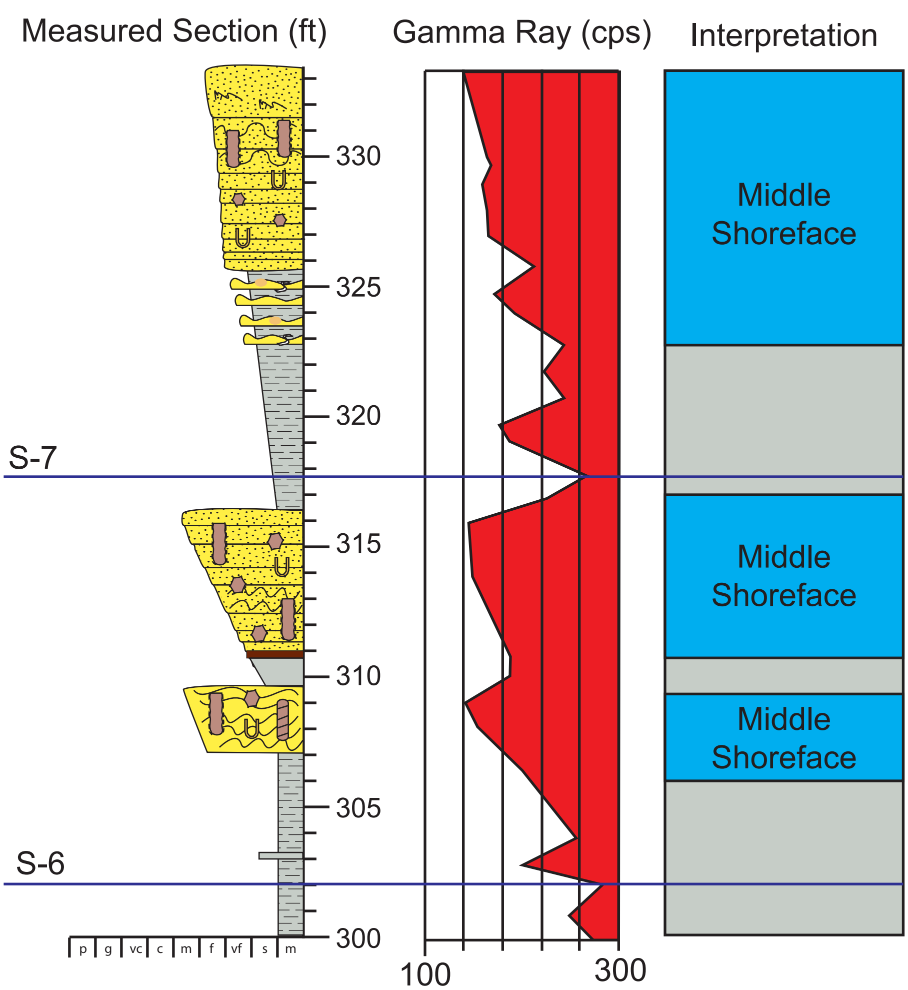
Measured Section (ft)
Gamma Ray (cps)
Interpretation
330
325
320
315
310
305
300
S-7
S-6
p
g
vc
c
m
f
vf
s
m
100
300
Middle Shoreface
Middle Shoreface
Middle Shoreface

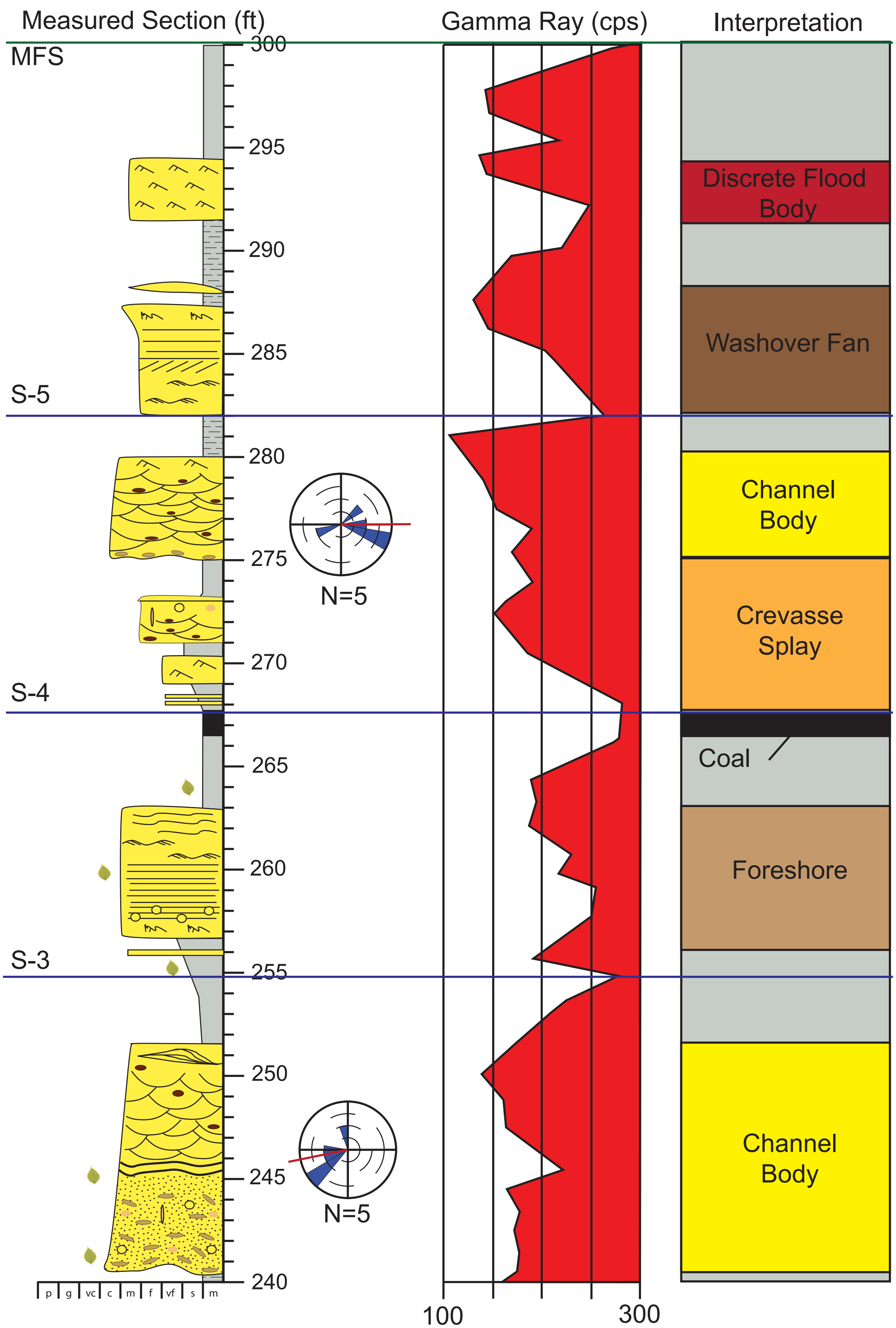

Measured Section (ft)
Gamma Ray (cps)
Interpretation
MFS
S-5
S-4
S-3
300
295
290
285
280
275
270
265
260
255
250
245
240
N=5
N=5
p g vc c m f vf s m
100
300
Discrete Flood Body
Washover Fan
Channel Body
Crevasse Splay
Coal
Foreshore
Channel Body

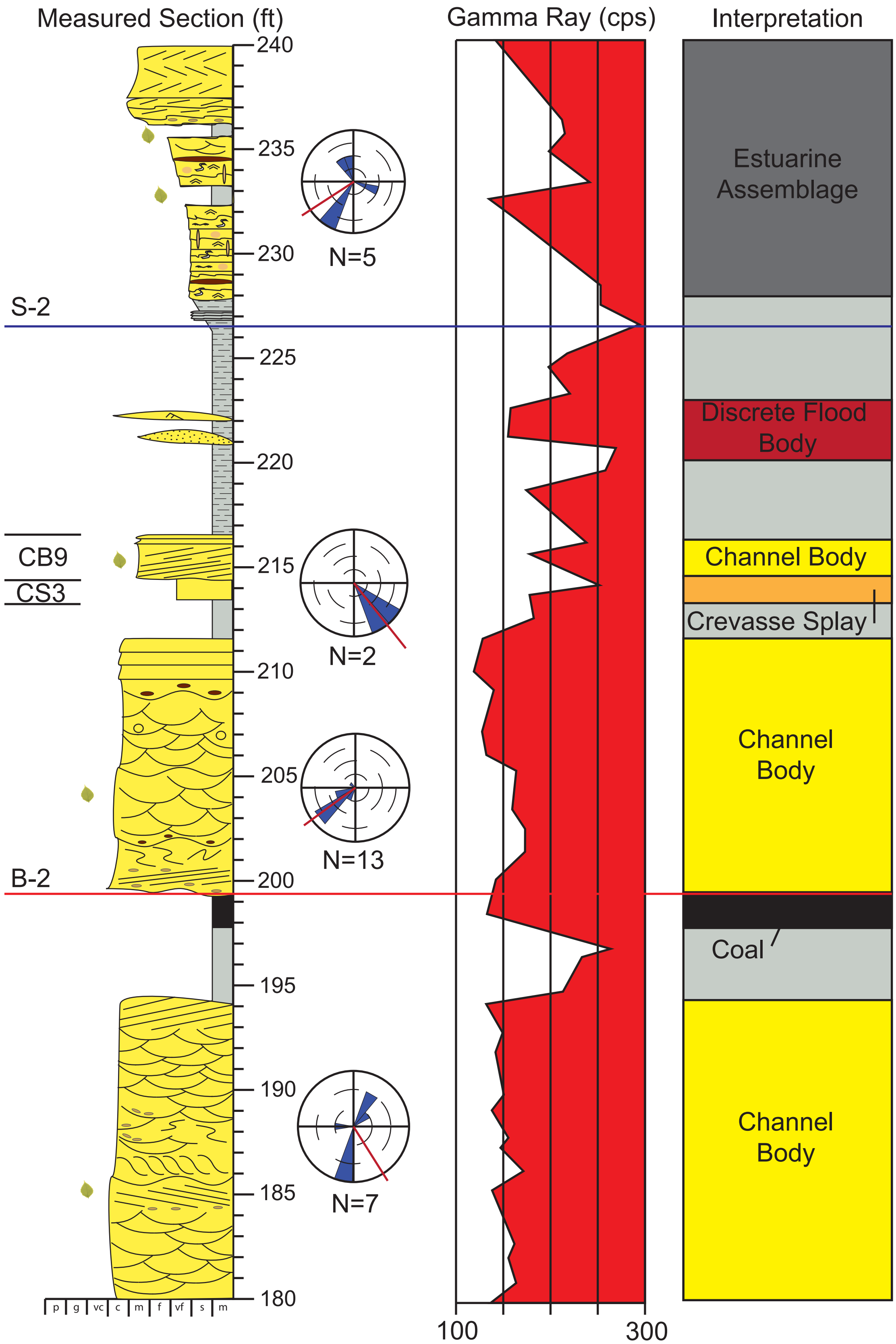
Measured Section (ft)
Gamma Ray (cps)
Interpretation
240
235
230
225
220
215
210
205
200
195
190
185
180
S-2
B-2
CB9
CS3
N=5
N=2
N=13
N=7
p g vc c m f vf s m
100
300
Estuarine Assemblage
Discrete Flood Body
Channel Body
Crevasse Splay
Channel Body
Coal
Channel Body

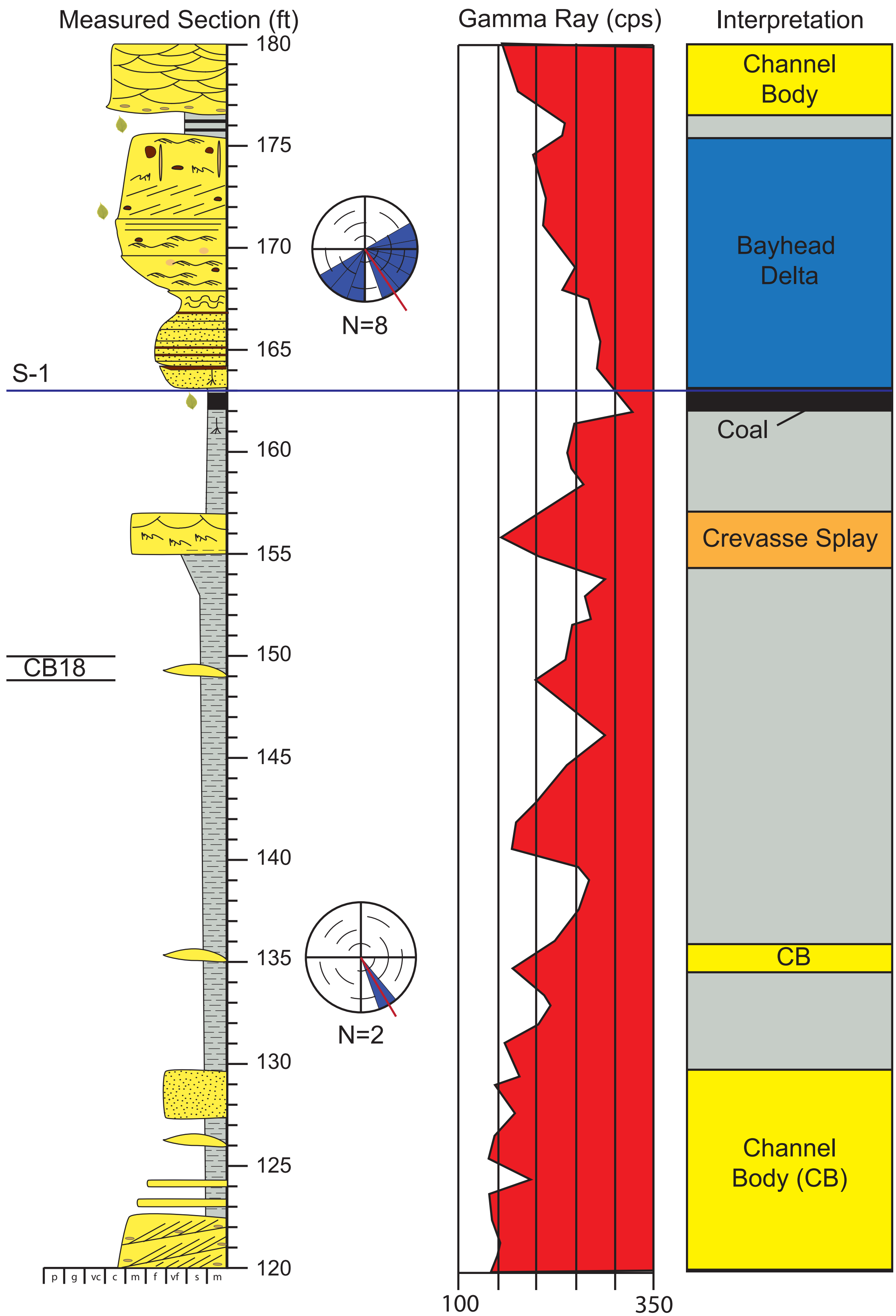

Measured Section (ft)
Gamma Ray (cps)
Interpretation
180
175
170
165
160
155
150
145
140
135
130
125
120
S-1
CB18
N=8
N=2
p
g
vc
c
m
f
vf
s
m
100
350
Channel Body
Bayhead Delta
Coal
Crevasse Splay
CB
Channel Body (CB)

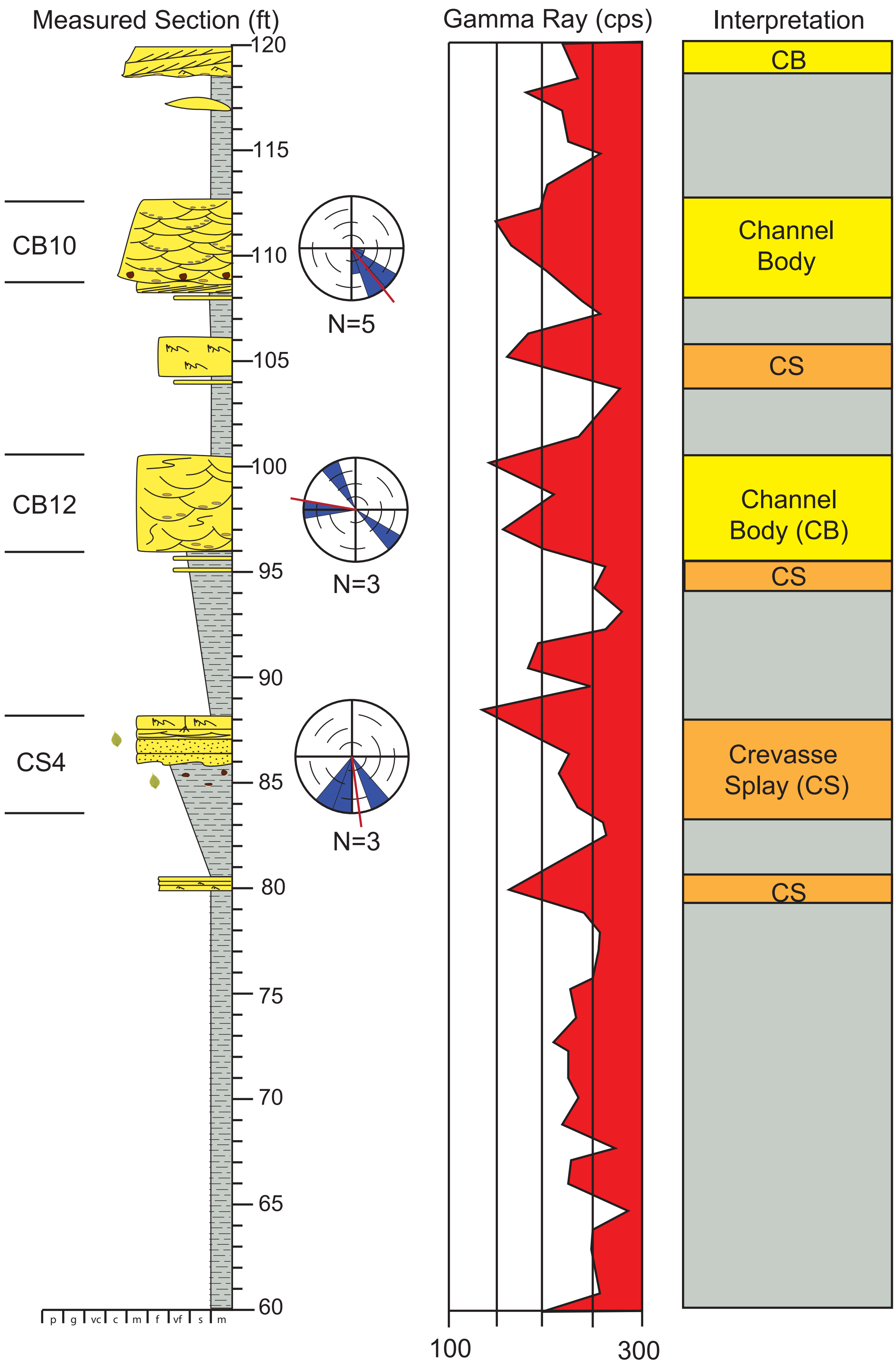

Measured Section (ft)
120
115
110
105
100
95
90
85
80
75
70
65
60
CB10
CB12
CS4
N=5
N=3
N=3
p g vc c m f vf s m
Gamma Ray (cps)
100
300
Interpretation
CB
Channel Body
CS
Channel Body (CB)
CS
Crevasse Splay (CS)
CS

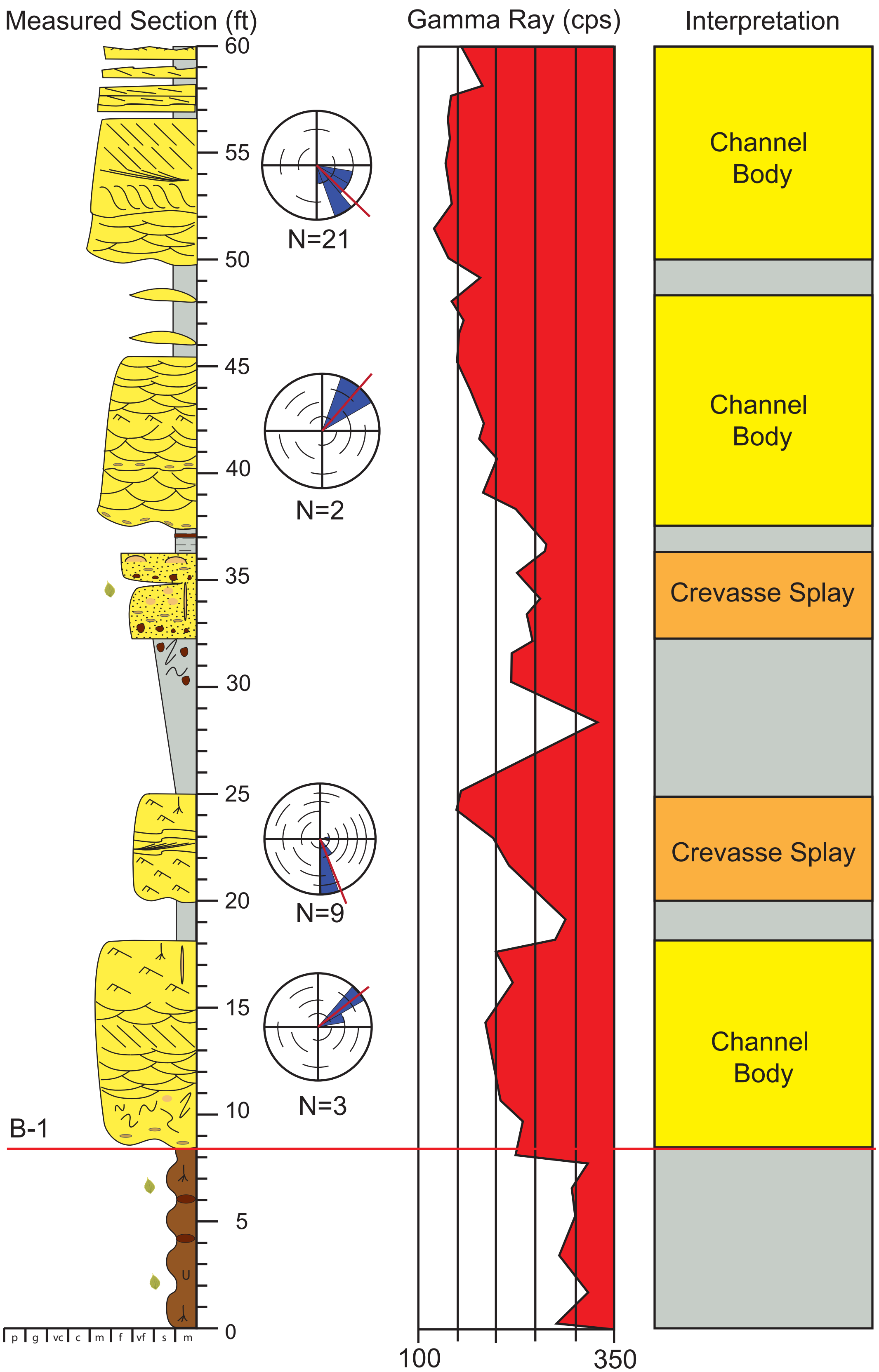
Measured Section (ft)
Gamma Ray (cps)
Interpretation
60
55
50
45
40
35
30
25
20
15
10
5
0
B-1
N=21
N=2
N=9
N=3
p g vc c m f vf s m
100
350
Channel Body
Channel Body
Crevasse Splay
Crevasse Splay
Channel Body

Appendix A3

State Bridge Draw East (SBE) Measured Section

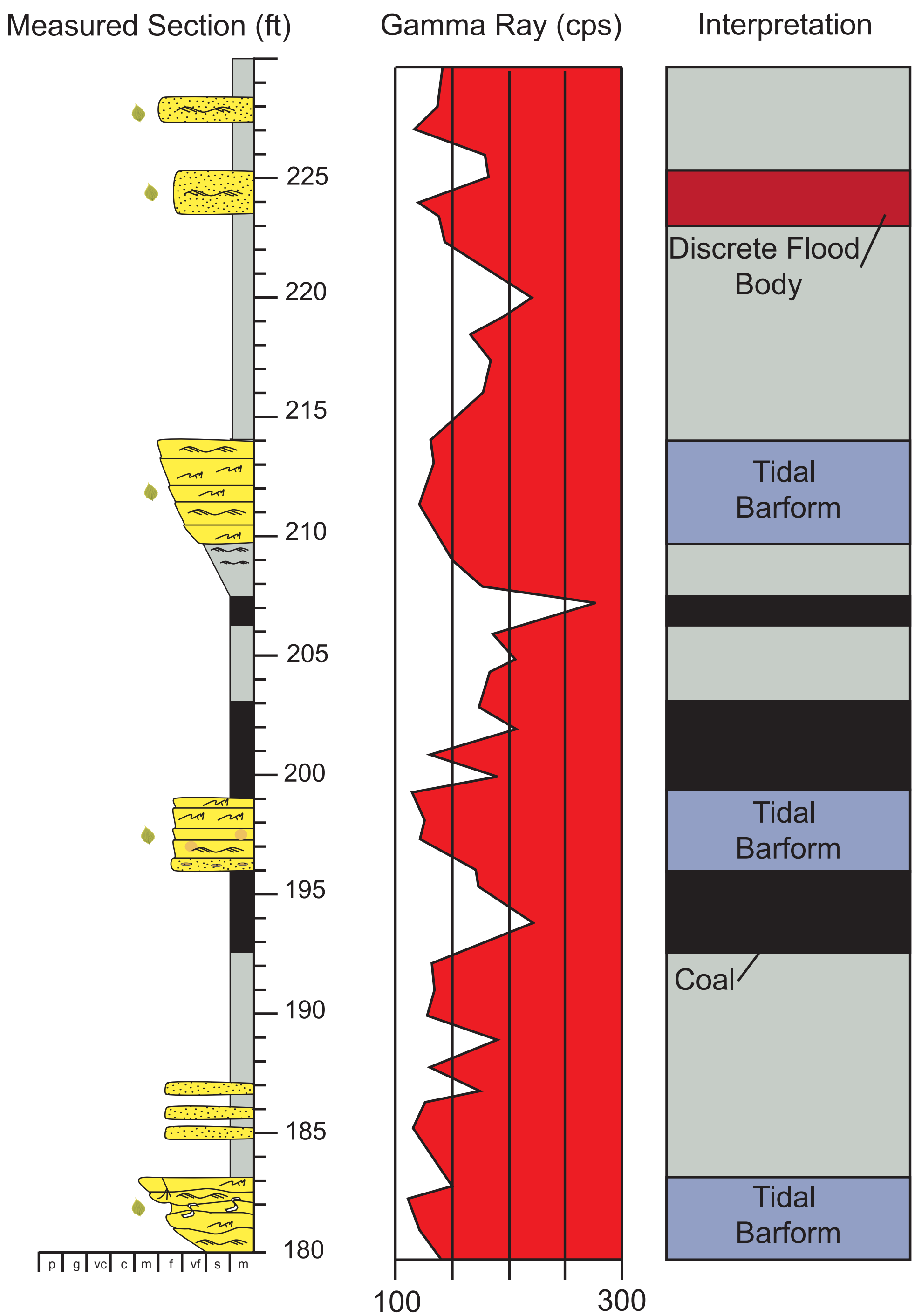
Measured Section (ft)
Gamma Ray (cps)
Interpretation
225
220
215
210
205
200
195
190
185
180
p g vc c m f vf s m
100
300
Discrete Flood Body
Tidal Barform
Tidal Barform
Coal
Tidal Barform

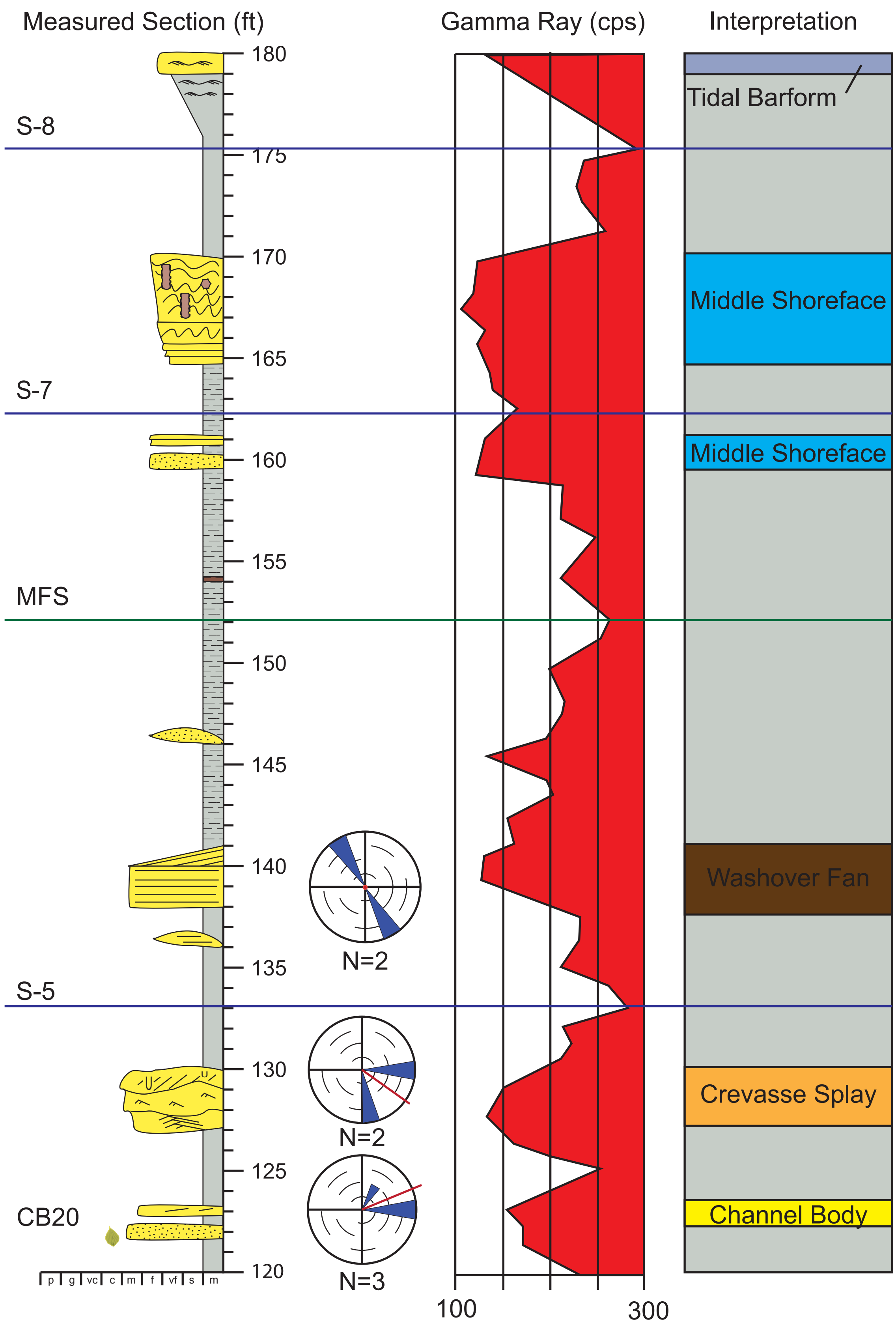

Measured Section (ft)
Gamma Ray (cps)
Interpretation
180
175
170
165
160
155
150
145
140
135
130
125
120
S-8
S-7
MFS
S-5
CB20
p g vc c m f vf s m
N=2
N=2
N=3
100
300
Tidal Barform
Middle Shoreface
Middle Shoreface
Washover Fan
Crevasse Splay
Channel Body

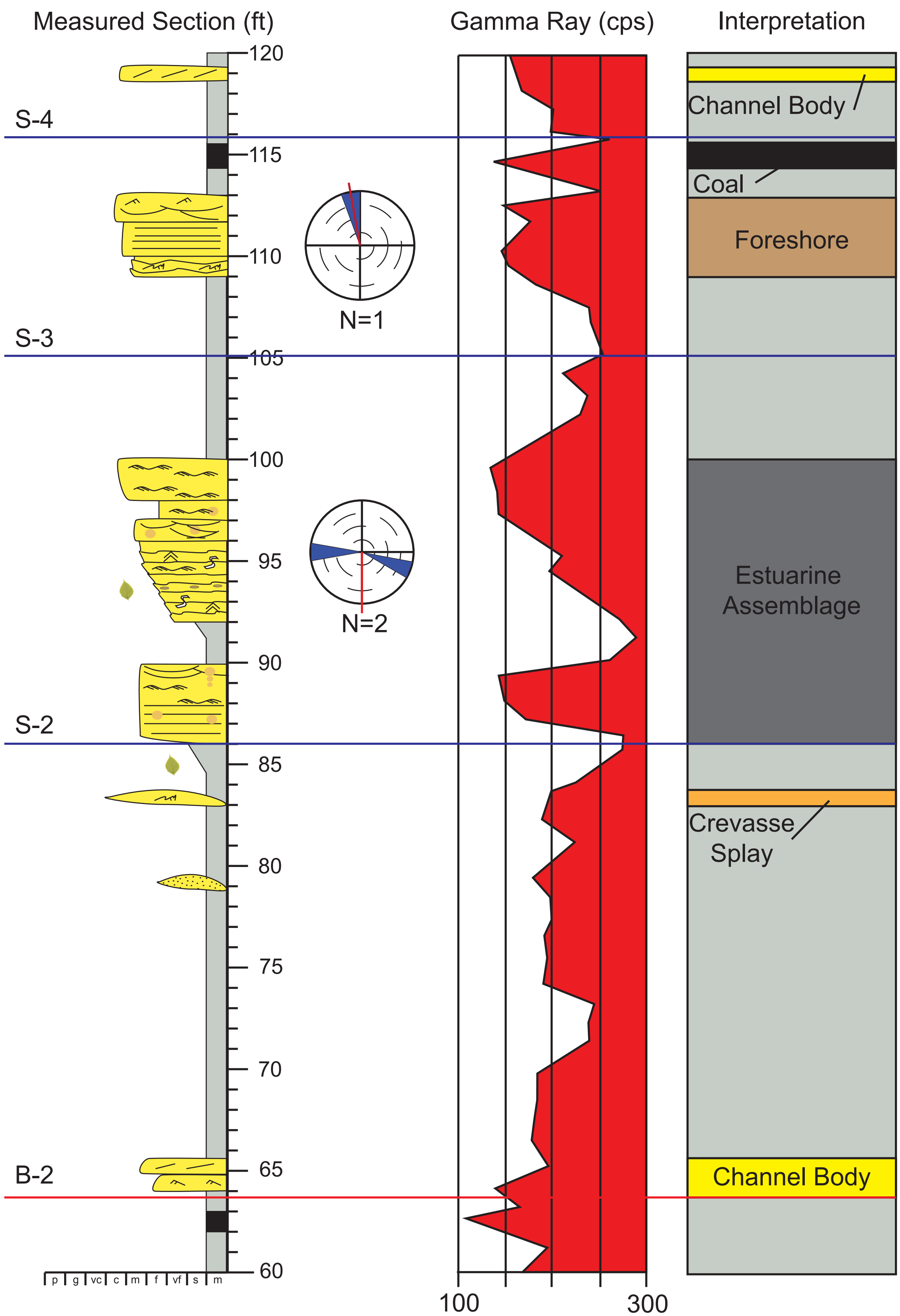
Measured Section (ft)
Gamma Ray (cps)
Interpretation
120
115
110
105
100
95
90
85
80
75
70
65
60
S-4
S-3
S-2
B-2
N=1
N=2
p g vc c m f vf s m
100
300
Channel Body
Coal
Foreshore
Estuarine Assemblage
Crevasse Splay
Channel Body

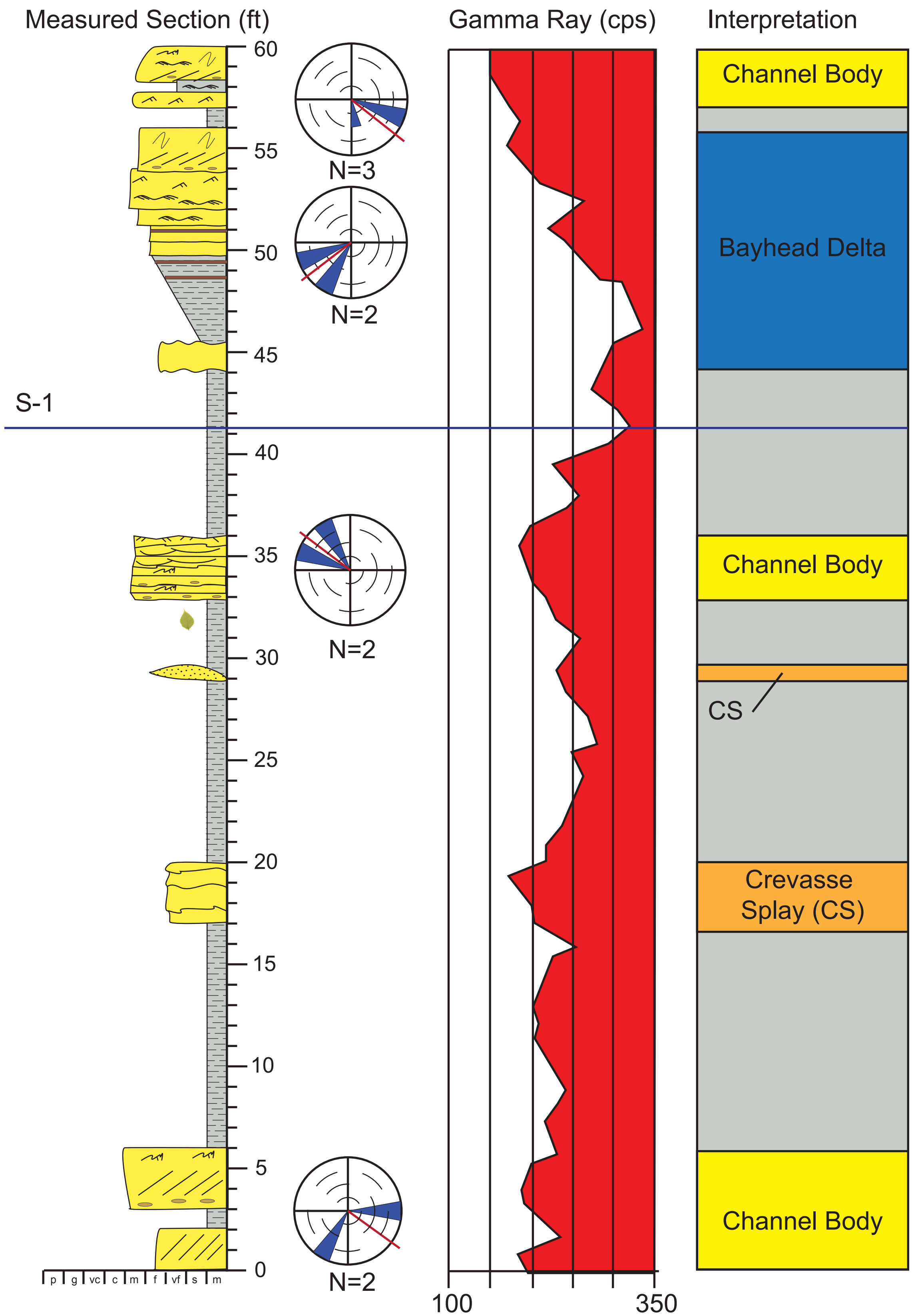
Measured Section (ft)
Gamma Ray (cps)
Interpretation
60
55
50
45
40
35
30
25
20
15
10
5
0
p g vc c m f vf s m
S-1
N=3
N=2
N=2
N=2
100
350
Channel Body
Bayhead Delta
Channel Body
CS
Crevasse Splay (CS)
Channel Body

Mini-Measured Sections: SBW

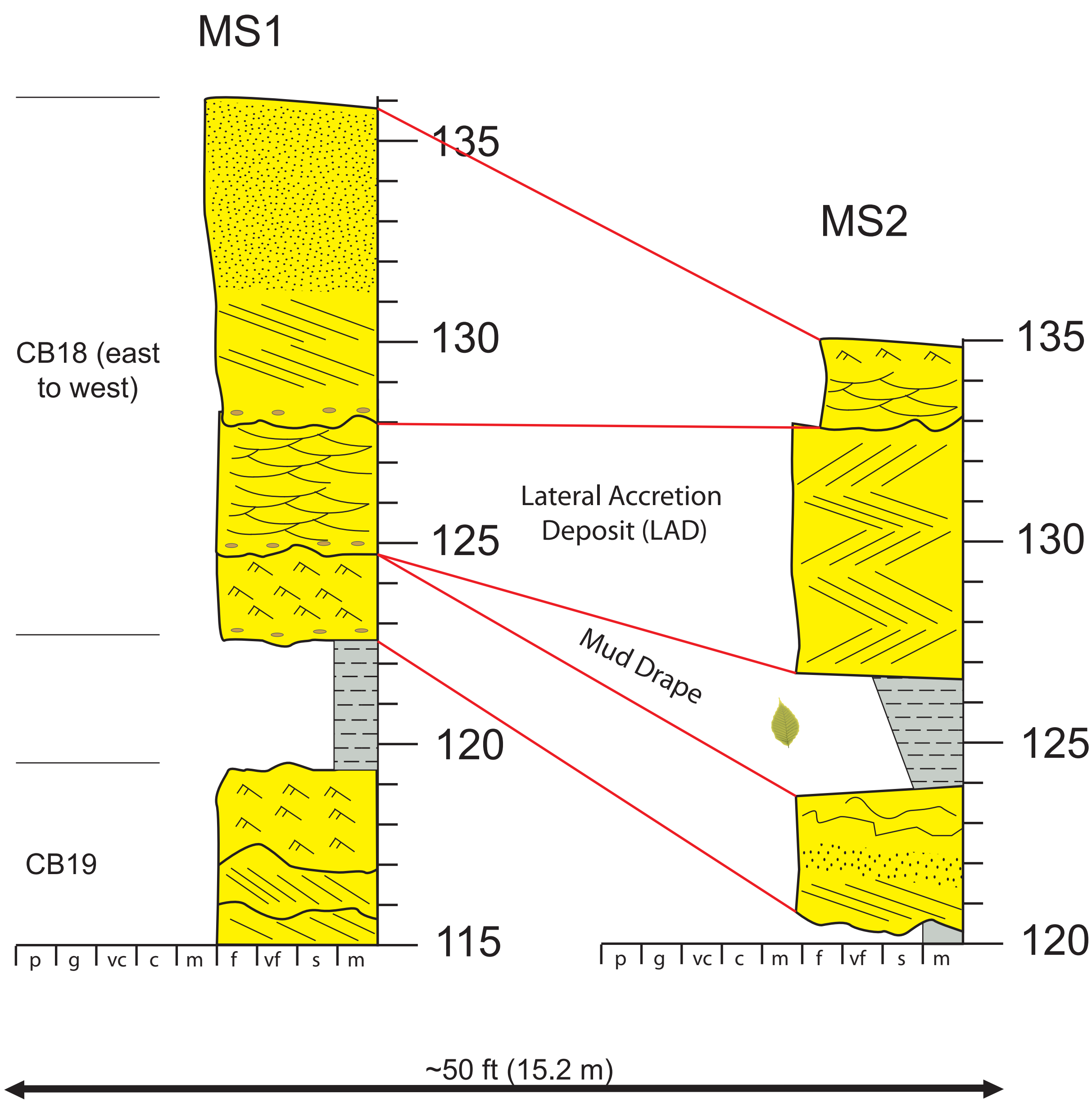

Appendix A4 Mini-measured sections (in feet) from the State Bridge Draw West (SBW) outcrop window. See Appendix A1 for locations. Footages are not exact. See Appendix C2 for location on photopan.

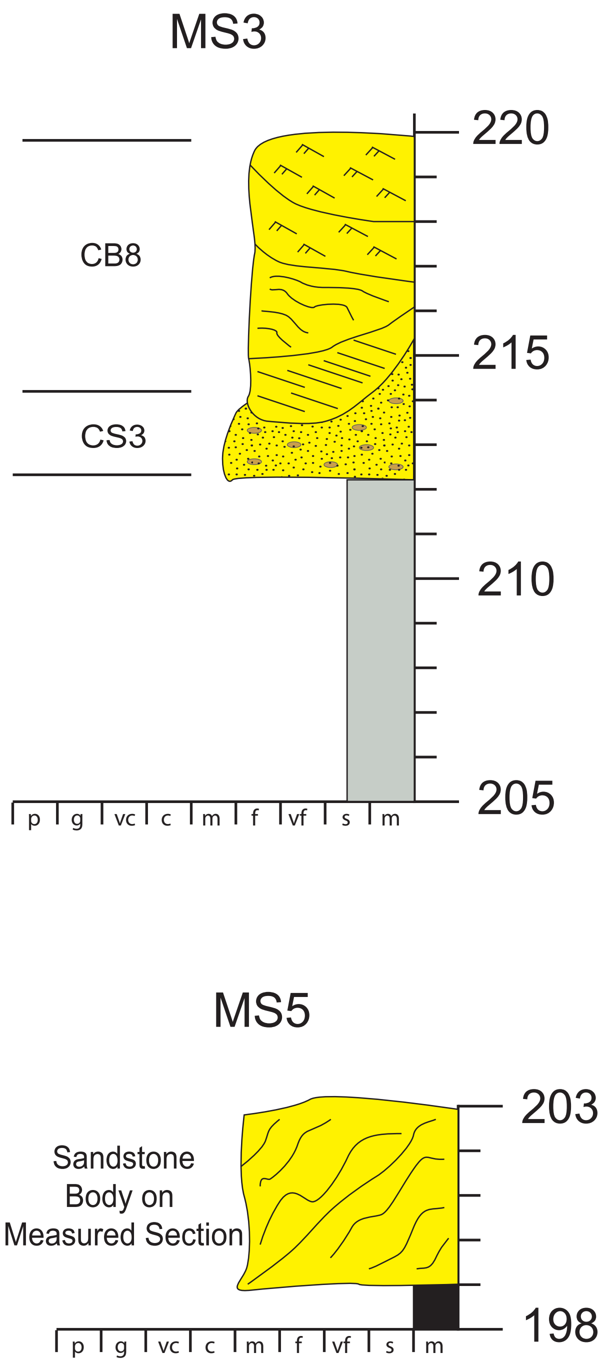

Appendix A4 Mini-measured sections (in feet) from the State Bridge Draw West (SBW) outcrop window See Appendix A1 for locations. Footages not exact. See Appendix C2 for locations on a photopan.

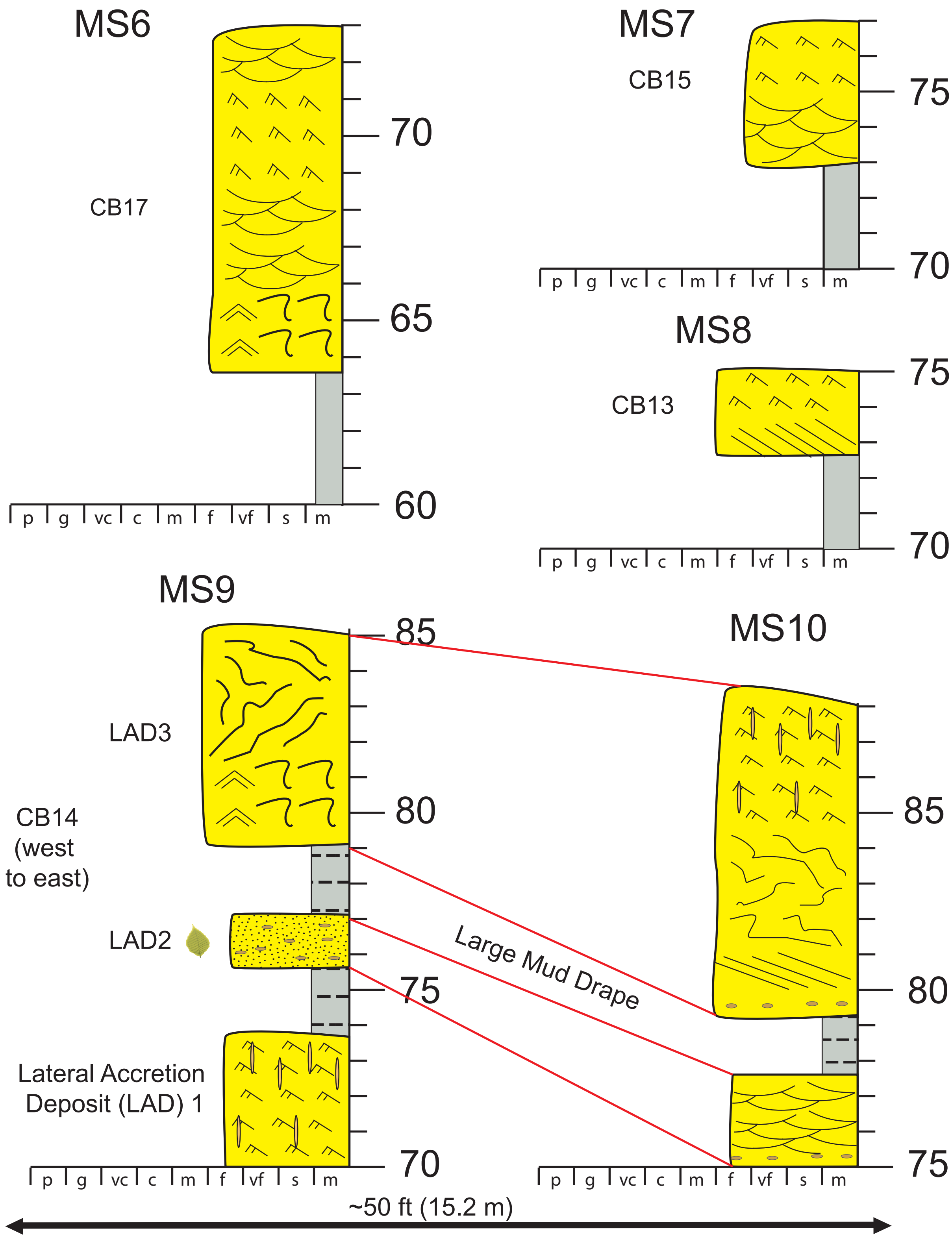

Appendix A4 Mini-measured sections (in feet) from the State Bridge Draw West (SBW) outcrop window. See Appendix A1 for locations. Footages not exact. See Appendix C2 for locationson photopan.

Mini-Measured Sections: VDS

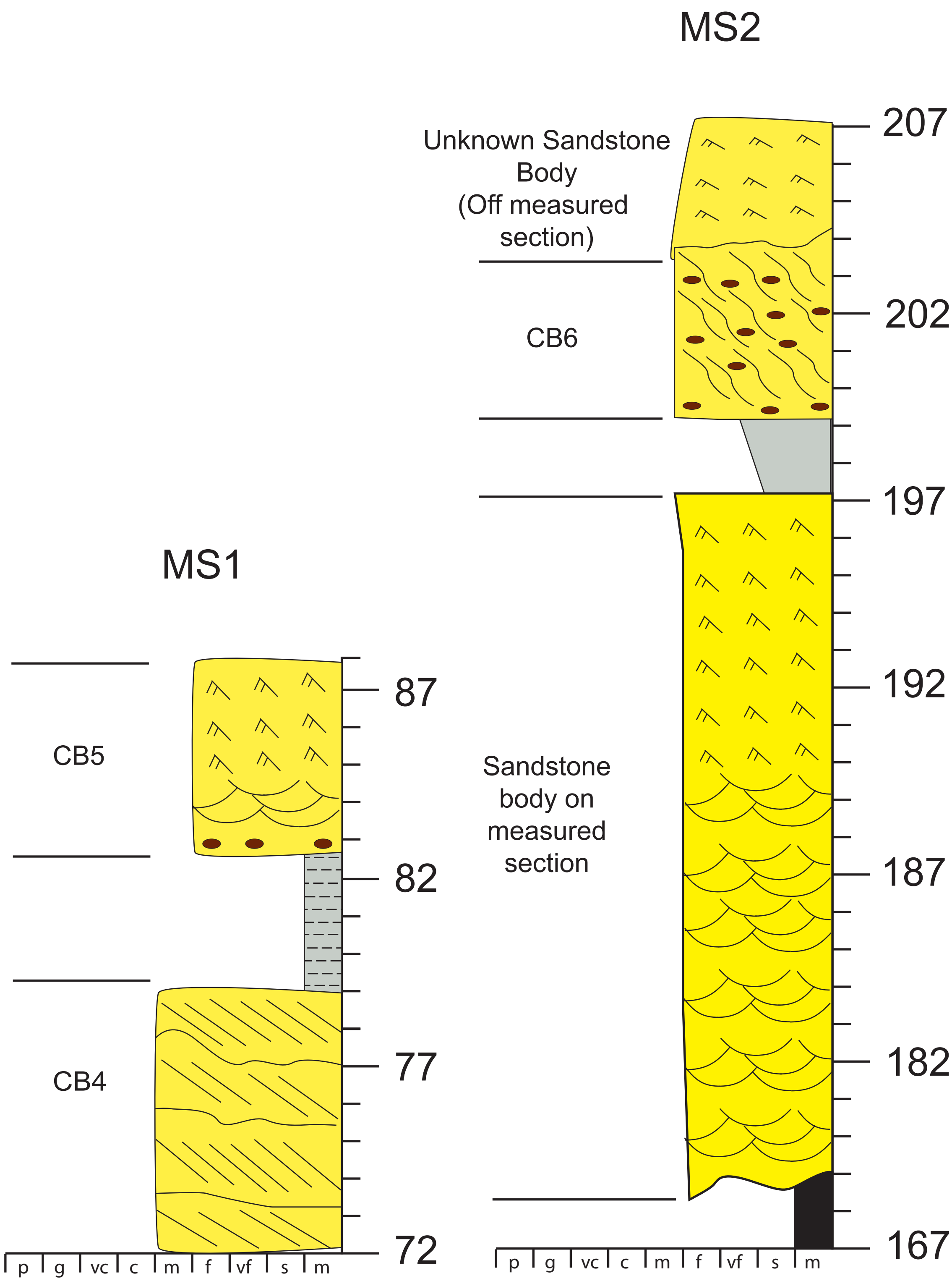

Appendix A4 Mini-measured sections (in feet) from the Vandamore Draw South (VDS) outcrop. See Appendix A1 for locations. Footages not exact. See Appendix C2 for locations on photopans.

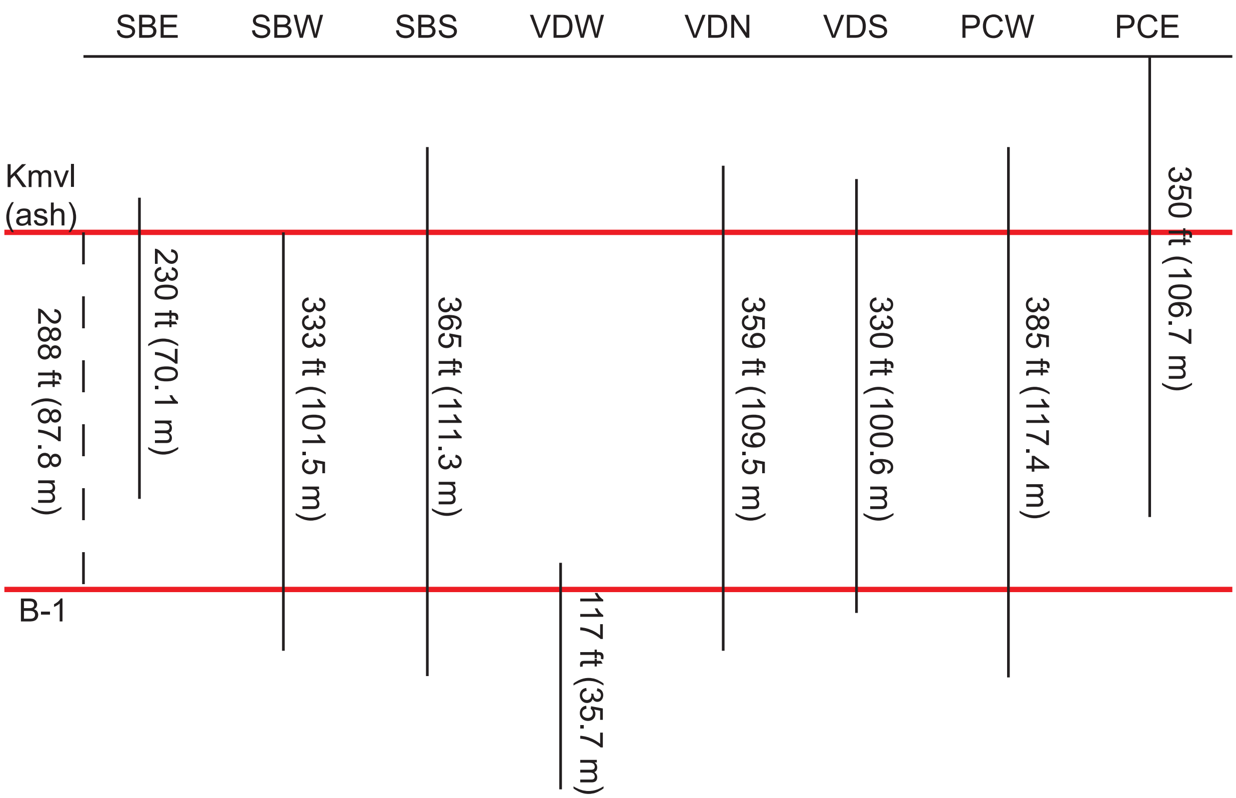

Appendix A5 Sampled intervals for all measured sections with relation to sequence boundary 1 (B-1) and the Kmvl boundary (or the ash). Footage shown to right is based on the thickness of the interval between B-1 and the ash on the SBS measured section. SBS is used as the type section of the study area.

APPENDIX B

1. Gamma-ray data spreadsheet

Philadelphia Creek East

Footage	Reading	Footage	Reading	Footage	Reading	Footage	Reading	Footage	Reading
350	111	297	118.5	244	180.5	191	185	138	220.5
349	120	296	138	243	180.5	190	236.5	137	220.5
348	133	295	138	242	178.5	189	180	136	203.5
347	135	294	130.5	241	178.5	188	166.5	135	203.5
346	138	293	130.5	240	170	187	166.5	134	183.5
345	140	292	136	239	170	186	177.5	133	190
344	154.5	291	136	238	172.5	185	177.5	132	201.5
343	160	290	121.5	237	172.5	184	186	131	230
342	170	289	121.5	236	188	183	186	130	257.5
341	180	288	134.5	235	188	182	191	129	230
340	186	287	134.5	234	188	181	166.5	128	211
339	185	286	148	233	188	180	166.5	127	220
338	183.5	285	148	232	178.5	179	166.5	126	224
337	176	284	137	231	178.5	178	167.5	125	199.5
336	171	283	137	230	142	177	167.5	124	199.5
335	180	282	164.5	229	142	176	176	123	199.5
334	190	281	164.5	228	234.5	175	176	122	217.5
333	195	280	170.5	227	234.5	174	183	121	217.5
332	199.5	279	170.5	226	151.5	173	183	120	186
331	199.5	278	192.5	225	151.5	172	211	119	186
330	190	277	192.5	224	136.5	171	211	118	172.5
329	190	276	189.5	223	136.5	170	201.5	117	172.5
328	168	275	165.5	222	150	169	170	116	172.5
327	168	274	165.5	221	150	168	230.5	115	172.5
326	157	273	165.5	220	177	167	230.5	114	173
325	157	272	159.5	219	177	166	190.5	113	173
324	267	271	159.5	218	176.5	165	190.5	112	277.5
323	267	270	153	217	176.5	164	207.5	111	250
322	182.5	269	153	216	155.5	163	207.5	110	182.5
321	182.5	268	140.5	215	155.5	162	185	109	190
320	174.5	267	140.5	214	150	161	185	108	209.5
319	174.5	266	156	213	150	160	183.5	107	220
318	153.5	265	156	212	157	159	183.5	106	236
317	153.5	264	156.5	211	157	158	180	105	230
316	169	263	156.5	210	219.5	157	200	104	244
315	169	262	134	209	219.5	156	231.5	103	200
314	131.5	261	134	208	427	155	231	102	172
313	131.5	260	119	207	204	154	231	101	172
312	143.5	259	120	206	204	153	231	100	170.5
311	143.5	258	137.5	205	204	152	223	99	175
310	164.5	257	150	204	160.7	151	223	98	188.5
309	164.5	256	118.5	203	160.7	150	224	97	190
308	159	255	118.5	202	191.5	149	224	96	207
307	159	254	108.5	201	191.5	148	236.5	95	200
306	129	253	108.5	200	228.5	147	236.5	94	199
305	129	252	125.5	199	177	146	188.5	93	180
304	150.5	251	125.5	198	177	145	188.5	92	183.5
303	150.5	250	214.5	197	177	144	195	91	185
302	153	249	214.5	196	173.5	143	195	90	197
301	153	248	226.5	195	173.5	142	196.5	89	197
300	137.5	247	226.5	194	174	141	196.5	88	255
299	153	246	172	193	174	140	220	87	255
298	118.5	245	172	192	185	139	220	86	195

Philadelphia Creek East			
Footage	Reading	Footage	Reading
85	195	32	245.5
84	205	31	240
83	180	30	236
82	163.5	29	230
81	165	28	221
80	176.5	27	240
79	176	26	251.5
78	173.5	25	200
77	175	24	211.5
76	177	23	200
75	176.5	22	221.5
74	176	21	218
73	176	20	213.5
72	176	19	220
71	175	18	243.5
70	180	17	230
69	215.5	16	226.5
68	215.5	15	164
67	240	14	164
66	258	13	166.5
65	258	12	166.5
64	234.5	11	175
63	199.5	10	175
62	199.5	9	184
61	180	8	184
60	178.5	7	167.5
59	179	6	167.5
58	180	5	175.5
57	180	4	175.5
56	200	3	175.5
55	200	2	264
54	257.5	1	264
53	257.5	78	173.5
52	177.5	77	175
51	177.5	76	177
50	199.5	75	176.5
49	203.5	74	176
48	203.5	73	176
47	203.5	72	176
46	213.5	71	175
45	213.5		
44	243.5		
43	215.5		
42	215.5		
41	200		
40	193		
39	200		
38	223		
37	220		
36	217		
35	170		
34	266		
33	255		

Philadelphia Creek West											
Footage	GR1	GR2	Average	Footage	GR1	GR2	Average	Footage	GR1	GR2	Average
385	153	172	162.5	330	198	154	176	275	268	200	234
384	178	163	170.5	329	182	177	179.5	274	248	267	257.5
383	175	165	170	328	172	147	159.5	273	233	241	237
382	200	208	204	327	134	157	145.5	272	149	155	152
381	133	156	144.5	326	195	182	188.5	271	171	145	158
380	151	145	148	325	141	154	147.5	270	145	165	155
379	149	153	151	324	147	157	152	269	192	195	193.5
378	145	141	143	323	137	151	144	268	186	201	193.5
377	134	141	137.5	322	152	132	142	267	248	261	254.5
376	141	131	136	321	143	152	147.5	266	214	215	214.5
375	135	139	137	320	232	194	213	265	221	235	228
374	130	146	138	319	245	236	240.5	264	132	226	179
373	141	132	136.5	318	231	245	238	263	228	197	212.5
372	139	126	132.5	317	260	264	262	262	227	210	218.5
371	175	201	188	316	235	230	232.5	261	141	159	150
370	190	182	186	315	209	203	206	260	138	173	155.5
369	250	247	248.5	314	264	231	247.5	259	146	153	149.5
368	227	217	222	313	207	191	199	258	142	140	141
367	232	232	232	312	130	144	137	257	145	161	153
366	200	191	195.5	311	148	154	151	256	155	137	146
365	193	202	197.5	310	178	150	164	255	138	160	149
364	277	249	263	309	176	181	178.5	254	152	166	159
363	263	269	266	308	186	178	182	253	132	162	147
362	217	222	219.5	307	175	175	175	252	176	164	170
361	225	210	217.5	306	165	168	166.5	251	147	145	146
360	223	236	229.5	305	168	153	160.5	250	165	176	170.5
359	208	186	197	304	151	141	146	249	157	182	169.5
358	226	216	221	303	135	143	139	248	175	150	162.5
357	221	217	219	302	200	197	198.5	247	167	172	169.5
356	180	167	173.5	301	217	210	213.5	246	152	175	163.5
355	202	213	207.5	300	260	233	246.5	245	162	162	162
354	229	210	219.5	299	274	259	266.5	244	192	164	178
353	299	294	296.5	298	176	170	173	243	157	187	172
352	146	153	149.5	297	222	205	213.5	242	194	172	183
351	141	132	136.5	296	223	216	219.5	241	208	196	202
350	150	147	148.5	295	205	247	226	240	188	213	200.5
349	141	150	145.5	294	296	238	267	239	155	163	159
348	138	165	151.5	293	233	271	252	238	168	151	159.5
347	146	162	154	292	248	252	250	237	186	176	181
346	153	165	159	291	209	239	224	236	192	186	189
345	172	135	153.5	290	209	240	224.5	235	161	181	171
344	157	141	149	289	248	258	253	234	194	187	190.5
343	157	159	158	288	177	176	176.5	233	210	221	215.5
342	149	174	161.5	287	192	176	184	232	235	240	237.5
341	194	183	188.5	286	210	222	216	231	268	247	257.5
340	171	201	186	285	227	256	241.5	230	270	246	258
339	224	227	225.5	284	149	169	159	229	263	260	261.5
338	202	188	195	283	143	147	145	228	205	238	221.5
337	180	171	175.5	282	189	190	189.5	227	206	225	215.5
336	198	177	187.5	281	152	134	143	226	258	271	264.5
335	177	198	187.5	280	180	172	176	225	253	247	250
334	177	171	174	279	210	216	213	224	138	170	154
333	146	132	139	278	210	216	213	223	140	114	127
332	149	139	144	277	234	213	223.5	222	127	140	133.5
331	157	156	156.5	276	234	213	223.5	221	162	127	144.5

Philadelphia Creek West

Footage	GR1	GR2	Average	Footage	GR1	GR2	Average	Footage	GR1	GR2	Average
220	177	192	184.5	165	156	169	162.5	110	192	212	202
219	183	230	206.5	164	204	202	203	109	243	238	240.5
218	238	256	247	163	210	196	203	108	177	204	190.5
217	190	185	187.5	162	185	197	191	107	177	204	190.5
216	173	179	176	161	172	185	178.5	106	207	195	201
215	194	196	195	160	148	154	151	105	225	254	239.5
214	202	213	207.5	159	240	247	243.5	104	236	249	242.5
213	219	200	209.5	158	240	239	239.5	103	185	222	203.5
212	229	229	229	157	229	255	242	102	183	195	189
211	179	209	194	156	265	265	265	101	165	170	167.5
210	229	183	206	155	291	261	276	100	209	182	195.5
209	212	216	214	154	242	280	261	99	230	278	254
208	187	202	194.5	153	237	219	228	98	225	224	224.5
207	157	191	174	152	254	230	242	97	272	289	280.5
206	127	175	151	151	244	249	246.5	96	266	279	272.5
205	182	174	178	150	262	300	281	95	290	307	298.5
204	170	186	178	149	279	290	284.5	94	303	329	316
203	205	174	189.5	148	250	267	258.5	93	269	277	273
202	189	182	185.5	147	258	247	252.5	92	265	300	282.5
201	147	153	150	146	232	266	249	91	284	291	287.5
200	188	154	171	145	257	239	248	90	288	283	285.5
199	176	192	184	144	262	277	269.5	89	291	290	290.5
198	179	193	186	143	227	233	230	88	275	303	289
197	168	185	176.5	142	208	230	219	87	267	290	278.5
196	191	164	177.5	141	241	207	224	86	258	287	272.5
195	188	200	194	140	229	221	225	85	260	286	273
194	172	211	191.5	139	258	248	253	84	211	254	232.5
193	165	190	177.5	138	266	284	275	83	213	250	231.5
192	191	168	179.5	137	265	273	269	82	177	200	188.5
191	166	179	172.5	136	211	241	226	81	158	183	170.5
190	172	177	174.5	135	222	252	237	80	154	167	160.5
189	159	142	150.5	134	191	223	207	79	199	203	201
188	240	218	229	133	262	279	270.5	78	242	240	241
187	221	248	234.5	132	208	192	200	77	213	219	216
186	220	245	232.5	131	202	187	194.5	76	202	181	191.5
185	185	206	195.5	130	187	192	189.5	75	215	216	215.5
184	223	248	235.5	129	195	181	188	74	238	220	229
183	252	267	259.5	128	192	195	193.5	73	246	296	271
182	240	244	242	127	182	199	190.5	72	235	254	244.5
181	256	215	235.5	126	171	185	178	71	187	234	210.5
180	231	264	247.5	125	200	185	192.5	70	194	190	192
179	273	281	277	124	147	174	160.5	69	181	188	184.5
178	190	206	198	123	149	182	165.5	68	215	227	221
177	234	228	231	122	184	206	195	67	184	180	182
176	235	253	244	121	133	169	151	66	193	211	202
175	279	270	274.5	120	217	216	216.5	65	204	202	203
174	281	310	295.5	119	177	197	187	64	162	156	159
173	178	194	186	118	164	152	158	63	180	178	179
172	137	116	126.5	117	163	150	156.5	62	163	169	166
171	144	141	142.5	116	167	192	179.5	61	177	183	180
170	231	243	237	115	213	214	213.5	60	164	155	159.5
169	179	185	182	114	180	225	202.5	59	178	185	181.5
168	203	203	203	113	162	203	182.5	58	167	187	177
167	189	183	186	112	188	163	175.5	57	201	187	194
166	209	193	201	111	162	177	169.5	56	194	174	184

Philadelphia Creek West

Footage	GR1	GR2	Average
55	230	242	236
54	202	170	186
53	191	176	183.5
52	161	183	172
51	140	171	155.5
50	172	180	176
49	185	191	188
48	190	x	190
47	170	x	170
46	200	x	200
45	200	x	200
44	205	x	205
43	210	x	210
42	205	x	205
41	210	x	210
40	170	x	170
39	200	x	200
38	200	x	200
37	200	x	200
36	180	x	180
35	180	x	180
34	180	x	180
33	180	x	180
32	180	x	180
31	200	x	200
30	200	x	200
29	200	x	200
28	180	x	180
27	180	x	180
26	185	x	185
25	202.6	x	202.6
24	210.6	x	210.6
23	200	x	200
22	181.8	x	181.8
21	179.5	x	179.5
20	182.5	x	182.5
19	182.2	x	182.2
18	171.5	x	171.5
17	187.7	x	187.7
16	197.5	x	197.5
15	285.3	x	285.3
14	225	x	225
13	288.6	x	288.6
12	251.5	x	251.5
11	237.7	x	237.7
10	306.8	x	306.8
9	286.9	x	286.9
8	271	x	271
7	259.5	x	259.5
6	243	x	243
5	203	x	203
4	238	x	238
3	289.1	x	289.1
2	288.1	x	288.1
1	259.4	x	259.4

Footage	GR1	GR2	Average
0	252	x	252

Vandamore Draw South											
Foot	GR1	GR2	Average	Foot	GR1	GR2	Average	Foot	GR1	GR2	Average
330	154	161	157.5	274	230	236	233	218	226	223	224.5
329	157	179	168	273	198	200	199	217	253	249	251
328	177	177	177	272	176	157	166.5	216	211	225	218
327	219	198	208.5	271	189	223	206	215	204	208	206
326	309	300	304.5	270	258	225	241.5	214	183	158	170.5
325	464	427	445.5	269	258	246	252	213	170	163	166.5
324	198	205	201.5	268	221	243	232	212	161	144	152.5
323	210	175	192.5	267	234	215	224.5	211	168	172	170
322	197	195	196	266	194	190	192	210	153	155	154
321	246	251	248.5	265	167	140	153.5	209	130	138	134
320	234	236	235	264	235	206	220.5	208	150	166	158
319	179	204	191.5	263	205	202	203.5	207	228	210	219
318	213	202	207.5	262	195	193	194	206	242	230	236
317	223	197	210	261	202	228	215	205	144	183	163.5
316	205	253	229	260	198	233	215.5	204	116	135	125.5
315	244	225	234.5	259	223	184	203.5	203	183	168	175.5
314	187	187	187	258	171	187	179	202	169	198	183.5
313	162	157	159.5	257	135	135	135	201	159	158	158.5
312	154	176	165	256	168	177	172.5	200	159	171	165
311	150	161	155.5	255	171	184	177.5	199	255	233	244
310	330	258	294	254	128	156	142	198	214	199	206.5
309	245	227	236	253	196	208	202	197	188	197	192.5
308	232	220	226	252	135	157	146	196	232	228	230
307	264	281	272.5	251	246	292	269	195	230	251	240.5
306	239	267	253	250	246	239	242.5	194	213	215	214
305	213	246	229.5	249	245	249	247	193	228	215	221.5
304	205	243	224	248	230	193	211.5	192	132	131	131.5
303	135	120	127.5	247	135	118	126.5	191	112	105	108.5
302	190	181	185.5	246	183	179	181	190	147	138	142.5
301	203	172	187.5	245	201	177	189	189	111	135	123
300	188	159	173.5	244	169	208	188.5	188	166	174	170
299	121	151	136	243	232	233	232.5	187	110	132	121
298	173	191	182	242	162	159	160.5	186	124	132	128
297	196	226	211	241	197	201	199	185	97	105	101
296	185	176	180.5	240	222	214	218	184	120	131	125.5
295	151	171	161	239	222	215	218.5	183	137	118	127.5
294	165	166	165.5	238	207	194	200.5	182	129	151	140
293	232	202	217	237	197	234	215.5	181	183	159	171
292	223	206	214.5	236	253	235	244	180	165	173	169
291	232	238	235	235	249	241	245	179	153	172	162.5
290	228	239	233.5	234	287	257	272	178	151	170	160.5
289	228	226	227	233	277	260	268.5	177	133	137	135
288	219	276	247.5	232	202	201	201.5	176	146	118	132
287	239	241	240	231	253	248	250.5	175	146	131	138.5
286	234	193	213.5	230	131	116	123.5	174	144	134	139
285	216	223	219.5	229	133	151	142	173	135	140	137.5
284	210	210	210	228	194	182	188	172	148	159	153.5
283	162	196	179	227	197	179	188	171	149	172	160.5
282	154	155	154.5	226	208	229	218.5	170	175	170	172.5
281	219	211	215	225	264	226	245	169	161	145	153
280	170	145	157.5	224	209	169	189	168	161	162	161.5
279	146	156	151	223	145	157	151	167	178	210	194
278	190	187	188.5	222	264	251	257.5	166	149	152	150.5
277	128	155	141.5	221	229	219	224	165	208	218	213
276	160	153	156.5	220	154	177	165.5	164	259	284	271.5
275	225	247	236	219	233	243	238	163	295	293	294

Vandamore Draw South											
Foot	GR1	GR2	Average	Foot	GR1	GR2	Average	Foot	GR1	GR2	Average
162	288	336	312	106	139	154	146.5	50	156	163	159.5
161	208	225	216.5	105	136	157	146.5	49	169	202	185.5
160	233	230	231.5	104	160	149	154.5	48	189	168	178.5
159	155	145	150	103	173	172	172.5	47	159	181	170
158	179	193	186	102	214	275	244.5	46	134	122	128
157	152	161	156.5	101	249	229	239	45	117	142	129.5
156	172	172	172	100	244	205	224.5	44	123	105	114
155	171	137	154	99	208	203	205.5	43	117	122	119.5
154	173	158	165.5	98	228	196	212	42	120	126	123
153	173	191	182	97	199	194	196.5	41	125	115	120
152	180	153	166.5	96	150	112	131	40	114	118	116
151	165	194	179.5	95	139	135	137	39	150	139	144.5
150	146	151	148.5	94	144	158	151	38	150	146	148
149	157	139	148	93	189	178	183.5	37	163	156	159.5
148	129	151	140	92	139	149	144	36	145	183	164
147	126	137	131.5	91	200	210	205	35	170	167	168.5
146	139	137	138	90	185	214	199.5	34	191	160	175.5
145	146	127	136.5	89	126	125	125.5	33	189	192	190.5
144	147	151	149	88	178	177	177.5	32	187	222	204.5
143	151	146	148.5	87	250	251	250.5	31	235	231	233
142	136	175	155.5	86	304	281	292.5	30	164	204	184
141	191	197	194	85	134	146	140	29	159	133	146
140	276	169	222.5	84	242	223	232.5	28	130	128	129
139	272	301	286.5	83	222	220	221	27	135	149	142
138	261	296	278.5	82	160	174	167	26	131	136	133.5
137	276	283	279.5	81	128	109	118.5	25	129	106	117.5
136	296	293	294.5	80	148	140	144	24	139	131	135
135	228	220	224	79	141	127	134	23	136	130	133
134	192	199	195.5	78	142	149	145.5	22	149	145	147
133	243	202	222.5	77	186	186	186	21	132	145	138.5
132	202	198	200	76	188	180	184	20	134	135	134.5
131	240	215	227.5	75	144	143	143.5	19	161	160	160.5
130	250	238	244	74	136	159	147.5	18	159	145	152
129	232	220	226	73	144	143	143.5	17	209	191	200
128	304	299	301.5	72	177	173	175	16	251	241	246
127	250	271	260.5	71	232	258	245	15	164	161	162.5
126	223	205	214	70	176	172	174	14	161	138	149.5
125	257	229	243	69	142	150	146	13	143	136	139.5
124	250	226	238	68	204	169	186.5	12	161	173	167
123	253	284	268.5	67	175	171	173	11	171	146	158.5
122	252	227	239.5	66	192	184	188	10	205	199	202
121	237	250	243.5	65	198	176	187	9	186	215	200.5
120	186	175	180.5	64	176	182	179	8	203	202	202.5
119	210	193	201.5	63	203	223	213	7	186	182	184
118	210	197	203.5	62	272	315	293.5	6	211	225	218
117	211	210	210.5	61	270	310	290	5	201	209	205
116	211	230	220.5	60	203	222	212.5	4	226	216	221
115	148	122	135	59	238	241	239.5	3	200	221	210.5
114	229	213	221	58	191	194	192.5	2	303	267	285
113	127	147	137	57	237	214	225.5	1	318	312	315
112	131	140	135.5	56	226	195	210.5	0	284	296	290
111	124	128	126	55	149	146	147.5				
110	149	138	143.5	54	149	146	147.5				
109	154	132	143	53	234	238	236				
108	137	143	140	52	233	218	225.5				
107	153	152	152.5	51	174	194	184				

Vandamore Draw North

Foot	GR1	GR2	Average	Foot	GR1	GR2	Average	Foot	GR1	GR2	Average
359	123	110	116.5	303	188	220	204	247	163	171	167
358	139	122	130.5	302	195	185	190	246	205	226	215.5
357	127	139	133	301	154	157	155.5	245	194	193	193.5
356	161	146	153.5	300	159	158	158.5	244	213	211	212
355	137	173	155	299	148	142	145	243	208	209	208.5
354	219	249	234	298	133	149	141	242	217	249	233
353	190	213	201.5	297	130	144	137	241	239	251	245
352	151	151	151	296	143	148	145.5	240	222	247	234.5
351	171	190	180.5	295	119	163	141	239	216	201	208.5
350	150	163	156.5	294	150	128	139	238	236	204	220
349	189	195	192	293	106	102	104	237	206	247	226.5
348	200	215	207.5	292	104	103	103.5	236	184	178	181
347	196	217	206.5	291	121	124	122.5	235	135	161	148
346	298	301	299.5	290	130	129	129.5	234	176	157	166.5
345	378	361	369.5	289	135	142	138.5	233	142	133	137.5
344	298	313	305.5	288	193	152	172.5	232	188	178	183
343	230	241	235.5	287	174	177	175.5	231	254	256	255
342	258	252	255	286	146	155	150.5	230	243	218	230.5
341	204	233	218.5	285	198	234	216	229	237	245	241
340	188	165	176.5	284	206	247	226.5	228	176	166	171
339	223	238	230.5	283	276	203	239.5	227	209	231	220
338	219	225	222	282	259	231	245	226	183	199	191
337	213	214	213.5	281	251	221	236	225	144	173	158.5
336	202	201	201.5	280	223	202	212.5	224	213	221	217
335	233	232	232.5	279	217	217	217	223	230	235	232.5
334	263	234	248.5	278	203	195	199	222	246	231	238.5
333	245	229	237	277	108	107	107.5	221	221	263	242
332	161	150	155.5	276	115	108	111.5	220	234	261	247.5
331	120	126	123	275	135	136	135.5	219	193	192	192.5
330	151	145	148	274	146	151	148.5	218	210	217	213.5
329	170	154	162	273	169	149	159	217	153	167	160
328	193	164	178.5	272	135	131	133	216	150	173	161.5
327	207	221	214	271	117	119	118	215	164	163	163.5
326	283	241	262	270	112	108	110	214	231	232	231.5
325	149	168	158.5	269	118	118	118	213	240	236	238
324	210	202	206	268	165	167	166	212	191	166	178.5
323	252	269	260.5	267	198	188	193	211	243	243	243
322	327	324	325.5	266	212	202	207	210	243	251	247
321	324	323	323.5	265	245	232	238.5	209	230	238	234
320	181	184	182.5	264	176	184	180	208	248	212	230
319	169	178	173.5	263	256	261	258.5	207	214	215	214.5
318	192	208	200	262	259	222	240.5	206	247	231	239
317	182	212	197	261	294	272	283	205	205	211	208
316	173	163	168	260	235	225	230	204	128	129	128.5
315	168	163	165.5	259	214	230	222	203	105	197	151
314	163	112	137.5	258	186	193	189.5	202	230	208	219
313	151	144	147.5	257	223	226	224.5	201	209	203	206
312	164	177	170.5	256	229	223	226	200	144	152	148
311	183	182	182.5	255	163	205	184	199	161	133	147
310	215	191	203	254	159	179	169	198	166	170	168
309	203	216	209.5	253	184	181	182.5	197	158	164	161
308	174	202	188	252	199	200	199.5	196	159	156	157.5
307	171	188	179.5	251	185	215	200	195	153	184	168.5
306	167	185	176	250	153	142	147.5	194	136	160	148
305	205	198	201.5	249	198	191	194.5	193	191	226	208.5
304	214	237	225.5	248	211	233	222	192	280	266	273

Vandamore Draw North											
Foot	GR1	GR2	Average	Foot	GR1	GR2	Average	Foot	GR1	GR2	Average
191	293	316	304.5	135	157	126	141.5	79	196	203	199.5
190	189	182	185.5	134	114	144	129	78	228	183	205.5
189	174	177	175.5	133	170	175	172.5	77	163	149	156
188	230	244	237	132	161	188	174.5	76	160	176	168
187	159	182	170.5	131	134	130	132	75	187	174	180.5
186	161	179	170	130	148	169	158.5	74	172	175	173.5
185	268	267	267.5	129	169	173	171	73	191	176	183.5
184	210	210	210	128	169	152	160.5	72	194	218	206
183	216	225	220.5	127	227	225	226	71	209	243	226
182	210	197	203.5	126	274	297	285.5	70	228	220	224
181	217	251	234	125	151	143	147	69	226	211	218.5
180	193	203	198	124	154	147	150.5	68	226	218	222
179	205	214	209.5	123	144	127	135.5	67	242	222	232
178	215	209	212	122	148	165	156.5	66	186	171	178.5
177	232	223	227.5	121	116	133	124.5	65	158	141	149.5
176	168	185	176.5	120	136	146	141	64	142	156	149
175	159	163	161	119	122	119	120.5	63	141	142	141.5
174	151	158	154.5	118	146	127	136.5	62	140	144	142
173	209	175	192	117	144	137	140.5	61	152	141	146.5
172	165	144	154.5	116	152	144	148	60	168	159	163.5
171	164	185	174.5	115	157	161	159	59	161	142	151.5
170	153	132	142.5	114	193	184	188.5	58	166	161	163.5
169	170	155	162.5	113	230	203	216.5	57	163	157	160
168	144	143	143.5	112	219	221	220	56	179	155	167
167	143	134	138.5	111	250	261	255.5	55	169	187	178
166	129	122	125.5	110	204	189	196.5	54	218	183	200.5
165	116	129	122.5	109	216	229	222.5	53	160	174	167
164	160	136	148	108	152	132	142	52	204	209	206.5
163	122	133	127.5	107	144	131	137.5	51	154	169	161.5
162	221	236	228.5	106	181	179	180	50	174	147	160.5
161	267	286	276.5	105	165	163	164	49	151	147	149
160	193	211	202	104	164	175	169.5	48	139	148	143.5
159	201	214	207.5	103	186	153	169.5	47	154	148	151
158	192	213	202.5	102	178	188	183	46	151	164	157.5
157	175	171	173	101	138	161	149.5	45	179	190	184.5
156	163	169	166	100	149	172	160.5	44	284	274	279
155	163	187	175	99	182	187	184.5	43	297	275	286
154	178	168	173	98	192	165	178.5	42	223	223	223
153	255	241	248	97	180	190	185	41	227	220	223.5
152	197	197	197	96	174	173	173.5	40	154	149	151.5
151	180	200	190	95	231	205	218	39	177	158	167.5
150	156	161	158.5	94	223	261	242	38	211	194	202.5
149	186	181	183.5	93	288	287	287.5	37	186	189	187.5
148	262	262	262	92	282	262	272	36	168	163	165.5
147	145	123	134	91	259	230	244.5	35	139	169	154
146	159	180	169.5	90	181	173	177	34	198	184	191
145	203	162	182.5	89	205	189	197	33	146	153	149.5
144	137	142	139.5	88	193	246	219.5	32	151	151	151
143	130	131	130.5	87	218	213	215.5	31	184	167	175.5
142	142	138	140	86	209	195	202	30	174	192	183
141	112	136	124	85	223	220	221.5	29	227	229	228
140	153	141	147	84	193	210	201.5	28	161	144	152.5
139	143	162	152.5	83	221	220	220.5	27	160	196	178
138	141	135	138	82	223	232	227.5	26	178	171	174.5
137	130	155	142.5	81	197	156	176.5	25	205	177	191
136	127	119	123	80	196	204	200	24	154	160	157

Vandamore Draw North			
Foot	GR1	GR2	Average
23	154	155	154.5
22	159	170	164.5
21	153	188	170.5
20	202	190	196
19	193	194	193.5
18	162	210	186
17	196	198	197
16	234	221	227.5
15	155	146	150.5
14	171	169	170
13	173	160	166.5
12	174	171	172.5
11	187	166	176.5
10	232	211	221.5
9	242	249	245.5
8	262	267	264.5
7	236	198	217
6	268	263	265.5
5	222	238	230
4	265	258	261.5
3	310	294	302
2	296	308	302
1	261	273	267
0	252	264	258

State Bridge Draw South											
Foot	GR1	GR2	Average	Foot	GR1	GR2	Average	Foot	GR1	GR2	Average
365	117	144	130.5	309	175	171	173	253	169	181	175
364	139	141	140	308	171	143	157	252	152	153	152.5
363	186	171	178.5	307	146	117	131.5	251	172	167	169.5
362	282	228	255	306	147	129	138	250	157	168	162.5
361	331	287	309	305	187	195	191	249	152	164	158
360	189	192	190.5	304	181	172	176.5	248	151	139	145
359	179	198	188.5	303	209	244	226.5	247	151	149	150
358	184	172	178	302	226	199	212.5	246	136	126	131
357	177	161	169	301	260	225	242.5	245	156	163	159.5
356	224	202	213	300	249	218	233.5	244	141	152	146.5
355	196	188	192	299	226	241	233.5	243	134	137	135.5
354	169	181	175	298	225	217	221	242	141	135	138
353	187	218	202.5	297	232	235	233.5	241	166	139	152.5
352	220	188	204	296	205	236	220.5	240	163	172	167.5
351	198	192	195	295	128	157	142.5	239	177	187	182
350	204	194	199	294	151	129	140	238	211	202	206.5
349	147	138	142.5	293	139	146	142.5	237	226	286	256
348	153	151	152	292	129	127	128	236	193	201	197
347	132	118	125	291	153	160	156.5	235	232	190	211
346	158	179	168.5	290	164	162	163	234	178	149	163.5
345	125	151	138	289	210	189	199.5	233	241	186	213.5
344	170	154	162	288	184	182	183	232	258	264	261
343	142	138	140	287	148	140	144	231	221	224	222.5
342	236	207	221.5	286	163	184	173.5	230	196	201	198.5
341	216	207	211.5	285	165	164	164.5	229	120	140	130
340	176	220	198	284	246	218	232	228	155	145	150
339	168	192	180	283	220	220	220	227	186	189	187.5
338	193	168	180.5	282	214	243	228.5	226	215	223	219
337	262	280	271	281	165	192	178.5	225	212	179	195.5
336	168	191	179.5	280	194	210	202	224	167	146	156.5
335	180	172	176	279	242	260	251	223	161	170	165.5
334	176	206	191	278	260	286	273	222	181	168	174.5
333	193	224	208.5	277	216	271	243.5	221	197	204	200.5
332	144	150	147	276	239	274	256.5	220	178	183	180.5
331	200	192	196	275	236	253	244.5	219	228	217	222.5
330	225	209	217	274	204	201	202.5	218	256	239	247.5
329	132	115	123.5	273	230	190	210	217	223	229	226
328	157	161	159	272	205	208	206.5	216	192	191	191.5
327	199	226	212.5	271	206	218	212	215	261	237	249
326	226	259	242.5	270	215	214	214.5	214	213	223	218
325	337	293	315	269	203	208	205.5	213	261	272	266.5
324	302	278	290	268	221	170	195.5	212	301	275	288
323	226	237	231.5	267	228	267	247.5	211	158	165	161.5
322	328	344	336	266	155	189	172	210	193	159	176
321	333	376	354.5	265	122	116	119	209	194	200	197
320	194	188	191	264	131	116	123.5	208	164	186	175
319	157	162	159.5	263	218	185	201.5	207	170	153	161.5
318	133	128	130.5	262	181	181	181	206	116	140	128
317	156	138	147	261	195	209	202	205	121	128	124.5
316	180	178	179	260	151	152	151.5	204	211	191	201
315	227	212	219.5	259	244	234	239	203	201	215	208
314	238	245	241.5	258	253	234	243.5	202	210	177	193.5
313	497	553	525	257	211	225	218	201	223	226	224.5
312	335	324	329.5	256	134	170	152	200	191	219	205
311	260	266	263	255	219	202	210.5	199	286	282	284
310	295	219	257	254	160	179	169.5	198	136	142	139

State Bridge Draw South											
Foot	GR1	GR2	Average	Foot	GR1	GR2	Average	Foot	GR1	GR2	Average
197	146	127	136.5	141	225	253	239	85	281	265	273
196	161	144	152.5	140	250	281	265.5	84	285	297	291
195	173	175	174	139	246	225	235.5	83	290	278	284
194	194	223	208.5	138	251	267	259	82	192	228	210
193	197	169	183	137	287	258	272.5	81	252	237	244.5
192	152	161	156.5	136	254	252	253	80	239	274	256.5
191	147	170	158.5	135	237	235	236	79	245	257	251
190	245	222	233.5	134	249	252	250.5	78	234	231	232.5
189	172	176	174	133	175	167	171	77	271	252	261.5
188	162	147	154.5	132	202	177	189.5	76	245	213	229
187	258	266	262	131	160	147	153.5	75	241	257	249
186	187	172	179.5	130	138	166	152	74	268	262	265
185	154	169	161.5	129	155	146	150.5	73	227	236	231.5
184	193	174	183.5	128	134	126	130	72	254	264	259
183	223	224	223.5	127	137	126	131.5	71	225	227	226
182	220	235	227.5	126	170	173	171.5	70	245	238	241.5
181	251	224	237.5	125	205	181	193	69	263	271	267
180	321	282	301.5	124	232	220	226	68	231	245	238
179	200	206	203	123	211	220	215.5	67	251	245	248
178	234	221	227.5	122	133	167	150	66	238	254	246
177	245	213	229	121	150	143	146.5	65	284	257	270.5
176	226	259	242.5	120	178	180	179	64	241	266	253.5
175	258	225	241.5	119	174	169	171.5	63	239	233	236
174	236	210	223	118	170	131	150.5	62	227	238	232.5
173	295	211	253	117	166	148	157	61	239	254	246.5
172	233	201	217	116	153	155	154	60	211	213	212
171	182	161	171.5	115	146	150	148	59	173	202	187.5
170	145	138	141.5	114	134	155	144.5	58	224	218	221
169	149	158	153.5	113	146	162	154	57	220	213	216.5
168	130	140	135	112	165	173	169	56	174	206	190
167	136	163	149.5	111	187	173	180	55	154	179	166.5
166	166	168	167	110	176	162	169	54	133	149	141
165	193	157	175	109	192	209	200.5	53	137	140	138.5
164	169	180	174.5	108	200	197	198.5	52	136	150	143
163	125	137	131	107	202	209	205.5	51	151	134	142.5
162	245	259	252	106	149	128	138.5	50	129	115	122
161	267	285	276	105	245	237	241	49	147	129	138
160	271	297	284	104	230	210	220	48	160	151	155.5
159	200	215	207.5	103	244	254	249	47	156	167	161.5
158	185	139	162	102	255	234	244.5	46	155	130	142.5
157	206	208	207	101	225	231	228	45	134	118	126
156	215	136	175.5	100	194	178	186	44	129	134	131.5
155	250	205	227.5	99	228	187	207.5	43	145	135	140
154	239	244	241.5	98	244	254	249	42	159	123	141
153	180	183	181.5	97	164	142	153	41	151	129	140
152	227	221	224	96	182	211	196.5	40	151	169	160
151	211	197	204	95	222	209	215.5	39	169	183	176
150	153	151	152	94	267	284	275.5	38	186	189	187.5
149	146	178	162	93	302	310	306	37	168	176	172
148	191	149	170	92	291	300	295.5	36	203	189	196
147	168	174	171	91	149	188	168.5	35	163	180	171.5
146	181	171	176	90	178	172	175	34	183	177	180
145	247	228	237.5	89	240	245	242.5	33	276	277	276.5
144	263	256	259.5	88	285	270	277.5	32	294	294	294
143	291	295	293	87	267	277	272	31	291	266	278.5
142	274	277	275.5	86	268	240	254	30	202	165	183.5

State Bridge Draw South			
Foot	GR1	GR2	Average
29	260	323	291.5
28	173	170	171.5
27	167	160	163.5
26	177	189	183
25	174	169	171.5
24	196	177	186.5
23	178	203	190.5
22	239	297	268
21	279	259	269
20	294	288	291
19	259	272	265.5
18	309	322	315.5
17	331	278	304.5
16	300	321	310.5
15	259	285	272
14	257	287	272
13	305	298	301.5
12	287	307	297
11	288	324	306
10	258	222	240
9	224	229	226.5
8	230	220	225
7	216	231	223.5
6	233	217	225
5	234	243	238.5
4	256	266	261
3	265	283	274
2	249	248	248.5
1	287	262	274.5
0	296	287	291.5

State Bridge Draw West											
Foot	GR1	GR2	Average	Foot	GR1	GR2	Average	Foot	GR1	GR2	Average
333	106	103	104.5	279	134	131	153	261	151	161	156
332	128	102	115	278	132	151	189	260	263	276	269.5
331	124	126	125	277	163	172	163	259	258	258	258
330	138	129	133.5	276	248	246	190	258	179	166	172.5
329	105	139	122	275	174	163	162.5	257	202	198	200
328	131	129	130	274	109	132	150.5	256	256	226	241
327	124	138	131	273	149	151	170.5	255	176	164	170
326	168	209	188.5	272	176	192	206	254	266	250	258
325	135	146	140.5	271	191	192	240.5	253	180	175	177.5
324	161	169	165	270	261	236	280	252	173	189	181
323	237	236	236.5	269	321	290	279.5	251	126	130	128
322	186	220	203	268	340	299	274.5	250	104	129	116.5
321	232	228	230	267	225	238	221.5	249	128	158	143
320	153	137	145	266	242	209	186.5	248	128	140	134
319	140	176	158	265	203	218	195	247	122	134	128
318	266	250	258	264	142	131	182	246	138	126	132
317	192	202	197	263	182	187	228	245	151	177	164
316	100	115	107.5	262	190	222	215	244	182	144	163
315	116	104	110	261	280	274	255.5	243	162	153	157.5
314	116	110	113	260	260	240	250	242	168	175	171.5
313	132	121	126.5	259	213	231	222	241	191	153	172
312	153	126	139.5	258	182	200	191	240	131	146	138.5
311	170	152	161	257	274	276	275	239	144	124	134
310	151	167	159	256	234	213	223.5	238	126	137	131.5
309	104	103	103.5	293	201	218	209.5	237	286	238	262
308	129	104	116.5	292	162	184	173	236	225	240	232.5
307	156	143	149.5	291	140	161	150.5	235	211	214	212.5
306	184	192	188	290	145	130	137.5	234	130	135	132.5
305	229	206	217.5	289	164	161	162.5	233	153	140	146.5
304	240	250	245	288	174	152	163	232	133	144	138.5
303	177	173	175	287	176	193	184.5	231	133	154	143.5
302	259	294	276.5	286	221	220	220.5	230	162	139	150.5
301	232	239	235.5	285	159	169	164	229	137	142	139.5
300	247	283	265	284	191	165	178	228	163	141	152
299	272	246	259	283	165	175	170	227	156	134	145
298	194	176	185	282	154	201	177.5	226	155	184	169.5
297	140	141	140.5	281	157	189	173	225	162	113	137.5
296	149	138	143.5	280	158	160	159	224	135	161	148
295	219	215	217	279	140	158	149	223	173	151	162
294	148	127	137.5	278	180	159	169.5	222	154	152	153
295	138	145	141.5	277	196	179	187.5	221	155	165	160
294	248	245	246.5	276	214	211	212.5	220	130	146	138
293	232	233	232.5	275	224	200	212	219	173	150	161.5
292	224	214	219	274	200	192	196	218	176	169	172.5
291	179	158	168.5	273	230	252	241	217	179	182	180.5
290	137	152	144.5	272	137	134	135.5	216	236	237	236.5
289	110	134	122	271	150	159	154.5	215	237	234	235.5
288	149	140	144.5	270	171	203	187	214	188	200	194
287	219	188	203.5	269	226	228	227	213	195	215	205
286	215	208	211.5	268	263	246	254.5	212	206	222	214
285	240	279	259.5	267	218	291	254.5	211	199	220	209.5
284	211	220	215.5	266	313	269	291	210	230	226	228
283	109	103	106	265	198	236	217	209	257	242	249.5
282	111	120	115.5	264	214	162	188	208	235	227	231
281	128	140	134	263	227	221	224	207	256	275	265.5
280	137	120	128.5	262	161	156	158.5	206	294	258	276

State Bridge Draw West

Foot	GR1	GR2	Average	Foot	GR1	GR2	Average	Foot	GR1	GR2	Average
205	277	289	283	149	196	208	202	93	144	131	137.5
204	271	280	275.5	148	223	234	228.5	92	151	135	143
203	310	290	300	147	254	260	257	91	119	125	122.5
202	296	349	322.5	146	168	194	181	90	141	147	139.5
201	233	264	248.5	145	166	152	159	89	199	192	179
200	239	238	238.5	144	200	212	206	88	169	168	142.5
199	243	242	242.5	143	284	271	277.5	87	167	161	158
198	261	259	260	142	253	251	252	86	151	135	150
197	235	224	229.5	141	222	231	226.5	85	141	126	151
196	166	143	154.5	140	96	184	140	84	130	138	157.5
195	197	208	202.5	139	168	182	175	83	140	159	168.5
194	304	272	288	138	207	210	208.5	82	146	116	181
193	246	281	263.5	137	142	170	156	81	158	149	176.5
192	270	272	271	136	183	213	198	80	173	149	201.5
191	240	239	239.5	135	245	277	261	79	153	161	181.5
190	239	229	234	134	247	258	252.5	78	171	185	234
189	195	169	182	133	284	277	280.5	77	188	197	262
188	212	229	220.5	132	274	239	256.5	76	208	216	264
187	266	235	250.5	131	190	195	192.5	75	168	195	219
186	286	290	288	130	197	169	183	74	189	230	255
185	244	233	238.5	129	245	248	246.5	73	195	210	233
184	194	237	215.5	128	134	133	133.5	72	295	297	247.5
183	187	199	193	127	176	174	175	71	281	336	221
182	153	188	170.5	126	229	221	225	70	295	320	216.5
181	156	179	167.5	125	211	220	215.5	69	249	270	259.5
180	245	264	254.5	124	237	220	228.5	68	330	321	325.5
179	267	271	269	123	228	297	262.5	67	294	271	282.5
178	253	253	253	122	251	276	263.5	66	226	200	213
177	231	245	238	121	186	216	201	65	148	161	154.5
176	239	209	224	120	164	158	161	64	160	138	149
175	167	174	170.5	134	240	241	240.5	63	164	176	170
174	196	200	198	133	256	259	257.5	62	211	191	201
173	210	223	216.5	132	252	263	257.5	61	220	209	214.5
172	213	192	202.5	131	257	247	252	60	239	246	242.5
171	151	166	158.5	130	236	211	223.5	59	289	284	286.5
170	186	171	178.5	129	247	220	233.5	58	265	283	274
169	135	154	144.5	128	214	201	207.5	57	204	193	198.5
168	171	168	169.5	127	239	205	222	56	213	229	221
167	159	128	143.5	126	209	242	225.5	55	189	219	204
166	153	120	136.5	125	231	248	239.5	54	178	197	187.5
165	175	209	192	124	213	220	216.5	53	177	206	191.5
164	141	141	141	123	281	265	273	52	177	214	195.5
163	135	152	143.5	122	238	220	229	51	185	214	199.5
162	155	152	153.5	121	238	213	225.5	50	218	190	204
161	159	143	151	120	280	293	286.5	49	227	242	234.5
160	129	154	141.5	119	252	241	246.5	48	202	247	224.5
159	229	217	223	118	246	246	246	47	323	310	316.5
158	238	232	235	117	259	239	249	46	296	292	294
157	170	192	181	116	264	245	254.5	45	313	292	302.5
156	201	232	216.5	115	194	202	198	44	300	284	292
155	230	217	223.5	114	161	164	162.5	43	289	275	282
154	275	240	257.5	113	160	203	181.5	42	295	306	300.5
153	189	215	202	112	141	147	144	41	327	306	316.5
152	199	189	194	111	126	145	135.5	40	286	266	276
151	159	140	149.5	110	141	144	142.5	39	153	161	76.5
150	150	189	169.5	109	131	134	132.5	38	171	185	85.5

State Bridge Draw West			
Foot	GR1	GR2	Average
37	188	197	262
36	208	216	264
35	168	195	219
34	189	230	255
33	195	210	233
32	295	297	247.5
31	281	336	221
30	295	320	216.5
29	249	270	259.5
28	330	321	325.5
27	294	271	282.5
26	226	200	213
25	148	161	154.5
24	160	138	149
23	164	176	170
22	211	191	201
21	220	209	214.5
20	239	246	242.5
19	289	284	286.5
18	265	283	274
17	204	193	198.5
16	213	229	221
15	189	219	204
14	178	197	187.5
13	177	206	191.5
12	177	214	195.5
11	185	214	199.5
10	218	190	204
9	227	242	234.5
8	202	247	224.5
7	323	310	316.5
6	296	292	294
5	313	292	302.5
4	300	284	292
3	289	275	282
2	295	306	300.5
1	327	306	316.5
0	286	266	276

State Bridge Draw East											
Footage	GR1	GR2	Average	Footage	GR1	GR2	Average	Footage	GR1	GR2	Average
230	108	135	121.5	178	214	217	215.5	126	257	250	253.5
229	128	147	137.5	177	255	264	259.5	125	205	190	197.5
228	124	105	114.5	176	292	293	292.5	124	158	151	154.5
227	226	132	179	175	237	236	236.5	123	174	173	173.5
226	187	177	182	174	225	234	229.5	122	172	176	174
225	120	117	118.5	173	230	236	233	121	228	240	234
224	125	147	136	172	256	261	258.5	120	163	150	156.5
223	135	147	141	171	188	193	190.5	119	173	163	168
222	179	178	178.5	170	130	118	124	118	207	194	200.5
221	220	221	220.5	169	116	118	117	117	196	200	198
220	198	208	203	168	105	112	108.5	116	259	263	261
219	167	166	166.5	167	124	136	130	115	136	140	138
218	181	184	182.5	166	124	119	121.5	114	266	237	251.5
217	167	186	176.5	165	133	143	138	113	139	145	142
216	150	145	147.5	164	135	140	137.5	112	184	169	176.5
215	124	134	129	163	164	163	163.5	111	132	163	147.5
214	148	122	135	162	142	140	141	110	152	150	151
213	128	129	128.5	161	129	127	128	109	179	184	181.5
212	120	124	122	160	111	135	123	108	238	245	241.5
211	135	128	131.5	159	203	224	213.5	107	242	236	239
210	144	147	145.5	158	219	204	211.5	106	249	261	255
209	178	175	176.5	157	242	252	247	105	215	209	212
208	270	280	275	156	219	239	229	104	244	232	238
207	182	190	186	155	216	206	211	103	220	236	228
206	214	195	204.5	154	229	227	228	102	189	204	196.5
205	169	200	184.5	153	265	263	264	101	161	175	168
204	171	176	173.5	152	250	255	252.5	100	130	134	132
203	219	194	206.5	151	221	215	218	99	155	131	143
202	130	130	130	150	197	200	198.5	98	144	145	144.5
201	180	200	190	149	223	209	216	97	172	185	178.5
200	120	104	112	148	204	225	214.5	96	214	208	211
199	128	117	122.5	147	180	200	190	95	190	188	189
198	125	115	120	146	137	135	136	94	224	221	222.5
197	168	178	173	145	201	193	197	93	273	271	272
196	167	178	172.5	144	207	194	200.5	92	304	274	289
195	220	223	221.5	143	168	145	156.5	91	262	260	261
194	163	182	172.5	142	158	166	162	90	133	158	145.5
193	128	131	129.5	141	130	127	128.5	89	149	149	149
192	123	140	131.5	140	114	145	129.5	88	174	170	172
191	120	131	125.5	139	174	172	173	87	268	278	273
190	179	200	189.5	138	230	231	230.5	86	270	278	274
189	126	130	128	137	217	239	228	85	228	230	229
188	170	177	173.5	136	206	218	212	84	196	202	199
187	127	124	125.5	135	264	259	261.5	83	191	183	187
186	115	112	113.5	134	287	277	282	82	226	219	222.5
185	131	137	134	133	206	220	213	81	209	200	204.5
184	146	153	149.5	132	218	224	221	80	183	180	181.5
183	124	92	108	131	211	216	213.5	79	193	207	200
182	116	120	118	130	156	158	157	78	205	196	200.5
181	145	134	139.5	129	137	140	138.5	77	200	177	188.5
180	146	130	138	128	131	135	133	76	196	188	192
179	173	185	179	127	169	179	174	75	184	198	191

State Bridge Draw East

Footage	GR1	GR2	Average
74	245	241	243
73	222	250	236
72	240	241	240.5
71	200	214	207
70	194	175	184.5
69	174	190	182
68	188	179	183.5
67	184	177	180.5
66	188	202	195
65	137	142	139.5
64	167	163	165
63	91	127	109
62	192	196	194
61	161	179	170
60	153	145	149
59	153	155	154
58	172	164	168
57	186	180	183
56	173	169	171
55	194	197	195.5
54	227	200	213.5
53	270	270	270
52	218	220	219
51	229	247	238
50	254	275	264.5
49	306	309	307.5
48	318	331	324.5
47	323	350	336.5
46	318	285	301.5
45	285	299	292
44	271	279	275
43	296	317	306.5
42	331	292	311.5
41	307	281	294
40	226	217	221.5
39	268	248	258
38	212	243	227.5
37	203	196	199.5
36	181	184	182.5
35	194	200	197
34	220	217	218.5
33	233	227	230
32	249	271	260
31	249	241	245
30	220	236	228
29	256	226	241
28	256	269	262.5
27	278	281	279.5
26	270	224	247
25	278	261	269.5
24	264	236	250
23	250	227	238.5
22	229	203	216
21	228	210	219
20	175	165	170
19	213	187	200
18	211	191	201
17	249	257	253
16	215	230	222.5
15	204	226	215
14	201	206	203.5
13	201	211	206
12	200	205	202.5
11	220	224	222
10	246	239	242.5
9	256	211	233.5
8	234	196	215
7	237	223	230
6	168	222	195
5	193	188	190.5
4	188	193	190.5
3	229	242	235.5
2	183	187	185
1	178	210	194

APPENDIX C

1. **Sandstone body coordinate spreadsheet**
2. **Sandstone body data spreadsheet**
3. **Sandstone body aerial-view traces**
4. **Sandstone body photopans**

Location	Footage	SSB ID	Date	Time	Datafile Name	GPS Elevation (ft)	Vertical Precision (ft)	Horizontal Precision (ft)	Northing	Easting
VDS	175-180'	NA	8/18/2010	08:56:20am	AT081808A.cor	5727.595	3.0	2.0	4420110.342	693052.791
VDS	175-180'	NA	8/18/2010	09:51:25am	AT081809A.cor	5979.119	2.6	1.6	4419932.104	693356.691
VDS	175-180'	NA	8/18/2010	10:17:40am	AT081809A.cor	6001.275	1.6	1.6	4419793.402	693355.219
VDS	87'	CB6	8/18/2010	10:08:55am	AT081810A.cor	6006.149	1.6	1.3	4419903.287	693354.979
VDS	87'	CB6	8/18/2010	10:12:30am	AT081810A.cor	6011.433	1.6	1.6	4419827.227	693354.652
VDS	87'	CB7	8/18/2010	10:20:25am	AT081810B.cor	6007.445	2.0	2.0	4419794.322	693359.064
VDS	87'	CB7	8/18/2010	10:22:40am	AT081810B.cor	6003.013	2.0	3.0	4419808.417	693347.235
VDS	155'	NA	8/18/2010	10:40:10am	AT081810C.cor	5977.154	3.6	4.6	4419877.854	693338.336
VDS	155'	NA	8/18/2010	10:45:05am	AT081810C.cor	5962.004	1.6	1.6	4419964.252	693340.490
VDS	141-151'	NA	8/18/2010	10:49:05am	AT081810D.cor	5953.928	1.6	1.6	4419981.428	693331.053
VDS	141-151'	NA	8/18/2010	11:07:00am	AT081810D.cor	5961.718	2.0	3.6	4419882.785	693330.588
VDS	100-115'	NA	8/18/2010	11:20:40am	AT081811A.cor	5931.932	2.3	1.3	4419703.948	693358.487
VDS	100-115'	NA	8/18/2010	11:36:05am	AT081811A.cor	5918.878	2.3	1.3	4419999.419	693341.631
VDS	76'	CB4	8/18/2010	11:46:30am	AT081811B.cor	5871.574	2.0	1.0	4420050.838	693361.766
VDS	76'	CB4	8/18/2010	12:02:05pm	AT081811B.cor	5889.014	3.6	2.3	4419851.349	693299.877
VDS	82'	CB5	8/18/2010	12:05:10pm	AT081812A.cor	5892.038	2.6	1.3	4419917.851	693295.927
VDS	82'	CB5	8/18/2010	12:07:00pm	AT081812A.cor	5894.147	2.3	1.3	4419905.632	693297.468
VDS	42'	CB2	8/18/2010	12:12:35pm	AT081812B.cor	5856.896	3.0	1.6	4419916.294	693280.232
VDS	42'	CB2	8/18/2010	12:18:40pm	AT081812B.cor	5843.471	2.0	1.0	4420064.302	693268.523
VDS	17-29'	NA	8/18/2010	12:25:25pm	AT081812C.cor	5822.869	2.3	1.3	4420097.563	693378.578
VDS	17-29'	NA	8/18/2010	12:47:05pm	AT081812C.cor	5828.990	3.3	1.6	4419872.392	693262.678
VDS	67'	CB3	8/18/2010	12:31:10pm	AT081812D.cor	5855.174	2.3	1.3	4420056.913	693275.897
VDS	67'	CB3	8/18/2010	12:35:50pm	AT081812D.cor	5869.918	3.6	1.6	4419975.910	693283.059
VDS	11-15'	NA	8/18/2010	12:52:10pm	AT081812E.cor	5810.356	2.3	1.3	4419853.919	693241.717
VDS	11-15'	NA	8/18/2010	01:07:55pm	AT081812E.cor	5801.720	2.3	1.6	4420047.307	693231.693
VDS	16'	CB1	8/18/2010	12:57:40pm	AT081812F.cor	5824.919	2.3	1.3	4419832.432	693251.099
VDS	16'	CB1	8/18/2010	01:01:00pm	AT081812F.cor	5821.049	2.3	1.3	4419892.007	693243.898
VDW	20-30'	NA	8/18/2010	03:35:40pm	AT081815A.cor	5741.624	3.0	2.6	4420590.788	693165.722
VDW	55'	CB21	8/18/2010	03:49:30pm	AT081815B.cor	5772.934	2.0	1.6	4420609.055	693177.940
VDW	55'	CB21	8/18/2010	03:54:35pm	AT081815B.cor	5772.820	2.0	1.6	4420646.247	693172.493
VDW	50-60'	CS8	8/18/2010	03:57:20pm	AT081815C.cor	5770.675	2.3	2.3	4420657.050	693171.149
VDW	50-60'	CS8	8/18/2010	04:04:00pm	AT081815C.cor	5757.814	2.6	2.0	4420755.281	693131.577
VDW	75'	CB22	8/18/2010	04:11:50pm	AT081816A.cor	5773.978	3.3	3.0	4420815.232	693127.270
VDW	75'	CB22	8/18/2010	04:48:50pm	AT081816A.cor	5802.497	4.6	2.0	4420576.639	693193.251
VDW	80-90'	CS9	8/18/2010	04:54:10pm	AT081816B.cor	5814.833	4.3	1.6	4420641.179	693190.319
SBW	216'	CB9	8/19/2010	09:23:45am	R081909A.cor	5966.612	2.6	1.6	4422126.609	693033.250
SBW	216'	CB9	8/19/2010	09:47:30am	R081909A.cor	5921.886	2.0	1.3	4422446.840	693025.066
SBW	Unk	NA	8/19/2010	10:06:50am	R081909B.cor	5937.400	2.0	1.6	4422271.996	693077.541
SBW	Unk	NA	8/19/2010	11:01:55am	R081909B.cor	5952.049	1.6	1.6	4422278.382	693088.356
SBW	199-211'	NA	8/19/2010	10:13:40am	R081910A.cor	5930.066	2.0	2.0	4422256.125	693056.566

Location	Footage	SSB ID	Avg. Thickness (ft)	Apparent Width (ft)	Comments	Included in Dataset?
VDS	175-180'	NA	16.6	455.0	Major Body above B-2	N, not completed
VDS	175-180'	NA	16.6	455.0	Major Body above B-2	N, not completed
VDS	175-180'	NA	16.6	455.0	Major Body above B-3	N, not completed
VDS	87'	CB6	2.3	249.5	Mini-Measured Section, MS2	Y
VDS	87'	CB6	2.3	249.5	Mini-Measured Section, MS2	Y
VDS	87'	CB7	3.0	60.4	NA	Y
VDS	87'	CB7	3.0	60.4	NA	Y
VDS	155'	NA	6.0	283.5	NA	N, not completed
VDS	155'	NA	6.0	283.5	NA	N, not completed
VDS	141-151'	NA	14.5	323.6	NA	N, not completed
VDS	141-151'	NA	14.5	323.6	NA	N, not completed
VDS	100-115'	NA	14.9	970.7	Tidal Point Bar	N, not completed
VDS	100-115'	NA	14.9	970.7	Tidal Point Bar	N, not completed
VDS	76'	CB4	7.7	685.1	NA	Y
VDS	76'	CB4	7.7	685.1	NA	Y
VDS	82'	CB5	2.7	40.4	Channel Fill, Mini-Measured Section, MS1	Y
VDS	82'	CB5	2.7	40.4	Channel Fill, Mini-Measured Section, MS1	Y
VDS	42'	CB2	5.7	487.0	Tidal Point Bar	Y
VDS	42'	CB2	5.7	487.0	Tidal Point Bar	Y
VDS	17-29'	NA	7.4	830.7	Amalgamated	N, not completed
VDS	17-29'	NA	7.4	830.7	Amalgamated	N, not completed
VDS	67'	CB3	1.0	266.7	NA	Y
VDS	67'	CB3	1.0	266.7	NA	Y
VDS	11-15'	NA	6.4	635.2	Major Body above B-1	N, not completed
VDS	11-15'	NA	6.4	635.2	Major Body above B-1	N, not completed
VDS	16'	CB1	2.3	196.8	NA	Y
VDS	16'	CB1	2.3	196.8	NA	Y
VDW	20-30'	NA	8.0	Unk	NA	N, not completed
VDW	55'	CB21	6.1	123.3	NA	Y
VDW	55'	CB21	6.1	123.3	NA	Y
VDW	50-60'	CS8	3.1	347.4	NA	Y
VDW	50-60'	CS8	3.1	347.4	NA	Y
VDW	75'	CB22	8.1	812.0	NA	Y
VDW	75'	CB22	8.1	812.0	NA	Y
VDW	80-90'	CS9	2.0	40.6	Hand Measured	Y
SBW	216'	CB9	5.0	1048.1	Tidal Point Bar	Y
SBW	216'	CB9	5.0	1048.1	Tidal Point Bar	Y
SBW	201'	NA	Unk	41.2	Mini-Measured Section, MS5	N, not completed
SBW	201'	NA	Unk	41.2	Mini-Measured Section, MS5	N, not completed
SBW	199-211'	NA	6.5	478.0	Major Body above B-2	N, not completed

Location	Footage	SSB ID	Date	Time	Datafile Name	GPS Elevation (ft)	Vertical Precision (ft)	Horizontal Precision (ft)	Northing	Easting
SBW	199-211'	NA	8/19/2010	10:22:55am	R081910A.cor	5951.704	2.0	1.6	4422114.173	693089.507
SBW	213-215'	NA	8/19/2010	10:31:05am	R081910B.cor	5956.641	2.0	1.6	4422147.830	693197.172
SBW	Unk	NA	8/19/2010	10:40:55am	R081910C.cor	5943.304	2.0	2.0	4422107.832	693135.179
SBW	Unk	NA	8/19/2010	10:53:50am	R081910D.cor	5930.489	2.6	2.0	4422103.480	693086.626
SBW	Unk	NA	8/19/2010	11:44:05am	R081910D.cor	5929.863	2.0	1.3	4422209.324	693010.724
SBW	220-225'	DF1	8/19/2010	11:09:15am	R081911A.cor	5964.778	1.6	1.3	4422110.874	693065.702
SBW	220-225'	DF1	8/19/2010	11:12:35am	R081911A.cor	5957.808	2.0	1.3	4422120.482	693031.162
SBW	213-214'	CS3	8/19/2010	11:18:50am	R081911B.cor	5964.798	2.0	1.3	4422113.491	693061.976
SBW	213-214'	CS3	8/19/2010	11:23:50am	R081911B.cor	5957.641	2.3	1.3	4422119.080	693017.975
SBW	213-217'	DF2	8/19/2010	11:30:55am	R081911C.cor	5968.108	2.0	1.0	4422119.190	693049.938
SBW	215'	CB8	8/19/2010	11:33:55am	R081911C.cor	5964.172	2.0	1.3	4422127.395	693032.939
SBW	215'	CB8	8/19/2010	11:36:15am	R081911C.cor	5965.887	2.0	1.0	4422125.504	693019.506
SBW	163-175'	NA	8/19/2010	11:51:25am	R081911D.cor	5919.075	2.3	1.3	4422137.113	692982.813
SBW	135'	CB18	8/19/2010	11:56:15am	R081911E.cor	5883.438	2.3	1.3	4422096.024	692968.515
SBW	135'	CB18	8/19/2010	12:02:10pm	R081911E.cor	5872.715	2.3	1.0	4422073.153	693081.140
SBW	Unk	NA	8/19/2010	12:05:35pm	R081912A.cor	5881.519	2.6	1.3	4422073.359	693029.945
SBW	105'	CB10	8/19/2010	12:15:50pm	R081912B.cor	5847.279	2.0	1.0	4422052.140	693097.091
SBW	105'	CB10	8/19/2010	12:43:15pm	R081912B.cor	5840.394	3.3	1.6	4422065.839	692960.363
SBW	120'	CB19	8/19/2010	12:21:20pm	R081912C.cor	5852.793	2.3	1.3	4422046.616	693054.695
SBW	120'	CB19	8/19/2010	12:40:30pm	R081912C.cor	5857.755	3.3	1.6	4422071.196	692958.920
SBW	110'	CB11	8/19/2010	12:36:50pm	R081912D.cor	5848.427	3.6	1.6	4422060.409	692973.814
SBW	110'	CB11	8/19/2010	01:46:35pm	R081912D.cor	5846.233	2.0	1.3	4422116.013	692920.532
SBW	98'	CB12	8/19/2010	01:52:05pm	R081913A.cor	5835.045	2.3	1.6	4422104.917	692913.486
SBW	98'	CB12	8/19/2010	02:02:10pm	R081913A.cor	5831.935	2.3	1.6	4422064.798	692951.726
SBW	86-88'	CS4	8/19/2010	02:08:40pm	R081914A.cor	5817.959	2.0	1.3	4422077.670	692900.710
SBW	86-88'	CS4	8/19/2010	02:13:50pm	R081914A.cor	5818.940	2.0	1.3	4422097.362	692905.033
SBW	77'	CB13	8/19/2010	02:23:15pm	R081914B.cor	5811.110	2.0	1.3	4422069.513	692863.270
SBW	77'	CB13	8/19/2010	02:25:35pm	R081914B.cor	5808.168	2.0	1.3	4422055.705	692829.022
SBW	77'	CB14	8/19/2010	03:54:05pm	R081915A.cor	5823.653	2.0	1.6	4422058.146	692811.172
SBW	77'	CB14	8/19/2010	03:56:40pm	R081915A.cor	5826.412	2.0	1.6	4422010.413	692769.676
SBW	77'	CB14,2	8/19/2010	04:16:15pm	R081915B.cor	5810.448	2.6	1.6	4422010.211	692777.597
SBW	77'	CB14,2	8/19/2010	04:18:40pm	R081915B.cor	5810.428	3.3	2.3	4422019.683	692780.056
SBW	~75-80'	NA	8/19/2010	04:06:00pm	R081916A.cor	5819.041	5.6	3.0	4422008.278	692769.023
SBW	~75-80'	NA	8/19/2010	04:21:30pm	R081916B.cor	5815.351	3.9	3.0	4422009.642	692769.262
SBW	~75-80'	NA	8/19/2010	04:25:30pm	R081916B.cor	5823.096	3.3	1.6	4422063.167	692822.888
SBW	77'	CB15	8/19/2010	04:36:55pm	R081916C.cor	5789.725	3.6	1.3	4422067.675	692782.659
SBW	77'	CB15	8/19/2010	04:42:30pm	R081916C.cor	5798.892	3.3	1.3	4422001.260	692774.147
SBW	77'	CB16	8/19/2010	04:51:25pm	R081916D.cor	5779.508	3.3	1.3	4422031.975	692743.748
SBW	77'	CB16	8/19/2010	04:56:45pm	R081916D.cor	5785.982	3.3	1.3	4421989.723	692787.533
SBW	50-60'	NA	8/19/2010	05:02:20pm	R081917A.cor	5767.408	3.9	1.3	4421976.807	692748.585

Location	Footage	SSB ID	Avg. Thickness (ft)	Apparent Width (ft)	Comments	Included in Dataset?
SBW	199-211'	NA	6.5	478.0	Major Body above B-2	N, not completed
SBW	213-215'	NA	3.9	Unk	NA	N, not completed
SBW	Unk	NA	Unk	Unk	NA	N, not completed
SBW	Unk	NA	16.2	427.2	Major Channel Body above Bayhead Delta	N, not completed
SBW	Unk	NA	16.2	427.2	Major Channel Body above Bayhead Delta	N, not completed
SBW	220-225'	DF1	2.3	117.6	NA	Y
SBW	220-225'	DF1	2.3	117.6	NA	Y
SBW	213-214'	CS3	2.3	145.5	NA	Y
SBW	213-214'	CS3	2.3	145.5	NA	Y
SBW	213-217'	DF2	1.0	61.9	Mini-Measured Section, Hand Measured	Y
SBW	215'	CB8	5.0	44.5	Channel Fill, Mini-Measured Section, MS3	Y
SBW	215'	CB8	5.0	44.5	Channel Fill, Mini-Measured Section, MS4	Y
SBW	163-175'	NA	7.8	Unk	Bayhead Delta	N, not completed
SBW	135'	CB18	18.5	377.0	Tidal Point Bar, Mini-Measured Section, MS1	Y
SBW	135'	CB18	18.5	377.0	Tidal Point Bar, Mini-Measured Section, MS2	Y
SBW	Unk	NA	Unk	Unk	Tidal Point Bar	N, not completed
SBW	105'	CB10	6.0	450.7	NA	Y
SBW	105'	CB10	6.0	450.7	NA	Y
SBW	120'	CB19	2.5	324.3	NA	Y
SBW	120'	CB19	2.5	324.3	NA	Y
SBW	110'	CB11	4.9	252.6	Tidal Point Bar	Y
SBW	110'	CB11	4.9	252.6	Tidal Point Bar	Y
SBW	98'	CB12	4.8	181.1	NA	Y
SBW	98'	CB12	4.8	181.1	NA	Y
SBW	86-88'	CS4	1.1	66.2	NA	Y
SBW	86-88'	CS4	1.1	66.2	NA	Y
SBW	77'	CB13	2.8	121.1	Mini-Measured Section, MS8	Y
SBW	77'	CB13	2.8	121.1	Mini-Measured Section, MS8	Y
SBW	77'	CB14	6.6	207.5	Mini-Measured Section, MS9	Y
SBW	77'	CB14	6.6	207.5	Mini-Measured Section, MS10	Y
SBW	77'	CB14,2	2.4	32.1	LAD of CB14, CB14 averaged	N, LAS of CB14
SBW	77'	CB14,2	2.4	32.1	LAD of CB14, CB14 averaged	N, LAS of CB14
SBW	~75-80'	NA	1.8	Unk	LAD of CB14, CB14 averaged	N, LAS of CB14
SBW	~75-80'	NA	1.6	248.5	LAD of CB14, CB14 averaged	N, LAS of CB14
SBW	~75-80'	NA	1.6	248.5	LAD of CB14, CB14 averaged	N, LAS of CB14
SBW	77'	CB15	3.7	219.6	Mini-Measured Section, MS7	Y
SBW	77'	CB15	3.7	219.6	Mini-Measured Section, MS7	Y
SBW	77'	CB16	2.6	199.6	NA	Y
SBW	77'	CB16	2.6	199.6	NA	Y
SBW	50-60'	NA	12.3	Unk	Tidal Point Bar, Mini-Measured Section	N, not completed

Location	Footage	SSB ID	Date	Time	Datafile Name	GPS Elevation (ft)	Vertical Precision (ft)	Horizontal Precision (ft)	Northing	Easting
SBW	65'	CB17	8/19/2010	05:12:45pm	R081917B.cor	5795.993	2.6	1.3	4422058.871	692922.534
SBW	65'	CB17	8/19/2010	05:16:50pm	R081917B.cor	5799.253	2.6	1.3	4422038.041	692975.324
SBW	60-70'	NA	8/19/2010	05:18:45pm	R081917C.cor	5798.981	2.6	1.6	4422039.651	692988.501
SBW	140'	CS7	8/19/2010	05:22:10pm	R081917D.cor	5811.337	2.3	1.3	4422023.977	693026.723
SBW	140'	CS7	8/19/2010	05:23:35pm	R081917D.cor	5809.756	2.6	1.3	4422021.193	693038.231
SBW	60-70'	NA	8/19/2010	05:26:05pm	R081917E.cor	5807.624	2.6	1.3	4422028.057	693075.852

Location	Footage	SSB ID	Avg. Thickness (ft)	Apparent Width (ft)	Comments	Included in Dataset?
SBW	65'	CB17	4.6	186.1	Tidal Point Bar, Mini-Measured Section, MS6	Y
SBW	65'	CB17	4.6	186.1	Tidal Point Bar, Mini-Measured Section, MS6	Y
SBW	60-70'	NA	8.7	Unk	Tidal Point Bar	N, not completed
SBW	140'	CS7	1.5	38.8	NA	Y
SBW	140'	CS7	1.5	38.8	NA	Y
SBW	60-70'	NA	Unk	Unk	NA	N, not completed

Appendix C1 Localities of sandstone-body coordinates (in northing and easting) and their statistics, and comments. SSB ID = Sandstone-body identification number, NA = Not Applicable, Unk = Unknown, LAD = Lateral Accretion Deposit Y = Yes, N = No.

Point Bars (PB)															
Architectural Element and Number	Location, Footage (ft)	Minimum Thickness (ft)	Maximum Thickness (ft)	Average Thickness (ft)	T1	T2	T3	T4	T5	T6	T7	T8	T9	T10	T11
CB1	VDS, 16'	1.0	3.5	2.3	3.5	2.3	1.0								
CB2	VDS, 42'	2.3	7.8	5.7	5.2	6.3	7.1	7.8	2.3						
CB3	VDS, 67'	1.0	1.0	1.0	1.0										
CB4	VDS, 76'	4.8	11.0	7.7	9.0	6.1	5.5	4.8	11.0	7.8	9.4				
CB5	VDS, 82'	2.1	3.7	2.7	2.1	3.7	2.4								
CB6	VDS, 87'	1.0	5.0	2.3	1.0	2.4	2.3	1.0	5.0						
CB7	VDS, 87'	3.0	3.0	3.0	3.0										
CB8	SBW, 215'	5.0	5.0	5.0	5.0										
CB9	SBW, 216'	3.6	7.4	5.0	4.1	7.4	3.6								
CB10	SBW, 105'	4.3	9.0	6.0	5.5	4.8	7.3	5.1	7.5	9.0	5.4	5.2	4.3		
CB11	SBW, 110'	4.1	5.4	4.9	4.1	5.2	4.8	5.4							
CB12	SBW, 98'	3.2	8.0	4.8	3.2	8.0	3.2								
CB13	SBW, 77'	2.1	3.6	2.8	3.6	2.8	2.1								
CB14	SBW, 77'	5.4	13.0	8.6	11.1	8.5	13.0	8.2	7.0	7.1	5.4				
CB15	SBW, 77'	3.0	4.3	3.7	3.0	4.3									
CB16	SBW, 77'	1.0	2.9	2.6	2.9	3.9	1.0								
CB17	SBW, 65'	2.6	7.3	4.6	3.9	7.3	6.5	2.7	2.6						
CB18	SBW, 135'	4.6	30.0	18.5	4.6	9.3	21.7	27.0	30.0						
CB19	SBW, 120'	2.5	2.5	2.5	2.5										
CB20	SBE, 121'	2.5	2.5	2.5	2.5										
CB21	VDW, 55'	3.2	8.4	6.1	3.2	6.7	8.4								
CB22	VDW, 75'	5.1	14.0	8.1	6.2	5.8	9.7	14.0	9.8	7.1	9.4	5.1	6.6	9.2	6.1
CB23	SBE, 125'	3.0	3.0	3.0	3.0										
CB24	SBS, 360'	3.7	5.4	4.4	4.0	4.0	3.7	5.0	5.4						
Totals	-	3.0	6.9	4.9											
Crevasse Splays (CS)															
Architectural Element and Number	Location, Footage (ft)	Minimum Thickness (ft)	Maximum Thickness (ft)	Average Thickness (ft)	T1	T2	T3	T4	T5	T6	T7	T8	T9		
CS1	VDS, 32'	2.5	2.5	2.5	2.5										
CS2	VDS, 55-57'	1.5	1.5	1.5	1.5										
CS3	SBW, 213-214'	1.0	4.5	2.3	3.2	3.0	1.0	1.0	1.0	4.5					
CS4	SBW, 86-88'	1.1	1.1	1.1	1.1										
CS5	SBW, 80'	1.0	1.0	1.0	1.0										
CS6	SBW, 96-100'	1.5	1.5	1.5	1.5										

Point Bars					
Architectural Element and Number	Location, Footage (ft)	Standard Deviation	Number of Measurements (Thickness)	Width (ft)	Width/Thickness Ratio
CB1	VDS, 16'	1.3	3	196.8	85.6
CB2	VDS, 42'	2.2	5	487.0	85.4
CB3	VDS, 67'	0.0	1	266.7	266.7
CB4	VDS, 76'	2.3	7	685.1	89.0
CB5	VDS, 82'	0.9	3	40.4	15.0
CB6	VDS, 87'	1.6	5	249.5	108.5
CB7	VDS, 87'	0.0	1	60.4	20.1
CB8	SBW, 215'	0.0	1	44.5	8.9
CB9	SBW, 216'	2.1	3	1048.1	209.6
CB10	SBW, 105'	1.6	9	450.7	75.1
CB11	SBW, 110'	0.6	4	252.6	51.6
CB12	SBW, 98'	2.8	3	181.1	37.7
CB13	SBW, 77'	0.8	3	121.1	43.3
CB14	SBW, 77'	2.6	7	228.0	26.5
CB15	SBW, 77'	0.9	2	219.6	59.4
CB16	SBW, 77'	1.5	3	199.6	76.8
CB17	SBW, 65'	2.2	5	186.1	40.5
CB18	SBW, 135'	11.1	5	377.0	20.4
CB19	SBW, 120'	0.0	1	324.3	129.7
CB20	SBE, 121'	0.0	1	134.0	53.6
CB21	VDW, 55'	2.7	3	123.3	20.2
CB22	VDW, 75'	2.6	11	812.0	100.2
CB23	SBE, 125'	0.0	1	132.0	44.0
CB24	SBS, 360'	0.7	5	83.0	18.9
Totals	-	1.7	92	287.6	72.5
Crevasse Splays					
Architectural Element and Number	Location, Footage (ft)	Standard Deviation	Number of Measurements (Thickness)	Width (ft)	Width/Thickness Ratio
CS1	VDS, 32'	0.0	1	48.0	19.2
CS2	VDS, 55-57'	0.0	1	30.0	20.0
CS3	SBW, 213-214'	1.5	6	145.5	63.3
CS4	SBW, 86-88'	0.0	1	66.2	60.2
CS5	SBW, 80'	0.0	1	55.0	55.0
CS6	SBW, 96-100'	0.0	1	43.1	28.7

CS7	SBW, 140'	1.5	1.5	1.5	1.5										
CS8	VDW, 50-60'	2.7	3.1	3.1	2.7	3.5	3.1	2.8	3.5						
CS9	VDW, 80-90'	2.0	2.0	2.0	2.0										
Totals	-	1.6	2.1	1.8											
Discrete Flood Body (DF)															
Architectural Element and Number	Location, Footage (ft)	Minimum Thickness (ft)	Maximum Thickness (ft)	Average Thickness (ft)	T1	T2	T3	T4	T5	T6	T7	T8	T9		
DF1	SBW, 220-225'	1.4	3.1	2.3	1.4	3.9									
DF2	SBW, 213-217	1.0	1.0	1.0	1.0										
DF3	SBE, 223-225	1.5	1.5	1.5	1.5										
DF4	VDW, 10'	1.0	1.0	1.0	1.0										
DF5	VDW, 0'	1.5	1.5	1.5	1.5										
DF6	SBS, 351-353'	1.4	3.4	2.6	3.0	3.4	2.5	1.4							
Totals	-	1.3	1.9	1.7											

CS7	SBW, 140'	0.0	1	38.8	25.9
CS8	VDW, 50-60'	0.4	5	347.4	112.1
CS9	VDW, 80-90'	0.0	1	40.6	20.3
Totals	-	0.2	18	90.5	45.0
Discrete Flood Bodies					
Architectural Element and Number	Location, Footage (ft)	Standard Deviation	Number of Thickness measurements	Width (ft)	Width/Thickness Ratio
DF1	SBW, 220-225'	1.8	2	117.6	51.1
DF2	SBW, 213-217	0.0	1	61.9	61.9
DF3	SBE, 223-225	0.0	1	29.0	19.3
DF4	VDW, 10'	0.0	1	56.0	56.0
DF5	VDW, 0'	0.0	1	20.0	13.3
DF6	SBS, 351-353'	0.9	4	84.6	32.5
Totals	-	0.4	10	61.5	39.0

Appendix C2 Measurement data for each of the architectural elements. T1-T11 are thickness measurements taken for each architectural element.

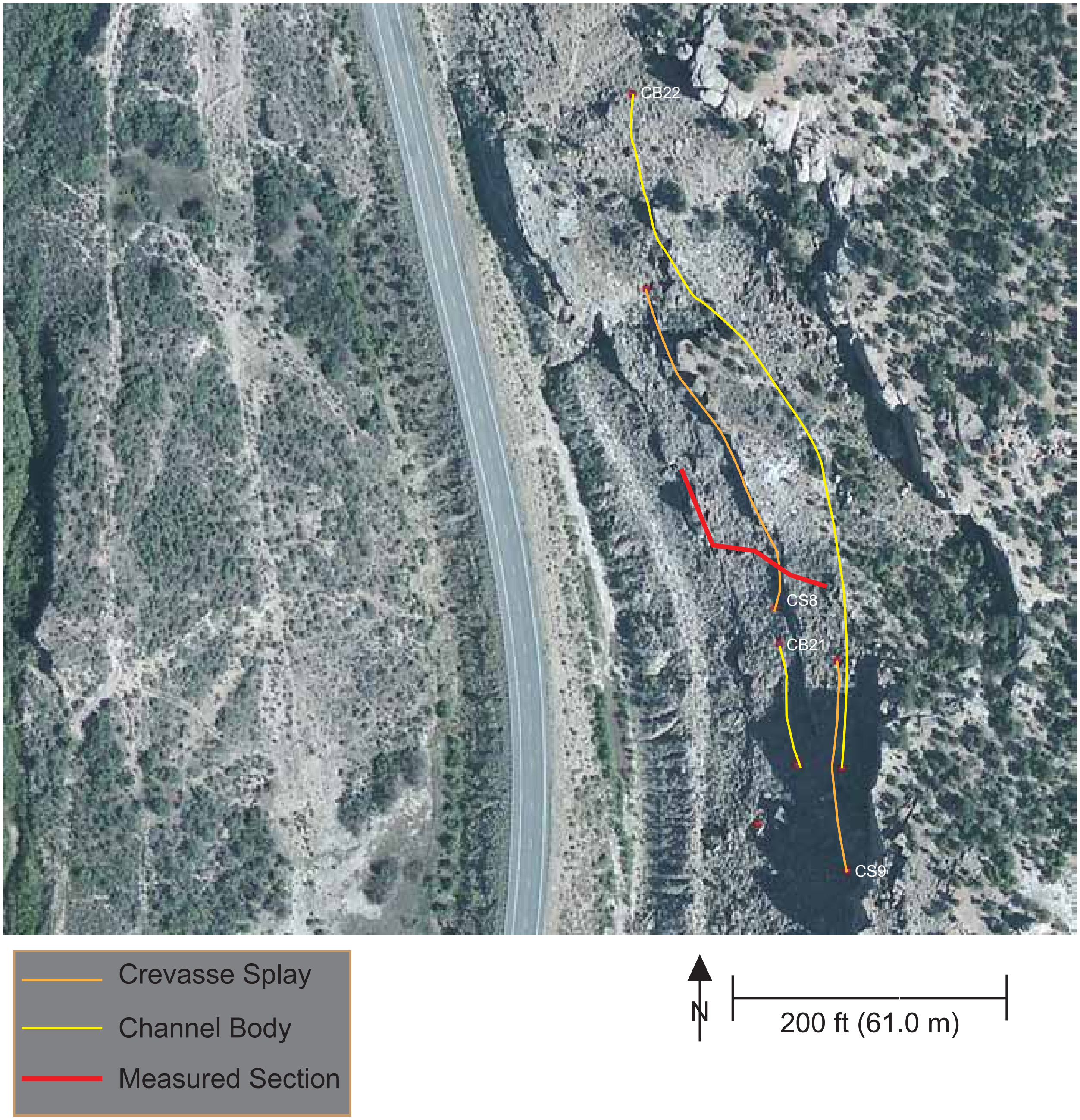

Appendix C3 Sandstone-body traces on the Vandamore Draw West measured section (red line) for crevasse splays (CS) 8-9, and channel bodies (CB) 21-22. Red dots show global positioning system (GPS) coordinates. Some GPS coordinates are not traced due to lateral extent. Discrete flood bodies 4-5 are not mapped using GPS, only hand measured, therefore, not shown in this diagram (see Appendix C1 for more information).

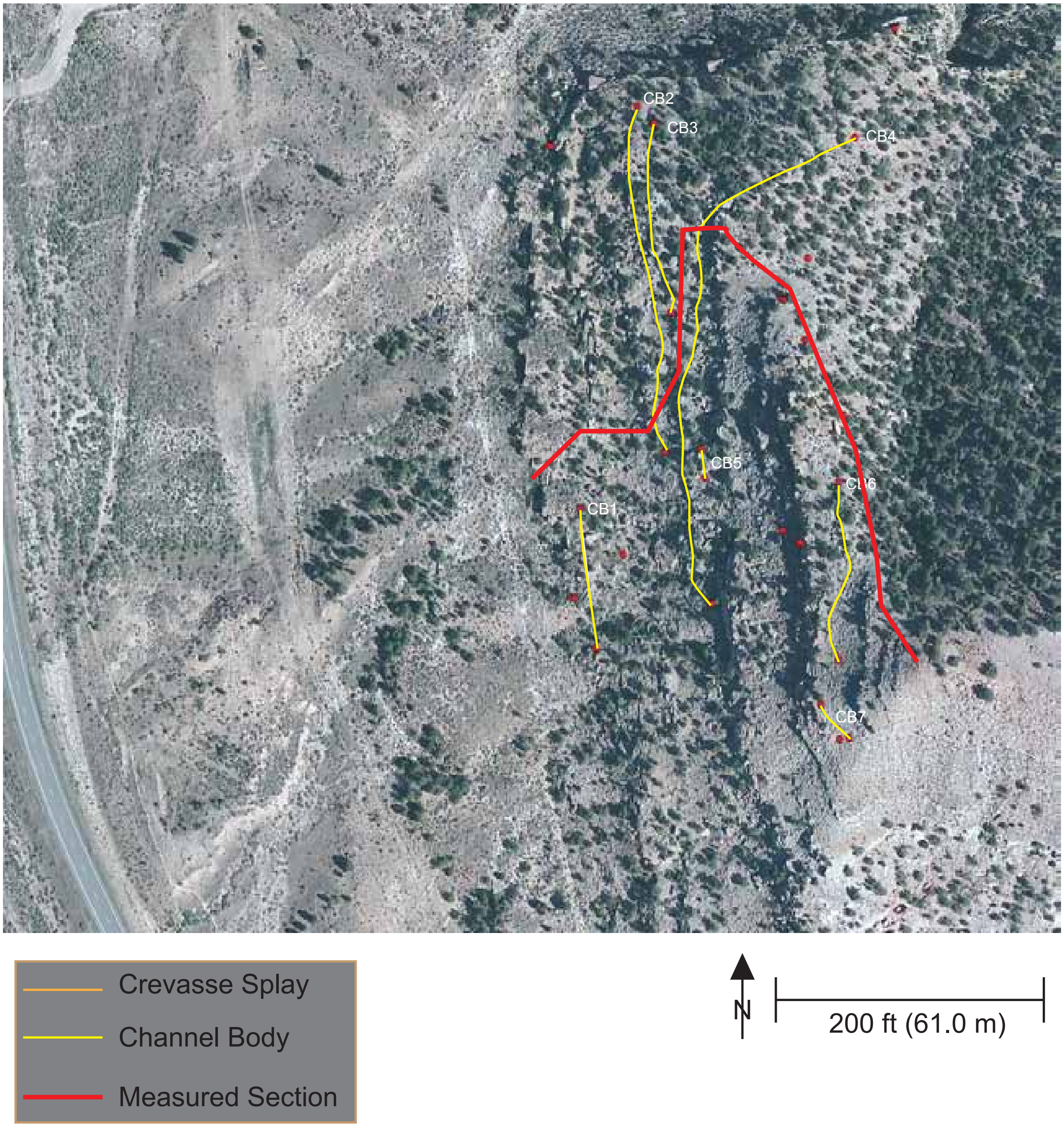

Appendix C3 Sandstone-body traces on the Vandamore Draw South measured section (red line) for channel bodies (CB) 1-7. Red dots show global positioning system (GPS) coordinates. Some GPS coordinates are not traced due to lateral extent. Crevasse splays 1-2 are not mapped using GPS, only hand measured, therefore, not shown in this diagram (see Appendix C1 for more information).

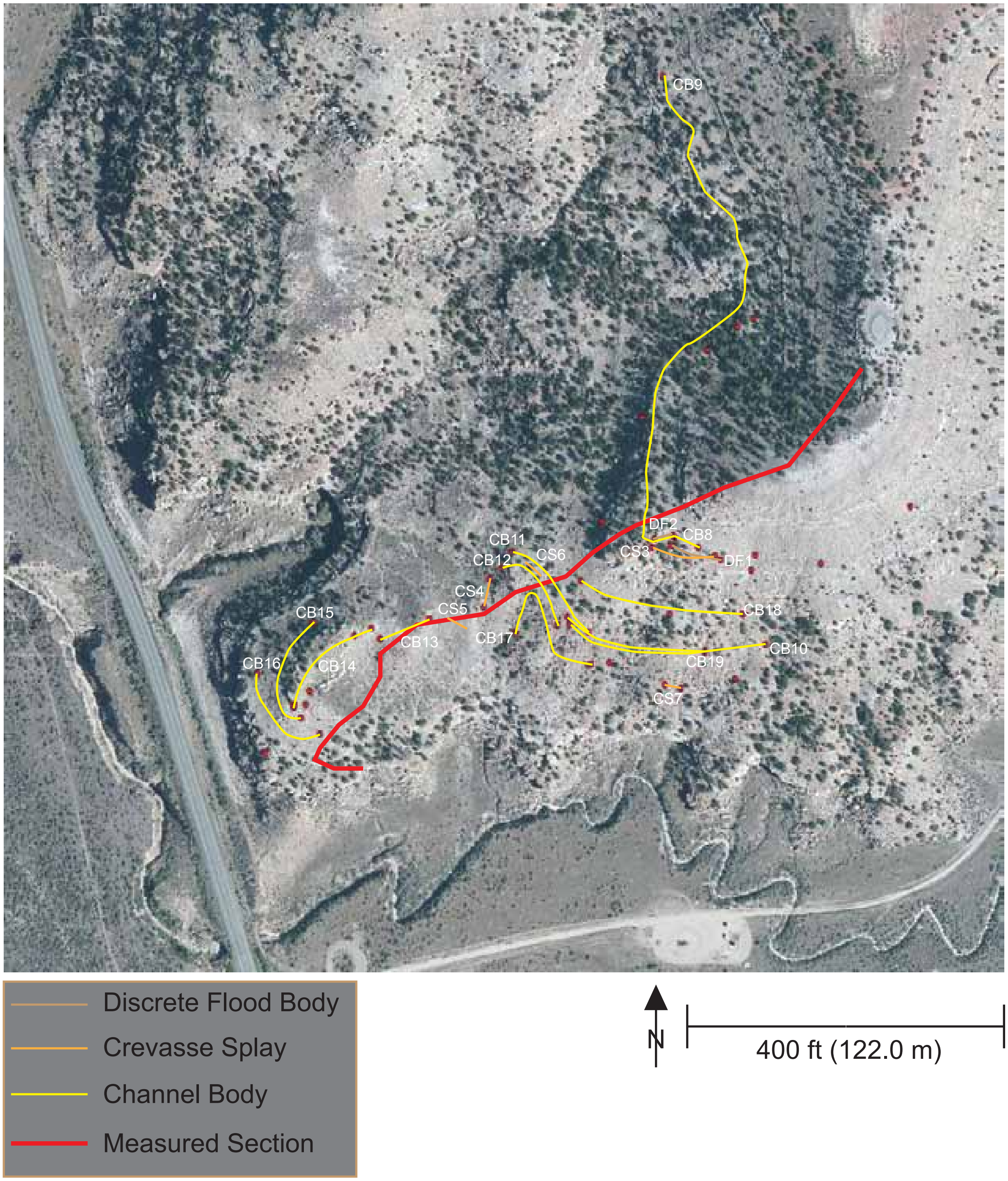

Appendix C3 Sandstone-body traces on the State Bridge Draw West measured section (red line) for discrete flood bodies (DF) 1-2, crevasse splays (CS) 3-7, and channel bodies (CB) 8-19. Red dots show global positioning system (GPS) coordinates. Some GPScoordinates are not traced due to lateral extent (see Appendix C1 for information).

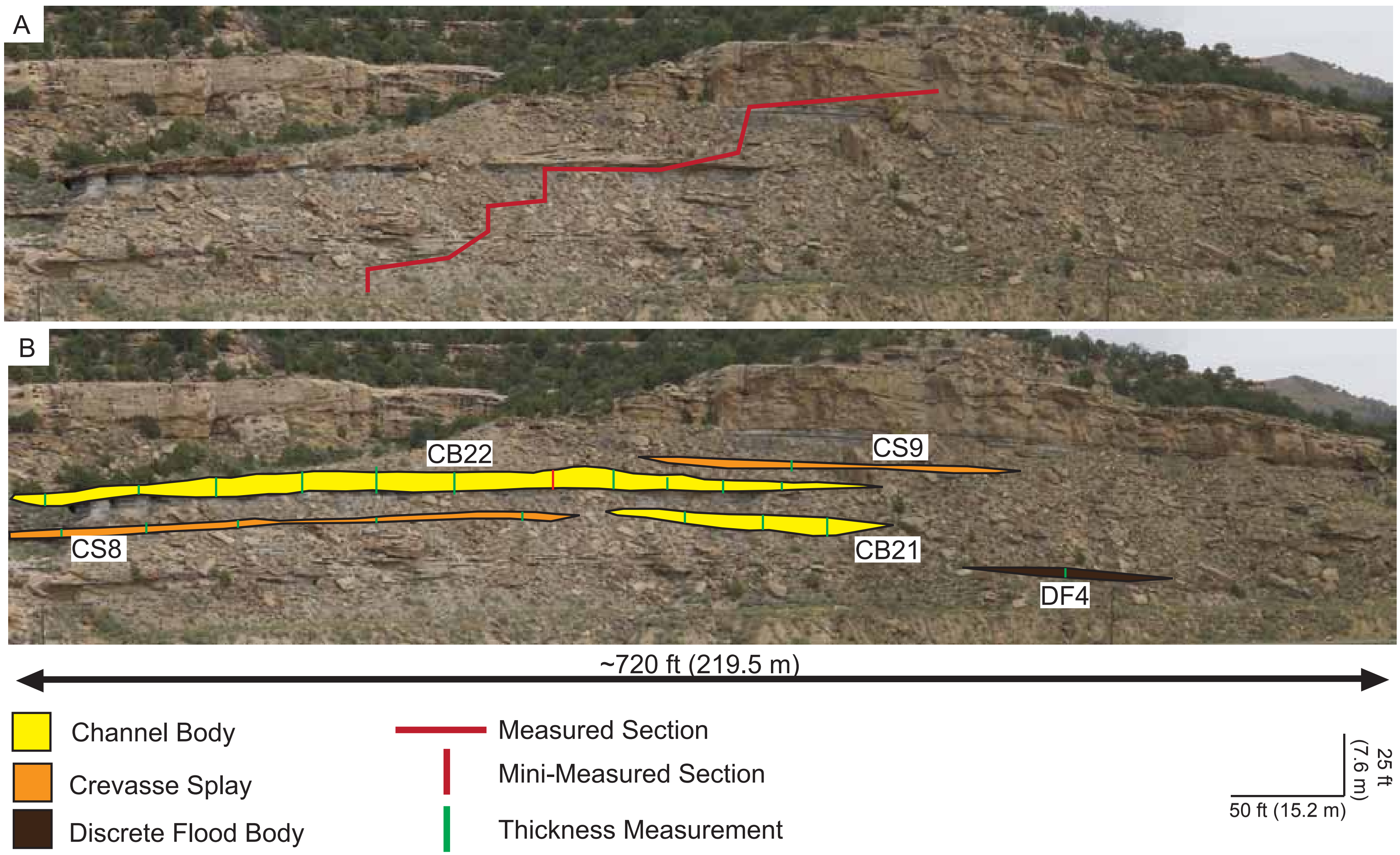

Appendix C Photopan of the Vandamore Draw West Measured Section (on red line) (Appendix A3). B) Interpred sandstone-body traces on the for crevasse splays (CS) 8-9, and channel bodies (CB) 21-22 and discrete flood body (DF) 4. Thickness and paleocurrent meaurements are shown on the green lines, and mini-measured sections are shown on the red lines, see Appendix A4 for more information. Discrete flood body 5 is not shown on this photopan.

Appendix C4 Photopan of the Vandamore Draw South Measured Section (on red line) (Appendix A3). B) Interpreted sandstone-body traces for channel bodies (CB) 1-6. Locations where thicknesses and paleocurrents were measured are shown on the green lines, and mini-measured sections (Appendix A4) are shown on the red lines. Channel body (CB) 7 is not visible on the photopan (it is to the south of the pan). Crevasse Splays (CS) 1-2 are not shown.

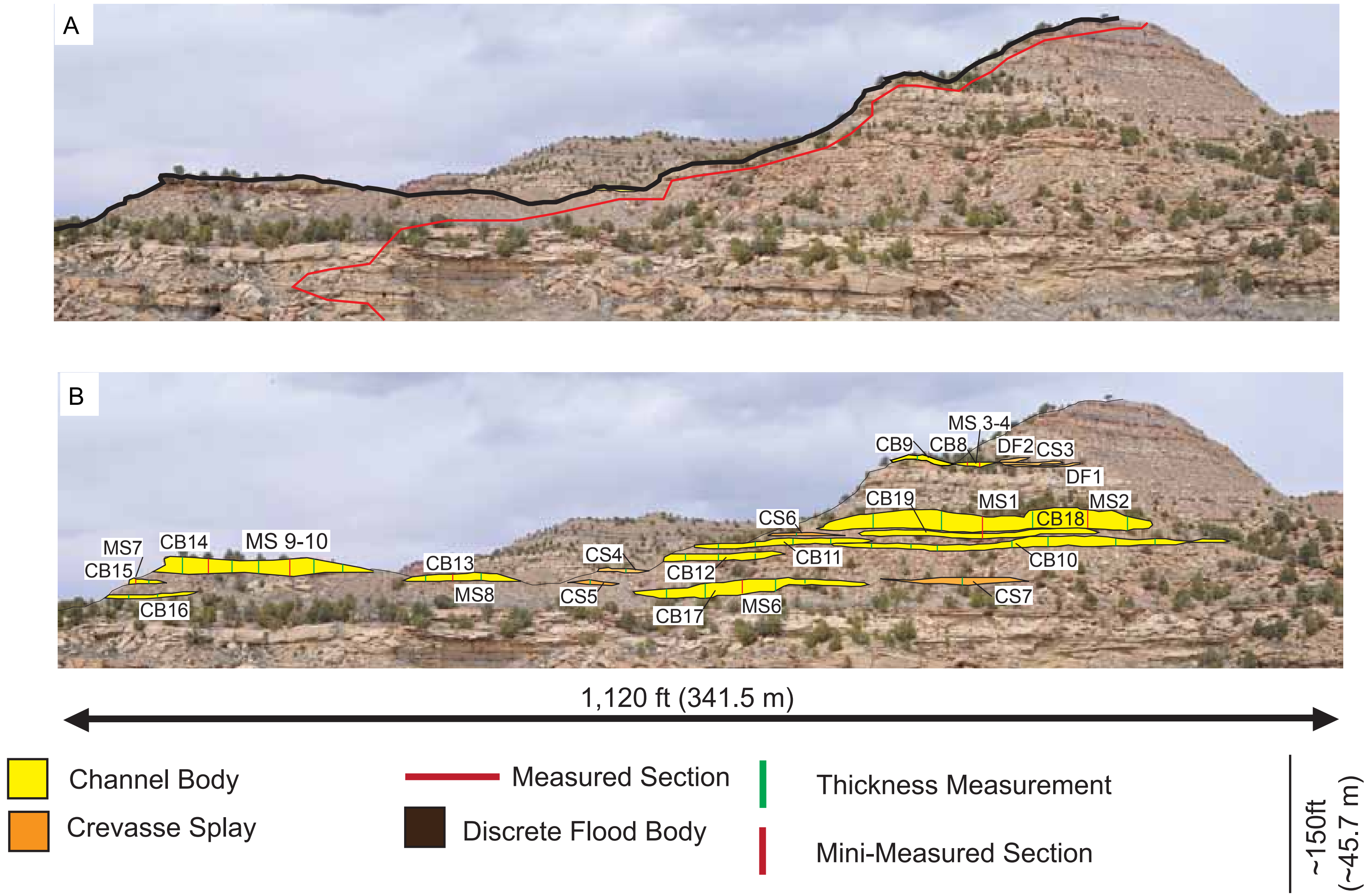

Appendix C4 Photopan of the State Bridge Draw West Measured Section (on red line) (Appendix A3). B) Interpreted sandstone-body traces for crevasse splays (CS) 3-7, and channel bodies (CB) 10-19 and discrete flood bodies (DF) 1-2. Thickness and paleocurrent meaurements are shown on the green lines, and mini-measured sections are shown on the red lines, see Appendix A4 for more information.

APPENDIX D

1. **Paleocurrent Data key**
2. **Paleocurrent Data for Measured Sections**

Paleocurrent Information

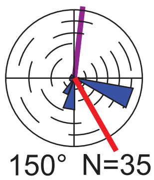

Rose Diagram (in upper right hand corner of all maps). Red line: average paleocurrent orientation. Purple line: vector mean of paleocurrent orientation of inclined heterolithic strata. “150°”: vector mean paleocurrent orientation. “N=35”: number of measurements.

Appendix D1 Paleocurrent rose-diagram key.

Philadelphia Creek East													
Architectural Element		**Paleocurrent Readings**											
	Footage	1	2	3	4	5	6	7	8	9	10	11	12
Crevasse Splay													
	3-10'	110	230	255	240	220							
	22-26'	130	160										
	315'	220											
Channel Body													
	8-15'	150	130										
	55-64'	225	170	120	260	260	270	350					
	44-54'	20	105	130	130	160							
	72-120'	300	260	205	85	345	40	215	160	340	250	150	220
	276-298'	260	140	135	160	300	170	190	50	320	40	260	335
	276-298' (2)	15	295	320	320	45							
	339-350'	60	60	20	0	280	330	45					
Bayhead Delta													
	35-45'	280	360										
Middle Shoreface													
	125-135'	350											
	140-145'	200											
Tidal Barform													
	210-220'	260	235	265	240	190							

Asymmetrical Ripples (Sra)
Bidirectional Ripples (Srb)
Lateral Accretion Surfaces
Planar Cross Stratification (Slp)
Measurement on a Log
Trough Cross Stratification (Slt)
Swaley Cross Stratification (Sls)

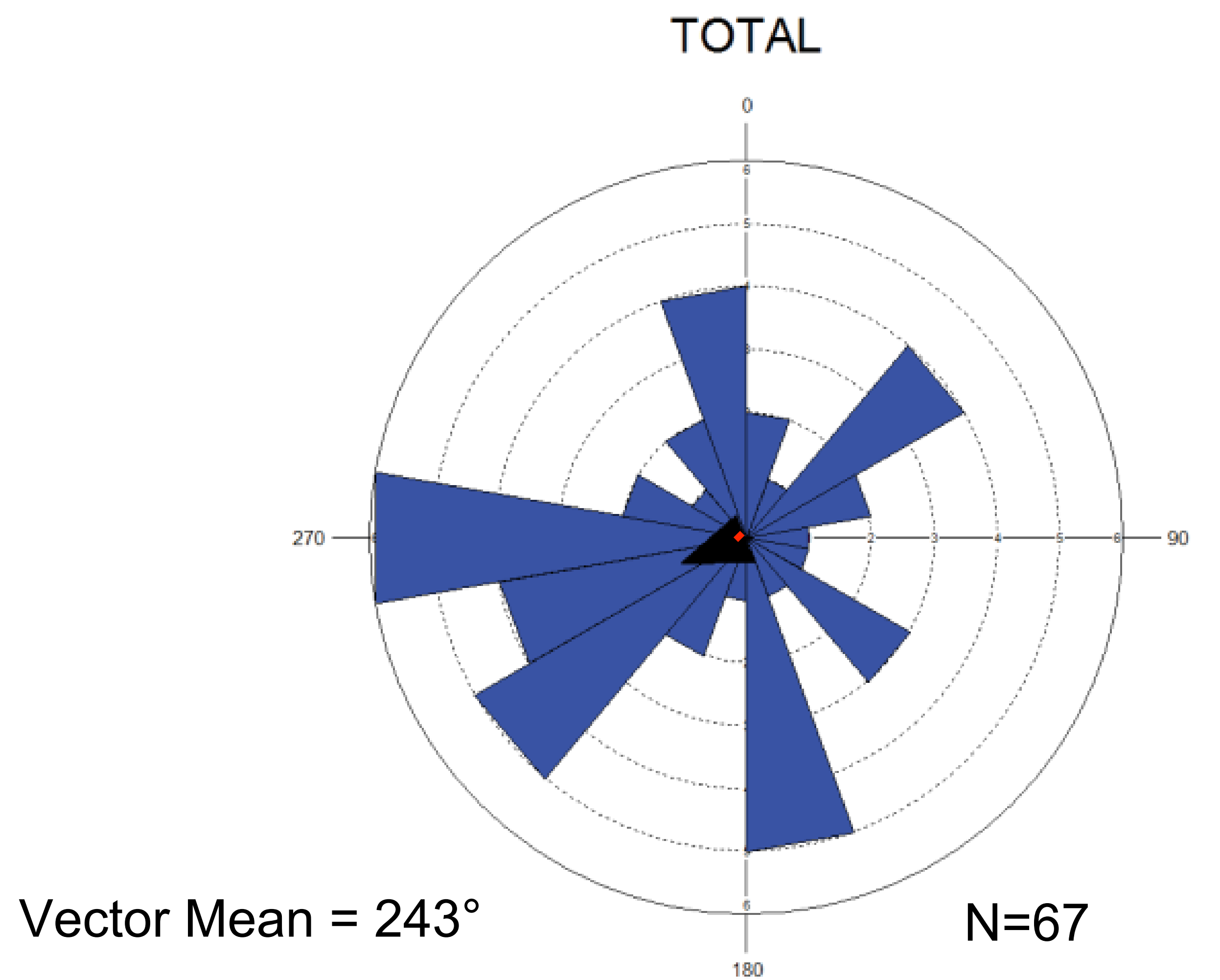

Appendix D2 Paleocurrent data for Philadelphia Creek East grouped by architectural element. Colors represent type of sedimentary structure from which paleocurrent was measured. Rose diagram shows the average paleocurrent orientation for PCE based on 67 measurements.

Philadelphia Creek West									
Architectural Element		Paleocurrent Readings							
	Footage	1	2	3	4	5	6	7	8
Crevasse Splay									
	15-20'	125	150	150					
	265-272'	145	140	140					
	354-355'	270							
Channel Body									
	50-60'	5	45	60					
	123-130'	10	305	220	190				
	170-175'	95	150						
	186-205	315	330	325	320	340	295	295	
	344-352'	160	130						
	370-380'	285	270	290	350	350	280	310	270
	380-390'	130	160	120					
Bayhead Delta									
	165'	345							
Estuarine Assemblage									
	210-225'	295	295	295	300	295			
Foreshore									
	280-285'	95	330	135	350	350			

Asymmetrical Ripples (Sra)
Bidirectional Ripples (Srb)
Trough Cross Stratification (Slt)
Planar Cross Stratification (Slp)
Measurement on a Log
Symmetrical Ripples (Srs)

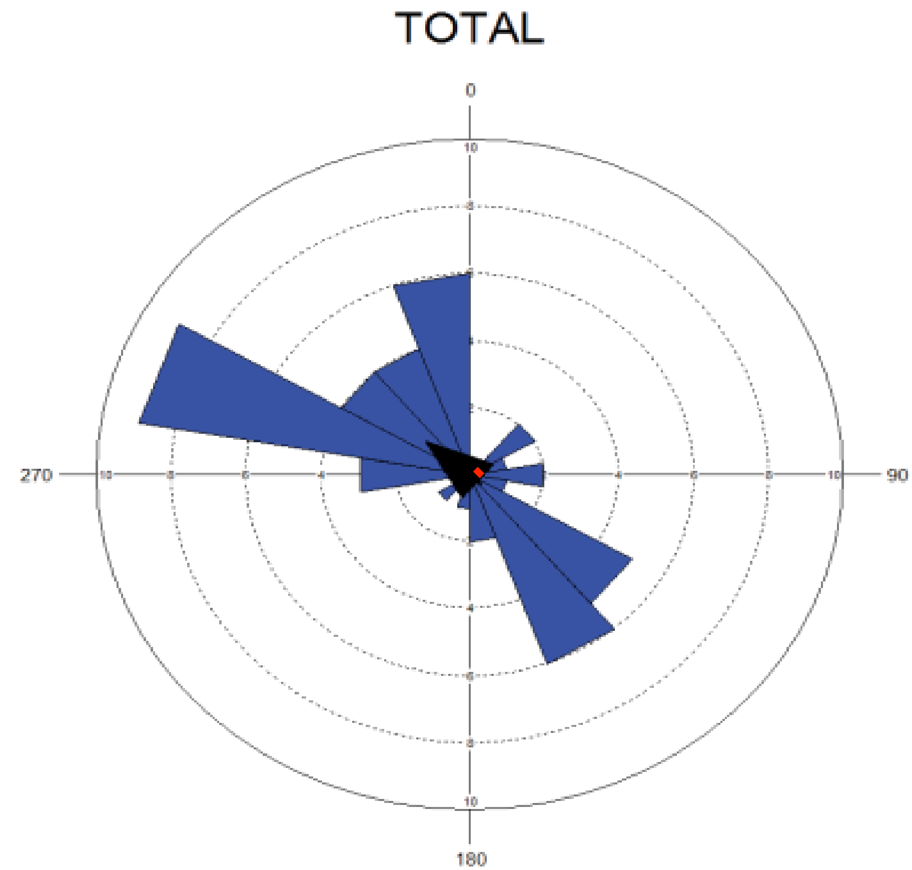

Vector Mean = 312°

N=47

Appendix D2 Paleocurrent data for Philadelphia Creek West grouped by architectural element. Colors represent type of sedimentary structure from which paleocurrent was measured. Rose diagram to right shows the average paleocurrent orientation for PCW, based on 47 measurements.

Vandamore Draw South										
Architectural Element		**Paleocurrent Readings**								
SSB#	**Footage**	1	2	3	4	5	6	7	8	9
Crevasse Splay										
	205-209'	305	325	315						
Channel Body										
CB1	~10-14'	180	190							
	17-29'	355	280	240	280	275	290			
CB2	39-46'	155	140	220	225	110	165			
CB4	72-80'	100	120	100	200	235	135	25	150	180
CB5	~82-83'	315								
	102-115'	130	180	190	105	115				
	164-190'	340	330	280	290	100	290	0		
	243-248'	205	195	200	215	240				
Estuarine Assemblage										
	222-230'	120	105	175	170	120				
Foreshore										
	250-257'	110	235	145	135	205	195			

Asymmetrical Ripples (Sra)
Trough Cross Stratification (Slt)
Planar Cross Stratification (Slp)

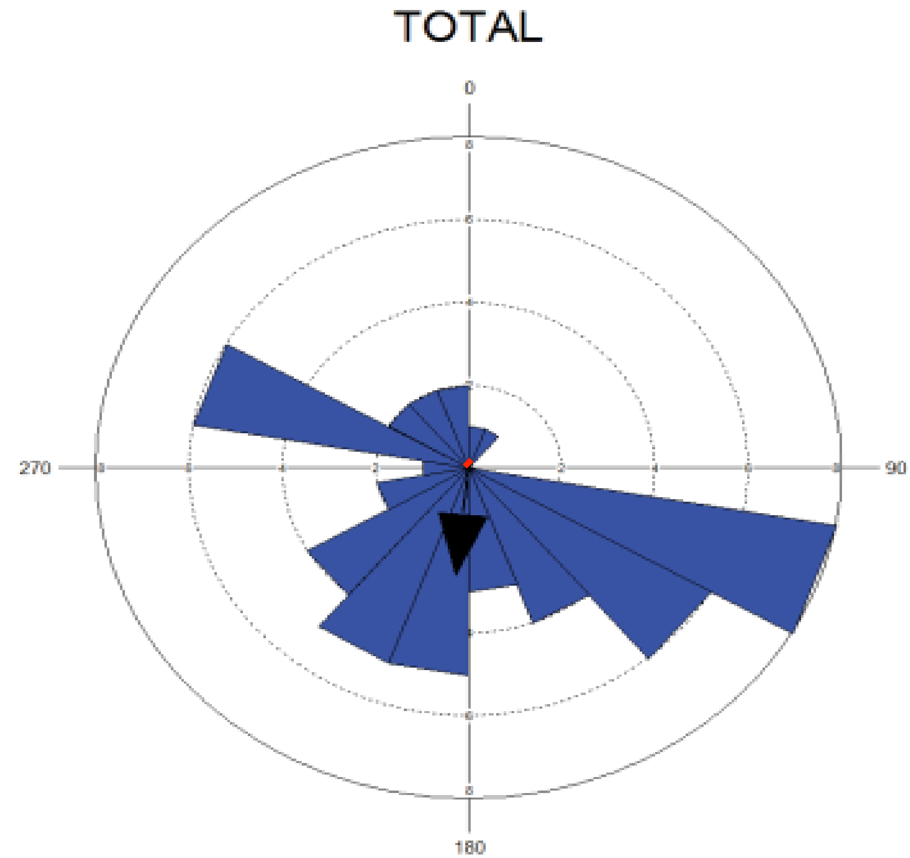

Vector Mean = 186°

N=55

Appendix D2 Paleocurrent data for Vandamore Draw South grouped by architectural element. Colors represent type of sedimentary structure from which paleocurrent was measured. Footages that are shown as approximate (~) are off section. Rose diagram to right shows average paleocurrent orientation based on 55 measurements.

Vandamore Draw North															
Architectural Element	Paleocurrent Readings														
Footage	1	2	3	4	5	6	7	8	9	10	11	12	13	14	15
Crevasse Splay															
145-146'	320														
185-187'	130														
212-218'	280	295	325	0	130	285									
Discrete Flood Body															
215'	40														
Channel Body															
10-15'	55	25													
25-35	335	260	350	240	50										
45-65'	210	95	95	200	30	20	280	340							
73-85'	150	200	100	290	280	40	190	280	20	30	0	30	30	195	
98-101'	75	315	150												
112-122'	45	285	350	280	350	155	170	215	80						
127-139'	20	50	10												
164-175'	325	305	295	285	285	315	60	60							
325-335'	315	310													
345-350'	30	30	60	55	50	30	60	40	65	75	60	10	35		
355-360'	330	340	310	240	250	230	115	100							
Bayhead Delta															
153-155'	230	100													
Estuarine Assemblage															
190-200'	190	240	230	290	220	60	220	60	280						
200-205'	300	200	80	80	80										
Foreshore															
220-225'	80														
230-235'	110														
245-250'	45	300													
Tidal Barform															
285-295'	310	315	260	260	330	30	80	300	100	210	310	290	310	115	325
327-332'	315	310													

Asymmetrical Ripples (Sra)
Lateral Accretion Surfaces
Planar Cross Stratification (Slp)
Measurement on a Log
Trough Cross Stratification (Slt)
Bidirectional Ripples (Srb)

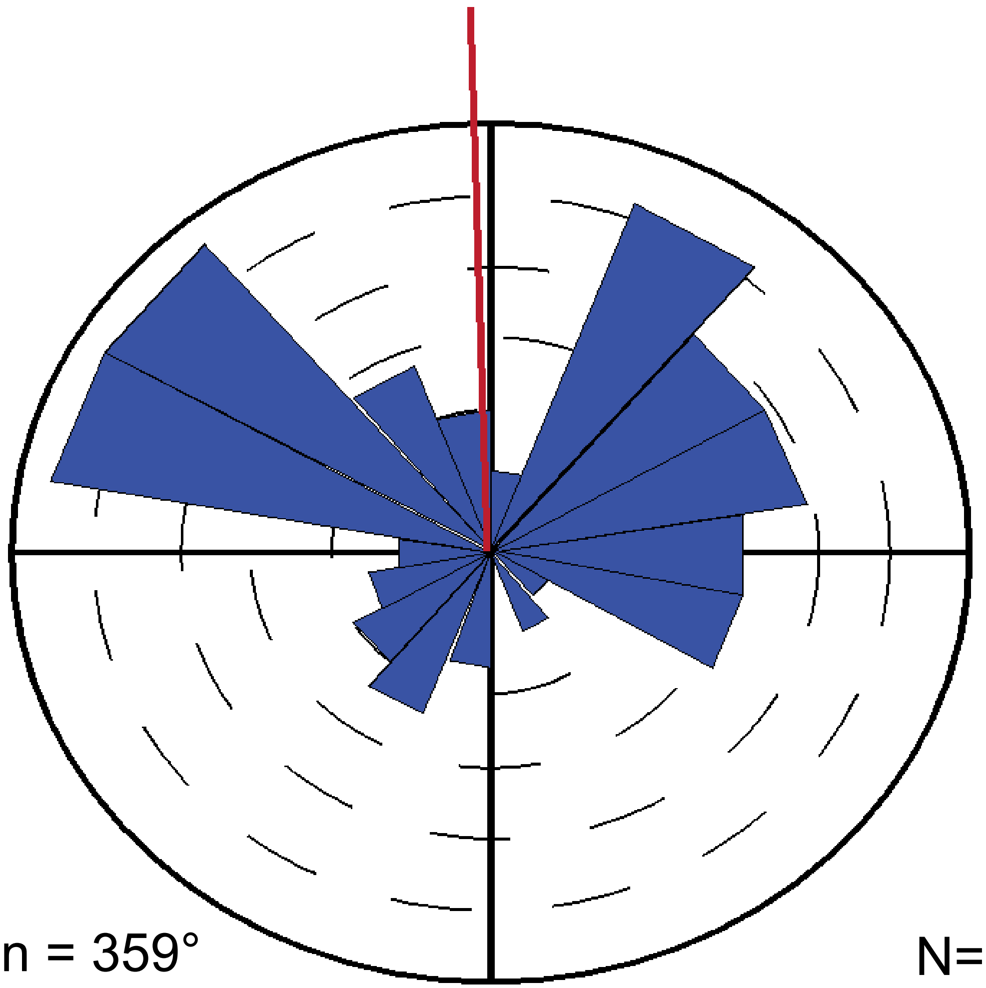

Appendix D2 Paleocurrent data for Vandamore Draw North grouped by architectural element. Colors represent type of sedimentary structure from which paleocurrent was measured. Rose diagram shows the average paleocurrent direction based on 121 measurements.

Vandamore Draw West									
Architectural Element		**Paleocurrent Readings**							
SSB#	**Footage**	1	2	3	4	5	6	7	8
Crevasse Splay									
CS8	47-53'	110	100	190					
Discrete Flood Body									
DF4	~9-12'	300	100	110					
Channel Body									
	21-27'	190	100	205	100	200	200	180	285
CB21	65-75'	100							
CB22	81-87'	195	105	150	240	180	200	180	190
CB22	81-87' (2)	95	130	100	115	160			

Asymmetrical Ripples (Sra)

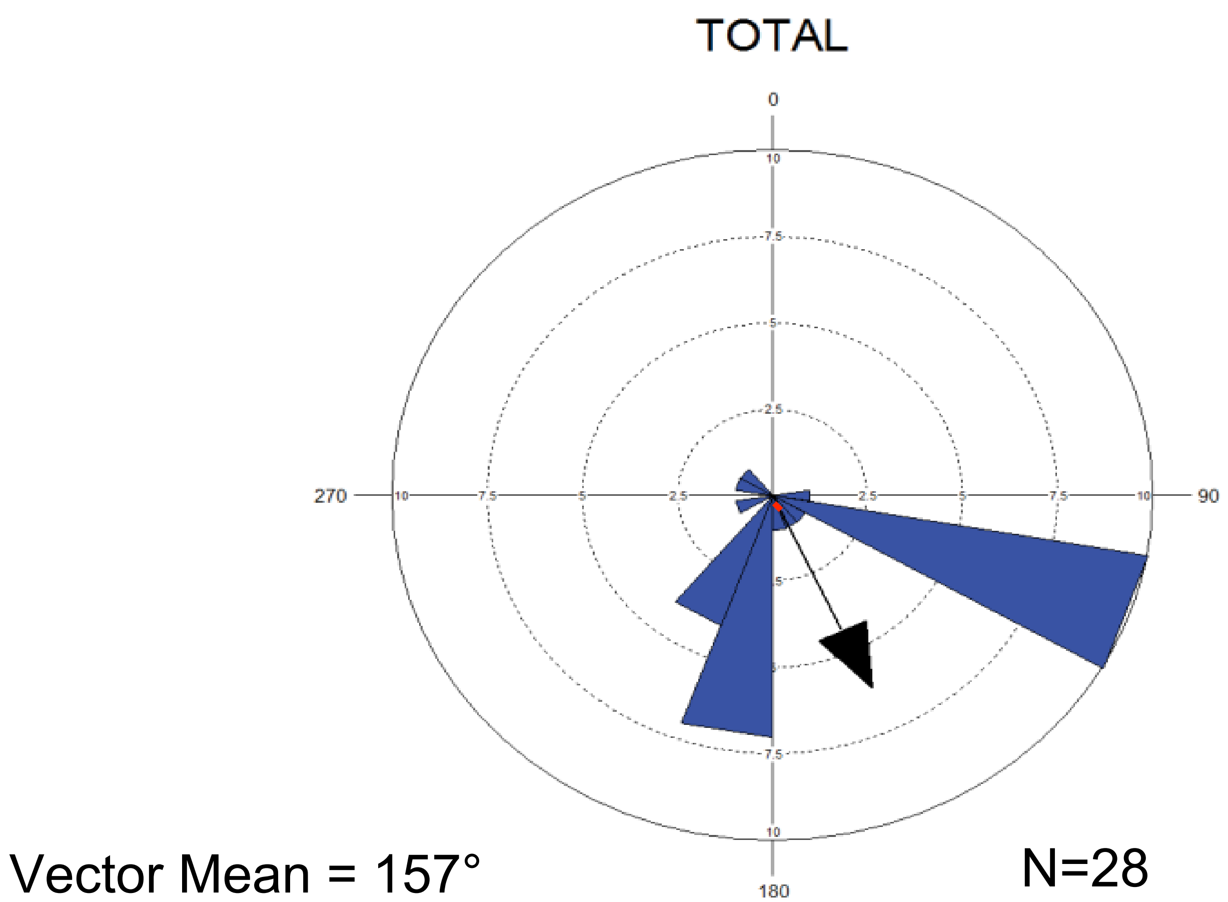

Appendix D2 Paleocurrent data for Vandamore Draw West grouped by architectural element. Colors represent type of sedimentary structure from which paleocurrent was measured. Footages which are approximate (~) are not on main measured section path. Twenty-eight total paleocurrents taken, and shown on the rose diagram.

State Bridge Draw South									
Architectural Element		**Paleocurrent Readings**							
SSB#	**Footage**	1	2	3	4	5	6	7	8
Discrete Flood Body									
	215'	40							
Channel Body									
	23-30'	235	105	110	100				
	33-55'	30	40	90					
	95-97'	120	260						
	106-114'	100	10	140	10	280	115	150	320
	115-120'	100	120	120					
	125-131'	310	290						
	164-171'	215	135	100	120				
	240-253'	45	35	40	30	120			
CB24	360-365'	70	60						
Bayhead Delta									
	144-150'	150	330						
Estuarine Assemblage									
	195-200'	330							
	200-206'	120	120	110	105				
Lower Shoreface									
	285-295'	240	260	280					
Tidal Barform									
	306-309'	0							
	316-320'	65	320						
	322-324'	30							

Asymmetrical Ripples (Sra)
Bidirectional Ripples (Srb)
Lateral Accretion Surfaces
Planar Cross Stratification (Slp)
Trough Cross Stratification (Slt)
Swaley Cross Stratification (Sls)

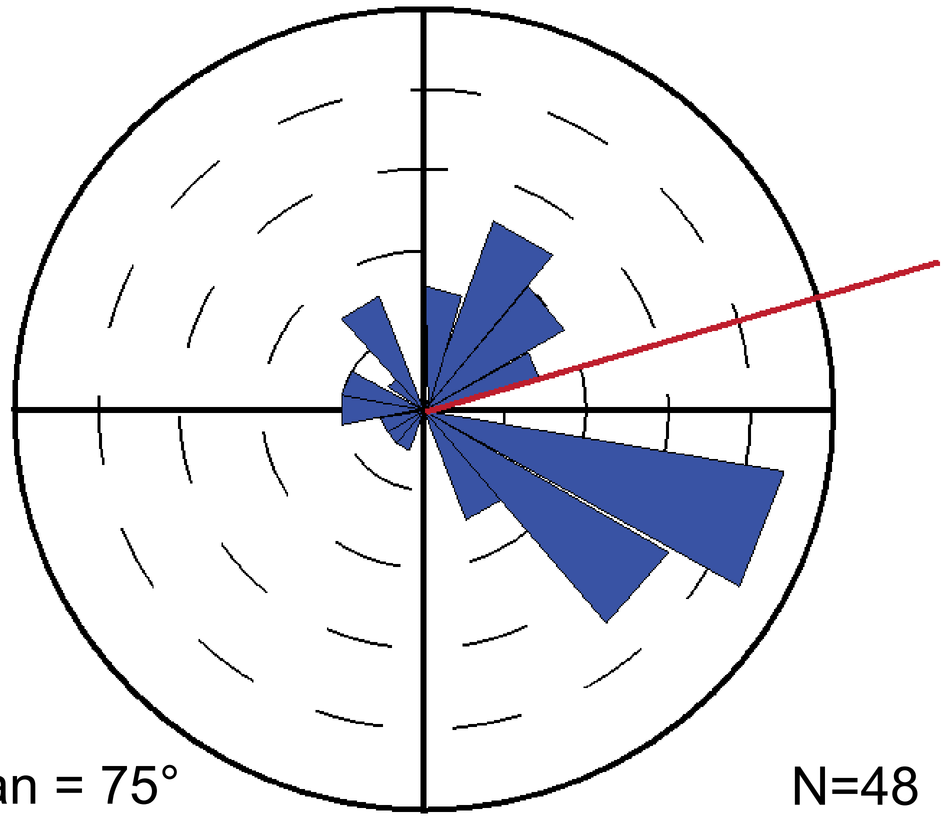

Appendix D2 Paleocurrent data for State Bridge Draw South grouped by architectural element. Colors represent type of sedimentary structure from which paleocurrent was measured. Rose diagram shows the average paleocurrent orientation for SBS based on 48 measurements.

State Bridge Draw West

Architectural Element		Paleocurrent Readings													
SSB#	**Footage**	1	2	3	4	5	6	7	8	9	10	11	12	13	14
Crevasse Splay															
	20-25'	170	170	170	170	175	175	140	145	90					
CS4	83-88'	200	140	180											
CS3	213-214'	110	180												
Discrete Flood Body															
DF2	~213-217'	100	140												
Channel Body															
	9-18'	40	40	70											
	37-46'	35	45												
	50-60'	140	145	160	130	145	115	135	100	50	160	140	90	80	160
	50-60' (2)	110	290	145	155	170	220	340							
CB16	~65-70'	150	135												
CB17	~60-70'	200	120	340											
	~60-70'	150	110	180	10	290	310	230							
	~60-70'	110	180												
CB15	~70-75'	100	110	120	180										
CB13	~75-80'	230	110	240	100										
CB14	~75-80'	350	210	270	330	350	210	300							
CB12	96-100'	130	265	320											
CB10	109-112'	160	70	90	155	150									
CB11	108-113'	130	165	155	160	130	135	155	115	140	150	125			
	118-130'	170													
CB18	135'	145	155												
	180-194'	260	50	30	35	190	190	185							
	200-211'	255	225	230	240	215	210	220	220	310	230	235	250	220	
CB9	214-216'	135	150												
	240-252'	230	350	250	230	265									
	275-280'	100	105	40	240	80									
Bayhead Delta															
	165-175'	65	135	105	60	210	190	150	220						
Estuarine Assemblage															
	230-240'	330	200	200	340	110									

Asymmetrical Ripples (Sra)
Bidirectional Ripples (Srb)
Planar Cross Stratification (Slp)
Lateral Accretion Surfaces
Trough Cross Stratification (Slt)

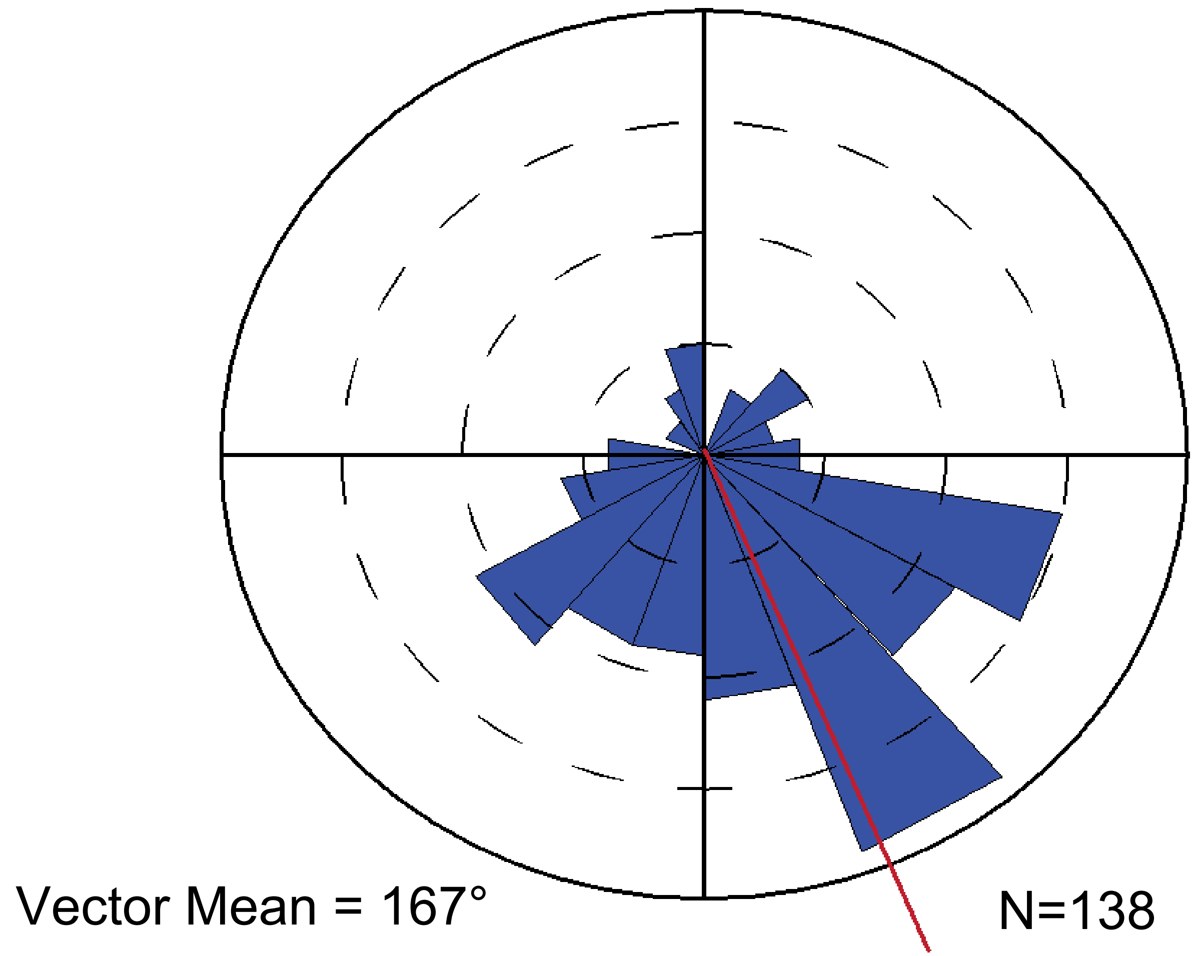

Appendix D2 Paleocurrent data for State Bridge Draw West grouped by architectural element. Colors represent type of sedimentary structure from which paleocurrent was measured. Footages which are approximate (~) are off the main measured section. Rose diagram shows average paleocurrent orientation for SBW with 138 measurements.

State Bridge Draw East				
Architectural Element		Paleocurrent Readings		
SSB#	Footage	1	2	3
Crevasse Splay				
	83-84'	100		
	127-130'	85	165	
Channel Body				
	3-6'	215	90	
	33-36'	280	335	
	64-66'	40	100	
CB20	122-123'	90	80	30
Bayhead Delta				
	50-56'	250	215	
	55-61'	110	110	170
Estuarine Assemblage				
	86-90'	260		
	92-100'	100		
Foreshore				
	109-113'	355		
Washover Fan				
	138-141'	325	150	

Asymmetrical Ripples (Sra)
Bidirectional Ripples (Srb)
Planar Cross Stratification (Slp)
Trough Cross Stratification (Slt)

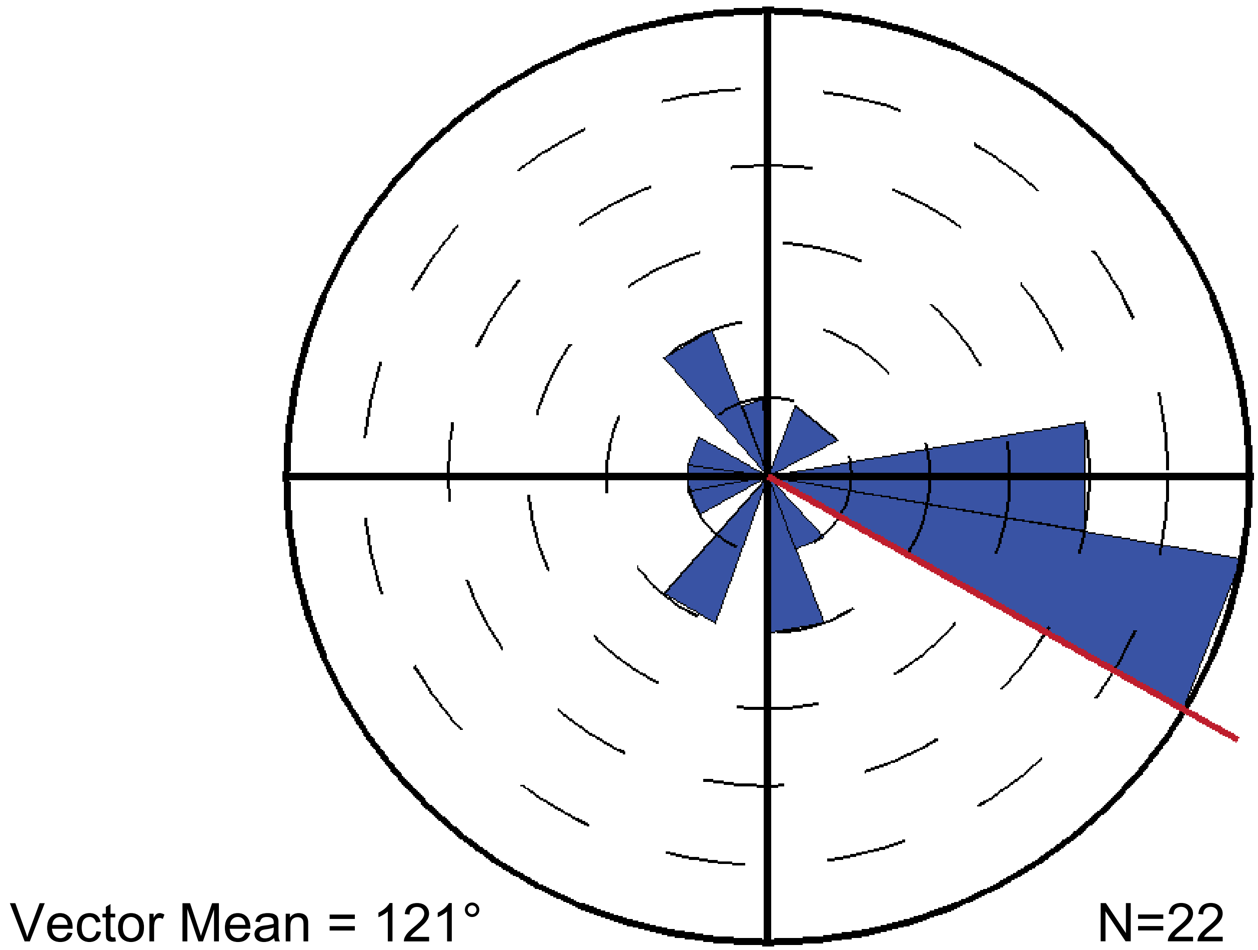

Appendix D2 Paleocurrent data for State Bridge Draw East grouped by architectural element. Colors represent type of sedimentary structure from which paleocurrent was measured. Rose diagram shows average paleocurrent orientation for SBE based on 22 measurements.

APPENDIX E

1. **Petrel individual-well user interface**
2. **Petrel cross-section user interface**

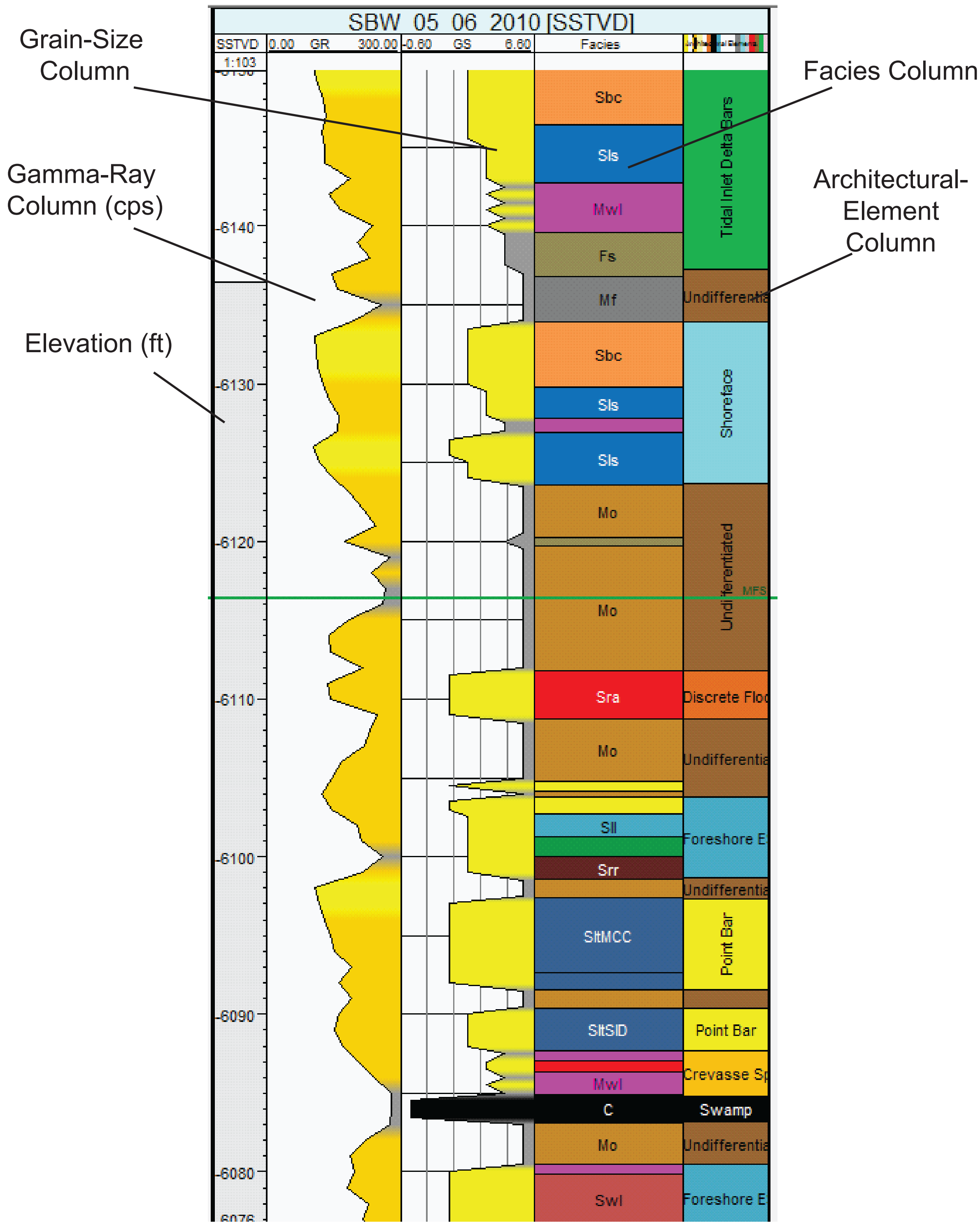

Appendix E1 Petrel user interface. Columns from left to right: Depth (elevation-ft), Gamma-Ray, Grain Size, Facies, Architectural Elements. Gamma-ray profile shown in counts per second (cps), from 0-300. Grain size assigned a value from 0-6: 0: coal, 1: coarse sand, 2: medium sand, 3: fine sand, 4: very fine sand, 5: silt, 6: mud. Facies assigned a code (as shown in Table 1) and color, and assigned using discrete logs. A rchitectural elements assigned using discrete logs.

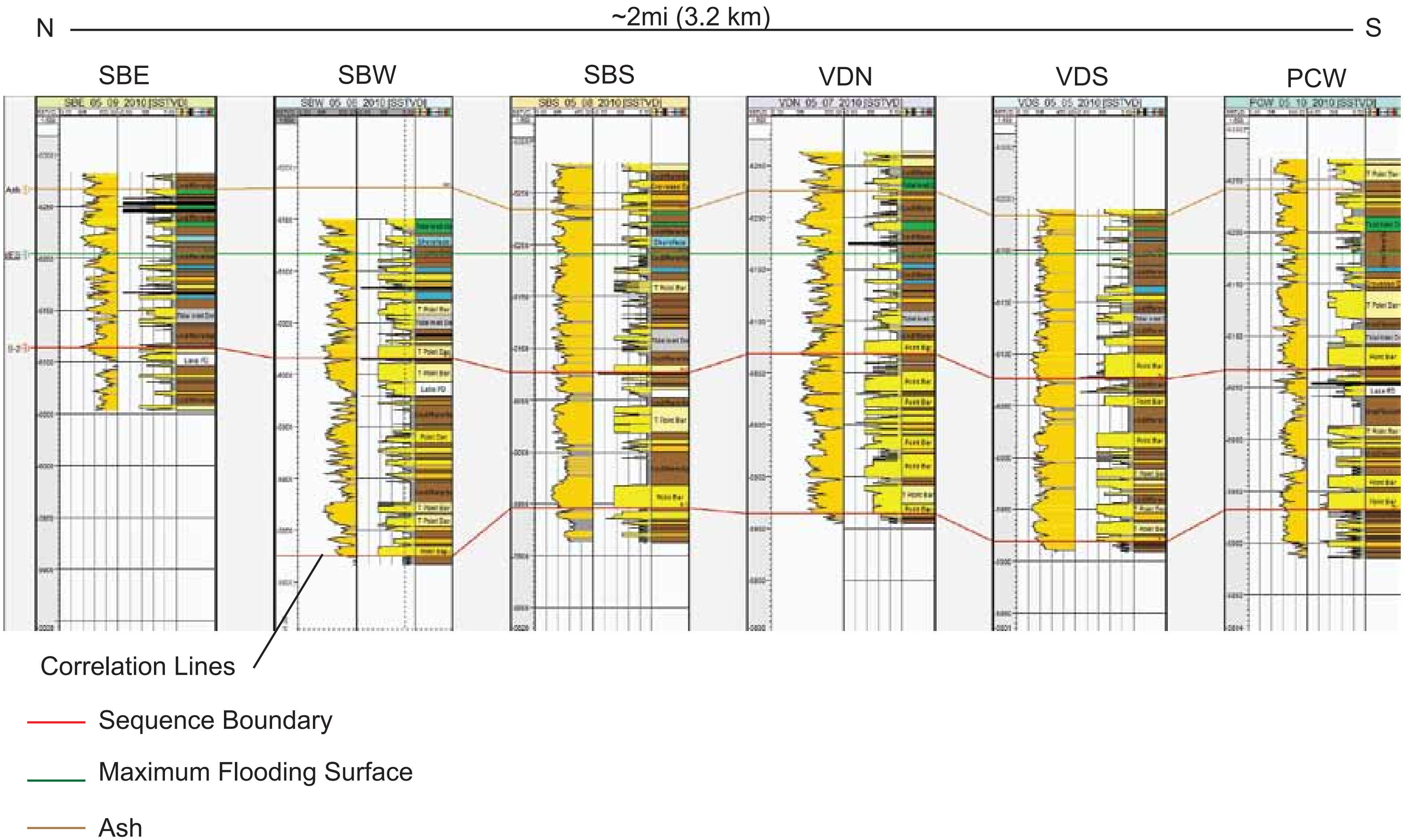

Appendix E2 Cross section from north to south of 6/8 of the measured sections (not including VDW or PCE). Columns for each measured section show (from right to left): elevation (ft), gamma-ray profile (cps), grain-size curve, and architectural-element assignment. All measured sections spaced equally. Lines between measured sections show correlation lines, or “surfaces”, assigned in Petrel. Note: gamma-ray curves for SBS and VDS are from 0-450 cps, rather than 0-300 cps in all other measured sections.

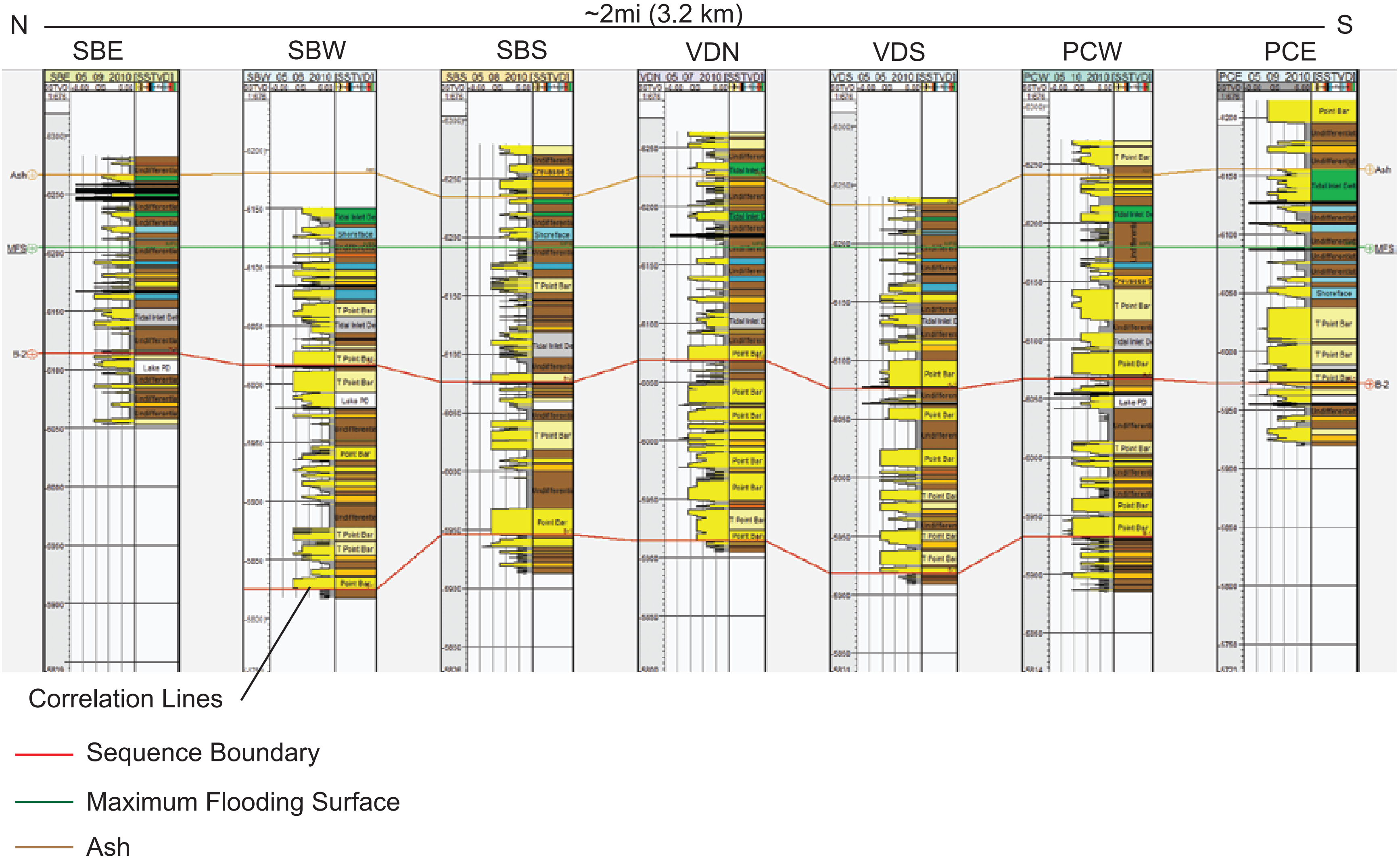

Appendix E2 Cross section from north to south of 7/8 of the measured sections (not including VDW). Columns for each measured section show (from right to left): elevation (ft), grain-size curve, and architectural-element assignment. All measured sections spaced equally. Lines between measured sections show correlation lines, or “surfaces”, assigned in Petrel.

APPENDIX F

1. Photos - Boundaries
2. Photos - Bioturbation/Trace Fossils
3. Photos - Estuarine Assemblage
4. Photos - Kmvl interval
5. Photos - Coal
6. Photos - Various

PCW at 50 feet - Heterolithic debris at B-1.

PCW at 290 feet - View of MFS .(fissile mudstone).

PCW at 50 feet - Outcrop-scale view of erosion at B-1 (on red line).

PCE 1 at 60 feet - Outcrop-scale viewof large sandstone bodies at B-2 (on red line).

SBW at 160 feet - Outcrop-scale view of S-1 (on red line) and EP1 (shown by arrow).

Appendix F1: Photographs of boundaries and surfaces observed in the study area.

SBE at 35 feet - Palm tree roots.

VDN at 320 feet - Large unknown burrow.

VDS at 245 feet - Unknown burrow.

SBS at 285 feet - *Ophiomorpha.*

SBS at 285 feet - *Arenicolites* and *Skolithos.*

SBS at 285 feet - *Skolithos.*

SBW at 130 feet - *Teredolites.*

SBW at 130 feet - unknown boring.

SBW ~70' - *Skolithos* or possible *Arenicolites.*

SBE at 165 feet - *Rhizocorralium.*

SBW at 308 feet - *Thalassinoides.*

VDN at 325 feet - Possible *Skolithos.*

Appendix F2 Photographs of observed types of bioturbation.

SBS at 195 feet - Basal sandstone unit of the estuarine assemblage (distal bayhead delta).

SBS at 205 feet - Upper sandstone unit of the estuarine assemblage (flood-tidal delta).

SBW at 225 feet - Syneresis cracks in plan view, middle muddy unit of the estuarine assemblage (central basin).

SBW at 230 feet - Upper unit of estuarine assemblage (flood-tidal delta).

VDN at 205 feet - Isolated, lenticular sandstone bodies within the muddy unit (central basin) of the estuarine assemblage.

SBE at 92 feet - Syneresis cracks in cross section and *Planolites* in cross-sectional view within the middle muddy unit of the estuarine assemblage (central basin).

Appendix F3 Photographs of the estuarine assemblage as observed in the study area.

VDS at 345 feet - Rooting.

PCW at 360 feet - Preserved tree branch.

PCW at 280 feet - Muddy tidally influenced channel fills.

VDN measured section - Ash Zone, consisting of at least 3 layers. Ash zone within red box and parts of ash beds outlined in white.

Appendix F4: Photographs from the kmvc interval, or the “clincker”.

VDS at 175 feet - Underdeveloped coal bed beneath EP1 with fissile mudstone above.

PCW at 175 feet - Underdeveloped coal bed beneath EP1.

PCE at 60 feet - Developed coal bed beneath B-2.

Appendix F5: Photographs of coal observed in the study area.

SBE at 50 feet - Isolated, lenticular sandstone bodies within the lower unit of the bayhead delta.

SBS at 290 feet - Unknown sedimentary feature - possible dinosaur footprint or soft-sediment deformation.

VDN at 235 feet - Symmetrical ripples.

SBS at 144 feet - Asymmetrical (climbing) ripple cross stratification.

VDS at 303 feet - Small-scale hummocky cross-stratification with *Ophiomorpha.*

VDN at 245 feet - Additonal photograph of the foreshore architectural element.

Appendix F6 Other photographs within the study area.

APPENDIX G

1. Thin Section Information

		Grains					
Sample #	AE*	Quartz	Chert	Biotite/ Muscovite	Feldspar	Illite/ Smectite	Others
PC6	CS	40	5	1	2	30	11% opaques, 1% calcite, 10% MCCs
PC22	PB	50	0	1	24	12	hematite, maybe siderite? (13%)
PC40	BD	77	1	<1	18	1	<2% rock frags, zircon
PC70	FTD	63	18	<1	6	6	hematite zircon, rock fragments (7%)
PC80	PB	70	6	2	4	8	10% opaques
PC110	PB?	68	4	<1	14	10	4% opaques
PC130	MS	60	10	2	6	22	NA
PC140	MS	62	10	4	20	4	NA
PC206	TB	79	5	0	2	14	zircon (<1%)
PC220	TB	68	8	0	8	12	hematite/opaques (4%)
PC230	TB	76	10	0	14	0	NA
PC235	TB	42	10	0	18	30	NA
PC251	PB?	60	16	0	2	20	2% opaques
PC345	PB	74	16	0	10	0	NA

Sample #	AE*	Grain Size	Roundness	Sorting	Cement	HCl reaction
PC6	CS	fU-mL	subang-subround	well sorted	Kaolinite (20%)	Low
PC22	PB	fL	subang-subround	moderate	kaolinite (1%)	Low
PC40	BD	vfU	subround-ang	mod-poor	NA	None
PC70	FTD	mL	subround-round	poorly sorted	kaolinite (10%)	Intense
PC80	PB	mL	subang-subround	moderate	kaolinite (10%) and calcite (7%)	Moderate to Intense
PC110	PB?	fU	ang-round	moderate-poor	kaolinite (10%)+ calcite (10%)	Moderate
PC130	MS	fU	subang-subround	moderate	NA	Moderate
PC140	MS	fL	subround-subang	moderate - well	NA	Moderate
PC206	TB	vfL-vfU	ang-round	moderate-well	NA	None
PC220	TB	vfU	ang - subround	moderate - well	NA	None
PC230	TB	fL	ang - subround	moderate - well	NA	None
PC235	TB	fL	subang - subround	moderate	NA	Moderate
PC251	PB?	fU	round - sunang	moderate - well	calcite (10%)	intense
PC345	PB	fL	sub-ang - ang	poor	calcite (40%)	intense

Sample #	AE*	Comments
PC6	CS	chacedonic quartz, sedimentary rock fragments (~1%), grain alteration, sutured grains, feldspar replacement
PC22	PB	grain replacement, hematite staining/iron, bioturbated, grain alignment, hematite creates lining, grains are aligned - bimodal distribution
PC40	BD	patchy clay, cryptic bioturbation, sharp grain size contrasts, grain dissolution
PC70	FTD	bedded, grain alignment, partially dissolved grains, quartz overgrowth, possible bioturbation, pseudomorphic replacement, ghosted chert
PC80	PB	hematite replacement, grain dissolution, grain replacement with illite/smectite
PC110	PB?	grain alignment, fine layers, drapes of mudrock, grain replacement, quartz overgrowth, hematite and replacement of grains with illite/smectite
PC130	MS	quartz overgrowth, not as much kaolinite
PC140	MS	kaolinite rare, Illite/smectite rare, quartz overgrowth, clay replacement, bedded
PC206	TB	simple composition, bioturbated, clear burrow, no kaolinite, grain replacement, hard to see grains
PC220	TB	grains hard to see, patchy clay, bioturbation, hematite rims around the burrow edge, very little kaolinite, hematite staining, lots of mud
PC230	TB	simple composition, tiny patches of mud, bioturbation,grain dissolution common
PC235	TB	contains lots of mud, laminated, grain alignment, very little kaolinite, lots more feldspar, orange looking replacement, not opaque?
PC251	PB?	Rounded grains, some have perfect cleavage and onlap, chert abundant, may have more feldsplar, bioturbation?, mud clasts, in situ mudrock
PC345	PB	very little mud, mostly calcite cement,

Appendix G Thin section statistics.